UNIVERSITY OF BIRMINGHAM

Advanced assessment of in-situ thermal Enhanced Oil Recovery (EOR) to promote co-production of both catalytically-upgraded oil and hydrogen gas

By

Ryan Claydon

A thesis submitted to the University of Birmingham

For the degree of

DOCTOR OF PHILOSOPHY

School of Chemical Engineering

College of Engineering and Physical Sciences

University of Birmingham

May 2021

Abstract

As the complexity of light oil reservoirs requires greater expense in exploration and production, it is likely that more accessible heavy oil and bitumen reserves become increasingly attractive targets for development. The energy industry is manoeuvring towards greener energy sources. However, the ongoing transitional period will continue to demand a significant oil supply. Heavy oil and bitumen have high viscosity, high content of polyaromatics, and high heteroatom content including sulphur, nitrogen and heavy metals. Energy intensive refinery schemes are required to upgrade these oil types. In Situ Combustion (ISC) uses a small portion of the oil as a fuel source to refine oil in the subsurface, while leaving the deleterious upgrading products within the reservoir and generating hydrogen gas as a by-product.

Heavy oil upgrading was studied using an inexpensive Layered-double hydroxide-derived Ni-enriched Mixed Metal Oxide (Ni-MMO), serving as an analogue to in situ reservoir minerals. The effects of upgrading were studied at 425°C, under both pure H_2 and N_2 gas environments, 30 minute reaction time, a loading of 0.02g/g catalyst to oil ratio and an agitation of 500 rpm. The Ni-MMO catalyst generated superior liquid characteristics, decreasing the viscosity from 811 to 0.2 mPa·s, with the highest proportion of light naphthas under N_2, increasing from 12.6% in the feed to 39.6% in the produced oil. The quantity of coke was saturated in sulphur indicating the generation of polyaromatic centres which served to remove the deleterious polyaromatic and asphaltic components from the oil.

A bespoke Mo-doped Ni-MMO was synthesised to improve the hydrogenation capability of the material. This was tested in the two-stage hydrogenation of naphthalene to tetralin and

decalin. A comparison was made with typical first and second-stage hydrotreating catalysts including NiMo-Al_2O_3 and $Pd_{1\text{-}5\%}$-Al_2O_3. It was apparent that the Mo-doped Ni-MMO generated comparable hydrogenation activity to $Pd_{2\%}$-Al_2O_3, while the NiMo-Al_2O_3, catalyst was comparable to the $Pd_{1\%}$-Al_2O_3 catalyst. Reaction rate constants were derived in agreement with the rate-determining step demonstrated in previous works, with the exception of the $Pd_{5\%}$-Al_2O_3 catalyst which demonstrated the naphthalene conversion to tetralin as the rate determining step. It was made clear that the Ni and Mo bearing catalysts favoured the cis decalin isomer as the end hydrogenation product. This is important for subsequent ring-opening stages. The Pd-bearing catalysts favoured more significant conversion to trans-decalin. It was concluded that the electronic configuration of the catalyst was responsible for the disparity, influencing the orientation of the intermediate octalin species over the catalyst surface.

A conceptualisation of an offshore in situ combustion thermal EOR process in the North Sea was made for a partially-depleted and water-flooded reservoir. A pilot well pairing in a 500 ft x 500 ft reservoir package was modelled. Production data was predicted using the Marx & Langenheim steam heating model, with the coke deposition as the fuel used to generate steam. The production of oil was supplemented with hydrogen gas estimates relating to dehydrogenation of the in situ oil, and compared to experimental work which focused on tetralin dehydrogenation activity to represent heavier feedstocks. The most favourable condition for oil production generated peak production at approximately 1100 barrels/day. It was evident that the dehydrogenation reactions could contribute to a modest co-production of hydrogen gas. Pd-Al_2O_3 catalysts showed the most promise in hydrogen generation at 250°C peaking at 78 Barrel of Oil Equivalent (BOE) H_2/day, while the Ni-MMO

catalyst species generated enhanced dehydrogenation activity over a range of 250 to 300°C compared to thermal dehydrogenation, reaching 35 boe H_2/day.

Acknowledgements

I would like to acknowledge both Professor Joe Wood and the Natural Environment Research Council (NERC), Centre for Doctoral Training (CDT) in Oil & Gas for providing me with the opportunity to undertake a well-resourced PhD at the renowned School of Chemical Engineering, University of Birmingham, in addition to the opportunities to complete external training schemes for both my personal and professional development.

I would further express my gratitude towards Dr. Jason Zhang, for his support and encouraging comments towards the later stages of my PhD studies, as well as Dr. Luis Román-Ramírez for his constructive feedback and support in the laboratory as well as his expertise in kinetic modelling.

I am eternally indebted to my friends and family who supported me through my studies, with special thanks to Stephanie Novasio, Dr. Emily Standell, Edward Pemberton, and both my parents Julia and Nicholas Claydon.

Table of Contents

List of Figures

List of Tables

Abbreviations

THAI	Toe-To-Heel- Air Injection
CAPRI	Catalytic upgrading Process In situ
WGS	Water Gas Shift
HYD	Hydrogenation
HDS	Hydrodesulphurisation
OIP	Oil In Place
(mm)BBL	(million) Barrels
STB	Stock Tank Barrel
BOE	Barrel of Oil Equivalent
XRD	X-Ray Diffraction
XRF	X-Ray Fluorescence
TGA	Thermogravimetric Analysis
SEM	Scanning Electron Microscopy
TEM	Transmission Electron Microscopy

Chapter 1

Motivation and Objectives

1.1 Introduction

Global heavy oil and bitumen resources represent a vast portion of the total global oil resources. The resource estimate for these oil types reach 3.4 and 5.5 trillion barrels, respectively (1). When drawing comparisons to conventional light oil with a resource estimate of 1.02 trillion barrels (2), it becomes clear that heavy oil and bitumen may be required to make a significant contribution to the energy and petrochemical markets in the future. With this in mind, however, over the course of this study governments around the world have accelerated projects to decarbonise their energy sectors. The transition away from fossil fuels is becoming the social and environmental bedrock of future energy sectors in developed countries. The UK for example have set a net-zero carbon emission target for 2050 (3). Emerging economies, though increasingly investing in greener and more renewable energy source, are however projected to demand a greater reliance on fossil fuel supply to continue vigorous industrialisation campaigns in a climate of increased globalisation, and mitigate the impact of huge population growth on energy consumption

(4). It has been suggested that these markets threaten to undermine the goals set by developed economies (5).

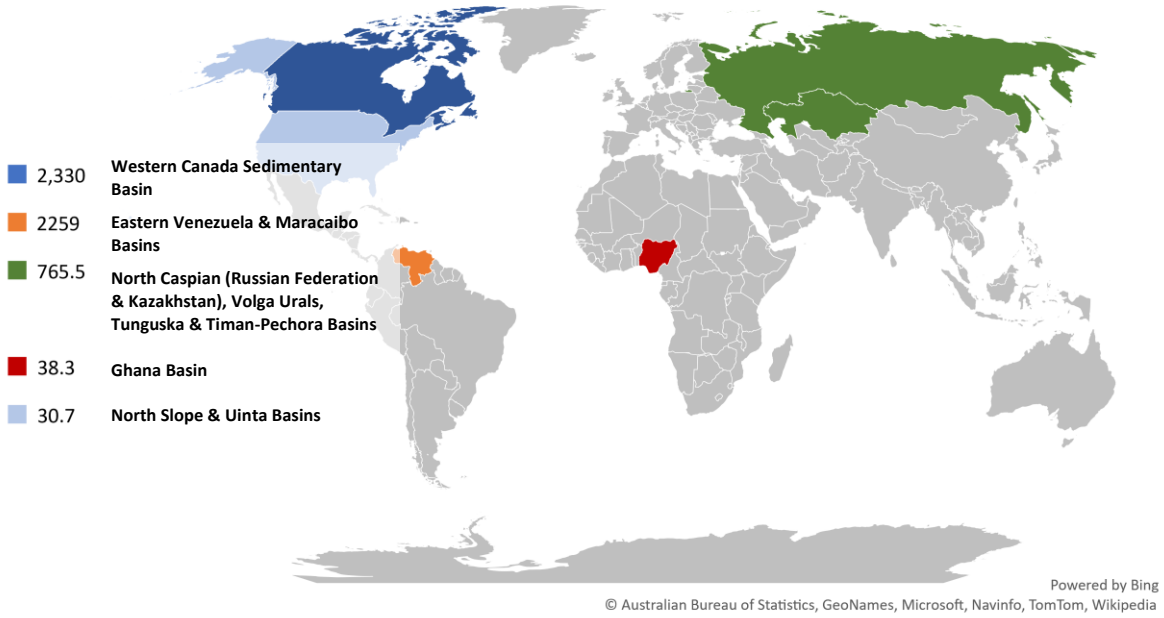

Fig 1.1 Distribution and OIP estimates (billion bbls), including prospective resource, of bitumen for the ten highest ranked basins.

Key differences between oil types are characterised by the volatility of their constituent groups including paraffinic, naphthenic and aromatic groups. Following fluid expulsion from the source host, lighter components in the oil are lost due to a bacterial degradation, evaporation and water washing. The resultant oil mixture will form a highly dense, viscous, asphaltic-enriched oil depleted in paraffins and naphthenes (1). The bacterial degradation also provides an active route for organic components such as nitrogen, sulphur and oxygen to be sequestered into the remaining oil mixture. Generally speaking, this process takes place at 5,000 ft or less beneath the surface. Evaporation plays a bigger part when the reservoir breaches the surface. The resultant fluids are subsequently characterised by their

viscosity and API gravity, those of which are used as benchmark characteristics to define oils in commercial oil markets.

If unconventional oil resources are to be adopted into the industry stream, a number of technical challenges will need to be overcome to extract and refine the resources more efficiently. Key factors representing these challenges include development of inexpensive catalytic materials to upgrade the oils. Furthermore, elevated oil prices are needed to justify the economics of a more intensive extraction programme (6). Also, environmental considerations need to be addressed to limit the carbon cost of new and existing projects. Consequently, there has been motivation for in situ conversion of the heavier oils to limit the environmental cost deficit, using a portion of the oil as the fuel therefore alleviating the need to use fuel from alternative sources (7–9).

The complex degradation of the oils accounts for the difficulty in conversion when drawing comparisons to lighter oils. Refinery programmes need to be redefined to cater for the more complex nature of the heavier feeds. Gray (10) provides a comprehensive account detailing the necessary units when processing large cuts of the residue fraction which defines heavy oils. Firstly, a portion of the oil will need to be distilled under vacuum to aid in the separation of the less volatile cuts. Rigorous thermal programmes, including delayed coking, produce a large amount of coke approximately 30 % by volume of the feed, are subsequently required to upgrade the oils into more useful feeds (11). Additionally, the higher quantity of organic heteroatoms deactivates refinery catalysts more easily. As such, the regeneration of catalysts is required more frequently. There are examples of purpose-built surface upgraders to refine heavy oils and bitumen. The Shell Scotford Upgrader facility is such an example which processes oil sands-derived bitumen in Alberta. Though this

facility is successful at upgrading the bitumen into value-added products, using energy intensive hydrogen-addition upgrading schemes, such as Shell Synthetic Light (31-32° API and 0.1% sulphur) (12), both the financial and environmental costs of such projects are vast, reaching values in excess of $1 billion and generating large quantities of greenhouse gas. The synthetic fuels must contain a sufficiently low nitrogen content to cater for catalytic reforming, while possessing adequate quality middle distillates to produce diesel, while the gas-oil fraction needs to be adequate for fluid cracking (10).

The often prohibitive costs of bitumen and heavy oil field development have asserted the motivation to explore more economically viable in situ upgrading and extraction techniques. Migrating the surface upgrading into the subterranean domain of the reservoir has underscored the continued development of in situ thermal EOR programmes. The types of EOR can be broadly split into two groups (a) steam-assisted and (b) combustion assisted. That said, many of the successful field-scale projects today have used a combination of the two (13,14). Steam assisted EOR techniques include Steam-Assisted Gravity Drainage (SAGD) and Cyclic Steam Stimulation (CCS) (15). Combustion-assisted recovery methods include In Situ Combustion and Toe to Heel Air Injection (THAI) (16). The steam-assisted variation has had far more popularity in recent years, with projects spanning from Canada, through to Egypt and the solar-thermal EOR project at the Amal oilfield (Oman) to aid in the development of heavy oil and bitumen reserves (17–19). Steam is injected into the reservoir to thermally condition the heavy oil so that viscosity can be reduced and the resultant mixture can flow easily to the producer well. While partial amounts of upgrading under aquathermolysis accompany this process, the amount of water needed in this process, in addition to the energy required to generate the steam, restrict this technology to certain operators which can manage high OPEX costs (20). The quantity of water required for each

produced bbl of oil can range from 2 to 4.5 barrels (21). Consequently, the impact on the environment can be immense with the coproduced contaminated water requiring rigorous treating methods.

The combustion-assisted EOR techniques use a portion of the in situ oil as a fuel thereby generating extensive thermal zones within the reservoir which can both aid in situ upgrading considerably while also minimising the need for injected steam. In recent years, the prospect of in situ catalytic upgrading has been advanced, wherein a catalytic liner (CAPRI) can be emplaced into the production well and aid in the upgrading of the oil before reaching the surface and thereby minimise the extent of surface upgrading (15). This mode of recovery remains in the experimental stage with only one known field trial, of which provided unclear results. As a result, if this technology is to be appropriated by the industry, significant changes must be made to demonstrate its effectiveness at upgrading and therefore offer the operators significant financial reward. A previous optimisation study carried out be Hart et al. (22) sought to understand how heavy oil upgrading could occur over a CAPRI-type production liner, simulated at lab scale. It was shown that the viscosity of the fluid could decrease significantly by up to 82%. Furthermore, under a hydrogen atmosphere the amount of coke could be inhibited significantly falling from 57.3 to 34.8 wt.%. It was clear that coke deposition and catalyst poisoning plays a limiting role in the CAPRI reactor and consequently a demonstration comparing a fixed catalytic bed to ultradispersed catalyst was undertaken (23). It was shown that when using ultradispersed catalyst sulphur and metal removal was superior to pelleted catalyst, reaching a 38.6% and 85.2%, respectively while viscosity reduction improved by 17% relative to the feed. The catalyst particle size is clearly correlated to the extent of upgrading. As the particle size decreases and therefore increasing the surface area, the diffusion pathway to the active

sites is shorter which helps to improve upgrading of the macromolecules associated with heavier, residue-rich feeds (24).

It is clear that augmenting the existing CAPRI add-on warrants the use of catalysts which can aid in the upgrading of the oil while suppressing coke formation and/or reducing heteroatom content, such as sulphur. Identifying pathways for the injection of catalysts may prove to be useful in conveying ultradispersed catalyst to the relevant thermal zones. Additionally, identifying reservoir minerals which could be used or augmented to generate catalytic properties could be a useful and inexpensive mode for in situ upgrading.

Furthermore, with the advent of hydrogen as a potentially wide-spread future energy resource, it is becoming clear that hydrocarbon deposits could be used as hydrogen-generating subterranean reactors (25–27). The coproduction of both oil and hydrogen gas may provide an adequate transition pathway for energy companies looking to expand into greener technologies, while maintain a foothold in the fossil fuel market. The in situ gasification, dehydrogenation and potential for WGS reactions remains an ideal mode of hydrogen generation. There have also been significant developments in the use of bespoke hydrogen filters which once installed within the reservoir could effectively limit the production mixture to a H_2 as a single component (27).

1.2 Aims and Objectives

To investigate the performance of catalysts under different conditions on heavy oil upgrading, via the evaluation of;

a. The impact of catalyst type on phase yields
b. The impact of catalyst type on sulphur removal

c. The impact of catalyst type on liquid and solid phase chemistry
d. The effect of H_2 and N_2 in the reaction gas media
e. To demonstrate how materials analogous to those found in reservoir formations may affect in situ upgrading
f.

To investigate the effect of bimetallic and monometallic catalyst type on model compound hydrogenation, via the evaluation of;

a. First and second stage naphthalene hydrogenation products
b. The impact of catalyst type on cis and trans decalin production
c. The impact of catalyst type on reaction rate constants

To investigate the production potential of a wet-mode ISC project offshore, via the evaluation of;

a. Oil saturation on production rate
b. Burn rate on production rate
c. Dehydrogenation potential of heavy oil feeds and coproduction potential of upgraded oil and hydrogen gas

1.3 Thesis Organisation

(i) Chapter 1 delivers the motivation of the study while highlighting the resource estimates and distribution of unconventional oil types. The identification of potential basins for the production of hydrogen is also made.

(ii) Chapter 2 comprises a thorough analysis of heavy oil and bitumen characterisation and refinement, followed by an in-depth overview of EOR methods adopted to improve product yield when developing oil fields.

(iii) Chapter 3 provides information regarding the experimental methodologies employed in the upgrading and analysis of oil products, in addition to the synthesis of catalyst species, to supplement experimental methodology in the subsequent chapters.

(iv) Chapter 4 details heavy oil upgrading based on previously optimised conditions. A comparison is made between various catalysts, both lab-synthesised LDH and refinery-grade Al_2O_3-supported, as well as non-catalytic thermal upgrading. In this chapter, the emphasis is on product distribution, with a detailed analysis of solid and liquid product composition, and how this is affected by the catalytic regime and reaction gas composition. The reaction gas media use in the experimental design, contrasted the effect of both pure H_2 and pure N_2.

(v) Chapter 5 studies the use of a model compound to represent the deleterious fraction of heavy oil would be ideal in further constraining the reaction pathway and mode of hydrogenation between catalysts. The hydrogenation capability of the LDH-based catalyst was improved by doping the material with Mo. A comparison was made between a typical $NiMo/Al_2O_3$ refinery catalyst as well as a series of Pd/ Al_2O_3 catalysts of differing Pd loadings. The effects of the metal species and support material were emphasised in product distribution of naphthalene hydrogenation. Furthermore, the reaction rate constants were determined using a pseudo-first order to further elucidate the reaction mechanism.

(vi) Chapter 6 deals with a proposed offshore in situ combustion project which could be applied to a partially waterflooded heavy oil field, The Alba field. Production figures were estimated using a Marx and Langenheim steam heating model, based on the coke and therefore fuel formation produced by the oil type. The production figures were further expanded on by estimating the amount of hydrogen produced in dehydrogenation reactions, using tetralin as a model component.

(vii) Chapter 7 presents concluding remarks on the results of the study and demonstrates a number of tangents along which further investigation is warranted.

1.4 References

1. Meyer, F, R.; Attanasi, D, E.; Freeman, A, P. Heavy oil and natural bitumen resources in geological basins of the world. US Geol Surv. 2007;Open File-:36.

2. Hein, J, F. Heavy oil and oil (tar) sands in North America: An overview & summary of contributions. Nat Resour Res. 2006;15(2):67–84.

3. Ofgem. Ofgem Decarbonisation Action Plan. Ofgem [Internet]. 2020;13. Available from: https://www.ofgem.gov.uk/system/files/docs/2020/02/ofg1190_decarbonisation_action_plan_revised.pdf

4. Finley, M. The oil market to 2030-implications for investment and policy. Econ Energy Environ Policy. 2012;1(1):25–36.

5. British Petroleum. Energy Outlook 2020 edition explores the forces shaping the global

energy transition out to 2050 and the surrounding that [Internet]. BP Energy Outlook 2030, Statistical Review. London: British Petroleum. 2020. Available from: https://www.bp.com/content/dam/bp/business-sites/en/global/corporate/pdfs/energy-economics/energy-outlook/bp-energy-outlook-2020.pdf

6. Ihejirika, N. The Canadian Oilsands and Strategic Approaches to Profitability. Oxford Inst Energy Stud. 2019;56(August):1–18.

7. Zhao, B, R.; Xia, T, X.; Luo, W, W.; Shi, L, Y.; Diao, J, C. Alteration of Heavy Oil Properties under In-Situ Combustion: A Field Study. Energy and Fuels. 2015;29(10):6839–48.

8. Greaves, M; Turta, A. Oil field in-situ combustion process. United States; 5626191, 1997.

9. Turta, A. In Situ Combustion. In: Enhanced Oil Recovery Field Case Studies. 2013.

10. Gray, R, M. Upgrading Petroleum Residues and Heavy Oils. Marcel Dekker; 1994.

11. Petroleum Coke : the coal hiding in the Tar Sands. 2013;(January).

12. Oil Sands Magazine. Upgrader Scotford [Internet]. 2021. Available from: https://www.oilsandsmagazine.com/projects/shell-scotford-upgrader

13. Bealessio, A, B.; Blánquez Alonso, A, N.; Mendes, J, N.; Sande, V, A.; Hascakir, B. A review of enhanced oil recovery (EOR) methods applied in Kazakhstan. Petroleum. 2020:1–9. Available from: https://doi.org/10.1016/j.petlm.2020.03.003

14. Panait-Patica, A.; Serban, D.; llie, N. Suplaco de Barcau Field - A Case History of a

Successful In-Situ Combustion Exploitation. In: SPE Europec/EAGE Annual Conference and Exhibition. 2006.

15. Hart, A. The novel THAI–CAPRI technology and its comparison to other thermal methods for heavy oil recovery and upgrading. J Pet Explor Prod Technol. 2014;4(4):427–37.

16. Xia, X, T.; Greaves, M.; Turta, A.; Ayasse, C. THAI - A “short-distance displacement” in Situ combustion process for the recovery and upgrading of heavy oil. Chem Eng Res Des. 2003;81(3):295–304.

17. Dong, X.; Liu, H.; Chen, Z.; Wu, K.; Lu, N.; Zhang, Q. Enhanced oil recovery techniques for heavy oil and oilsands reservoirs after steam injection. Appl Energy. 2019;239(March 2018):1190–211. Available from: https://doi.org/10.1016/j.apenergy.2019.01.244

18. POWER TECHNOLOGY. Miraah Solar Thermal Project. 2021. Available from: https://www.power-technology.com/projects/miraah-solar-thermal-project/#:~:text=Translated as “mirror” in Arabic,officially inaugurated in February 2018.

19. Gupta, S.; Guédez, R.; Laumert, B. Market potential of solar thermal enhanced oil recovery-a techno-economic model for Issaran oil field in Egypt. AIP Conf Proc. 2017;1850.

20. Giacchetta, G.; Leporini, M.; Marchetti, B. Economic and environmental analysis of a Steam Assisted Gravity Drainage (SAGD) facility for oil recovery from Canadian oil sands. Appl Energy. 2015;142:1–9. Available from:

http://dx.doi.org/10.1016/j.apenergy.2014.12.057

21. Jordaan, M, S. Land and Water Impacts of Oil Sands Production in Alberta. Environ Sci Technol [Internet]. 2012; Available from: http://eutils.ncbi.nlm.nih.gov/entrez/eutils/elink.fcgi?dbfrom=pubmed&id=22364164&retmode=ref&cmd=prlinks

22. Hart, A.; Shah, A.; Leeke, G.; Greaves, M.; Wood, J. Optimization of the CAPRI process for heavy oil upgrading: Effect of hydrogen and guard bed. Ind Eng Chem Res. 2013;52(44):15394–406.

23. Hart, A.; Greaves, M.; Wood, J. fixed-bed and dispersed catalytic upgrading of heavy crude oil Opus : University of Bath Online Publication Store Please cite only the published version using the reference above . of heavy crude oil using-CAPRI. 2015;213–23.

24. Al-Marshed, A.; Hart, A.; Leeke, G.; Greaves, M.; Wood, J. Effectiveness of Different Transition Metal Dispersed Catalysts for In Situ Heavy Oil Upgrading. Ind Eng Chem Res. 2015;54(43):10645–55.

25. Kapadia, R, P.; Wang, J.; Kallos, S, M.; Gates, D, I. Practical process design for in situ gasification of bitumen. Appl Energy. 2013;107:281–96. Available from: http://dx.doi.org/10.1016/j.apenergy.2013.02.035

26. Kapadia, R, P.; Kallos, S, M.; Gates, D, I. Potential for hydrogen generation from in situ combustion of Athabasca bitumen. Fuel. 2011;90(6):2254–65. Available from: http://dx.doi.org/10.1016/j.fuel.2011.02.038

27. Parker, D. Proton Technologies mining low-cost, green energy from aging oil wells

[Internet]. Calgary Herald. 2021. Available from:

https://calgaryherald.com/business/commercial-real-estate/proton-technologies-mining-low-cost-green-energy-from-aging-oil-wells

Chapter 2

Review of heavy oil upgrading and catalysis

2.1 Introduction

Hydrocarbons represent a group of organic compounds that have been used over the centuries for a variety of purposes, of which one fundamental use centres around combustion to harvest energy. These compounds are generated by the decomposition of organic matter, with the subsequent heat and pressure applied in the subsurface over time to slowly produce a chemical compound composed almost entirely of carbon and hydrogen, with the addition of smaller amounts of impurities. One group of hydrocarbon compounds, in a liquid form, is known as crude oil.

Today, crude oil represents a significant component of the global energy mix, as well as the non-combusted use of fuels in the petro-manufacturing sector (1). The current polito-socioeconomic trend, however, focuses on the gradual removal of crude oil from both the energy and manufacturing sectors over the coming decades. Such a debate is highly controversial, albeit underlined by clear and unmistakable environmental implications. It is becoming clear that the world has a greater amount of oil than will likely be needed for the 21st century given the acceleration of natural gas consumption and renewable energy development. As a result, one side of the argument in risk mitigation suggests that the development of existing fields should be favoured over the engagement in new drilling campaigns in underexplored basins, many of which are located in environmentally-sensitive areas such as in the Arctic Circle or deep-sea Atlantic settings (2).

The abundance of proven high viscosity oil reserves around the world ultimately offers a clear motivation for development. Huge deposits in Canada, found chiefly in the Western Canada Sedimentary oil province, equate to approximately 1.7 trillion bbls in reserves with additional prospective resources (3,4), while large reserves of heavy oil can be found in Western and Eastern Siberia, among other locations including the Orinoco heavy oil belt in Venezuela in which there are resources in excess of 1.9 trillion bbls of extra heavy crude (4,5). Currently limited by conventional methods of extraction, further exploration into new technological frontiers will make these known reserves increasingly more attractive.

Heavy oil represents one of the least desirable fractions of oil that can be found in the subsurface. On a geological scale, biodegradation of the comparatively low temperature shallow deposits have preferentially removed the more desirable, lighter liquid compounds leaving an abundance of long chain, polyaromatic, organo-metalliferous and heteroatom-enriched hydrocarbon compounds in addition to a high methane content (4,6). This results in a high abundance of resin and asphaltene fractions which are deleterious for the transport and combustion of oils.

That said, there are production and mining companies around the world that are committed to developing heavy oil deposits (7). This is due in part to the relative high abundance of this hydrocarbon type, but also due to technological facilitation in refining these compounds to remove the undesirable compounds. In some cases, this is done at great expense, but methods to minimise the costs of synthesising highly active catalysts used in the refinery process will continue to be explored to facilitate economically viable upgrading operations.

2.2 Components in Heavy Oil

The typical parameters cited include viscosity, the measure of a fluid's resistance to flow, and the American Petroleum Institute's index of gravity, aka API gravity, which details how heavy or light an oil is with respect to water. Generally, oils can be divided into the following groups as shown in Table 2.1 (4):

Table 2.1 A comparison of oil types using viscosity and API gravity as defining parameters

Type	API gravity (°)	Viscosity (cP)
Conventional	25	-
Medium	25 > 20	< 100
Heavy	20 > 10	> 100
Bitumen	> 10	> 10,000

However, while this scheme is useful to efficiently compare oils around the world and quickly assign value, there are many additional factors contributing to the low quality of an oil and consequently the difficulty found in its processing.

Oils can be classified into fractions based on solubility and adsorption characteristics. For example, in this particular scheme, there are four classes:

- Coke and solids: insoluble in tetrahydrofuran
- Preasphaltenes: Soluble in THF and insoluble in benzene
- Asphaltenes: soluble in benzene and insoluble in n-pentane
- Maltenes: Soluble in n-pentane

The maltenes can, however, be separated into four fractions saturates, aromatics, resins and oils (asphaltenes). This separation protocol is acronymised to SARA and is a commonly adopted classification tool.

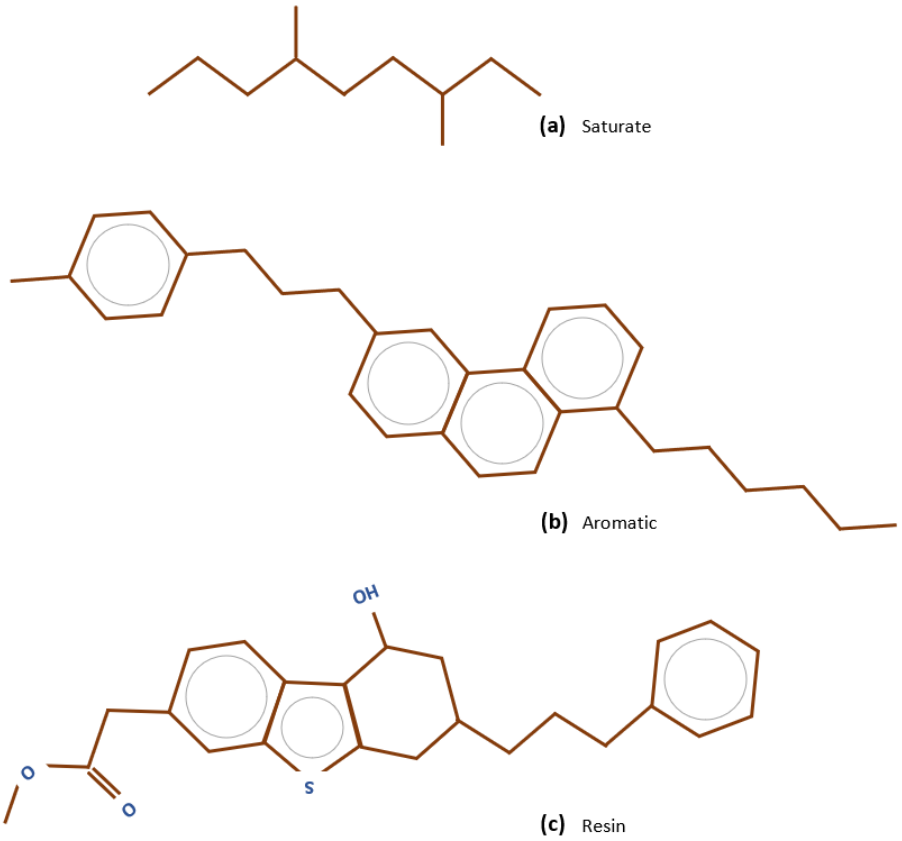

Figure 2.1 Molecular structures of components typically found in oils (a) saturates (b) aromatics (c) resins

The saturate fraction contains aliphatic compounds. The aromatic group comprises aromatic compounds typically substituted with saturated groups or bridges to other aromatics. Resins contain a higher concentration of aromatic carbon and exhibit more heteroatoms. The asphaltene group, aromatic-soluble and paraffinic-insoluble, represent the most deleterious fraction representing the highest molecular weight and most polar compounds. It is the latter groups which are most important in characterising heavier feeds.

Residuum comprises the fraction of petroleum that cannot be distilled under vacuum with atmospheric equivalent boiling points exceeding 520°C. While conventional deposits accumulate between 10-30% residuum, heavier feeds exceed 40% (8). The constituents of residuum encompass polyaromatic compounds which make up the resinous and asphaltenic components typically found in the oil, key constituent of the SARA analysis. An example of the molecular structure is demonstrated in Figure 2.2.

When identifying the viability of fuel materials, knowledge of the hydrogen to carbon ratio (H/C) provides insights into heating and combustion values. As a result, in order that residuum can be processed into useful transportation distillates, the feed must undergo severe disproportionation to remove the carbon, or hydrogenation in which hydrogen from another source is added to the feed.

Moreover, residuum contains heteroatoms which are elements present in addition to carbon and hydrogen. Sulphur, nitrogen, oxygen, vanadium and nickel comprise the most common heteroatoms. Typical values found in heavy oils exceed the acceptable range of oils processed in conventional refinery programmes (8). Consequently, pre-treatments are used to reduce the heteroatom proportions.

The asphaltenes are the most complex molecules present in petroleum and microstructure analysis has revealed that they are made up of large aromatic sheets piled upon one another with associated metalloporphyrins and PI-PI interactions between the sheets stabilising the structure (9,10). With the biggest contribution to parameters such as viscosity which can have significant impacts on pipeline transportation, their structures remain poorly defined, occurring in great variation and in need of further understanding. Consequently, it has become more important to define this group by the solvent used to

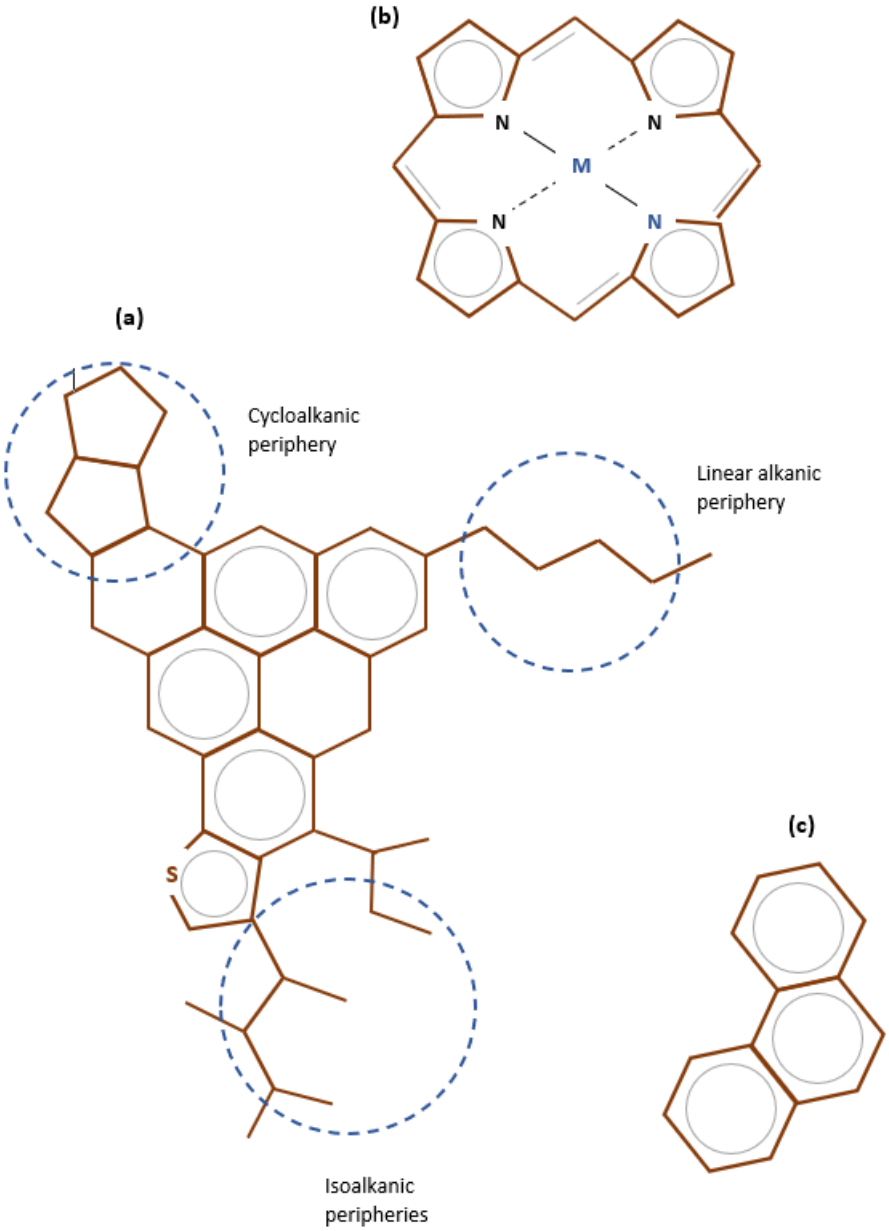

Figure 2.2 Molecular structures of components typically found in heavier feeds (a) poly-aromatic species with a polar component and multiple alky substitutions (b) metal porphyrin and (c) simple aromatic.

precipitate them, or the make-up of the remaining solute from which it has precipitated. This is important as the type of precipitant used to isolate the asphaltene fraction can have a marked effect on the structure of the precipitated asphaltene molecules. For example, a detailed review covered the use of several precipitants which highlighted the precipitant-dependent formation of asphaltenes dominated by either naphthene peripheral groups, branched peripheries or those with long linear hydrocarbon perhiperies (11). As a result, the

type of precipitant is directly related to the rheological properties of the solution that remains. This can help to understand the processes which should be adopted for a specific feed to obtain the optimum characteristics, weighted against cost.

2.3 Traditional Extraction Methods

Oil mining is the term attributed to surface or shallow subsurface (typically up to 250 ft) excavation of oil-saturated sand and clay, which is then processed using on-site washing, floatation and retorting instruments (12). The finished product is a blend of syncrude which can then be economically transported for further refinement.

As with much mining activity around the world, it does not come without cost. This cost follows a clear environmental tangent. The mining sites are often vast which consequently spoils large swathes of otherwise natural landscape and the accompanying complex ecosystems which thrive witihn (13). Furthermore, mine spoils are abundant, containing many deleterious organic and inorganic species which, if not managed correctly, can leak into waterways causing hugely detrimental environmental problems. What's more, the shear quantity of material that makes up the spoil heaps may be sufficient to instigate failure leading to liquefaction (14).

That said, the wide-scale use of mining in this manner has been justified previously as the proportion of unconventional oil (Athabasca region) that can be mined represents six times the quantity of conventional recoverable oil in Canada. Furthermore, Athabascan oil which can be mined is estimated to make up approximately 7% of the total Athabascan reserves (12). However, the remaining 93% rely on more costly operations and future technological developments which can draw companies away from the comparatively efficient mining operations.

2.4 EOR

There is growing interest in Enhanced Oil Recovery (EOR) with respect to the extraction of heavy oil due to the significant increase in extraction efficiency obtained using new technologies. EOR methods comprise those that are applied after primary production and secondary production are exhausted, or if they are unable to provide economic production (12). Primary production uses the natural energy in the reservoir to produce oil, while secondary production utilises co-produced water and/or gas to be subsequently injected, thereby compensating the reservoir with additional pressure to enhance the production. There remain a number of different methods ranging from miscible fluid drive, chemical to thermal methods (15,16).

All of these methods seek to improve the heavy oil recovery, however, given the chemical nature of the oil it is still necessary to partially upgrade the oil while at surface so that the oil can be efficiently transported to refinery plants. Surface upgraders and heavy oil processing facilities are key to this process as they provide on-site conversion to reduce the viscosity of the oil (17).

2.4.1 Miscible Displacement

Miscible displacement comprises an injection well and production well, whereby the injection fluid can dissolve into the crude either at contact or after several contacts. This process can reduce the interfacial tension and improve oil displacement on the microscopic level. Gases are preferable as the significant density difference between the oil and gas is sufficiently large enough to increase sweep efficiency. Carbon dioxide is commonly selected as the miscible gas due to its low cost as compared to LPG or methane. However, due to its low volumetric sweep efficiency a CO_2-salinated water injection method has been

developed to help mitigate the resistance of water in allowing CO_2 to diffuse into the oil ganglia (18).

In the Alberta area, numerous successful miscible floods have been implemented but typically the project target has comprised a light to medium oil. However, there have been a number of heavy oil targets including both The Suffield Upper and Lower Mannfield J pools (19).

2.4.2 Chemical Flooding

On the pore scale, the interfacial tension between the relevant phases can present a huge problem in mobilising oil to the production borehole. However, an array of chemicals can be used to reduce this interfacial tension and consequently enhance the sweep efficiency. Surfactants and alkaline-based chemicals form the predominant groups of chemicals used in this EOR technique.

Polymers can also be used to increase sweep efficiency in a process known as polymer drive, depicted in Figure 2.3. Polymers are typically used when high permeability or fracture zones reduce the efficiency of a waterflood. Polymer or crosslinked gel can be injected and diverted to shut-off the high permeability 'thief' zones (20), while water-soluble varieties promote the movement of water through the reservoir rock thereby increasing sweep efficiency.

Inhibiting factors in assessing the applicability of this technique include the high cost of chemicals and the lack of practical evidence on large-scale reservoirs. Typically, this technique has been applied to reservoirs bearing relatively low viscosity oil. However, with the advent of new technologies including horizontal wells and improvements in polymer

manufacturing, oils with viscosity on the order of thousand centipoise have been targeted with this particular brand of EOR.

Micellar polymer flooding presents an efficient type of chemical flood. The mixture consists of surfactant, alcohols serving as cosurfactants, water and electrolyte which together with oil, sweeps through the reservoir, releasing trapped oil. The chemical complexity of the micellar slug also makes it the most expensive method, but the sweeps have been indicated as highly effective at unlocking oil pools in highly heterogeneous reservoirs (21).

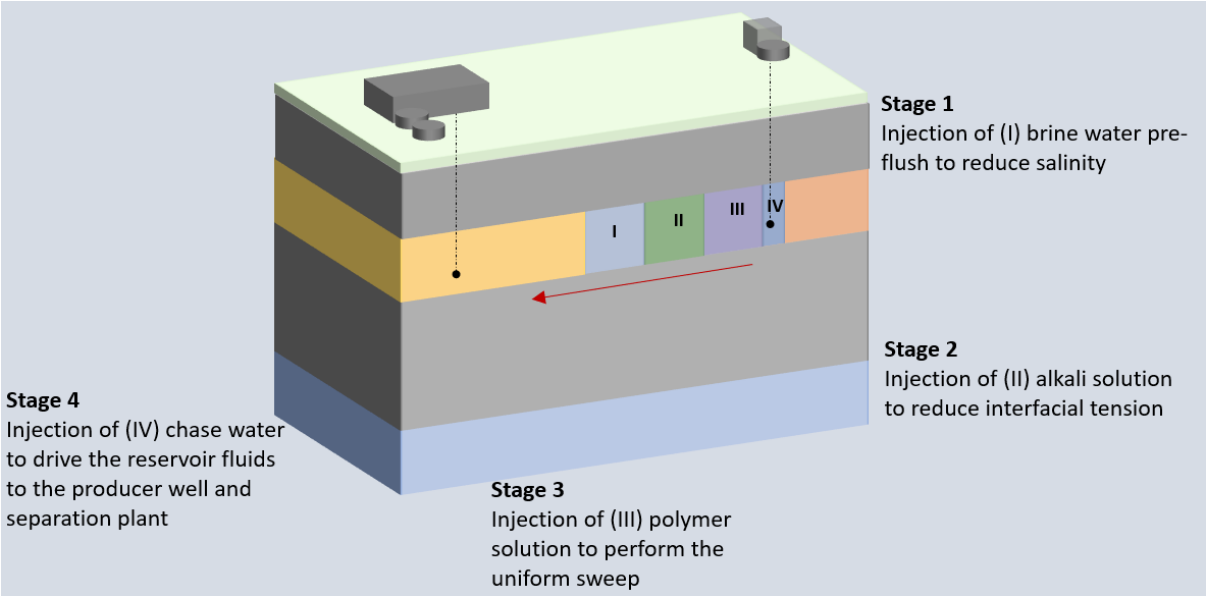

Figure 2.3 A visualisation of the multi-stage chemical flood of an oil reservoir using a polymer drive mechanism

The SZ36-1 field in Bohai Bay was targeted as a polymer flooding candidate following poor recovery under waterflooding. It has been reported that the test in 2002 became the first offshore example of polymer flooding realising a water cut drop from 66 to 50% accompanied by an incremental oil recovery of more than 145,000 STB by 2006 (22). The success of this test catalysed the implementation of a further 52 pilot tests. The average oil

recovery from the overall development program in the NB35-2 field, Bohai Bay, achieved 20.2% (23).

2.4.3 Thermal Stimulation

Thermal recovery methods set forth an additional tangent of EOR methods.The concept centres on the use of heat to reduce the viscosity of the oil and accelerate the flow of oil towards production wells (24).

These methods have existed in both theory and practice throughout the last century, with particular attention afforded by production companies in both the United States of America and former-Soviet Union (25). As a result, it is in these two territories that a wealth of information regarding the viability of such techniques can be found.

The selection of a heat source, however, has remained a matter of debate for production companies. Heat sources have ranged from the use of steam, electromagnetic heating elements *in situ*, combustion of a proportion of the oil *in situ* and even the somewhat daunting 1950s conceptualisation of harnessing atomic energy, the latter of which included the plan to detonate a nuclear device at a depth of 1250 ft just below the target reservoir (26). That said, with the exception of a handful of electrical heating element trials, thermal recovery has frequentloy centred on the use of steam flooding and *in situ* combustion.

2.4.3.1 Steam Flooding

Harnessing the latent energy of steam is an effective method of heating. This has subsequently been applied to the context of Heavy oil reservoirs. Injecting steam into an oil reservoir to saturate it in heat has been widely applied with the intention of reducing

viscosity, and developing a relatively low water to oil mobility ratio thereby promoting oil displacement and recovery.

A multitude of configurations have been adopted including simple vertical injectors and vertical producers, in addition to more complex steam pads comprising multiple horizontal well pairings. In this latter set-up, aka Steam-Assisted Gravity Drainage (SAGD), the well pairing encompasses two horizontal wells, one a few meters above the other as shown in Figure 2.4. When steam is injected through the shallower horizontal well, thermal communication is established with the deeper horizontal producer well as latent heat is released into the formation (27). A "steam chamber" is developed leading to the countercurrent gravity drainage of oil and condensed water. Although total recovery can extend towards 70%, the major drawback is the vast amount of water required in addition to the necessary, but financially restrictive, heating facility to generate steam. Heat loss during injection has also been an inhibiting factor in steam operations, particularly in regions with thick permafrost sequences overlying the reservoir. Consequently, Moussa et al. (28) modelled a SAGD variation which included in situ steam generation to successfully mitigate the problems with heat loss and achieve high project profitability.

Current operations include the Long Lake facility in Alberta which began operations in 2008 with a production capacity of 72000 boe/d (29). Furthermore, the Yarega heavy oil deposit in the Republic of Komi, Russia has an expanding SAGD operation with an expected annual production reaching 25 million bbls (24).

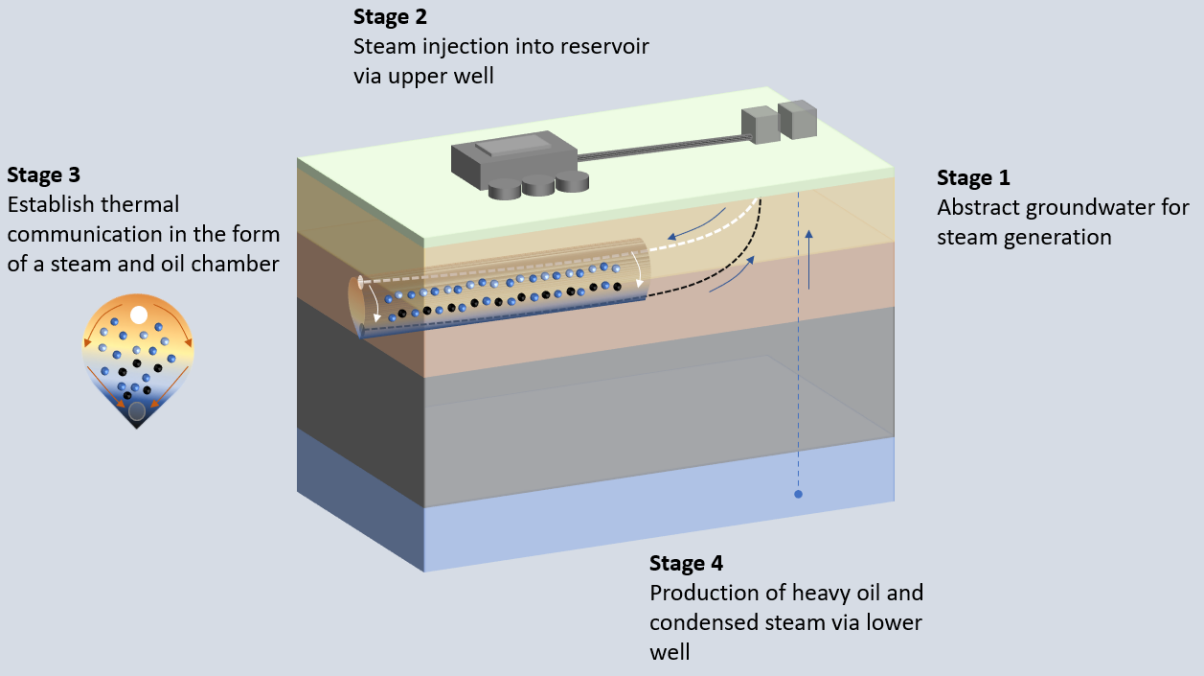

Figure 2.4 A visualisation of the double horizontal well configuration of the SAGD process accounting for the key process stages

2.4.3.2 *In situ* combustion

From technical, environmental and social perspectives, the *in situ* combustion process is, to say the least, a tumultuous concept. A portion of the OIP is burned in the ground to provide sufficient heat to promote coking reactions for fuel laydown while enhancing the displacement of the in situ oil. This is done through increasing the mobility ratio, oil vaporisation, steam and flue gas drive as well as miscible displacement. In addition, pyrolysis reactions stimulate upgrading through cracking, hydrogenation and hydrodesulphurisation reaction pathways, catalytically enhanced by minerals present in the reservoir in theory. This in essence turns a subsurface reservoir into a subterranean refinery, while providing for an EOR with a unique mechanism to increase the $/stock tank barrel (STB)rather than just simply increase the total stb/development, which would normally be the case when introducing high expense tertiary EOR mechanisms.

During this combustion process, a series of complex reaction zones are created, moving through the reservoir as the combustion front progresses towards the production well. Broadly, these zones can be split into the (I) burned zone, (II) combustion zone, (III) cracking zone, (IV) condensation zone and (V) native zone. A high temperature exothermic oxidation reaction between the native hydrocarbons and oxygen-enriched air, leads to high temperatures in the reservoir which are favourable when reducing the viscosity of the heavy oil and also promoting the pyrolysis reactions. The oxidation, pyrolysis and hydrogen generating reactions can be simplified to the following:

Oxidation of heavy oil:

Heavy Oil + O_2 → CO + CO_2 + H_2O

Pyrolysis of heavy oil:

Heavy Oil → Light Oil + hydrocarbon gas + coke

Steam reforming of heavy oil:

$C_mH_n + mH_2O \rightarrow mCO + (m + 0.5n) H_2$

Pyrolysis of hydrocarbon gas:

$CH_4 \rightarrow C + 2H_2$

Oxidation of coke:

Coke + O_2 → CO + CO_2 + H_2O

Water-Gas-Shift:

$CO + H_2O \rightleftharpoons CO_2 + H_2$

Initially, the native oil is oxidised and the heat generated promotes pyrolysis reactions to generate coke, the process fuel, and the fuel is then subsequently oxidised to sustain the heat generation for further oxidation and pyrolysis. In theory, this basic reaction scheme is replicated as the combustion front propagates along the reservoir.

That said, the complexity and therefore uncertainty of this process has prevented wide-scale implementation. A predominant constraint on the process is the uneven penetration of the combustion front. The velocity contrast between the injected air and the native formation fluids leads to preferential channelling through the most permeable networks. It has also been demonstrated that excessive coke lay-down can sink greater amounts of oxygen and therefore inhibit the growth and movement of the combustion front. Additionally, lighter oils are unable to produce sufficient quantities of coke which is a rigid requirment to sustain the combustion front.

In traditional well construction, a production casing is cemented in place along the most productive zones in a reservoir. Unfortunately, conventional equipment is not designed to accommodate the extreme temperatures, pressures and corrosive fluids that accompany the in-situ burning reactions. There have been numerous reports of temperatures reaching approxioamtely 550°C (1000°F) leading to the failure of tubing, casing and cement, thereby significantly destabilising the integrity of the well construction, leading to buckling or collapse (30). Furthermore, highly acidic fluids can corrode the equipment. These issues have the potential to not only halt the production and irrevocably compromise the initial investment in cases, but also provide deleterious leakage pathways into the environment, especially if the reservoirs are shallow.

2.5 Wide-scale Adoption

The attention towards *in situ* combustion in the US was underpinned by the relative successes of a handful of thermal projects in heavy-oil reservoirs and the tar sands. A notable example included the successful field test in the Delaware-Childers field by Sinclair Oil and Gas, highlighting a combustion efficiency of over 80%. Consequently, in combination with the vast quantity of poor viscosity, heavy oil reservoirs in the US and relative high OIP responding to poor primary and secondary production, and in a time of ever-increasing oil demand, thermal projects looked an attractive opportunity.

A definitive analysis of heavy-oil resources in the US, their amenability to thermal exploitation was made in 1967, dividing potential reservoirs into one of three classes, including a review of previous and existing thermal projects (30). These classes assessed the individual reservoir characteristics in terms of their potential success for thermal stimulation. It was concluded that as of 1966, 45.9 out of 106.8 billion heavy oil stb were in class 1 reservoirs i.e. those with the perceived highest success rate, the majority of which situated in southern California (30). By January 1966, 63 ISC projects and 2 steam-ISC combinations had been started in heavy-oil reservoirs, with many more to follow in subsequent years.

The former Soviet Union hosted some of the biggest *in situ* combustion projects known in the world today, with numerous examples situated in the former Azerbaijan, Ukraine and Russia SSRs. The oldest *in situ* combustion project dates back to 1933 with the Shirvan oil field pilot project (26). This later gave way to larger and more ambitious projects within the Pavlova Gora and Zybza oil fields. However, possibly the most widest known today is the Karazhanbas oilfield of the former Kazakhstan SSR. Karazhanbas is a 400 million barrel heavy

oil field which has seen field-scale application of both steam flooding and in-situ combustion over 40 years (31). Under wet-mode combustion an incremental recovery of between 32-40% has been achieved over conventional production mechanisms.

A detailed analysis of thermal projects, both steam injection and in-situ combustion, can be found in the literature, and it is clear that through both success and failure, sufficient interest in this tertiary EOR technique has lasted through the times to today. The Suplaco de Barcau field in Romania is an example of an on-going successful thermal ISC project, commencing in the 1960s and still producing today (32). Furthermore, the Mayorovskoye field is the site of an ISC project in the Samara region, Russia, having commenced in 2019, demonstrating the remaining current interest in using thermal techniques to develop highly viscous oils (33).

2.5.1 Technical Variations

Continued experimentation has led to distinct variations in its implementation which have accounted for successful EOR projects. For example, reverse combustion, wet-mode combustion, pressure-up/blowdown combustion (34) and Toe-to-Heel Air Injection (THAI) all represent unique variations of the *in situ* combustion process . The problem remains that there is no quick-fit method of adoption, rather, project models tailored to the reservoir geometry, rock type and hydrocarbon properties are required to mitigate the risk. This is costly, time-consuming and in many instances unviable unless there is a unified and well-funded determination for an organisation to enter the thermal EOR arena.

The Toe-to-Heel Air Injection method, shown in Figure 2.5 is a relatively new variation on the conventional in situ-combustion process. This variation proposes a vertical injection well and horizontal production well pattern. The proposal by Greaves and Turta (35) generates a

number of intrinsic properties which promote a more successful project. Firstly, the well pattern configuration is characterised by a short displacement mechanism. The partially-upgraded, mobilised oil ahead of the combustion front is drawn-down into the horizontal producer i.e. taking the shortest pathway to the well instead of mixing with the cold native oil zone as in conventional thermal methods. Additionally, a stable process condition persists during the process, preventing oxygen-enriched air bypassing which is a problem with conventional methods. The ignition and acceleration of the air injection is concentrated to the top section of the oil lens. Heat conduction to the lower part of the oil lens generates the mobile oil zone. It was suggested by Xia et al. (36) that the stability of THAI is then coordinated by a continuous and highly exothermic oxidation process at the top of the reservoir (representing a controlled and complementary form of gas override), and a sequential sealing of the horizontal producer by heavy residue coking at the base prevents preferential gas channelling into the production well. The results of their experimental model indicated that temperatures in excess of 500°C could be achieved with an accompanying upgrade of 5-7 ° API.

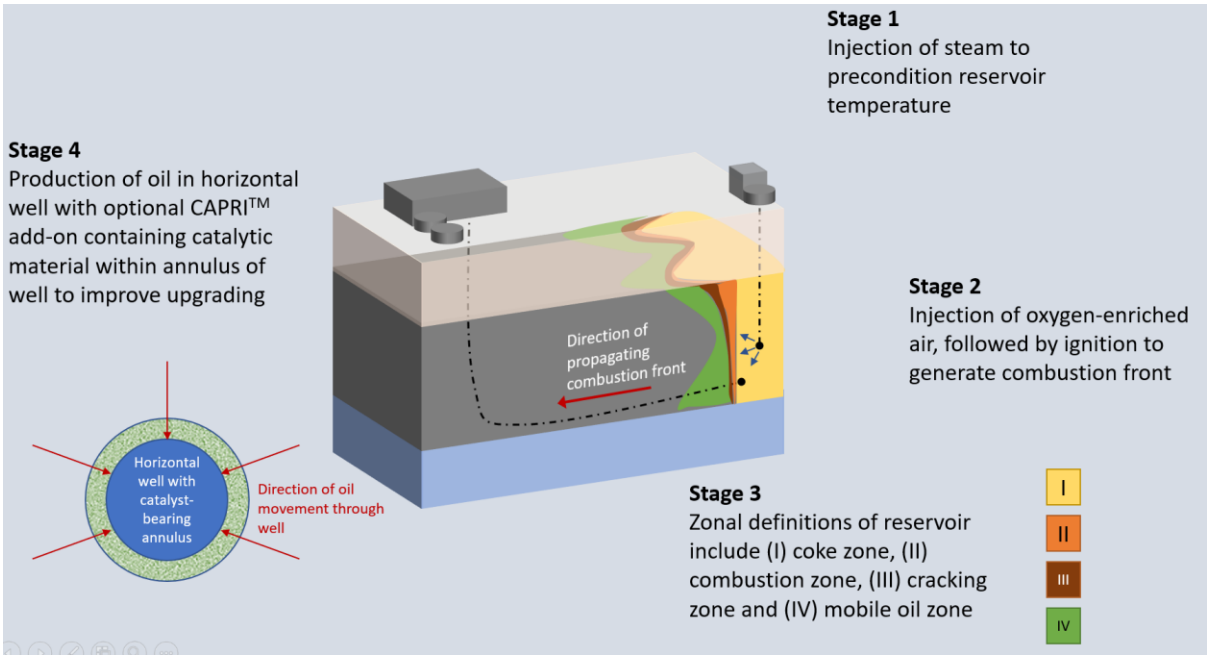

Figure 2.5 A visualisation of the Toe-To-Heel configuration of the horizontal and vertical wells configured when adopting the THAI process.

The short-displacement property localises the in-situ combustion process into smaller cells, demonstrating the inhibition of deleterious heterogeneity, while also preserving and concentrating the extent of thermal and reservoir-mineralogically enhanced upgrading.

The THAI process has since been tested in the field by Petrobank in 2005 (16), while conceptual modifications have been researched in abundance. A CAPRI 'add-on' provided the horizontal well with a pseudo-refinery catalytic upgrading pattern in the annular spacing. This new definition of THAI provides the opportunity to further upgrade the oil through the use of various catalytic materials at the high temperatures encountered during combustion. Choice of the catalytic material is constrained by a balance between cost and effectiveness. However, given the variation of oil quality that this process can be applied to, individual characteristics of a reservoir's oil will dictate the material used, while this choice can easily be accommodated in the annular spacing.

Since this conceptualisation was first announced, numerous other variations have been hypothesised and researched, varying from the injection of nanoparticles into the formation, to increase the localised zone of catalytic upgrading, as well as, engineering a subsurface heating element which can essentially 'top-up' the temperature to a required level, optimising the upgrading reactions (37). Furthermore, this could be promoted using a mobile electrical heater which migrates along the horizontal well as the combustion front migrates through the reservoir. Adam et al. (37) investigated the use of a downhole microwave-assisted heating mechanism, contradicting previous claims that heavy oil could not be heated to adequate upgrading temperatures using this method. In the absence of a microwave susceptor, temperatures reached 425°C accompanied with strong indications of HDS with a reduction exceeding 12%. Furthermore, viscosity was reduced to below 100 cP from 880 cP therefore successfully converting a heavy oil to within the range of a more upgradable medium quality oil.

Furthermore, the ISC method has since evolved into a process which could aim to capture a portion of the green energy market through the production of hydrogen as a by-product of the gasification of bitumen in the Canadian tar sands (3,38). It has been reported that during the Maguerite Lake ISC pilot, under wet-mode combustion, up to 20. mole percent of hydrogen was generated in the gas stream.

2.5.2 Offshore planning

Air injection as an offshore concept remains in its infancy. However, given the potential to increase the productivity of heavy oil fields in their decline, as well as potentially unlock a huge supply of hydrogen, renewed interest in field development can be sought to apply air

injection. However, wet-combustion has been acknowledged as a more effective thermal EOR option. It has the potential to reduce coke formation, increase the burning rate, yield higher production rates by impacting a greater area of the reservoir and produce H_2 gas (32).

While several proposals have been made to introduce HPAI into offshore reservoirs, the majority field projects to be undertaken have been located onshore, mainly in the US (39). It is therefore more difficult to assess the viability of offshore candidates, particularly those in different geological regimes. Despite this, offshore TEOR is not a completely new frontier. An offshore ISC pilot project was implemented successfully in the comparatively thick 96.8m Gao 3-6-18 reservoir within the Liaohe Oil field. The oil recovery improved from approximately 29.1 t/d to 47.3 t/d (40). Furthermore, successful Steam-Assisted Gravity Drainage (SAGD) pilot tests have been conducted offshore in Bohai Bay, China as well as the Emeraude Vapeur project, offshore Congo (41,42). Some of the significant differences between ISC and its thermal counterparts include the fact that ISC can operate at much greater depths, as heat loss is not a significant factor. This is because the heat is generated in the reservoir when using air injection, whereas SAGD uses injected steam to condition the reservoir and this process suffers from heat loss during its transport via the injection well.

There have been some key acknowledgements to high pressure air injection's potential as an offshore EOR technique. The fractured reservoirs of the Litoral de Tabasco and Sonda de Campeche basins have been considered as air injection candidates by the joint venture of PEP-BO (43). The project aimed at applying air injection to light oil-saturated naturally fractured carbonate reservoirs. The estimated benefits were split across two predicted processes. This includes immiscible flooding of the air and LTO mode of the combustion

which is thought to contribute gains at least equivalent to a nitrogen injection. Additional recovery is predicted to relate to the thermal process-induced pressure increase.

2.6 Chemistry of Upgrading

Heavier oils typically comprise a higher fraction of the deleterious components typically found in oils across the world. A higher density of sulphur, poly-aromatics, metals and asphaltenes leads to the requirement to more rigorously upgrade these oils. Often several stages of treatment will complement any refining programme to sequentially remove these components in as efficient a manner as possible.

However, broadly upgrading is achieved through both cracking and hydrogenation reactions. These reactions can be purely thermally-operated or catalytically-augmented through the addition of active metal and support materials. The operation of cracking is constrained to the carbon-carbon separation of a hydrocarbon molecule, requiring temperatures in excess of 420°C to achieve any useful conversion rates (8). This reaction produces highly reactive radical intermediates that can undergo a series of supporting reactions. One such common result is the quenching of the radical via hydrogenation, thereby generating a molecularly-lighter and often more valuable hydrocarbon. However, in the presence of multiple radicals and a lack of activated hydrogen, adducts can be formed from two or more of these cracked molecules. This in turn can produce macromolecular varieties forming coke, a carbonaceous toluene-insoluble solid phase. The amount of coke produced is controlled by reaction conditions, and while this can be minimised to great extents, its formation remains an unescapable certainty of heavy-feed upgrading reactions.

The crackability of a residue mixture is determined by the individual constituents. Crackability is typically increased in the presence of higher molecular weight species due to the fact that there is a higher concentration of easily ruptured bonds in complex molecules (8). This increases the chances of bond breakage. Furthermore, the variation of radical intermediates interact with different species during the degradation process. Broadly speaking the following trend exists from most reactive to least reactive: paraffins > linear olefins > naphthenes > cyclic olefins > aromatics.

2.6.1 Visbreaking and coking

Visbreaking is the name of a technique which uses relatively mild conditions to reduce the viscosity of the oil. A schematic of the process is demonstrated in Figure 2.6. A 5-10% conversion to naptha can impart significant reductions in viscosity, while the relatively low residence time of the oil prevents significant coke formation. The mixture is then quenched following completion of the visbreaking reactions, inhibiting further thermal reactions. The visbreaking process has also been augmented to include steam in the presence of a homogeneous catalyst. This process is called aquaconversion and generates a more stable product (12). The catalyst promotes the transfer of hydrogen from the water, to the reactive species generated by the thermal process, under the same conditions of visbreaking. While hydrogen incorporation in this process is not as significant under high hydrogen partial pressures found in hydroconversion processes, it is sufficient to enhance viscosity reduction and distillate production. Lakhova (44) investigated the use of a series of zinc and aluminium nano-oxide additives which have shown to reduce the proportion of asphalt-resinous substances in the product.

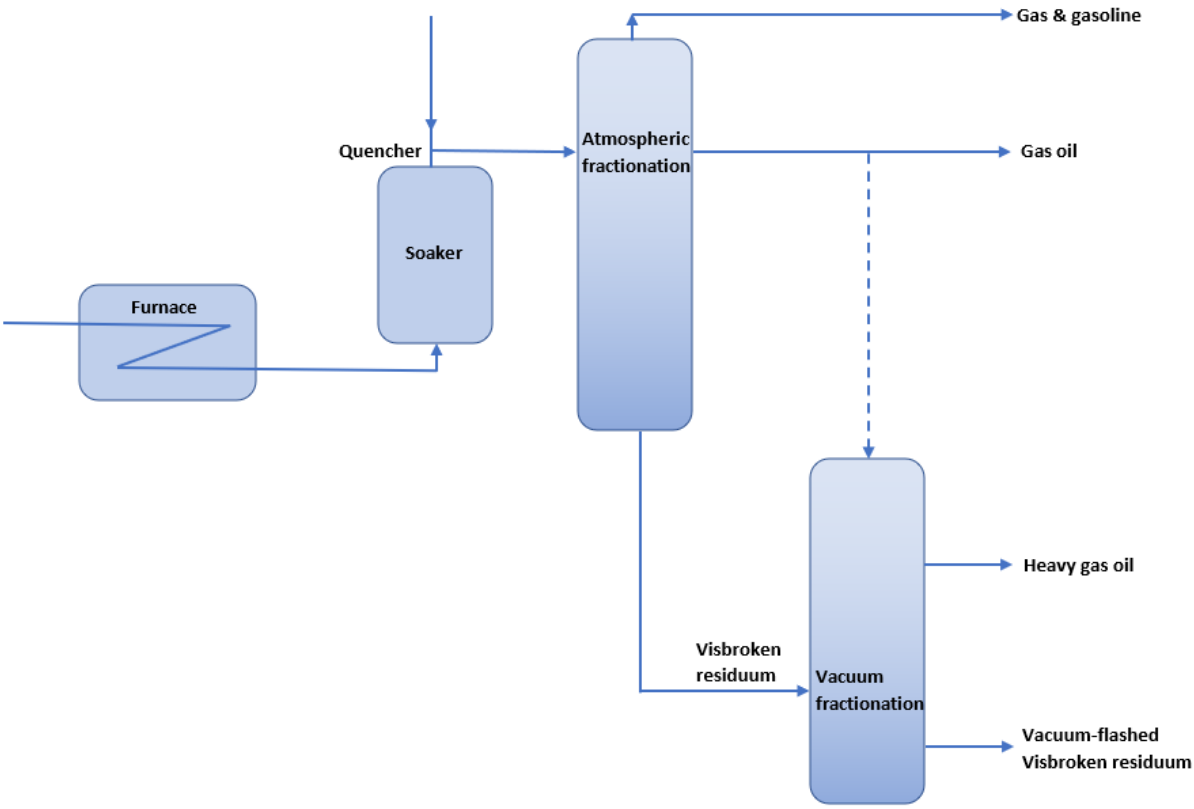

Figure 2.6 Schematic of a visbreaking unit designed primarily as a low-energy process to aid in the transport of heavy oil. This variation includes the optional soaker and vacuum fractionation column.

A more rigorous thermal upgrading process is known as coking which is depicted in the schematic Figure 2.7. This process is used to generate a higher quality distillate components at the expense of significant coke and gas production. A fired heater is used to pre-heat the vacuum residue to approximately 500°C, encouraging some thermal conversion. The fluid is then charged into the reactor vessel, whereupon a temperature exceeding 400°C and pressures between 15-80 psig are used. Volatile components are cracked from the mixture and discharged overhead, which in turn leads to a coke fractionator, while the solid residue remains in the drum. When the drum is filled with solid carbonaceous material, the heated fluid is charged to the second vessel, while the "coked-up" drum is shut down for cleaning

purposes. The residual coke, however, has some residual value. The type of coke produced depends on the initial oil composition and various studies have looked into understanding

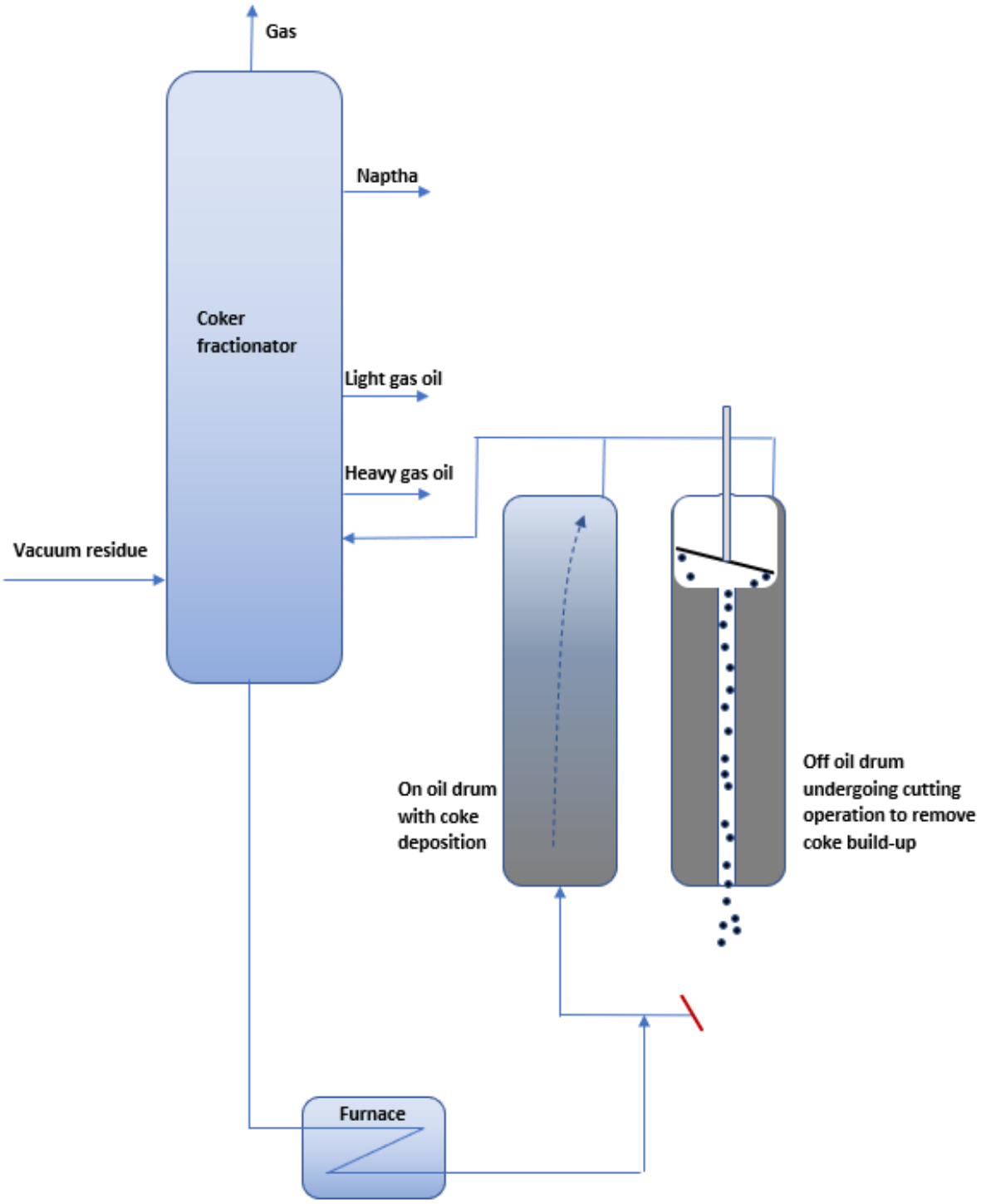

Figure 2.7 Schematic of a coker unit highlighting the de-coking of the 'off' oil drum and continuous charging of the 'on' oil drum.

this relationship (45,46). Green coke is one such type which can be produced, serving as a feed for the manufacture of industrial anodes and graphitic carbon manufacture (8).

2.6.2 Hydroprocessing

Hydroprocessing covers the catalytic treatment of oil at elevated hydrogen pressure, resulting in an increase in the hydrogen proportion of the products and decrease in heteroatom impurities. Okunev et al. (47) presents a review of the complex process involving a number of chemical reactions ranging from hydrocracking, hydrodesulphurisation, hydronitrogenation and hydrometallisation. The preliminary removal of these impurities is essential for further Residue Catalytic Cracking. This is because the catalysts used in RCC can be highly sensitive to heteroatoms, particularly metals such as V and Ni which can block the active sites, while nitrogen base compounds can migrate to acid sites and result in an inhibitory effect on conversion.

The hydrocracking process typically involves two reactors. The first reactor contains a catalyst which favours the removal of heteroatoms while the resultant oil is passed through the second reactor which contains a hydrocracking-specific catalyst.

HDM reactions can be summarised as a two-step process in which porphyrins undergo hydrogenation via tetrapyrrole ring cleavage followed by metal deposition on the catalyst surface. HDN involves two key reactions. The nitrogen rings are hydrogenated while the specific C-N bond undergo hydrogenolysis which yields ammonia and hydrocarbons. HDS reactions can either proceed as direct desulphurisation yielding aromatic hydrocarbons and hydrogen sulphide or are aided by hydrogen to partially or fully saturate the ring structures.

Hydrocracking involves a multitude of simultaneous and sequential reactions which includes the cleavage of high molecular weight molecules as a result of the catalyst acid sites and the hydrogenation of the cleaved products over metal sulphide active sites. Hydrodealkylation reactions proceed over the alkyl-branches while isomerisation, polymerisation and condensation reactions can occur which may promote coke formation.

2.6.3 Principle cracking sequences

The reaction sequence of heavy oil upgrading to produce lighter oils has been generalised to a few distinct reaction stages under thermal treatment, of which the simple cracking of an n-alkane in solvent is used as an example:

Initiation:

$P \rightarrow 2R\cdot$

Propagation:

$R\cdot + P \rightarrow RH + P\cdot$ (chain transfer)

$P\cdot \rightarrow R\cdot + O$ (β-scission)

Termination:

$R\cdot + R\cdot \rightarrow$ products

P and P· represent the parent alkane and corresponding radical, while R· and RH represent the resultant lower molecular weight alkyl radical and alkane, respectively. The symbol O represents a lower olefin molecule.

The reactions of olefins are affected significantly by the reaction conditions (8). For instance, in the absence of hydrogen and catalytic active sites, a number of free radical reactions can

occur including hydrogen abstraction, β-scission and addition reactions, similar to their alkane counterparts. In the presence of hydrogen and a suitable catalytic material, hydrogenation can occur as well as the addition of a radical to simulate reverse β-scission reactions.

As the quality of oil decreases, the complexity of the hydrocarbon structures increases as well as the abundance of such types. The residue fraction of oil is rich in naphthenic compounds, bridged to other structures and substituted with complex side chains. The cracking of such compounds release naphthenic groups and their side chains, with the more favourable points for breakage adjacent to the ring structure (8). Subsequently, naphthenic groups can dehydrogenate to form aromatics in the absence of hydrogen, highlighted by the conversion of decalin to naphthalene.

However, alkylaromatic products which can be produced from naphthenic structures participate in condensation reactions. These reactions stimulate the production of a complex network of fused ring structures which provide the precursors for coke (8). However, in the presence of suitable catalytic materials, hydrogen gas and a hydrogen acceptor, the production of hydroaromatics and naphthenes can be predetermined.

In the context of subsurface upgrading, it is likely that the complexity of reactants present in the reservoir render a comprehensive suite of reactions possible in the CAPRI process, including cracking reactions, hydrogenation and dehydrogenation, desulphurisation, hydrogen transfer and isomerisation to name but a few. In this way, the heavy oil will undergo a great amount of physio-chemical change producing an oil with more favourable properties, equating to higher value, at the surface. However, control over products will be

limited by the constantly-changing conditions prevalent throughout the zone, as well as variations in textural and chemical properties of the reservoir rock.

2.7 Catalysts

The addition of catalytic materials has a marked influence of the quality of the products during upgrading. Catalysts lower the energy barrier for a reaction pathway and result in an increase in molecular degradation and conversion. Molecules will diffuse through the catalyst pore network and coordinate with the active sites, react and diffuse back through the pores into the reaction mixture.

However, the sensitivity of the catalysts to coke deactivation, when dealing with heavy residue feeds, makes a number of pre-treatment processes necessary before catalytic upgrading. These include processes such as deasphalting, demetallisation and some hydrotreating reactions.

Presently, there is a huge array of catalyst types that can be used in petroleum refining. A refinery program involves a complex system of refinery units each carrying out specific reactions dependent on the feed. As such the nuances of each process objective can be tied to specific individual catalytic materials. Catalytic reforming, polymerisation, isomerisation, alkylation, hydrotreating, hydrocracking are all examples of these process units which require combinations of augmented materials to increase the efficiency of the refinery program.

Refineries which have been modified to increase the amount of heavier feeds, as well as purpose built surface upgraders, the latter of which are constructed in close proximity to

the heavy oil deposits, require multiple units exclusively focused on upgrading heavier feeds. Solvent deasphalting, *vis* breaking, hydroprocessing which itself includes an entire repertoire of hydrogenation desulphurisation-related facilities, as well as the non-catalytic coking process remain typical upgrading units used in heavy oil upgrading and refining. With the exception of coking, catalyst selection is crucial. Insufficient catalyst lifetime is an on-going problem which inhibits heavy oil upgrading and related processes such as THAI CAPRI.

The CAPRI process was studied using a series of microreactors to scale the field well section to a laboratory model. It was found that catalyst fouling and deactivation occurs over a short period. This specifically involved asphaltene, metal and coke deposition on the catalytic active sites, inhibiting the full capability of the catalyst. In addition, pore blocking as a result of the metal accumulation acts as a precursor for substantial pressure drop and reduction in accessible active site area (8). This ultimately reduces the recovery rate of the process while inhibiting the upgrading (16). It has been stipulated that in reactions such as steam reforming, once initiated, the pore plugging and deactivation of the catalyst can reduce its lifetime to the order of hours (48).

It has been reported that A carbon guard bed was utilised in the microreactor to represent a potential multi-layered catalyst-bearing annulus within the CAPRI well. The results indicated that that the addition of a guard bed helped to prolong catalyst lifetime by acting as an adsorption medium for asphaltene molecules which would ordinarily polymerise to form macromolecular coke deposits on the catalytic active sites. Specifically, when using the guard bed, an additional 8.5% viscosity reduction and an additional increase of API by 2° was described when comparing to the HDS/HDT catalyst used independently (49). Moreover, further advancements to the CAPRI process have included looking at potential hydrogen

donors to support the hydroprocessing reactions. The growth of macromolecules under polymerisation can demonstrably impact catalytic activity and liquid hydrocarbon yield. Hart et al. (50) experimented with a number of gas environments to quantify its impact on oil quality during the CAPRI process. An inert gas made up of N_2 was compared to CH_4, acting as a hydrogen donor, and H_2 atmospheres. The results were clear in highlighting the positive impact of active hydrogen in preventing the cross-linking of asphaltene molecules. The final content of asphaltene in the oil dropped by 10.7, 51.6 and 43.4%. In combination with the coke production it is clear that hydrogen from both pure hydrogen and methane atmospheres, inhibited the conversion into coke with the coke content representing 23.5, 20.4 and 17.4 wt.%, respectively.

It is clear that hydrogen would therefore be a useful additive to the CAPRI process, however, the limitation resides in its transportation into the wellbore. As a result, hydrogen donors either as gases or liquids have been hypothesised to provide active hydrogen. What's more a simultaneous steam and air injection under wet-mode combustion may provide suitable means for hydrogen generation via the water-gas shift reaction.

Pyrolysis of the heavy oils and bitumen can lead to coke adsorption over the catalyst which is a predominant route towards catalyst deactivation (15). Where the typical lifetime of a hydrotreating catalyst varies from 6 months to 1 year, catalysts used for heavy oil upgrading suffer from comparatively much shorter periods before catalytic deactivation (51,52). Hart (16) outlines the stages of deactivation, commencing with the initial adsorption of asphaltenic and resinous molecules onto the surface of the catalyst. The adsorbed species subsequently undergoes dehydrogenation, leading to a greater adherence onto the catalyst of the resulting poly-aromatic molecule. As hydrogen is continually extracted from these

molecules, the molecules undergo gradual condensation and polymerisation reactions which result in the formation of coke. This coke can remain deposited on the surface of the catalyst, preventing hydrocarbon components from reaching the active sites. Gradual deposition of the metalloid components from porphyrin and non-porphyrin types structures, onto the catalyst eventually result in complete catalyst deactivation (51).

Sulphur remains a key constituent responsible for the deactivation of catalysts. Heavy oils have an enrichment of sulphur in comparison to conventional oils. This sulphur can attack the active sites on sulphur-intolerant metals, irreversibly binding to them and preventing any further coordination of reactants. However, some catalysts can be treated and augmented to target sulphur in the presence of hydrogen so that it may be removed in the gaseous form of hydrogen sulphide as depicted in Figure 2.8.

A serious consideration therefore should focus on the catalyst which is required to efficiently promote heavy oil upgrading. A major obstacle in catalyst development remains with cost. This is relevant both on the surface and in the subsurface. However, surface catalysts are used on the order of months and what's more are often directed into regeneration units so that they can be reactivated. This factor is not relevant in the subsurface due to the inability to recover the catalyst emplaced within the annulus of a production well. Furthermore, the contact time at maximum temperature will be on the order of days rather than months. This is evidenced from the movement of the combustion front observed in many field trials ranging between 0.125 and 0.5ft/day (39). That said, the expanding thermal regions ahead of the combustion and coke zones will subjugate the catalytic liner to high temperatures for prolonged periods which raises the potential for carbonaceous deposition. That said, for the comparatively shorter contact time within the

reservoir, the catalyst should be inexpensive as well as able to cater for the highly sulphurous heavy oil. This therefore limits the concentration of Platinum Group Element (PGE) and Rare Earth Element (REE) metals due to the considerable costs involved. With this in mind, the development of catalysts and nanoparticle solutions for the CAPRI and similar technologies should be focused on material benefiting from facile synthesis, bearing comparatively inexpensive transition metal components, and exhibit high surface area and pore volumes suitable.

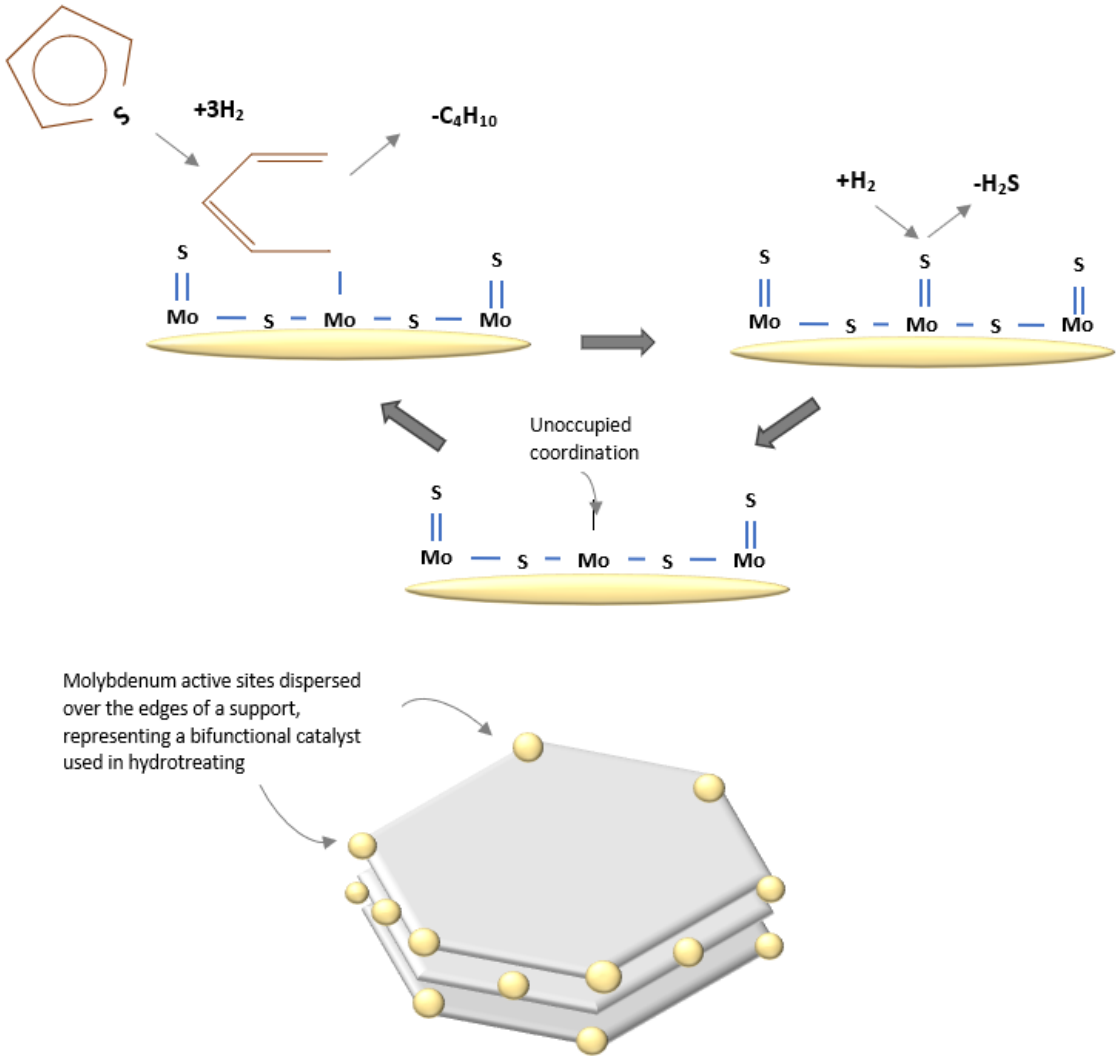

Figure 2.8 The mechanism of molybdenum on sulphur bearing aromatics to produce hydrogen sulphide as a by-product, limiting the exposure of sulphur to other prevalent active sites and completing the dearomatisation of the oil constituents.

2.7.1 Clays

Clay minerals typically belong to the family of phyllosilicates containing two-dimensional hydrous silicate tetrahedra linked by three of four sharing corners. These tetrahedral are linked to octahedral sheets containing cations such as aluminium and/or magnesium with variable amounts of another cation species (53).

The extensive use of clays and clay-modified materials in the refining and petrochemical industry relies upon key intrinsic characteristics including its swelling, adsorption, ion exchange capacity and high surface areas. Specifically, the unique crystalline structure of clay promotes a reversible exchange with organic or inorganic cations, subsequently generating active sites which are crucial in the catalysis process (54). Notable examples of which include kaolinite, smectite, palygorskite and sepiolite, all of which offer different properties and optimisations to enrich specific upgrading pathways.

The clay's catalytic activity can be manipulated using a variety of modification techniques. Techniques including thermal-, acid- and cation exchange can export clays with a larger surface area, higher porosity and thus permeability, enhanced thermal stability and increased acidity. Furthermore, the exchange capacity of a clay allows impregnation of foreign metal oxides to assist in its catalytic function, as well as interlayer chemical substitution or addition, the latter of which produces pillared clays (54).

2.7.1.1 Hydrotalcites

Hydrotalcite is a synthetic compound comprising hydroxycarbonates of magnesium and aluminium (55). Brucite-like sheets containing magnesium and aluminium ions, octahedrally

coordinated by hydroxyl ions, result in edge-shared layer stacks. The substitution of trivalent aluminium ions for divalent magnesium ions generates a positive charge which is compensated for by the interlayer anions to keep them electronically neutral (56). The interlayer sites comprising the anions also contain crystallised water (57). The general formula of a hydrotalcite is $[M_x^{II}M_y^{III}(OH)2x+2y](An-)(y/2).mH_2O$, where M^{II} and M^{III} are the divalent and trivalent cations, respectively. A class of isostructural materials can be generated by the interchange of cations and anions, and both variations of the stoichiometric coefficients and water content (56). This class of material is known as the layered double hydroxides (LDHs) or anionic clays and is graphically depicted in Figure 2.10.

Hydrotalcites have been used successfully as supports for HDS and HYD catalysts (58). Typically, hydrotreatment catalysts target the removal of N, S, O and metallic-heteroatoms using alumina-supported binary metallic pairs such as CoMo or NiMo. However, the increase in heavy oil-cut in refineries has demonstrated a need to elucidate more cost-effective catalysts. While the typical binary LDH comprise divalent and trivalent cations, recent research has led to the formulation of a LDH containing divalent and hexavalent cations, where Mostafa et al. (59) successfully produced a CoMo-LDH, through the incorporation of a hexavalent Mo species into the LDH complex. It was successfully used in the treatment of Suez crude petrolatum, leading to the removal of sulphur and aromatic species as well as low melting waxes, the latter of which can be repurposed for industrial applications. Linares et al. (58) highlighted an increase in the HDS/HYD ratio (using thiophene as the desulphurisation subject and cyclohexene as the hydrogenation subject) when using CoMo-HT, over its conventional alumina-supported counterpart, in FCC gasoline upgrading. Specifically, a calcined quaternary hydrotalcite containing Al, Co, Ni and Zn, respecting a 0.25 molar ratio ($M^{3+}/ M^{3+} + M^{2+}$), impregnated with Co and Mo achieved a selectivity

(HDS/HYD) of 2.3 compared to the CoMo/alumina with only 1.05 (58). Additionally, Zhao et al. (60) investigated the use of a CoMo-impregnated, alumina complex with a Zn-Al HT support as a catalyst in the desulphurisation and olefin hydrogenation tests of FCC gasoline. It was clear that with the addition of hydrotalcite, in comparison to a CoMo-alumina supported catalyst, the selectivity of hydrodesulphurisation reactions was enhanced over hydrogenation reactions. This highlights hydrotalcite's potential the upgrading of high sulphur-containing crude.

Thermal treatments can be used to modify the structure of the LDHs to increase surface area, enhance stability against sintering and produce an elevated metal dispersion once reduced. Furthermore, the incorporation of additional metallic elements, to achieve greater selectivity and optimisation of the upgrading process, has led to the formulation of ternary and quaternary LDHs (58).

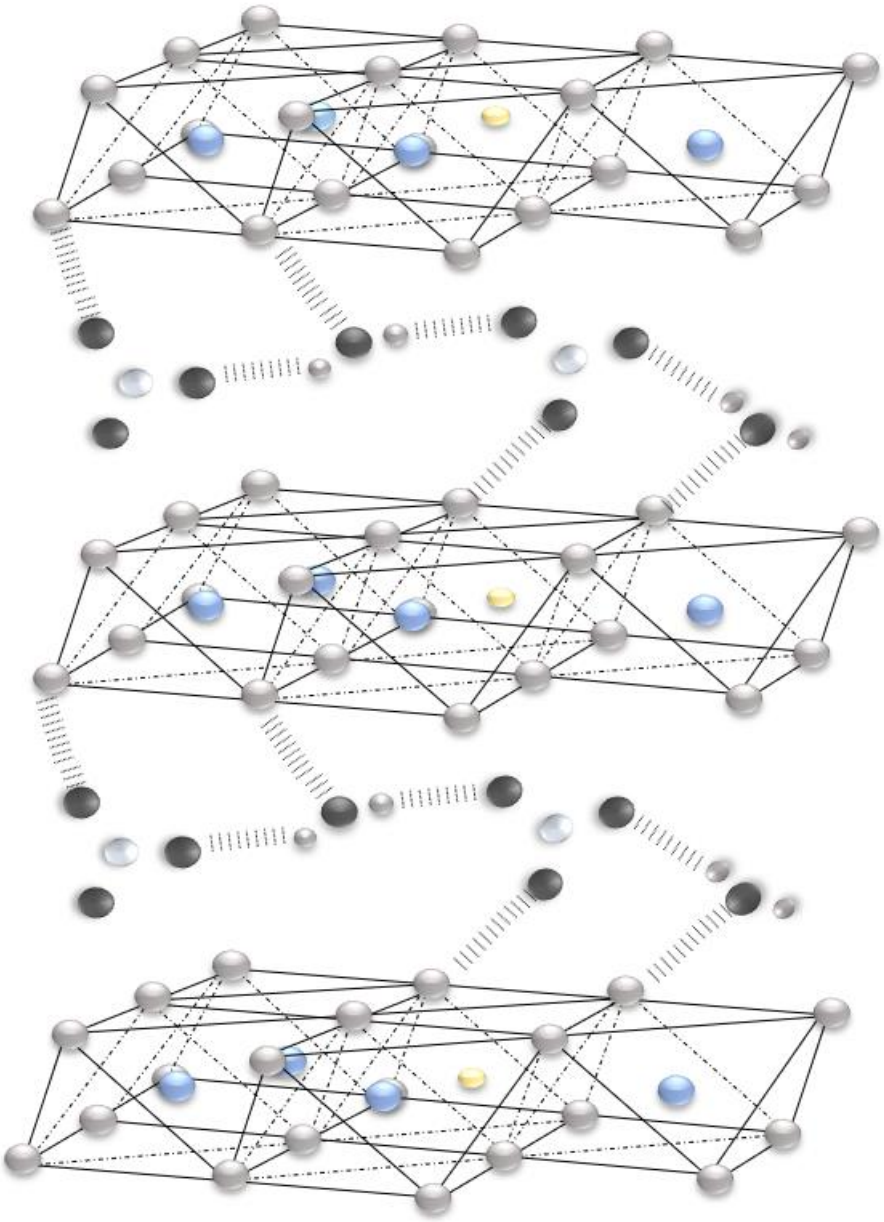

Figure 2.9 A molecular model of the cation-exchanged octahedrally-coordinated metal hydroxide layers supported by interstitial water molecules and anionic species

2.7.2 Zeolites

These are crystalline hydrated aluminosilicates of varying metals, widely used in petroleum refining due to their highly organised and interconnected shapes which produce high surface area molecular sieves (61). While zeolites can be found naturally, Kaolinite, a natural clay mineral, is used to manufacture synthetic zeolites through the process involving

metakaolizination followed by zeolitization to achieve the activated form (62). Zeolite Y is widely used in Fluid Catalytic Cracking (FCC) due to its selectivity to gasoline and distillate fractions.

The zeolites found naturally in deposits worldwide must be activated to enhance the catalytic activity. This can be done either with simple heating or treatment with acids and bases.

Recent works, however, have looked at the optimisation of natural zeolites for use in heavy oil upgrading (63). The results have indicated that the higher the acid strength and the greater the Silica to Aluminium ratio, the more effective the mineral is at undertaking catalytic cracking. Furthermore, Merissa et al. (63) reported that the addition of natural zeolite (0.5 wt%) on mixed heavy oil and water in an autoclave, imposed a decrease in viscosity by up to 65% after 6 hours of upgrading at 200°C.

An abundance of natural zeolites can be found in Venezuela, which may therefore accommodate increasing pressure to refine the poor oil quality found widely in the Venezuelan Orinoco heavy oil belt.

Clinoptilolite has also been investigated as a potential sorbent for hydrogen sulphide, attracting much attention as an abundant naturally-occurring zeolite. Yasyerli et al. (64) conducted experiments in a fixed-bed reactor, looking at the capacity of Clinoptilolite as a hydrogen sulphide sorbent over varying temperatures. Results indicated that Clinoptilolite is effective up to a maximum of 600°C, while regeneration of the sorbent is relatively easy compared to many mixed oxides which are potential sorbents (64).

2.7.3 Alumina

Conventionally, alumina or amorphous silica-alumina is used as a catalyst support, offering a high density of acid sites which can promote the carbon-rejection stage of processing. However, these active sites are inhibited by nitrogen-containing compounds and contribute to the generation of coke macromolecules, slowly deactivating the catalyst. When heavier products such as jet fuel and diesel are required, a reduction of acid sites on the catalyst is desired. Consequently, the implementation of dealumination steps during the catalyst activation process is sought, a notable example of which includes the commercial zeolite Y (65).

A typical hydrotreating catalyst includes the alumina supporting a molybdenum sulphide, promoted by varying ratios of Cobalt and Nickel. This configuration significantly enhances hydrogenation activity thereby preventing the generation of large amounts of coke and consequently prolonging the life of the catalyst (66). Alumina is used as a support due to its strong interaction with the active molybdenum species, delivering high dispersion and stability (65).

2.7.4 Nano-Dispersed Catalyst

Nanoparticle catalysts can offer several advantages over their pelleted counterparts, including the presence of a much greater surface area to volume ratio, the ability to maintain in ultra-dispersion within the reactor thereby increasing rates of contacts between reactants, far shorter diffusion routes which accommodates the interaction between macromolecules and active sites, absence of a fixed-bed thereby increasing run-time, in

addition to inhibiting the amount of produced greenhouse gases by trapping them in the reservoir (46,67).

Hart, Greaves and Wood (68) trialled a Co-Mo/Al_2O_3 catalyst in both its pelleted form and a dispersed ultrafine powder using a fixed-bed reactor and batch reactor, respectively. Results demonstrated a significant increase in upgrading when using the dispersed catalyst. This is reported to have resulted from the higher surface area to volume ratio, reducing the amount of pore plugging, as well as a higher active site activity and a greater ability to crack the macromolecules (68).

These results have suggested that the THAI CAPRI process could be augmented to cater for the application of dispersed catalyst throughout the Mobile Oil Zone (MOZ). Hart, Greaves and Wood (68) suggest several techniques including the injection of a catalyst-based slurry, pneumatically conveying the catalyst into the MOZ or creating the catalyst in-situ. If magnetic material is used, the introduction of a local-scale magnetic field may present an effective method to stimulate movement of the catalyst and separation from the reaction media (69). Furthermore, there is the potential to use both nano-dispersed catalyst and pelleted catalyst, the latter of which will remain packed around the borehole annulus, to stimulate multiple upgrading reactions varying spatially. This could attempt to optimise conditions of particular catalysts with specific functions, sensitive to varying operating conditions which may include sulphur-content or temperature.

A more recent conceptualisation of a thermal EOR includes the In-Situ Upgrading Technology (ISUT) (70). This novel process approaches thermal EOR from a new avenue, using a partially closed circuit of continuous vacuum residue re-injection as depicted in Figure 2.9. Initially, dispersed catalyst in vacuum residue is injected into the formation at a

temperature of at least 300°C. Following sufficient deposition of the catalyst within the formation localised around the injection well, catalyst injection is stopped. However, vacuum residue injection with hydrogen continues. The heat from the injected fluid, coupled with the catalytic nano particles, is sufficient to promote upgrading. The hydrogenation reactions produce upgraded oil components as well as evolved gas migrate laterally to the producer well. As these fluids are produced, they enter a vacuum distillation tower. The resultant vacuum residue is sent to be re-injected, while the upgraded lighter components are piped away for further refinement. The process capitalises on the benefits of nano-dispersed catalyst, while using the upgrading components as an effective solvent to mobilise the oil. The experiments indicated that 50 wt.% of the asphaltenes were upgraded to predominantly saturated hydrocarbons.

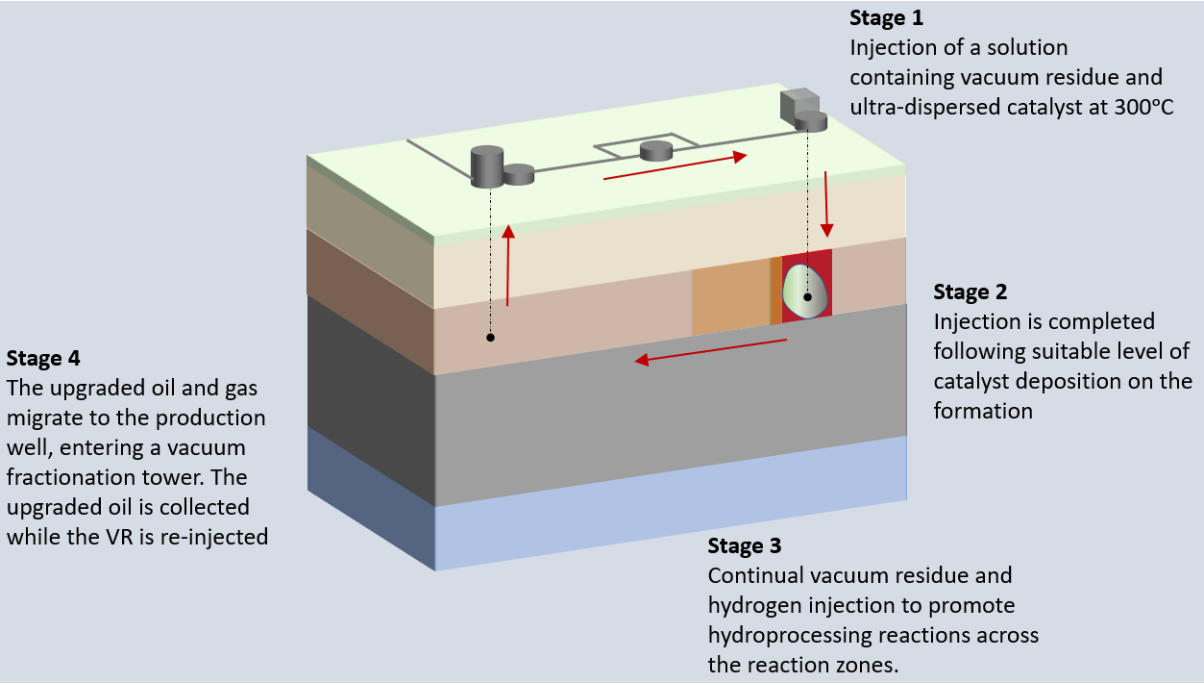

Figure 2.10 A visualisation of the novel ISUT thermal EOR highlighting the use of a vacuum fractionator continuously producing the heated vacuum residue for re-injection.

2.7.5 Biogenic Catalyst

A number of novel methods of catalyst generation have been suggested including the production of unsupported biogenic transition-metal catalysts. Unsupported Iron Oxide (Fe_2O_3) nano-catalyst is reported to offer high activity in terms of inhibiting coke formation in comparison to thermal cracking (46). This may support prolonged catalyst lifetime. Under hydroprocessing conditions, the sulphur-rich heavy oil can stimulate the production of iron sulphides which aids in the activation of hydrogen which in turn promotes hydrogenation activity. Furthermore, the remaining coke which is produced offers a sponge-type character, in contrast to typically produced coke, which can have residual value as an industrial fuel. Basavegowda (69) demonstrated the successful utilisation of Cyprus Rotundus L. to prepare stable and highly magnetic α-Fe_2O_3 nanoparticles, using an eco-friendly, fast and relatively facile method.

It has also been suggested that an efficient mechanism of an iron oxide production includes utilising subsurface Fe(III)-reducing bacteria *Geobactor Sulfurreducens* which has been scaled up successfully to pilot plant-scale production (Byrne et al., 2015). Brown et al. (52) synthesised a biogenic magnetite using a *Geobactor Sulferreducens* culture as the reducing compound in the presence of an Fe (III) salt. Surface-sorbed Fe(II) dispersion provided necessary electron donors for the reductive precipitation of palladium, thereby producing bi-functional bionanomagnetite hydrogenation catalyst. This study examined the effect of a microbially-synthesised nanoscale iron oxide (Fe_3O_4) catalyst, with varying Palladium loadings, on heavy oil upgrading reactions. The results showed favourable upgrading properties of the catalyst. This included a significant increase in liquid fraction production, reduction in coke and gas.

Brown et al. (52) suggested the palladium successfully initiated hydrogen transfer from the gas phase to the oil phase. This assisted an increase in the liquid content by ~11% to ~90%, a viscosity reduction of 99.4%, and an incremental increase of 7.8° API gravity, in comparison to 5.3 for thermal cracking of the same oil, when using a 9.5 wt.% with respect to palladium. Finally, the amount of coke produced with the catalyst was recorded as 3 wt.% for the catalyst in comparison to 10 wt.% for thermal cracking. The performance over conventional thermal cracking demonstrated the significance of this biocatalyst.

2.7.6 Sulfur removal

Sulphur compounds liberated via the in-situ combustion process may take the form of hydrogen sulphide, depending on the origin of the sulfur. Hydrogen sulphide in very low concentrations has a tendency to irreversibly adsorb onto heterogeneous catalysts, poisoning the active sites and therefore preventing catalytic upgrading. In traditional upgrading set-ups, such as FCC units, catalyst regeneration kilns constitute a part of the system to reactivate the spent catalyst following poisoning, however, in the subsurface this presents a challenge. Consequently, sulphur tolerant catalysts need to be developed and employed in order that the high sulphur heavy oil can be upgraded efficiently.

2.7.7 Dolomite

Dolomite has been used as a sulfur absorbent in both oxidising and reducing environments. Yrjas et al. (71) suggested that dolomite should be half-calcined to optimise its performance in hydrogen sulfide absorption. Half-calcined dolomite however can be split into both a

stable and unstable zone, dependent on the partial pressure of carbon dioxide and temperature:

Dolomite will thermally-decompose into half-calcined dolomite, at relatively low temperatures of less than 400°C, according to the following equation:

$$MgCO_3.CaCO_3\ (s) \rightarrow MgO.CaCO_3\ (s) + CO2$$

The stability of dolomite is dependent on the carbon dioxide partial pressure in the system and the equilibrium carbon dioxide partial pressure. If the dolomite enters the unstable zone, it will begin to decompose into its fully calcined form which exhibits more limited hydrogen sulphide absorption.

The reaction for hydrogen sulphide absorption by dolomite is given as follows:

$$MgO.CaO(s) + H_2S(g) \rightarrow MgO.CaS\ (s) + CO2\ (g) + H_2O\ (g)$$

It has been indicated that that the half-calcined dolomite should be in a system where the temperature is at a maximum, slightly above the interface between the stable and unstable zones at its. This is because with half-calcined dolomite, the equilibrium hydrogen sulfide partial pressure decreases with an increase in temperature, at given carbon dioxide and water vapour partial pressures (71).

As dolomite can be found in many carbonate reservoirs worldwide, the mineral could potentially be exploited *in situ* by acting as a large-scale pseudo guard bed before the oil enters the production well. In this way, theoretically-speaking a greater reduction in sulphur content could be achieved which would help mitigate the added complications of sulphur removal in surface upgraders and refineries. This presents a natural analogue to the augmentation of the THAI CAPRI in which an activated carbon guard bed was positioned

ahead of the catalyst bed, in a simulated CAPRI set-up, to promote catalyst longevity and improved upgrading (49). Additionally, clay minerals have also been shown to promote desulphurisation pathways (72). This therefore proposes a use for the abundant clay minerals present within certain reservoirs.

2.8 Heavy oil reservoir as a source for in-situ catalyst formulation

A number of elements and compounds that may be used as suitable upgrading catalysts are present within the oil sands reservoirs.

The oil sands in Indonesia have been shown to contain significant quantities of calcite, generating an oil-wet system (73). Sands in the Athabasca region, Canada are composed mainly of quartz. However, fines are prevalent in the reservoirs comprising various mineralogies. Kaminsky (53) highlighted the extensive composition of heavy metal compounds in addition to clay minerals which possess potential catalytic upgrading potential. Oxenford and Coward (74) reviewed the potential recycling of Heavy Mineral Concentrations (HMC) from oil sands tailings, indicating the relative abundance of minerals such as titanium oxide and zircon. Other minerals comprising the heavy mineral assemblages from the oil sands include pyrite, ilmenite, altered ilmenite, leucohexenea, goethite tourmaline and zircon.

If these compounds can be effectively mobilised to produce catalysts, it could provide a means to alleviate the reliance of expensive industry-produced catalysts. Furthermore, the processes may prove to be key in formulating nano-particles which offer a great number of advantages over their conventional pelleted counterparts (67). This includes the ability to

alleviate problems associated with constrained placement within the production borehole, as well as pore blocking and poisoning of the active sites due to organometallic components. Lapeira (75) studied the relationship between particle size and HDS activity for molybdenum sulphide catalysts when upgrading Vacuum Gas Oil (VGO). In this study, HDS activity was doubled when using nanocatalyst with a size of 10nm compared to bulk molybdenum sulphide.

Formulating these compounds into viable catalysts in-situ however, may pose a problem. There are several methods used to synthesise nanocatalysts, including bottom-up and top-down methods. The former incorporates the usage of molecular components as starting materials, followed by nucleation and growth, while the later uses bulk materials as the starting material followed by distribution techniques such as laser beam processing, quenching and photolithography (67).

The water-in-oil emulsion process is one of a number of bottom-up methods which can be been used to synthesise hydroprocessing catalysts (76). An emulsion constitutes two separate phases; water and oil phase, and a surfactant to create a dispersed phase within a continuous phase. A significant advantage relating to the use of emulsions or micro-emulsions, which is an optically isotropic and thermodynamically stable water, oil and surfactant system, is the ability to control the size of the droplets and therefore size of resulting particles (67,76). Subsequently, the particles may be precipitated from the emulsions using a number of techniques such as a destabilising agent to disassemble the emulsion. Vasquez (76) prepared ultra-dispersed bimetallic catalysts via water-in-oil emulsions and an emulsion decomposition zone was used, wherein the water was vaporised out of the emulsion. The catalyst size was generally constrained to the hundreds of

nanometers scale while the smallest recorded particle size was 50 nanometers. Chen et al (77) used a $Cu(OH)_2$ precursor within a microemulsion to synthesise a CuO aquathermolysis catalyst in the heavy oil phase, aiding in the reduction of viscosity for Shengli heavy oil.

Zekel et al. (78) proposed a mechanism for the formation of Pseudo-Homogenous Catalysts (PHC), associated with catalysts characterised by sizes from 0.01 to 0.04 micrometers with similar properties to colloidal solutions. The study proposed a mechanism for catalyst formation via emulsions such that from 120-150°C, the emulsion begins to boil resulting in vaporisation of the water from solution, initiating salt crystallisation. As boiling, accompanied by micro-explosions of the dispersed droplets within the emulsion, continues it is suggested that the crystals form a spherical globule via agglomeration which unfavourably increases the size of the particles. This is dependent on the nature of the solute and concentration of the solution.

Additionally, Lapeira (75) studied the use of transient emulsions to produce nanocatalysts, entailing the application of energy to generate the emulsion. This energy can then be inhibited to destabilise and break-up the emulsion.

If emulsions can be adequately emplaced in the reservoir, it could provide a means through which catalytic materials may be synthesised using the mineral enriched-reservoirs. It could provide a more cost-effective route to catalyst generation and minimise the coking-up of catalyst pellets used in the THAI-CAPRI process. That said, formation of the emulsion through optimum injection of the surfactant in the desired location is a process difficulty that must be considered.

Zou et al. (73) investigated the use of ultrasonic waves to promote the migration of chemical reagents into the pores of the Buton oil sands. Ultrasonic waves can be used to activate

certain chemical processes in addition to enhancing heat and mass transfer processes through cavitation, heating and intense agitation. Consequently, this may provide a solution to generating the emulsions once a surfactant has been injected into the reservoir.

2.9 Mining Waste

Additional sources of materials which may provide the means from which catalytic materials can be synthesised include mine wastes. Acid mine drainage, for instance, represents a huge problem in many historic mining sites in which dewatering systems have been abandoned due to the cost. The mixing of the rising groundwater with the exposed minerals and slag heaps represents a huge problem in terms of environmental damage. These metal-enriched acidic solutions, however, present an opportunity for catalyst synthesis and simultaneous environmental remediation. For *example, hydrotalcites may be formed from these mine and pit water due to the prevalence of M^{2+} and M^{3+} cations found in typical gangue minerals in addition to the target mineral structures. The Baal Gammon mine water was the subject of a trial in which a controlled amount of magnesium salts and hydroxide solution was added to the pit water to generate extensive hydrotalcite deposits. The hydrotalcite formation reaction offers rapid kinetics and the ability to entrain colloidal materials. In this instance, the hydrotalcite formation led to the removal of a vast array of elements of interest due to their catalytic potential and environmental concern, including: Al, Cd, Co, Cr, Cu, Fe, In, Mn, Mo, Ni, V and Zn (79).

Furthermore, bauxite mining presents similar challenges to the mining industry with the generation of large deposits of “red mud” as a by-product of the Bayer process. However, red mud supernatant treatment with sea-water generates an alkali solution which can be

subsequently used to remediate acid mine waters, generating hydrotalcite materials in the process (80).

2.10 Model Compounds

The distillates and residues of petroleum are highly complex groups of hydrocarbons, not all of which can be accurately resolved. However, kinetic parameters are required so that large-scale reactors or indeed subsurface processes can be designed, while mechanisms can be more properly understood. That said, the complexity of the reaction mixture may be broken down into pseudo groups, to represent certain components of a hydrocarbon mixture over particular boiling ranges (8). A wealth of studies have been undertaken to represent the deleterious components found in heavier feeds, so that useful kinetic data may be obtained and certain conditions during the process may be optimised. It is also useful to understand how the catalytic material can introduce different mechanisms on a given reaction, so that cost-effective augmentations may be achieved, while desired product yields are attained.

Sabtier and Senderence conducted a catalytic hydrogenation study of aromatics in 1901. This was the first such study that led to the successful conversion of benzene to cyclohexane over a nickel catalyst. Benzene is an important feedstock in the petrochemical industry. Benzene conversion to cyclohexane alone accounts for approximately 4.6 mT, while the broader use of benzene uses approxmiamtely 46 mT in total. Consequently, benzene has since been a well-used component in model hydrogenation reactions to examine catalyst activity (81–83).

Sano et al (84), first considered the hydrogenation of monoaromatics over protonic zeolitic catalysts. The proposed mechanism accounts for the hydrogenation activity closely related

to the protonic sites. The results demonstrated a preference for benzene ring-opening at high temperature and pressure of 573°C and 39.3 bar, respectively. This was contrasted by hydrogenation activity resulting in cyclohexane at a lower temperature of 300°C.

It is also clear that metal dispersion, crystallite size and the support play an important role in influencing the catalytic activity. However, it has been stated that studies on benzene hydrogenation have produced conflicting results. This has underpinned the idea that hydrogenation of benzene is highly complex and catalyst-specific. It is suggested that the hydrogenation is highly dependent on both the support material and crystal system of the metal species, that which can considerably modify the electronic properties of the catalyst and shape-dependent reaction selectivity, respectively. A study which looked at platinum-based catalysis found that the products of benzene hydrogenation varied with the crystal surfaces of the catalyst. Pt(111) and Pt(100) surfaces produced cyclohexene (an intermediary) and cyclochexane, and purely cyclohexane, respectively (83). These surfaces are dependent on the crystal system of the platinum particles, with cubeoctahedral crystals exhibiting Pt(111) and cubic crystals giving rise to a preponderance of Pt(100) crystal faces.

Other useful materials for model compound studies include aromatics containing heteroatoms such as sulphur, nitrogen and oxygen. During the HDS process there are two reaction pathways (i) direct desulfurisation and (ii) the two-step hydrogenation and desulfurisation. This specific reaction scheme may be demonstrated clearly using components which would represent the fraction which would typically undergo this treatment. Ahmed et al. (85) used benzothiophene and dibenzothiophene molecules to model the deep HDS of gas oils which is required to meet ever more stringent specifications on the sulphur content within diesel fuel. The results in study concluded that when using Co

and Mo supported by alumina at different metal molar ratios, the concentration of Co/(Co+Mo) was found to be optimum when equal to 0.4. The findings also presented results indicating that DBT was converted predominantly by the DDS route while Co/(Co+Mo) ratio affected only the DDS pathway not the HYD pathway. The HDS of BT and DiHydroBenzoThiophene (DHBT) was studied over a Mo-doped Al_2O_3 catalyst. The results indicated that the C-S bonds were broken by the action of hydrogenolysis. It was also indicated that the presence of H2S as a by product of HDS inhibited the hydrogenation and hydrogenolysis significantly, particularly with the latter.

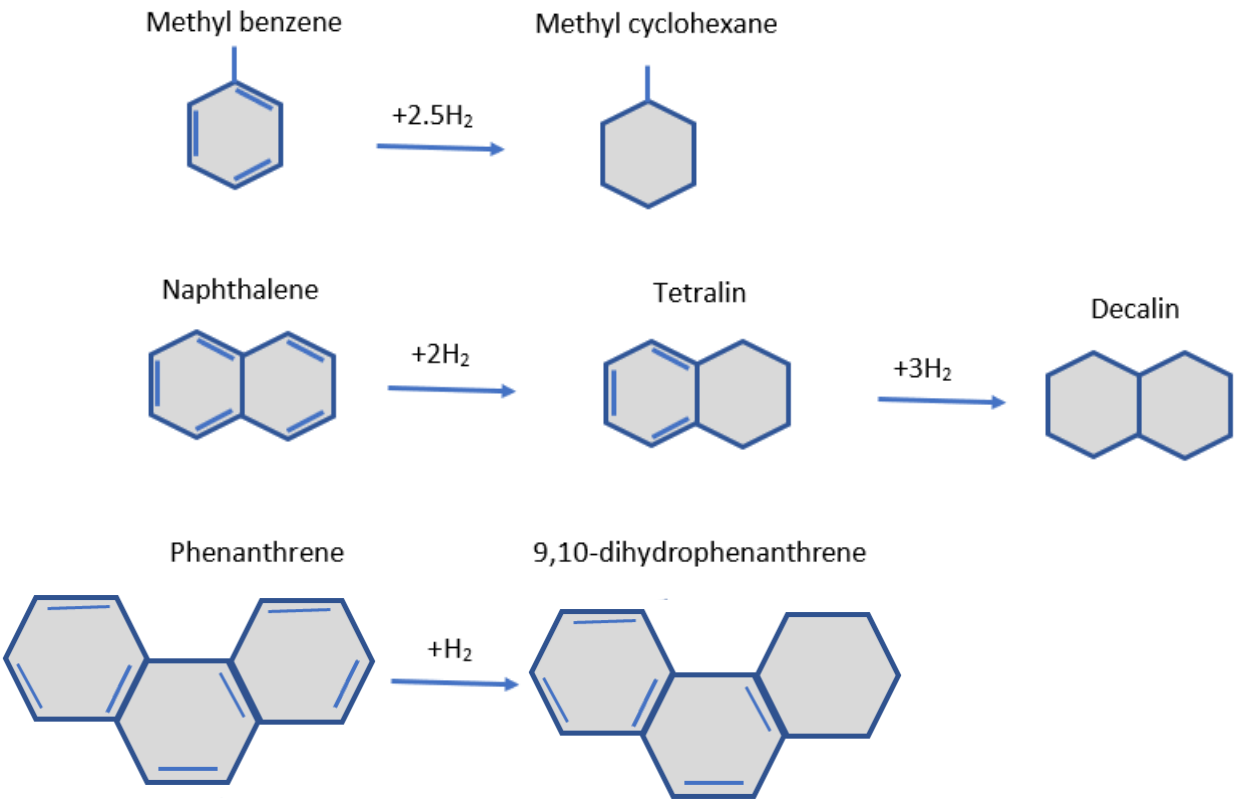

Figure 2.11 A visualisation of the hydrogenation reaction schemes for (a) methyl benzene, (b) naphthalene and (c) phenanthrene.

Aromatics undergo hydrogenation to yield both naphthenes and hydroaromatics. While benzene rings have a high resonance energy which in turn gives them high stability, the more rings a cluster presents, the hydrogenation reactions becomes more thermodynamically stable (8). As such polynuclear aromatics are more easily treated via hydrogenation. Naphthalene, phenanthrene and alkyl benzenes are examples of more easily hydrogenated aromatic compounds which have been studied previously, demonstrated in Figure 2.11. Though many studies have been devoted to mono-aromatic hydrogenation, naphthalene can be used as diaromatic to represent multi-ring pre-processed species found in heavier feeds which require further hydrogenation. It is important to saturate the ring structures so as to improve cetane number and reduce soot emissions which are relevant to middle distillates yielding widely-used diesel fuels. This is a well-studied reaction scheme which has helped to understand the optimum catalytic conditions for conversion, as well as coke reduction (86–88).

Under catalysis, the active sites serve to exchange hydrogen with the liquid components, producing saturated ring structures. Given the compositional characteristics of heavy oils and residues, clear that hydrogenation reactions are an important factor in upgrading the aromatic content. What's more, the process of catalytic hydrogenation is reversible i.e. dehydrogenation reactions can be stimulated. This however depends much on the specific aromatic components, as well as the temperature and catalytic material.

Escobar et al. (89) prepared a series of Pt-based catalysts over acid-base supports of varying ratios, represented by Al_2O_3 and MgO. The results indicated that Pt-supported by a binary carrier with 2wt.% MgO content contributed to the most efficient naphthalene and tetralin conversion. This indicates the possible deviation from conventional thought wherein mainly

protonic supports are used in hydrogenation reactions. The kinetics of the study were based on a pseudo-first order model accounting for an excess of H_2. Furthermore, Fang et al. (90) used a Ru-doped MgO catalyst in the context of mono and poly-cyclic arenes, hypothesising a dual mechanism wherein dual-site heterolytic hydrogen splitting and surface ionic hydrogenation pathways were discovered as a function of the interaction between the basic support and metallic nanoparticles.

It is widely accepted that naphthalene hydrogenation to the decalin derivatives is characterised by a two-step process, in which the first transformation to the tetralin intermediate has a greater rate, inhibited by the second transformation to the decalins, demonstrated as the rate-determining step. This has opened up the possibility of narrowing the gap between the two transformations, by way of manipulating the catalytic material which in turn can help to elucidate the mechanism. When considering the intermediates between tetralin and decalin – the octalins, it was previously discovered that the yields of cis and trans decalin were subordinate to the intermediate octalin structure, composed of either $\Delta^{1,9}$-octalin or $\Delta^{9,10}$-octalin (91). The former structure can yield both cis and trans decalin, while the latter, only cis-decalin. The difference in octalin hydrogenation stems from the orientation of the species on the catalytic surface and the location of the hydrogen atom occupying position 10. Furthermore, the double bond in $\Delta^{1,9}$-octalin is not as stable as that within $\Delta^{9,10}$-octalin. This allows the former octalin species to undergo isomerisation to $\Delta^{9,10}$-octalin to favour a cis-decalin-enriched product.

A vast range of materials have been adopted for the catalytic conversion of naphthalene. PGE metals offer outstanding aromatic saturation, and more broadly hydrogenation, reactivity and do not require as high a metal loading as the cheaper non-PGE alternatives.

Platinum has been shown to have a higher selectivity towards decalin production than palladium, however, palladium generates a higher trans-decalin yield compared to platinum under the same conditions. The major obstacle with these materials, however, is the high cost and poor availability. Transition metal based catalysts, often in sulfided form, present challenges in the form of inhibited hydrogenation activity. To improve the activity often severe operating conditions are needed. Metal in their carbide and nitride forms are also used, however, when in the presence of a high sulfur content the metals deactivate. This therefore makes them an unlikely alternative when dealing with heavier feeds which are typically in high aromatics with sulfur heteroatoms.

The crystal structure of materials is also an important factor to consider. Crystal edges and corner systems facilitate richer active sites which promote hydrogenation. The exposure of unsaturated coordinated atoms will catalyse the uptake of hydrogen (92). Stacked rhombohedral or prismic structures, which generate more of the unsaturated active sites, could therefore facilitate greater rates of hydrogenation reactions.

2.11 Conclusions

Heavy oil recovery has been the subject of much debate over the last few decades. The relative abundance of this oil type has accelerated the desire to augment existing extraction techniques to develop a more efficient, environmentally-friendly EOR method. In situ combustion is a technique which has seen fragmented application over the decades since its initial inception in 1933. However, there have been an abundance of modifications to attempt to make the process more economic for production companies. The advancement of the technique to the THAI CAPRI configuration, opened up the possibility of higher

efficiency using a specific well pattern, in addition to the introduction of catalytic upgrading. This latter element has the potential to aid in oil recovery, in addition to promoting dehydrogenation reactions for the production of hydrogen gas. There remains an abundance of catalysts available for all manners of refinery programmes, however, the need to find more cost effective variations to be used *in situ* frames an interesting research debate. Within the subsurface, an abundance of minerals can be found in reservoirs which could potentially be used in the synthesis of cheap catalytically active materials.

Clay minerals are in abundance and these have occupied one of the cornerstones in catalytic materials used in refineries. These materials are also typically present in the subsurface oil reservoirs. Hydrotalcites represent a group of, easily-synthesised, economically cost-effective and highly tuneable clay materials. Consequently, given the need to find catalysts which can promote upgrading of heavy oils but may also be sourced from reservoir materials, hydrotalcites form a substantial part of the work as presented in this research thesis. The ease of synthesis reflects the option to use reservoir minerals to construct anionic-clay like materials in situ. What's more, these materials present major adsorptive architecture which could therefore prove to be a useful tool to channel undesirable components from the reservoir oil. These components include but are not limited to heteroatoms and metallo-organic components which could also use the clay materials as support materials and under thermal treatment may present useful activation components to form quasi-industry-style catalysts. Redefining limitations and novelty in the synthesis of exotic hydrotalcite species, the subsequent testing of these materials in heavy oil samples could yield useful information with respect to the upgrading mechanisms to form lighter, more useful oils. Furthermore, the use of these materials with model compound environments will provide a useful assessment on their hydrogenation capability, which can

further delineate their importance in potential heavy oil upgrading. As such, it is plausible that these materials could be adopted in the THAI CAPRI method in addition to other EOR methods, or more generally, surface upgrading units and refineries dedicated to the processing of heavier feeds.

2.12 References

1. British Petroleum. Energy Outlook 2020 edition explores the forces shaping the global energy transition out to 2050 and the surrounding that [Internet]. BP Energy Outlook 2030, Statistical Review. London: British Petroleum. 2020. Available from: https://www.bp.com/content/dam/bp/business-sites/en/global/corporate/pdfs/energy-economics/energy-outlook/bp-energy-outlook-2020.pdf

2. Grantz, A.; Hart, E, P. Petroleum prospectivity of the Canada Basin, Arctic Ocean. Mar Pet Geol. 2012;30(1):126–43. Available from: http://dx.doi.org/10.1016/j.marpetgeo.2011.11.001

3. Kapadia, R, P.; Kallos, S, P.; Gates, D, I. Potential for hydrogen generation from in situ combustion of Athabasca bitumen. Fuel . 2011;90(6):2254–65. Available from: http://dx.doi.org/10.1016/j.fuel.2011.02.038

4. Meyer, F, R.; Attanasi, D, E.; Freeman, A, P. Heavy oil and natural bitumen resources in geological basins of the world. US Geol Surv. 2007.

5. Attanasi, D, E.; Meyer, F, R. Natural Bitumen and Extra-Heavy Oil. Surv Energy Resour. 2007;World Ener:119–43.

6. Head, M, I.; Jones, M, D.; Larter, R, S. Biological activity in the deep subsurface and the origin of heavy oil. Nature. 2003;426(6964):344–52.

7. MINING OPERATIONS, BITUMEN PRODUCTION. Oil Sands Magazine [Internet]. 2020; Available from: https://www.oilsandsmagazine.com/projects/oilsands-mining

8. Gray, R, M. Upgrading Petroleum Residues and Heavy Oils. Marcel Dekker; 1994.

9. Rana, S, M.; Sámano, V.; Ancheyta, J.; Diaz, I, A, J. A review of recent advances on process technologies for upgrading of heavy oils and residua. Fuel. 2007;86(9 SPEC. ISS.):1216–31.

10. Rueda-Velásquez, I, R.; Freund, H.; Qian, K.; Olmstead, N, W.; Gray, R, M. Characterization of asphaltene building blocks by cracking under favorable hydrogenation conditions. Energy and Fuels. 2013;27(4):1817–29.

11. Ilyin, S.; Arinina, M.; Polyakova, M.; Bondarenko, G.; Konstantinov, I.; Kulichikhin, V.; Malkin, A. Asphaltenes in heavy crude oil: Designation, precipitation, solutions, and effects on viscosity. J Pet Sci Eng. 2016;147:211–7. Available from: http://dx.doi.org/10.1016/j.petrol.2016.06.020

12. Speight, G, J. Enhanced Recovery Methods for Heavy Oil and Tar Sands. Houston: Gulf Publishing Company; 2009.

13. Lowey, M. Energy and Environment: Toward Achieving the Balance in Alberta. In: Developments in Environmental Science. 1st ed. Elsevier Ltd.; 2012. p. 35–45. Available from: http://dx.doi.org/10.1016/B978-0-08-097760-7.00003-2

14. Lade, V, P.; Yamamuro, A, J. Evaluation of static liquefaction potential of silty sand slopes. Vol. 48, Canadian Geotechnical Journal. 2011. p. 247–64.

15. Shah, A.; Fishwick, R.; Wood, J.; Leeke, G.; Rigby, S.; Greaves M. A review of novel techniques for heavy oil and bitumen extraction and upgrading. Energy Environ Sci. 2010;3(6):700. Available from: http://xlink.rsc.org/?DOI=b918960b

16. Hart, A. The novel THAI–CAPRI technology and its comparison to other thermal methods for heavy oil recovery and upgrading. J Pet Explor Prod Technol. 2014;4(4):427–37.

17. Canadian Natural. Pelican Lake Crude Oil [Internet]. 2021. Available from: https://www.cnrl.com/disclaimer.html?redirect=https://www.cnrl.com/corporate-responsibility/stewardship-report/

18. Salehpour, M.; Riazi, M.; Malayeri, R.; Seyyedi, M. CO2-saturated brine injection into heavy oil carbonate reservoirs: Investigation of enhanced oil recovery and carbon storage. J Pet Sci Eng. 2020;195:107663. Available from: https://doi.org/10.1016/j.petrol.2020.107663

19. Galas, C.; Clements, A.; Jaafar, E.; Jeje, O.; Holst, D.; Holst, R. Identification of Enhanced Oil Recovery Potential in Alberta Phase 2 Final Report for Energy Resources Conservation Board. 2012.

20. Fink, K, J. Petroleum Engineer's Guide to Oil Field Chemicals and Fluids. 2012. Gulf Professional Publishing;

21. Dang, C, Q, T.; Chen, Z.; Nguyen, N, B, T.; Bae, W. The potential of enhanced oil recovery by micellar/polymer flooding in heterogeneous reservoirs. Energy Sources, Part A Recover Util Environ Eff. 2014;36(14):1540–54.

22. Saboorian-Jooybari, H.; Dejam, M.; Chen, Z. Heavy oil polymer flooding from

laboratory core floods to pilot tests and field applications: Half-century studies. J Pet Sci Eng. 2016;142:85–100.

23. Shi, L, T.; Zhu, S, J.; Zhang, J.; Wang, S, X.; Xue, X, S.; Zhou, W.; Ye, Z, B. Research into polymer injection timing for Bohai heavy oil reservoirs. Pet Sci. 5AD;(12):129–34.

24. Chekhonin, E.; Parshin, A.; Pissarenko, D.; Popov, Y.; Romushkevich, R.; Safonov, S.; Spasennykh, M.; Chertenkov, V, M.; Stenin, P, V. When rocks get hot: Thermal properties of reservoir rocks. Oilf Rev. 2012;24(3):20–37.

25. Elkin, E, L. Thermal, Solvent And Improved Gas-Drive Oil-Recovery Methods. In: History of Petroleum Engineering. American Petroleum Institute; 1961.

26. Elkins, E, L. THERMAL , SOLVENT AND IMPROVED GAS-DRIVE. In: History of Petroleum Engineering. 1961. p. 883–906.

27. Shen, C. Chapter 17 - SAGD for Heavy Oil Recovery. In: Enhanced Oil Recovery Field Case Studies. 2013. p. 413–45.

28. Moussa, T.; Mohamed, M.; Mokheimer, A, M, E.; Al-Shehri, D.; Patil, S. Heavy Oil Recovery Using In Situ Steam Generated by Thermochemicals: A Numerical Simulation Study. Jounral Energy Resour Technol. 2019;141(12).

29. Oil Sands Magazine. In Situ Long Lake. Oil Sands Magazine [Internet]. 2020 Jul; Available from: https://www.oilsandsmagazine.com/projects/nexen-long-lake-sagd

30. Mineral Resource Office. Heavy crude oil: resource, reserve, and potential production in the United States. 1967.

31. Bealessio, A, B.; Blánquez Alonso, A, N.; Mendes, J, N.; Sande, V, A.; Hascakir, B. A

review of enhanced oil recovery (EOR) methods applied in Kazakhstan. Petroleum. 2020;(March):1–9. Available from: https://doi.org/10.1016/j.petlm.2020.03.003

32. Panait-Patica, A.; Serban, D.; llie N. Suplaco de Barcau Field - A Case History of a Successful In-Situ Combustion Exploitation. In: SPE Europec/EAGE Annual Conference and Exhibition. 2006.

33. И.А. девон. RITEK launches in situ “combustion” of high-viscosity oil in the Samara region. 2019; Available from: https://iadevon.ru/news/Technologies/ritek_zapuskaet_vnutriplastovoe_«gorenie»_visokovyazkoy_nefti_v_samarskoy_oblasti-9299/

34. Hallam, J. R.; Hajdo, E. L.; Donnelly, K, J.; Baron, R. P. Thermal Recovery of Bitumen at Wolf Lake. SPE Reserv Eng. 1989;4(02): 178-186.

35. Greaves, M.; Turta, A. Oil field in-situ combustion process. United States patent; 5626191, 1997.

36. Xia, X, T.; Greaves, M.; Turta, T, A.; Ayasse, C. THAI - A “short-distance displacement” in Situ combustion process for the recovery and upgrading of heavy oil. Chem Eng Res Des. 2003;81(3):295–304.

37. Adam, M.; Anbari, H.; Hart, A.; Wood, J.; Robinson, P, J.; Rigby, P, S. In-situ Microwave-assisted Catalytic Upgrading of Heavy Oil : Experimental Validation and Effect of Catalyst Pore Structure on Activity Author names and affiliations : Chem Eng J [Internet]. 2020;127420. Available from: https://doi.org/10.1016/j.cej.2020.127420

38. Kapadia, R, P.; Wang, J.; Kallos, S, M.; Gates, D, I. Practical process design for in situ gasification of bitumen. Appl Energy. 2013;107:281–96. Available from:

http://dx.doi.org/10.1016/j.apenergy.2013.02.035

39. Sarathi, P, S. In-Situ Combustion Handbook - Principles and Practices. Natl Pet Technol Off US Dep Energy. 1999;

40. Yao, J.; Song, Y. Dynamic analysis approach to evaluate in-situ combustion performance for heavy oil production. J Oil, Gas Petrochemical Sci. 2019;2(1):42–7.

41. Aquitaine, E.; Larribau, A. EMERAUDE VAPEUR - AN OFFSHORE STEAM PILOT. 1989;2:179–91.

42. Han, X.; Liu, Y.; Liu, H.; Wang, Q.; Zou, J.; Zhang, H.; Wang, H.; Wu, X. Case Study: Realization and Evaluation of Cyclic Steam Stimulation Pilot for Offshore Oilfield, China. In: SPE EOR Conference at Oil and Gas West Asia. Society of Petroleum Engineers; 2018.

43. Rodríguez, F.; Christopher, A, C. Overview of Air Injection Potential for PEMEX. AAPG Int Conf. 2004;October 24(89612):1–6.

44. Lakhova, A.; Petrov, S.; Ibragimova, D.; Kayukova, G.; Safiulina, A.; Shinkarev, A.; Okekwe, R. Aquathermolysis of heavy oil using nano oxides of metals. J Pet Sci Eng. 2017;153:385–90.

45. Siskin, M.; Kelemen, S.; Gorbaty, L, M.; Ferrughelli, T, D.; Brown, D, L.; Eppig, A.; Kennedy, J, R. Chemical approach to control morphology of coke produced in delayed coking. Energy and Fuels. 2006;20(5):2117–24.

46. Al-Marshed, A.; Hart, A.; Leeke, G.; Greaves, M.; Wood, J. Effectiveness of Different Transition Metal Dispersed Catalysts for In Situ Heavy Oil Upgrading. Ind Eng Chem Res. 2015;54(43):10645–55.

47. Okunev, G, A.; Parkhomchuk, V, E.; Lysikov, I, A.; Parunin, D, P.; Semeikina, S, V.; Parmon, N, V. Catalytic hydroprocessing of heavy oil feedstocks. Russ Chem Rev. 2015;84(9):981–99.

48. Argyle, D, M.; Bartholomew, H, C. Heterogeneous catalyst deactivation and regeneration: A review. Catalysts. 2015;5(1):145–269.

49. Hart, A.; Shah, A.; Leeke, G.; Greaves, M.; Wood, J. Optimization of the CAPRI process for heavy oil upgrading: Effect of hydrogen and guard bed. Ind Eng Chem Res. 2013;52(44):15394–406.

50. Hart, A.; Leeke, G.; Greaves, M.; Wood, J. Down-hole heavy crude oil upgrading by CAPRI: Effect of hydrogen and methane gases upon upgrading and coke formation. Fuel. 2014;119:226–35. Available from: http://dx.doi.org/10.1016/j.fuel.2013.11.048

51. Maity, K, S.; Blanco, E.; Ancheyta, J.; Alonso, F.; Fukuyama, H. Early stage deactivation of heavy crude oil hydroprocessing catalysts. Fuel. 2012;100:17–23. Available from: http://dx.doi.org/10.1016/j.fuel.2011.11.017

52. Brown, R, A.; Hart, A.; Coker, V.; Lloyd, J.; Wood, J. Upgrading of heavy oil by dispersed biogenic magnetite catalysts. Fuel. 2016;185:442–8. Available from: http://dx.doi.org/10.1016/j.fuel.2016.08.015

53. Kaminsky, A, H. Characterization of an Athabasca oil sand ore and process streams. Diss Abstr Int Sect B. 2008;70(2):9–18. Available from: http://login.ezproxy.library.ualberta.ca/login?url=http://search.ebscohost.com/login.aspx?direct=true&db=pta&AN=1073720&site=eds-live&scope=site

54. Emam, E.; Centi, G.; Perathoner, S.; Vaccari, A. Clays as Catalysts in Petroleum

Refining Industry. Appl Clay Sci. 2008;3(4):161–98. Available from: http://www.ejournalofscience.org/archive/vol3no4/vol3no4_5.pdf

55. Cavani, F.; Trifirò, F.; Vaccari, A. Hydrotalcite-type anionic clays: Preparation, properties and applications. Catal Today. 1991;11(2):173–301.

56. Salomão, R.; Milena, M, L.; Wakamatsu, H, M.; Pandolfelli, C, V. Hydrotalcite synthesis via co-precipitation reactions using MgO and Al(OH)3 precursors. Ceram Int. 2011;37(8):3063–70.

57. Obadiah, A.; Kannan, R.; Ravichandran, P.; Ramasubbu, A.; Kumar, V, S. Nano hydrotalcite as a novel catalyst for biodiesel conversion. Dig J Nanomater Biostructures. 2012;7(1):321–7.

58. Linares, F, C.; Vásquez, M.; Castillo, R.; Bretto, P.; Solano, R.; Rincón, A. Applications of CoMo/calcined quaternary hydrotalcites for hydrotreatment reactions. Fuel Process Technol. 2015;132:105–10. Available from: http://dx.doi.org/10.1016/j.fuproc.2014.12.043

59. Mostafa, S, M.; Mohamed, H, N. Towards novel adsorptive nanomaterials: Synthesis of Co2+Mo6+ LDH for sulfur and aromatic removal from crude petrolatum. Egypt J Pet. 2016;25(2):221–7.

60. Zhao, R.; Yin, C.; Zhao, H.; Liu, C. Synthesis, characterization, and application of hydotalcites in hydrodesulfurization of FCC gasoline. Fuel Process Technol. 2003;81(3):201–9.

61. Degnan Jr, F, T. Applications of zeolites in petroleum refining. Top Catal. 2000;13:349–56. Available from:

http://link.springer.com/article/10.1023/A%3A1009054905137

62. Abdullahi, T.; Harun, Z.; Othman, D, H, M. A review on sustainable synthesis of zeolite from kaolinite resources via hydrothermal process. Adv Powder Technol. 2017;28(8):1827–40. Available from: http://dx.doi.org/10.1016/j.apt.2017.04.028

63. Merissa, S.; Fitriani, P.; Iskandar, F.; Abdullah, M.; Khairurrijal. Preliminary study of natural zeolite as catalyst for decreasing the viscosity of heavy oil. 2013;2013(2013):131–4. Available from: http://scitation.aip.org/content/aip/proceeding/aipcp/10.1063/1.4820302

64. Yaşyerli, S.; Ar, İ.; Doğu, G.; Doğu, T. Removal of hydrogen sulfide by clinoptilolite in a fixed bed adsorber. Chem Eng Process. 2002;41(9):785–92.

65. Ma, Z.; Wei, L.; Zhou, W.; Jia, L.; Hou, B.; Li, D.; Zhao, Y. Overview of catalyst application in petroleum refinery for biomass catalytic pyrolysis and bio-oil upgrading. RSC Adv. 2015;5(107):88287–97.

66. Semeykina, S, V.; Parkhomchuk, V, E.; Polukhin, V, A.; Parunin, D, P.; Lysikov, I, A.; Ayupov, B, A.; et al. CoMoNi Catalyst Texture and Surface Properties in Heavy Oil Processing. Part I: Hierarchical Macro/Mesoporous Alumina Support. Ind Eng Chem Res. 2016;55(12):3535–45.

67. Hashemi, R.; Nassar, N, N.; Pereira-Almao, P. Nanoparticle technology for heavy oil in-situ upgrading and recovery enhancement: Opportunities and challenges. Appl Energy. 2014;133:374–87. Available from: http://dx.doi.org/10.1016/j.apenergy.2014.07.069

68. Hart, A.; Greaves, M.; Wood, J. fixed-bed and dispersed catalytic upgrading of heavy

crude oil Opus : University of Bath Online Publication Store Please cite only the published version using the reference above . of heavy crude oil using-CAPRI. 2015;213–23.

69. Basavegowda, N.; Mishra, K.; Lee, R, Y. Synthesis, characterization, and catalytic applications of hematite (α-Fe2O3) nanoparticles as reusable nanocatalyst. Adv Nat Sci Nanosci Nanotechnol. 2017;8(2).

70. Elahi, M, S.; Khoshooei, A, M.; Ortega, C, L.; Scott, E, C.; Chen, Z.; Pereira-Almao, P. Chemical insight into nano-catalytic in-situ upgrading and recovery of heavy oil. Fuel. 2020;278:118270. Available from: https://doi.org/10.1016/j.fuel.2020.118270

71. Yrjas, P.; Hupa, M. Limestone and dolomite as sulfur absorbents under pressurized gasification conditions. 1996;75(1):89–95.

72. Shakirullah, M.; Ahmad, W.; Ahmad, I.; Ishaq, M.; Khan, I, M. Desulphurization of liquid fuels by selective adsorption through mineral clays as adsorbents. J Chil Chem Soc. 2012;57(4):1375–80.

73. Zou, C.; Zhao, P.; Ge, T.; Li, D.; Ye, H.; Huang, G. Bitumen recovery from Buton oil sands using a surfactant under the effect of ultrasonic waves. Energy Sources, Part A Recover Util Environ Eff. 2016;38(2):270–6. Available from: http://dx.doi.org/10.1080/15567036.2012.762701

74. Oxenford, J.; Coward, J.; Bulatovic, S.; Lui, Q. Heavy minerals from Alberta ' s oil sands — setting new standards ? SGS Miner Serv - Tech Bull. 2001;12.

75. Lapeira, C. Development of a new methodology for preparing nanometric ni, mo and nimo catalytic particles using transient emulsions [Internet]. 2009. Available from:

doi:10.11575/PRISM/3212

76. Vasquez, A. Synthesis, Characterization and Model Reactivity of Ultra Dispersed Catalysts for Hydroprocessing. Unpublished Master's Thesis. University of Calgary, Calgary, AB. 2007.

77. Chen, M.; Li, C.; Li, G, R.; Chen, Y, L.; Zhou, C, G. In situ preparation of well-dispersed CuO nanocatalysts in heavy oil for catalytic aquathermolysis. Pet Sci. 2019;16(2):439–46. Available from: https://doi.org/10.1007/s12182-019-0300-3

78. Zekel', A, L.; Maloletnev, S, A.; Ozerenko, A, A.; Shpirt, Y, M. Basics of synthesis and application of pseudohomogeneous coal and petroleum feedstock hydrogenation catalysts. Solid Fuel Chem. 2007;41(1):31–7. Available from: http://www.springerlink.com/index/10.3103/S0361521907010077

79. Douglas, B, G. Contaminant removal from acidic mine pit water via in situ hydrotalcite formation. Appl Geochemistry. 2014;51:15–22. Available from: http://dx.doi.org/10.1016/j.apgeochem.2014.09.005

80. Kaur, G.; Couperthwaite, J, S.; Millar, J, G. Acid Mine Drainage Treatment Using Bayer Precipitates Obtained from Seawater Neutralization of Bayer Liquor. Glob Challenges. 2018;2(12):1800061.

81. Zhang, P.; Wu, T.; Hou, M.; Ma, J.; Liu, H.; Jiang, T.; Wang, W.; Wu, C.; Han, B. The hydrogenation of aromatic compounds under mild conditions by using a solid Lewis acid and supported palladium catalyst. ChemCatChem. 2014;6(12):3323–7.

82. Sharma, K, S.; Sidhpuria, B, K.; Jasra, V, R. Ruthenium containing hydrotalcite as a heterogeneous catalyst for hydrogenation of benzene to cyclohexane. J Mol Catal A

Chem. 2011;335(1–2):65–70. Available from: http://dx.doi.org/10.1016/j.molcata.2010.11.015

83. Bratlie, M, K.; Kliewer, J, C.; Somorjai, A, G. Structure Effects of Benzene Hydrogenation Studied with Sum Frequency Generation Vibrational Spectroscopy and Kinetics on Pt(111) and Pt(100) Single-Crystal Surfaces. 2006;111:17925–30.

84. Sano, T.; Shoji, H.; Okabe, K.; Saito, K.; Hagiwara, H.; Hosoya, T.; Takaya, H. Hydrocracking of benzene over various zeolite catalysts. 1986;29(5):20–30.

85. Ahmed, W, K.; Ali, A, S.; Ahmed, S.; Al-Saleh, A, M. Simultaneous hydrodesulfurization of benzothiophene and dibenzothiophene over CoMo/Al2O3 catalysts with different [Co/(Co + Mo)] ratios. React Kinet Mech Catal. 2011;103(1):113–23.

86. Popescu (Stanica), I, A.; Bombos, M.; Popovici, D.; Bombos, D.; Bolocan, I. Hydrogenation of Naphtalene on Pt-Pd Catalyst. Rev Chim. 2017;68(2):210–4.

87. Monteiro-Gezork, A, C, A.; Natividad, R.; Winterbottom, M, J. Hydrogenation of naphthalene on NiMo- Ni- and Ru/Al2O3 catalysts: Langmuir-Hinshelwood kinetic modelling. Catal Today. 2008;130(2–4):471–85.

88. Kirumakki, R, S.; Shpeizer, G, B.; Sagar, V, G.; Chary, R, V, K.; Clearfield, A. Hydrogenation of Naphthalene over NiO/SiO2-Al2O3 catalysts: Structure-activity correlation. J Catal. 2006;242(2):319–31.

89. Escobar, J.; Barrera, C, M.; Santes, V.; Terrazas, E, J. Naphthalene hydrogenation over Mg-doped Pt/Al2O3. Catal Today. 2017;296:197–204. Available from: http://dx.doi.org/10.1016/j.cattod.2017.04.064

90. Fang, M.; Sánchez-delgado, A, R. Ruthenium nanoparticles supported on magnesium

oxide : A versatile and recyclable dual-site catalyst for hydrogenation of mono- and. J Catal. 2014;311:357–68. Available from: http://dx.doi.org/10.1016/j.jcat.2013.12.017

91. Dokjampa, S.; Rirksomboon, T.; Osuwan, S.; Jongpatiwut, S.; Resasco, E, D. Comparative study of the hydrogenation of tetralin on supported Ni, Pt, and Pd catalysts. Catal Today. 2007;123(1–4):218–23.

92. Jing, Y, J.; Wang, Z, J.; Liu, C, D.; Qie, Q, Z.; Bai, C, H.; Li, Y, W. Naphthalene Hydrogenation Saturation over Ni2P/Al2O3Catalysts Synthesized by Thermal Decomposition of Hypophosphite. ACS Omega. 2020;5(48):31423–31.

Chapter 3

Materials and Methods

3.1 Introduction

Though current technological and environmental trends indicate a progressively reduced reliance on crude oil, demand is expected to continue until 2050. This demand is characterised by transportation fuels, as well as feedstocks for a host of ancillary industries including but not limited to the production of plastics, medicines and hydrogen.

In situ combustion is characterised by the supply of thermal energy to the petroleum reservoir to induce cracking reactions with the aim to coproduce oil and hydrogen at the surface. The thermal conversion also drives catalytic upgrading over both the reservoir rock minerals, in addition to subsurface catalytic liners incorporated into the production string. The vast number of components found in the oil undergo a great number of conversion mechanisms, some of which include removal of sulphur, reduction in viscosity, hydrogen addition and thermal cracking reactions.

Indicators used to assess the performance of catalytic upgrading comprise viscosity measurements, simulated distillation profiles of the produced liquid phase, the analysis of liquid sulphur content as well as, measurements over the solid phase including both elemental and textural properties.

When using model compounds to simulate heavy oil hydrogenation, gas chromatography was utilised to measure the individual components during multi-stage conversion.

The experimental methods in this study including catalyst synthesis, upgrading of both crude oil feedstock and model compounds, in addition to subsequent analysis of the products are highlighted in this chapter. The intention is to supplement additional information provided in the following results chapters, in which catalyst-specific characterisation methods and results are included, with fundamental operating principles of the equipment used in the experimental work.

The treatment of experimental error including repeating each in-house experiment for at least three repetitions, raising to five repetitions where indicated, while the graphs illustrated in the thesis include the standard error of mean unless otherwise stated. With regards to the outsourced characterisation techniques, including the sulphur determination for upgraded oil and Brunauer-Emmett-Teller analysis, the error treatment used was consistent with the specific organisations' policy on procedures.

3.2 Coprecipitation of anionic clay

The method of coprecipitation was selected to synthesise Layered-Double Hydroxides as either stand-alone catalytic materials and in addition to support materials. The varieties synthesised comprised carefully selected metals known to be useful species in petroleum upgrading.

A temperature-controlled reactor was used to initiate material synthesise as observed in Figure 3.1. Three separate solutions were made up, (i) the metal salt solutions containing the metals in the appropriate molar ratio, governed by equation [3.1] (ii), a sodium or ammonium hydroxide solution to enable careful adjustment of the pH and (iii) the solution

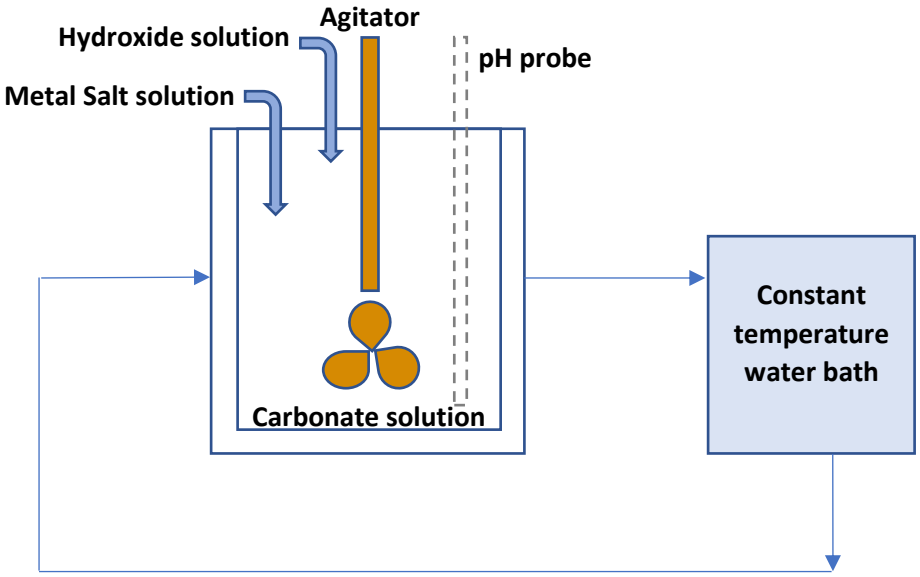

Figure 3.1 Schematic of the coprecipitation catalyst synthesis

of either sodium or ammonium carbonate dissolved in deionised water, in the reaction vessel, to which the first two solutions were slowly added. The appropriate molar concentration of the $[CO_3]^{2-}$ was governed by equation [3.2]. The exact metal salts and molar ratios used are detailed in sections **4.2** and **5.2.1**. A peristaltic pump was used to add the metal salt and hydroxide solutions into the main reaction vessel. Careful selection of the pH was required to optimise the formation of the LDH materials, while a pH probe continually monitored the pH of the solution in the reaction vessel. If the pH deviated from the optimised pH constraints, the hydroxide solution would be sequentially added or inhibited until the pH was in the optimum range.

$$[M^{II}_{(1-x)}M^{III}_{x}(OH)_2]_x+[A^{n-}]_{x/n}mH_2O \qquad \textbf{[3.1]}$$

$$[CO_3]^{2-}/[M^{III}] = 0.5 \qquad \textbf{[3.2]}$$

Agitation was fixed at 500 rpm, while the temperature of the solution in the reaction vessel was selected and maintained by an external water bath which fed water through the double jacket of the reaction vessel.

Upon completion of the metal salt addition, the agitation was stopped and thermal treatment for 12 hours was continued to aid in the crystallisation process.

Following crystallisation, the LDH precipitant was washed with hot deionised water several times, before being vacuum filtrated and dried in an oven for a further 12 hours.

Both the synthesised and refinery catalyst types were characterised using X-Ray Diffraction, X-Ray Fluoresence, Scanning Electron Microscopy, Transmission Electron Microscopy, Thermo-Gravimetric Analysis, Temperature Programmed Desorption and Temperature Programmed Reduction and Brunauer-Emmett-Teller, the methods of which and accompanying results are detailed in sections **4.3.1** and **5.3.1**.

3.3 TGA

A NETZSCH-Geratebau GmbH, TG 209 F1 Iris® was used to undertake ThermoGravimetric Analysis (TGA). This analysis was conducted over both catalysts and petroleum coke samples, the latter of which were collected from the autoclave following upgrading of heavy

oil. 20 mg samples were taken and placed in a platinum crucible, set upon the microbalance. The program used to analyse the samples comprised a ramp temperature range of RT –

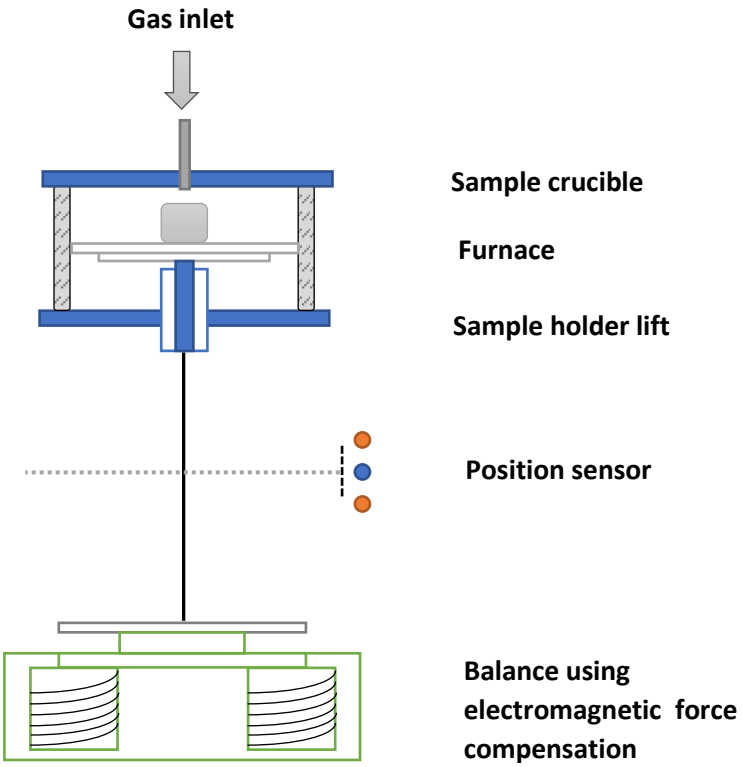

Figure 3.2 Schematic of the thermo gravimetric analytical instrument equipped with an electromagnetic compensation balance.

900°C, with a heating rate of 10 K min^{-1} and a flow rate of air set at a constant 50 mL min^{-1}. This ramping phase was followed by an isothermal phase, the length of which comprised 10 minutes. Proteus® software was used to analyse the data, producing graphs illustrating both mass change and the rate of mass loss as the temperature is ramped. The sensitive microbalance was vacuum-tight, using electromagnetic power compensation to accurately determine the mass loss of the sample upon exposure to the air during the temperature ramping as shown in Figure 3.2.

3.4 Rheometer

An AR 1000 rheometer was used to measure the viscosity of the oil both pre and post reaction, demonstrated in Figure 3.3. The system comprised a sample holder with parallel plate geometry. The aluminium parallel plate was 40 mm in diameter. The viscometry mode used in the analysis measured rheological properties as a function of shear stress vs shear rate. The parallel plate gap size was set at 100 µm. The measurements were performed using a shear rate of 100 s^{-1}, performed at 25°C. The data was averaged across five data points to provide an accurate account of viscosity reduction.

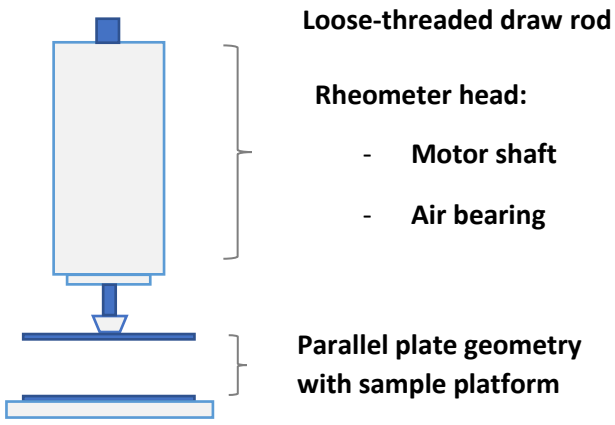

Figure 3.3 Schematic of the AR 1000 Rheometer.

3.5 Asphaltene Measurement

Asphaltenes were collected using n-heptane separation to form a precipitate, while the remaining portion of the liquid comprised a mixture of saturates, aromatics and resins, commonly referred to as the maltene fraction. The method used was in accordance with ASTM D2007-80.

1g of the liquid sample was collected following completion of the reaction. This was mixed with 40 mL of n-heptane. The mixture was agitated under magnetic stirring for 4 hours. Following agitation, the mixture was left for 24 hours. The precipitated asphaltenes was subsequently vacuum filtrated and washed with additional n-heptane until no maltenes could be detected within the solvent. The precipitant was subsequently dried for a further 24 hours to allow for the evaporation of residual n-heptane. The percentage of asphaltene

$$\text{Asphaltene content (wt. \%)} = \left\{ \frac{\text{dried asphaltene precipitate (g)}}{\text{heavy oil sample used for the analysis (g)}} \right\} \times 100$$

was calculated using the following equation:

3.6 Sulfur Analysis

The sulphur content of the heavy oil, both before and after the upgrading reaction, was measured using total sulphur analysis by titration (Exeter Analytical UK Ltd). The results. The results were obtained as a percentage of sulfur removed through the various mechanisms of desulphurisation, providing both a sulfur % wt/wt and reduction with respect to the feed (%).

$$\text{Sulphur removal (wt. \%)} = \left\{ \frac{\text{Sulphur \% (wt/wt)}_{\text{feed}} - \text{Sulphur \% (wt/wt)}_{\text{upgraded}}}{\text{Sulphur \% (wt/wt)}_{\text{feed}}} \right\} \times 100$$

3.7 Combustion Tube for CHNS analysis

The solid coke samples were weighed out into tin capsules for subsequent introduction into the combustion tube, a schematic of which is shown in Figure 3.4. A mixture of inert carrier

gas, He, in addition to high purity O_2 were supplied to the combustion tube. Following combustion, the products are passed over high purity Cu, to remove any residual O_2. Detection of the gaseous products was carried out by GC separation using a thermal conductivity detection system.

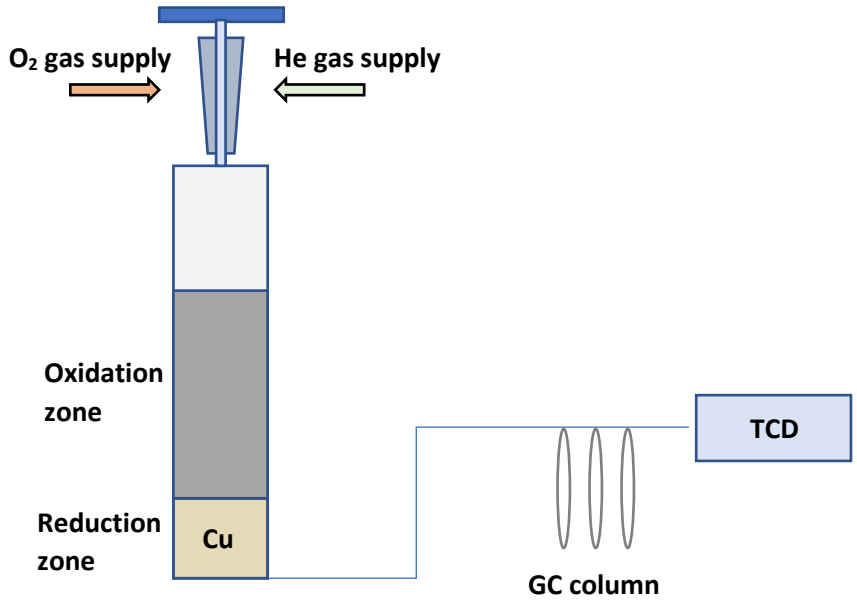

Figure 3.4 Schematic of the combustion tube apparatus.

3.8 Scanning Electron Microscopy

In terms of product characterisation, Scanning Electron Microscopy (SEM) was used to demonstrate the textural properties of the produced solid phase comprising the toluene-washed solids. The SEM used was an Hitatchi TM3030Plus. A sputter coater was used to thinly coat the solid particles in an appropriate conductive metal to maximise the resolution of the textural properties.

3.9 Baskerville reactor

Heavy oil upgrading-g using dispersed microcatalyst was conducted in a Baskervillle batch autoclave reactor, Figure 3.5, encompassing a 100 mL internal reactor sleeve. The catalyst to oil ratio used equated to 0.36g to 18g heavy oil. Agitation in the reactor was performed by an electric stirrer comprising a dual-bladed impeller. Previous optimised conditions were used to undertake the upgrading reactions, at 425℃ and an initial ambient pressure of 20 bar. The reaction gases used were either 100% N_2 or 100% H_2. Upon reaching the maximum reaction temperature, the pressure appropriately increased to between 60 and 70 bar, reaction gas and catalyst dependent.

Before experimentation could commence, the gas inlet and outlet valves were used to purge the reactor vessel with N_2, utilising successively higher N_2 pressures. The experiment was taken at time point zero when the reaction temperature had been reached.

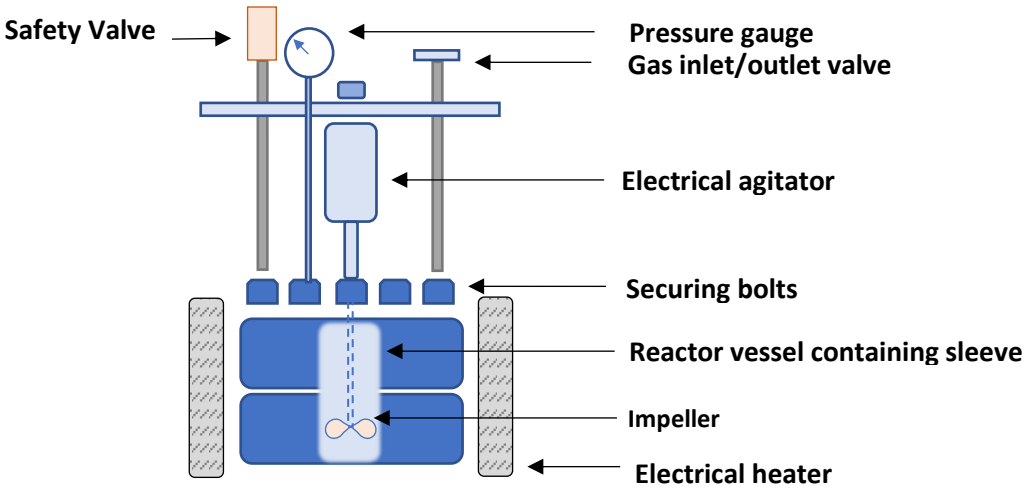

Figure 3.5 Schematic of Baskerville reactor used for heavy oil upgrading.

3.10 Anton Parr reactor

The Anton Parr reactor was used in conjunction with an external temperature controller. The reactions were conducted to measure naphthalene hydrogenation and tetralin dehydrogenation. The reactor comprised a gas inlet valve and sample outlet valve, a magnetic stirrer and external electric heater. The gas inlet valve enabled comprehensive purging prior to reaction, as well as gas adjustment immediately after sampling. The reaction conditions were set at 0.12g of catalyst and 0.18g of naphthalene reactant, the latter of which dissolved in 60 mL *n*-hexadecane. A low N_2 pressure, set at 1 bar, was used during the heating period to reaction temperature to prevent hydrogenation reactions taking place. At reaction temperature, the N_2 was evacuated from the reactor and replaced with 40 bar H_2. Following each 20 minute sampling interval, H_2 was fed into the reactor to retain a pressure of 40 bar.

3.11 Gas Chromatography

3.11.1 Simulated Distillation

To analyse the boiling point distribution of the produced liquid, the ASTM-D2887-08 method was adopted using an Agilent 6850N Gas Chromatography (GC). A DB-HT capillary column was fitted to the system, characterised by the following dimensions: 5m length, 0.53 mm

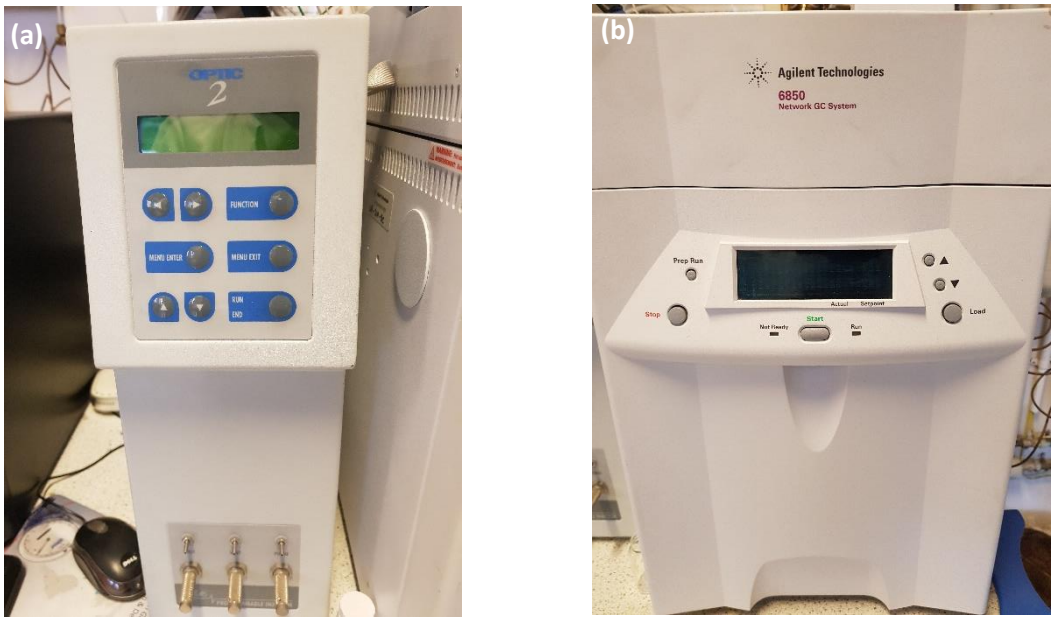

Figure 3.6 A photo to demonstrate the PVT injector (a) and Agilent 6850N GC (b).

internal diameter and 0.5 um film thickness. Prior to injection, the produced liquid was diluted using a miscible, low boiling point solvent, CS_2 under a fixed volumetric ratio of 1 to 10. One of the key features required by the solvent is a low response factor over the Flame Ionisation Detector (FID). An injection volume of 0.1 ul was taken manually and injected into the GC. A Programmed Temperature Vaporisation (PTV) injector rapidly heated up the injected sample to 350℃ so that it may be vaporised prior to introduction into the GC. The FID itself was maintained at 260℃ with a constant flow of 450, 40 and 32.3 mL min^{-1} for air,

hydrogen and nitrogen, respectively. The temperature ramping program comprised a 0oC min^{-1} rate through 40 to 260℃.

The boiling point range was separated into distinct regions; light naphtha, middle distillates and above 343℃, the latter of which details the more undesirable heavy fractions.

3.11.2 Model compound

An Agilent Technologies 6890N Gas Chromatography analyser was used to separate the individual components remaining in the filtered samples. A 7683 B Series injector was used to commence the analysis, the capillary column of which was an Agilent 19091J-413

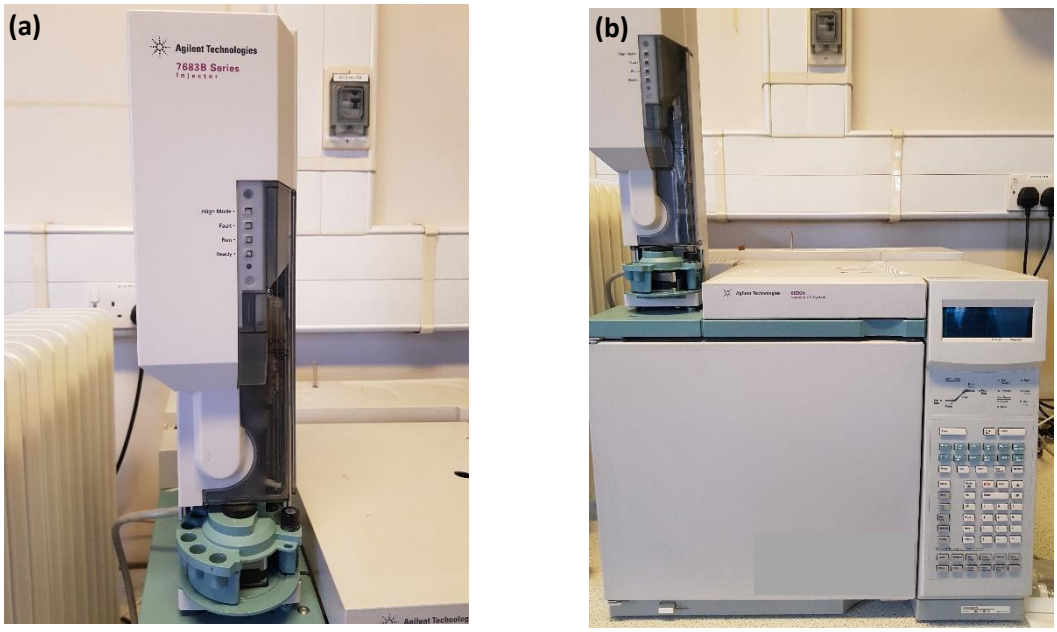

Figure 3.7 The A 7683 B Series injector (a) and the Agilent 6850N GC (b).

capillary column (nominal length, diameter and film thickness at 30.0m, 320.0 µm and 0.25 µm, respectively). The following method was used to optimize the resolution and quality of the data: equilibration time of 3 min, with a ramp from 80 to 135℃ over 9 min and second

stage to 300℃ over 4 min. Depending on the nature of experimentation, the separated components were assigned to first and second stage naphthalene hydrogenation products, or tetralin dehydrogenation products. Consequently, five-point calibrations were made for naphthalene, tetralin, cis-decalin and trans-decalin. The calibrations were conducted as virgin components in the solvent while also in the presence of the other products/reactants. This was to ensure no complications were prevalent in the analysis of reactant and product mixture.

Claydon, R.; Wood, J. A Mechanistic Study of Layered Double Hydroxide (LDH)-Derived Nickel-Enriched Mixed Oxide (Ni-MMO) in Ultradispersed Catalytic Pyrolysis of Heavy Oil and Related Petroleum Coke Formation. Energy Fuels 2019, 33 (11), 10820−10832.

Chapter 4

Chapter 4: A mechanistic study of Layered-Double Hydroxide (LDH)-derived nickel-enriched mixed oxide (Ni-MMO) in ultradispersed catalytic pyrolysis of heavy oil and related petroleum coke formation

4.1 Introduction

Petroleum demand is expected to grow over the coming decades before being phased out by renewable alternatives. The BP Energy Outlook (1) predicts that hydrocarbons as an energy supply will cease to grow between 2030 and 2040. However, conventional reserves are slowly depleting and with this in mind, heavy oil and bitumen resources may be able to mitigate this concern. There are an estimated 8 trillion barrels of heavy oil and bitumen remaining in Canada and Venezuela (2). However, primary production in these petroleum

reservoirs is limited by both the physical and chemical properties of the oil. These unfavourable properties constitute an excessive viscosity, which significantly limits the flow rates of production wells. Consequently, Enhanced Oil Recovery (EOR) techniques are employed to partially upgrade these heavy oils. In-Situ Combustion (ISC) and Steam-Assisted Gravity Drainage (SAGD) are examples of thermal EOR methods that have previously been employed. A number of EOR techniques have been tested in conjunction with downhole catalysts to ascertain their role in upgrading the oil in-situ. High temperatures may be achieved in the reservoirs as a result of thermal techniques, with a notable example Toe-to-Heel Air Injection (THAI) leading to temperatures exceeding 450℃ and peaking up to 600℃ in laboratory simulations (3,4). This is an adequate temperature to promote catalytic upgrading and as such has lent itself to the development of an in-well catalyst interface otherwise known as CAtayltic upgrading PRocess In-situ (CAPRI) comprising a fixed bed of hydroprocessing catalysts within the annulus of the production liner.

Additionally, surface upgrading units are used to further improve the quality of the oil including the sulphur content. This property is tied into both the overall petroleum quality and environmental legislation. For example, the United States government implemented new legislation, beginning 2017, which limited the total content of sulphur to 10 ppm in gasoline (5) As such, it is of great importance to minimise this constituent and its consanguineous fractions. Additional performance markers highlight the proportion of valuable gasolines and distillates and petroleum coke composition. Additional performance markers assess the proportion of valuable gasolines and distillates and petroleum coke composition.

Anionic clays, commonly referred to as Layered Double Hydroxides (LDHs), are a class of multicomponent catalysts which have been used previously in both reforming and hydrogenation reactions, as well as acting as catalytic supports (6,7). These compounds comprise brucite-like metal hydroxide layers, octahedrally-coordinated containing at least two cations with a different ionic charge. The difference in ionic charge gives rise to layers, comprised of both anions and water, between the metal hydroxide layers. Consequently, sheet-like stacks of metal hydroxides with negatively charged interlayer regions are formed to generate the overall anionic clay structure, as illustrated in Figure 4.1 (6,7). While there has been some use of anionic clays as petroleum upgrading catalysts and additives as shown in Mostafa and Mohamed (8) and Zhao et al. (9), much work is needed to understand the mechanism of upgrading and to realise the true potential of metal-doped anionic clays on upgrading across all facets of the upgrading products.

One critical characteristic of these anionic clays is the ability to exchange different metals into the metal hydroxide structure. This enables the tailoring of the catalyst to a specific function. For instance, a well-studied anionic clay in literature is the Mg^{2+}/Al^{3+} anionic clay in a 3:1 ratio (6). Petroleum upgrading reactions typically use metals such as nickel, cobalt and molybdenum (10,11). Consequently, the substitution of nickel into the anionic clay has been chosen to tailor its use in petroleum catalytic upgrading reactions at a relatively cost-effective premium. Additionally, upon heating the layered clays lose their interstitial water and anion layers to form high-surface area mixed oxides (6,7). This may act to release activated components into the reaction mix as well as leaving behind host sites. There are very few limitations to the nature of anions incorporated into the anionic clay structure,

consequently, the vacant sites may accommodate the removal of deleterious fractions of the oil during the simultaneous upgrading and re-lamination of the mixed oxides (6). The mixed oxides possess both Lewis acidic and Lewis basic sites which may sufficiently accommodate both hydrogenation and deprotonation reactions which are valuable in petroleum upgrading (6). The thermal stability of the resultant mixed oxides which are synthesised in-situ, combined with the high level of metal dispersion across the layers, also contribute to its potential viability as an upgrading catalyst.

The purpose of this study is to achieve a lower cost in-situ activated alternatives to hydroprocessing catalysts. The catalysts have the potential for usage in conjunction with the THAI-CAPRI as an ultradispersed catalyst reflecting a new CAPRI contacting pattern. Specifically, the study will evaluate the effect of a Nickel-Enriched Mixed Metal Oxide (Ni-MMO) catalyst derived from the in-situ delamination of NiAl-LDH on heavy oil recovered from the THAI wells. The performance of the catalyst was placed into the context of both thermal upgrading and catalytic upgrading with the use of a commercial refinery catalyst (Co-Mo/Al_2O_3).

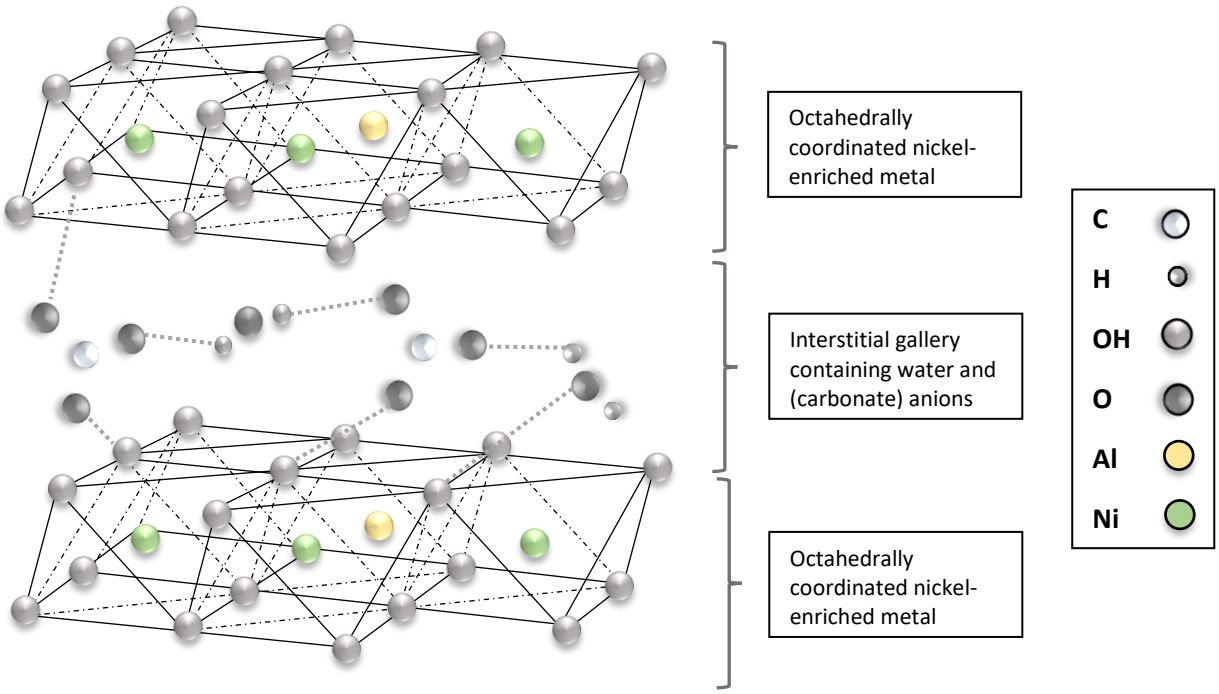

Figure 4.1 Graphical representation of the Layered-Double Hydroxide (LDH) prior to thermal treatment.

4.2 Materials and Methods

The heavy oil used in this study was obtained from a pre-mixed series of samples from eight different THAI production wells at Kerrobert, Saskatchewan, Canada. A representative bulk sample -was taken for use during the experimentation with the properties of the heavy oil shown in Table 4.1.

Table 4.1 Properties of the heavy oil feedstock prior to pyrolysis

Parameter	**Value**
Viscosity at 20℃ (mPa·s)	811
Sulphur (wt%)	3.32
Asphaltene (wt%) by nC_7H_{16}	14
ASTM D2887 Distillation	
IBP - 200 ℃ (%)	12.6
200 - 343 ℃ (%)	27.6
343 ℃ - FBP (%)	59.8

The LDHs were synthesised using the co-precipitation method under constant pH. Solutions containing the cation salts were dissolved in distilled water and co-precipitated into a carbonate solution, the concentration of which is defined by the limit $[CO_3^{2-}]/[M^{3+}] = 0.5$. The metal salts were mixed in ratios appropriate to yield anionic clays with the desired compositions. A sodium hydroxide solution was used to maintain the optimum pH for homogenous precipitation. Following the complete addition of the metal salt solutions, the system was left to age overnight at a constant temperature of 60˚C. The precipitate was vacuum filtrated and washed several times with distilled water. Ni/Al (3.3:1) anionic clays were synthesised using the co-precipitation method, where the metal salts,

$Ni(NO_3)_2{\cdot}6H_2O$ and $Al(NO_3)_3{\cdot}9H_2O$, were mixed in given ratios (x:y), conforming to the limits of metal ratios exhibited by anionic clays (6). Properties of the anionic clay catalysts are shown in Table 4.2 with the corresponding commercial refinery catalyst properties, following extended crushing into a fine powder.

Powder X-ray Diffraction (PXRD) patterns were obtained with a Bruker D2 X-ray diffractometer using a cobalt source and nickel filter. This was used to determine the atomic arrangement of the mineral crystals. A scan speed of 30 minutes with a step size of 0.370 was used over a 2theta range 10-100˚.

Furthermore, Thermo-Gravimetric Analysis (TGA) experiments were used to determine the chemical changes to the structure as the temperature within the reactor increases, helping to further delineate the reaction mechanism. 22 mg of catalyst was added to a platinum crucible before being heated up at a rate of 10 K/minute from 25℃ to the maximum temperature of 900℃, under a constant flow set at 10 mL/min of air.

Scanning Electron Microscopy (SEM) photographs were taken to highlight the morphology of the catalyst species. The sample was mounted on a carbon disc, before being sputter coated in gold to improve conductivity and consequently morphological resolution. This helped in the identification of the anionic clays, while highlighting the morphological differences prevalent when intercalating new metal species into the clay layers. Additionally, EDX was used to estimate the cation ratio in the brucite-like layer.

Temperature Programmed Reduction (TPR) and Desorption (TPD) was performed to evaluate the reduction temperature of the Ni-MMO. A Quantachrome ChemBet Pulsar

equipped with a Thermal Conductivity Detector (TCD) was used in conjunction with approximately 20 mg of the catalyst loaded into a quartz U-tube reactor. The temperature was ramped from room temperature to 900℃ using a ramp rate of 10℃/min while recording the intensity of H_2 uptake using a H_2 (5%) in Ar gas mix. TPD measurements were taken using the same apparatus but with a NH_3 (5%) in He gas mix. Approximately 40 mg of the catalyst was heated under He to 300℃, before holding for 1 hour and cooling to room temperature. The NH_3 (5%) in He was introduced for 2 hours before switching the gas back to He and ramping from room temperature to 900℃ using a ramp rate of 10℃/min.

For the oil upgrading reactions, a 100mL capacity (Baskerville) stirred batch reactor, set in a removable high-temperature electrical heater, was used to facilitate the heating, agitation and upgrading, with which parameters were selected following a previous optimisation study (12). Details of the experimental set-up are highlighted in Section 3.2.

After collecting the liquid fractions, a range of measurements were taken to analyse the quality of the product. The asphaltene content was estimated using 40mL of n-heptane (precipitating agent) added to 1 g of upgraded oil, followed by constant agitation for 4 hours. An AR 1000 (TA Instruments Ltd, UK) rheometer was used to measure the viscosity of the liquid products at temperature of 25℃. GC method ASTM D2887 with the Agilent 6850N GC calibration mix comprising C_5-C_{44}, in addition to the ASTM D2887 reference gas oil mix No.1 Lot 2, was used to determine the percentage yield of light naphtha (IBP - 200℃), middle distillates (200 - 343℃) and residues (343℃+). This is a standard test method to determine the boiling range distribution of petroleum samples by gas chromatography.

Total Sulphur Analysis by titration to determine sulphur wt.%/wt was carried out by Exeter Analytical.

Coke quantification using the TGA curve of asphaltene and wax saturated coke particles is the commonly adopted method demonstrated in previous studies. This method makes the assumption that coke constitutes all components burnt-off at and above 600˚C rather than accounting for compositional variations in coke (4,13-15). However, this paper sought to use a more accurate method of coke quantification and characterisation. Consequently, toluene-insoluble coke precipitation and subsequent TGA of the product was employed (16). Additionally, both elemental (CHNS) and SEM analysis were undertaken on the coke samples. This provided new insights into the mechanism of coke formation and the differences between thermal upgrading and catalytic upgrading.

Table 4.2. Results of the nitrogen sorption analysis conducted on the ultrafine catalysts

Catalyst	**BET area(m^2/g)**	**Pore size (nm)**	**Total pore volume (cm^3/g)**
Ni-Al/LDH	96.4	5.62	0.13
Co-Mo/AL2O3	198.2	6.06	0.07

4.3 Results and Discussion

4.3.1 Layered-Double Hydroxide Characterisation

4.3.1.1 PXRD

Successful synthesis of the layered anionic clay structure was confirmed using Powder X-Ray Diffraction (PXRD) analysis. The diffractogram of NiAl-LDH in Figure 4.2 highlights the various reflections corresponding to the crystal lattice of an anionic clay, the peaks of which having been picked and matched to a material with the same crystal lattice formulation to PDF 00-056-0953, a nickel aluminium LDH with Ni:Al 2:1 molar ratio. A slight deviation from the matched LDH reflects the difference in molar ratio between Ni and Al. The three narrow peaks occurring at low 2theta values (2θ = 14.1, 27.8 & 41.5) can be assigned to the lattice planes (003), (006) and (012). These reflect the ordering of the layered clay structure and highly crystalline nature of the clay, while the overall peak distribution accurately reflects typical anionic clay XRD patterns (6,7).

Furthermore, to validate the process of in-situ delamination of the anionic clay, during the temperature build-up of the reaction, the anionic clay was calcined at 425℃ before being re-analysed using XRD. The subsequent delaminated anionic clay diffractogram, illustrating large broad peaks which are highly indicative of an amorphous structure relating to the resultant Ni-MMO. The peaks have been picked as perfect match using the PDF 00-047-1049 for Bunsenite, a nickel oxide, while it is inferred that the poor crystallisation of aluminium oxides has led to its absence in the diffractogram. They do however remain active components in the resultant mixed oxide material. Upon calcination Ni-Al LDH forms

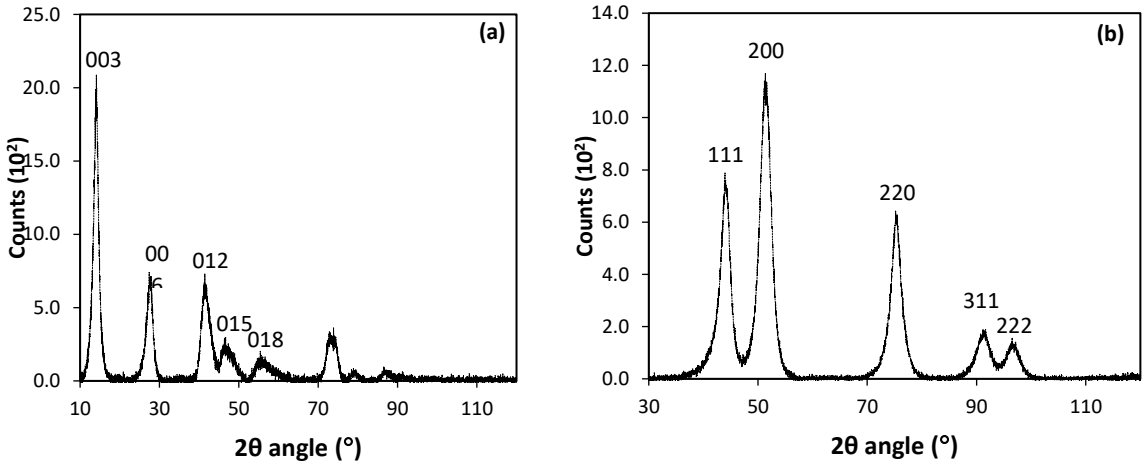

Figure 4.2 (a) PXRD peaks of NiAl-LDH highlighting successive (003), (006) and (012) peaks indicative of the layering in the LDH, in addition to (b) PXRD of resultant mixed oxides following calcination at 425℃.

polyphasic Ni-MMO containing; a NiO phase, a quasi-amorphous spinel-type phase and a Ni-doped alumina phase grafted to the spinel phase (7).

4.3.1.2 TGA

The TGA analysis in Figure 4.3 highlights the thermal stability of the catalyst when subject to rising temperature. The results clearly demonstrate two zones prior to reaching 425˚C, the reaction temperature, which can be classified into dehydration and dehydroxylation stages,

at approximately 100℃ and 250℃ respectively, the latter of which is accompanied by decarboxylation to a lesser extent (6,7). These peaks correspond with the XRD-post thermal

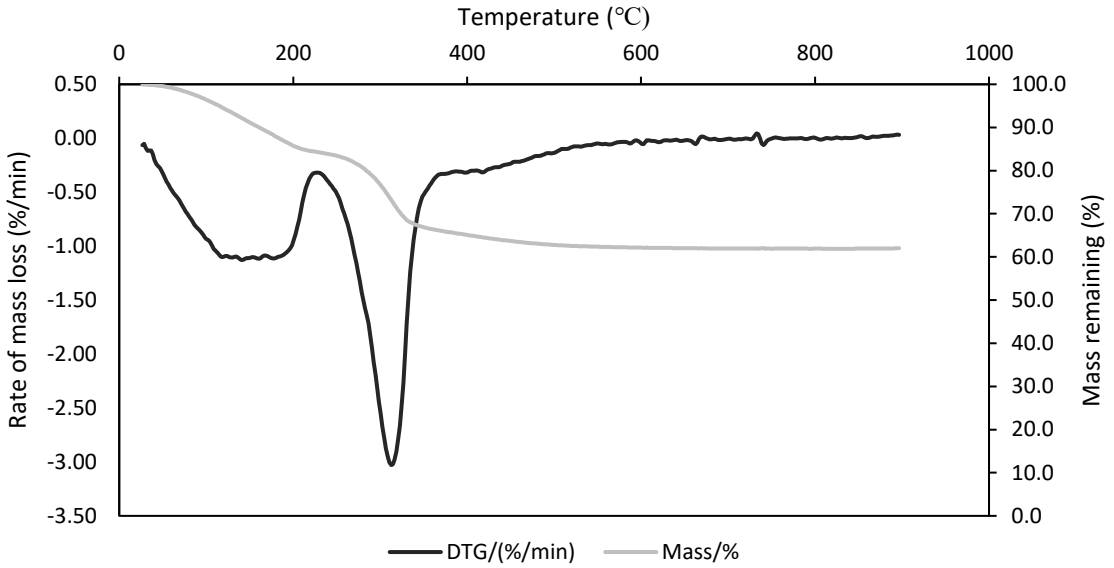

Figure 4.3 Thermo-gravimetric analysis of the catalyst prior to the upgrading reaction.

treatment highlighted in Figure 4.2 (b) wherein the delamination has led to the production of a high-surface area tri-phasic metal oxide. These layers contain active zones on which cracking, hydrogenation and desulphurisation can take place (7). It is also thought that the liberation of water molecules and hydrogen may serve to supply an activated hydrogen donor at reaction temperature and pressure.

Furthermore, the vacant sites left by the elimination of water and carbonate in anionic clays, highlighted by the mass loss peaks in Figure 4.2, are known to accommodate the re-uptake of other anionic and polar species (6). This inherent property of delaminated anionic clays may therefore prove to be useful in removing deleterious species within the hydrocarbon mixture, thereby undergoing re-lamination to possibly form a complex anionic clay derivative.

4.3.1.3 SEM and TEM

The images in Figure 4.4 highlight the morphological structure of the NiAl-anionic clay as well as an approximation of the particle size, pertaining to approximately 1 µm crystallites, forming approximately 3 µm agglomerates. The anionic clay demonstrates a plate-like structure comprising an undulating structure with hexagonal crystallites, typical of the LDH morphology. TEM imaging better highlights the agglomeration of hexagonal plates inherent in the structure of LDHs (6).

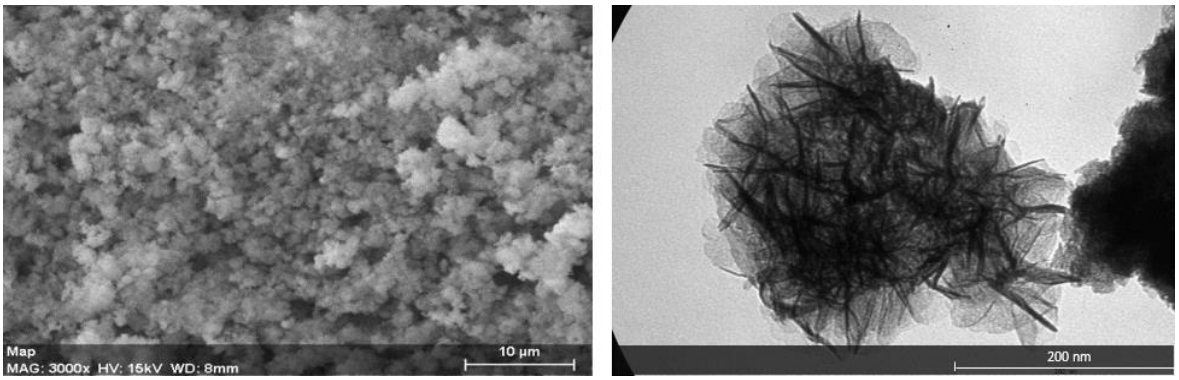

Figure 4.4 Scanning Electron Micrograph at a 10um scale (a) and Transmission Electron Micrograph at a 200nm scale (b) of the NiAl-LDH ultrafine catalyst powder.

Results obtained from EDX in Table 4.3, highlights the elemental content of the material. As shown, the intercalation of Ni and Al into the brucite-like layer was confirmed with a molar ratio at 3.3:1. This demonstrates the successful enrichment of nickel into the LDH during the co-precipitation synthesis method. The carbon and oxygen represent the oxygen within the CO_3^{2-} anions, H_2O molecules and within the –OH groups representing the brucite-like layer. It is worth noting that EDX does not detect hydrogen atoms, as a result absolute quantification of the chemical structure cannot be confirmed.

Table 4.3 EDX results of NiAl-LDH catalyst

Element	**Atomic number**	**Atom (at.%)**
Oxygen	8	68.56
Carbon	6	15.14
Nickel	28	12.51
Aluminium	13	3.79
		100

4.3.1.4 TPR and TPD

Figure 4.5 demonstrates the peaks of reduction and extent of NH_3 desorption across the temperature range. H_2 (5%)-TPR was performed to evaluate the reduction profile of Ni-MMO. The intensity of reduction peaked at 602.6℃, following a less intense reduction profile which peaked at 344.0℃. NH_3 (5%)-TPD was performed to investigate the acidity of the catalyst. The total number of acid sites has been calculated at 0.368 mmol g^{-1}.

A typical HDS CoMo-(γ)alumina catalyst with a similar surface area to the one used in these experiments at 204.24 m^2/g was shown to have an acid site density of 1.5134 mmol/g (17).

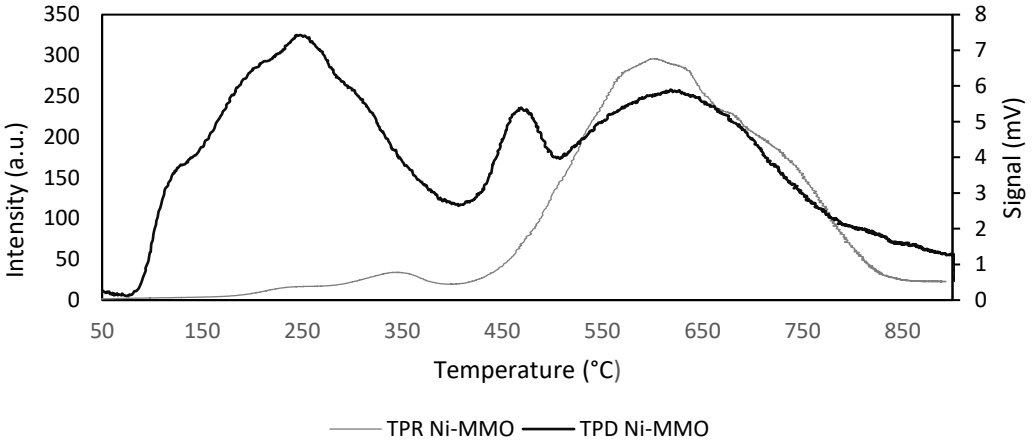

Figure 4.5 TPR and TPD profiles for the Ni-MMO catalyst.

The significant difference in acidity between the prepared and refinery catalyst is influenced by the alumina support. This has been shown to heavily influence catalyst acidity and promote coke-generating reactions in previous work (14).

4.3.2 Comparison of petroleum upgrading with anionic clays, refinery-grade catalyst and thermal upgrading

The upgrading experiments were performed in a Baskerville batch reactor under the following parameters; a reaction time of 30 minutes, Catalyst-To-Oil (CTO) ratio of 0.02 g/g, agitation speed 500 rpm and initial pressure 20 bar, 425℃ reaction temperature with N_2 reaction gas followed by hydrogen reaction gas, denoted in the paper by (N_2) and (H_2), respectively.

4.3.2.1 Effect of catalyst on product distribution

The preliminary steps taken within the analysis of petroleum upgrading comprise the mass balance. This is used to quantify the following three phases produced by the reactions; gas, oil and petroleum coke (the latter containing a mixture of condensed asphaltenes, resins, waxes and deactivated catalyst). Broad upgrading trends are subsequently identified before a more detailed analysis on the various products is discussed.

Gas (wt%) = 100 – liquid yield (wt%) – solids and residue yield (wt%)

The “solids and residue yield” is subsequently split into two components following toluene washing; (i) petroleum coke (and coked-up catalyst) (ii) liquid phase. Subsequently, TGA curves identified the amount of catalyst remaining following coke burn-off.

The normative aim concludes that the amount of oil produced should be high relative to the other phase products (10,14). However, there is invariably a trade-off between quality and quantity that directly affects the choice of processing methods employed by a refinery. This is mostly satisfied by market factors wherein the supply and demand relationship of different quality fuels and products becomes significantly influential on the refinery processing programmes (18).

The reaction environment is host to a great deal of reactions all of which impact both the quality and quantity of products. Cleavage of C-C, C-H and C-heteroatom bonds generates intermediate radicals which in turn can undergo several transformations depending on the catalyst involved and reaction environment. If hydrogen is not present in large quantities at high-pressure, it is more difficult for the radicals to undergo rearrangement and termination

reactions, leading to the formation of radical adducts forming. As a result, an increase in the amount of solid residue in the form of petcoke is in effect (14).

The relative proportions of the phases produced, shown in Figure 4.4, are used to provide a general insight into the reaction mechanisms occurring between thermal and catalytic upgrading. The general trends and corresponding interpretations are carefully considered, but at this stage do not represent the significant differences shown by subsequent analytical techniques employed on the liquid and solid phases.

From Figure 4.6, it can be observed that the liquid yield decreases in the following order: Thermal (H_2)> Ni-MMO (H_2)> Thermal (N_2)> CoMo-Al_2O_3 (H_2)> CoMo-Al_2O_3 (N_2)> Ni-MMO (N_2). When using hydrogen gas as a hydrogen donor in the presence of catalysts, it is observed that the mass balance is distinctly altered as opposed to using a N_2 atmosphere, which is supported in previous works (13).

With respect to the Ni-MMO, the addition of H_2 led to a marked increase in liquid yield from 70.3 to 78.9% with consequent reductions in wt% coke from 10.4 to 6.40%, and wt% gas reduction from 18.3 to 13.8%. This is significant when accounting for the average error margin across the resultant phases of only 1.78% as it clearly demonstrates the role of hydrogen gas as an active hydrogen donor in hydrogenation reactions and consanguineous coke suppression roles.

When using a CoMo-Al_2O_3 catalyst the addition of hydrogen led to a marginal increase in liquid yield from 72.6 to 74.2% with consequent reductions in wt% coke from 9.5 to 8.6%,

and wt% gas reduction from 15.7 to 15.3%. Combined with the error margin, the catalyst has made a minimal impact on the mass balance under different gas regimes.

It is shown that both the Ni-MMO (N_2) and CoMo-Al_2O_3 (N_2) give rise to elevated quantities of petroleum coke relative to the other reaction conditions. In particular, the thermal upgrading regimes both generated the least amount of coke at a steady 6.2%.

The acid site-containing alumina within the CoMo-Al_2O_3 catalyst structure leads to acid-catalysing C-C and C-heteroatom cleavage (11,19). Under a N_2 atmosphere it is difficult to cap the resultant free radicals because active $H^{\bullet}$ is scavenged from the mixture rather than being freely available under a H_2 atmosphere. Under a N_2 environment, carbon rejection is predominant while activated hydrogen is redistributed among the hydrocarbon molecules [20]. The increase in liquid fraction by 1.6% for CoMo-Al_2O_3 under a H_2 relative to N_2 atmosphere highlights the effect of hydrogenation on the product yield.

While the Ni-MMOs yield the largest quantity of petroleum coke at 10.4% under N_2, the theory behind this is decidedly different. Initial interpretations indicate that the condensation of radicals to petcoke is accommodated by the uptake of polarised asphaltic and resinous radicals by the positively-charged metal oxide sheets to ultimately generate polyaromatic-saturated layered structures – a pseudomorph of the initial anionic clay layered structure prior to heating. This theory is highly plausible given that interstitial anions present within anionic clays can have widely complex structures including complex organic and organometallic forms, while the mixed oxides have a strong tendency to reproduce the original layered structure when in solution (6). NiO nanoparticles have previously

demonstrated active asphaltene sorption sites, which is later supported by analysing the asphaltene content of the upgraded liquid and sulphur content of the petroleum coke (21). The asphaltene-saturated active sites may then be responsible for a multitude of side reactions culminating in the production of adducts as a coke-precursor. Under a H_2 environment, the yield of coke dropped significantly by 4% (0.52% and 0.59% error for N_2 and H_2 atmosphere-derived coke, respectively). The Ni-MMO undergoes in-situ partial reduction during the heat-up phase to 425℃ (under a 100% H_2 atmosphere), thereby contributing to the hydrogenation function. Fast-diffusing active hydrogen species ($H^{\cdot}$) led to an increase in hydrogenation and hydrocracking reactions. Specifically, free radicals generated by the carbon rejection routes are capped-off thereby inhibiting the condensation reactions which leads to petroleum coke formation (22).

The thermal regimes both generated the least amount of coke at 6.2%. The 2.4% difference in yield of liquid between the two reaction environments was accommodated by the yield of gaseous products, with which thermal (N_2) demonstrated over-cracking into smaller gaseous hydrocarbon molecules due to the unavailability of active hydrogen. Without metallic active sites and a support, the magnitude of both hydrogenation and cracking is limited, hence there was no difference in the coke production between N_2 and H_2 gas atmospheres. This also explains why the Al_2O_3-supported CoMo catalyst produced a higher amount of coke in both the N_2 and H_2 regimes, yielding an additional 3.3 and 2.4% of coke for CoMo-Al_2O_3 (N_2) and (H_2) over the thermal regime counterparts. The increased amount of carbon rejection pathways leading to free radical generation and condensation, accommodated by the acid-cracking alumina. This can culminate in an increase in free radical condensation and

simultaneous pore blockage in the catalyst, therefore enhancing the coke quantity. Moreover, this is supported by previous studies wherein one such example alumina produced the greatest quantity of coke in comparison to Pd-doped Al_2O_3 and Pd-doped carbon again demonstrating the significance of the acid-catalysing role of Al_2O_3 in upgrading (14).

Overall, the mass balance is a useful tool in obtaining an initial understanding of the upgrading process. Ultimately, the aim is to generate most significant amount of liquid phase with the smallest possible gas and coke phases. However, it is clear that the Ni-MMO catalyst has a complex impact on reaction pathways such that more gas and coke is produced at the expense of the liquid phase. However, subsequent analysis on the products shows distinct differences in the quality of the liquid and solid phases between the catalysts

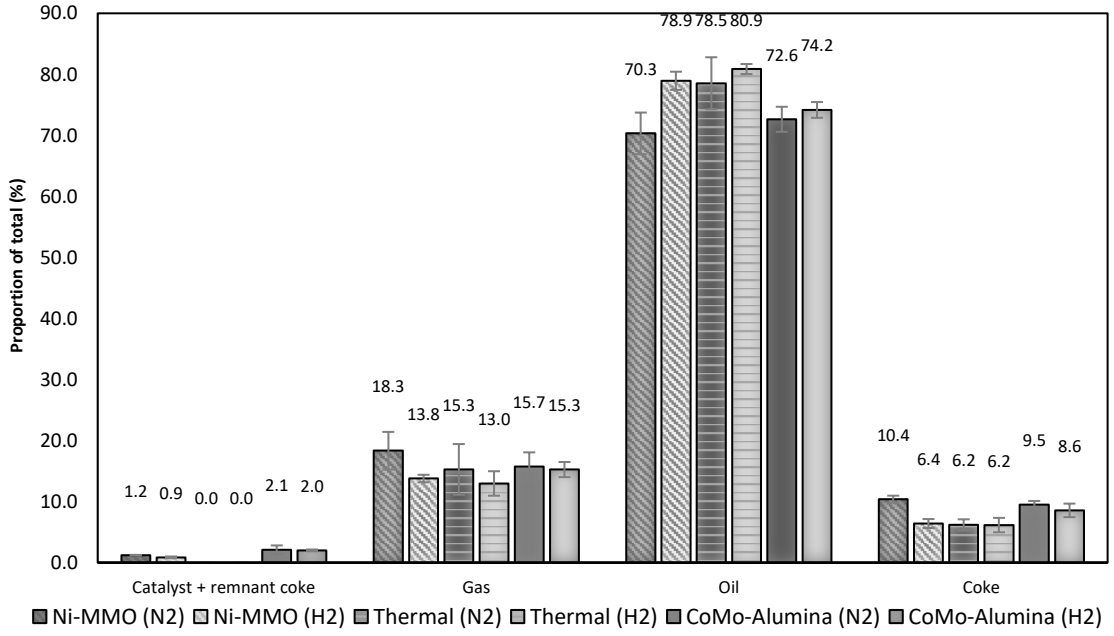

Figure 4.6 Mass balance following upgrading reactions highlighting coke, oil, gas and catalyst and remnant coke applicable constituents. Error bars demonstrate standard error of mean.

and thermal upgrading reactions which form the basis of an initial mechanistic understanding of Ni-MMO in heavy oil upgrading.

4.3.2.2 Effect of catalyst on liquid fraction sulphur

In terms of heavy oil, the sulphur content is a deleterious component which is typically removed using hydrotreating reactors at the refinery. Its significance rests on the fact that oils with a greater density and viscosity typically contain higher amounts of sulphur, as the higher boiling fractions are usually enriched in sulphur species (10,23). Furthermore, the combustion of oils with high sulphur content produces sulphur oxides and derivatives. The damage to the environment caused by such pollutants remains a big challenge for global environmental agencies. As such, maximum sulphur reduction achieved by upgrading facilities is necessary to conform to ever more strict environmental regulations (5).

The quantity of sulphur within the liquid oil is crucial in understanding the relative upgrading mechanism of the catalyst. The amount of sulphur can correlate most closely with the relative proportion of polyaromatic hydrocarbons, since it is these molecules which constitute heteroatoms of this type (24).

It is clear from the results in Table 4.4 that desulphurisation is enhanced by the catalysts. The results show an obvious trend emphasising sulphur removal following upgrading of the oil. To begin with, referring to the thermal (N_2) and thermal (H_2) conditions, sulphur reduction relative to the feed was 26.5 and 22.6%, respectively. There is a discernible difference of 3.9% favouring sulphur reduction in the absence of H_2. During the H_2 donor gas

condition, the long-chain polyaromatic hydrocarbon components are thought to be capped off by activated hydrogen species, thereby preventing the extent of over-cracking and subsequent generation of hydrocarbon gases. Consequently, there remains a higher yield of the residue fractions, supported by subsequent simulated distillation data, and therefore a higher yield of polyaromatic components which contain a significant portion of the sulphur heteroatoms. This is in broad agreement with the mass balance which highlights an increase in liquid yield at the expense of the gas yield under a H_2 gas atmosphere.

The Ni-MMO follows a similar pattern but demonstrates more significant desulphurisation. Ni-MMO catalyst achieved 31.6 and 30.4% reduction relative to the feed for N_2 and H_2, respectively. What is indicated is that under a N_2 atmosphere, the tri-phasic metal oxide sheets favour asphaltene removal, and by extension sulphur removal given the higher abundance of heteroatoms in asphaltenes, from the liquid phase (24). While under a H_2 atmosphere, the petcoke formation is limited by the active hydrogen availability and polyaromatic removal is inhibited by the reduction and potential in-situ sulfidation of the metal sites. A higher yield of middle distillates and residue fractions at the expense of light naphtha is attained which proves that the amount of hydrogenation of higher molecular weight species increased. With this, an increased percentage of sulphur-bearing aromatics is likely to have been maintained in the liquid phase relative to the inert environment. Nonetheless, even under hydrogenation conditions the significance of using Ni-MMO is apparent. Relative to thermal upgrading, Ni-MMO achieved a further reduction in sulphur relative to the feed oil by 5.1 and 7.85% for N_2 and H_2 atmospheres, respectively.

Table 4.4 Sulphur analysis of liquid phase, obtained through titration.

Catalyst Condition	Sulphur %wt/wt	Reduction w.r.t feed (%)
Feed Oil	3.32	-
Thermal (N_2)	2.44	26.5
Thermal (H_2)	2.57	22.6
Ni-MMO (N_2)	2.27	31.6
Ni-MMO (H_2)	2.31	30.4
CoMo-A (N_2)	2.31	30.4
CoMo-A (H_2)	2.07	37.6

A difference of 4% in the petcoke produced between Ni-MMO (H_2) and Ni-MMO (N_2) has already been noted in the mass balance analysis. The highest amount of petcoke produced, at 10.4%, coincides with a reduction in sulphur, at 31.6% relative to the feed oil. Consequently, this may corroborate the idea that the sulphur is being transferred into the petcoke through polyaromatic sorption reactions rather than HDS, the reaction mechanism of a typical refinery catalyst such as CoMo-Al_2O_3. This is again demonstrated by the fact that the Ni-MMO (N_2) reaction regime favoured the lowest yield of asphaltenes.

When CoMo-Al_2O_3 is utilised in conjunction with H_2 gas, a significant increase in desulphurisation is apparent – a 37.6% reduction - pertaining to the HDS function of the in-situ activated cobalt and molybdenum species. The trend between N_2 and H_2 environments is reversed. Under a H_2 environment, the removal of sulphur is accommodated by the

liberation of hydrogen sulphide gas, owing to the HDS mechanism involving the sulphide-molybdenum slabs promoted by cobalt which is demonstrably a more effective desulphurising agent.

4.3.2.3 Effect of catalyst on viscosity and asphaltene content

It is clear that viscosity plays an instrumental role in assessing the value of the hydrocarbon oil. Ultimately, a high viscosity oil is difficult to transport as it contains a higher proportion of heavier, higher boiling point hydrocarbon fractions. Heavy oils are typically defined as oils with a viscosity greater than 200mPa·s which can extend up to 10,000mPa·s, above which is often defined as bitumen (derived from oil sands) (25). Where necessary and economically feasible, diluents such as naphtha and condensates are used to reduce the viscosity to below a typical maximum pipeline viscosity of 400 mPa·s (26). Consequently, any hydrocarbon upgrading process will aim to achieve a significantly lower viscosity relative to the feed oil. The viscosity of the oil however is inter-dependent on a number of factors which will be subsequently explored.

Asphaltenes should contribute towards the viscosity of an oil with the greatest significance (27). While the specific molecular architecture of asphaltenes remains highly diverse and poorly understood, asphaltenes are thought to compose polyaromatic cores with peripheral-aliphatic chains, and contain both highly polar and non-polar groups (21,24,28). The presence of asphaltenes in oil may lead to colloidal aggregates, a phenomenon leading to high viscosity of the oil and consequent problems such as wellbore and pipeline clogging.

They are, however, nominally designated as macromolecules precipitated by a given solvent during their extraction e.g. n-heptane precipitation (ASTM D4124). The generalisation exists because they are highly complex and can differ in structure greatly.

The feed oil viscosity of 811 mPa·s is greatly reduced by thermal upgrading to 7.5 mPa·s. This represents a huge reduction relative to the feed oil, which is highly beneficial to the sweep efficiency and production during its recovery and subsequent transportation. However, when using the catalysts under a N_2 atmosphere, the viscosity reduction increases further to 0.2 and 4.3 mPa·s for Ni-MMO and CoMo-alumina, respectively. Interestingly, when a H_2 reaction gas is added there is a conflicting relationship yielding a reduction in a further reduction in viscosity to 3.9 and 4.3 mPa·s with respect to thermal and the CoMo-alumina catalyst, but an increase in viscosity to 4.9 mPa·s for the Ni-MMO catalyst.

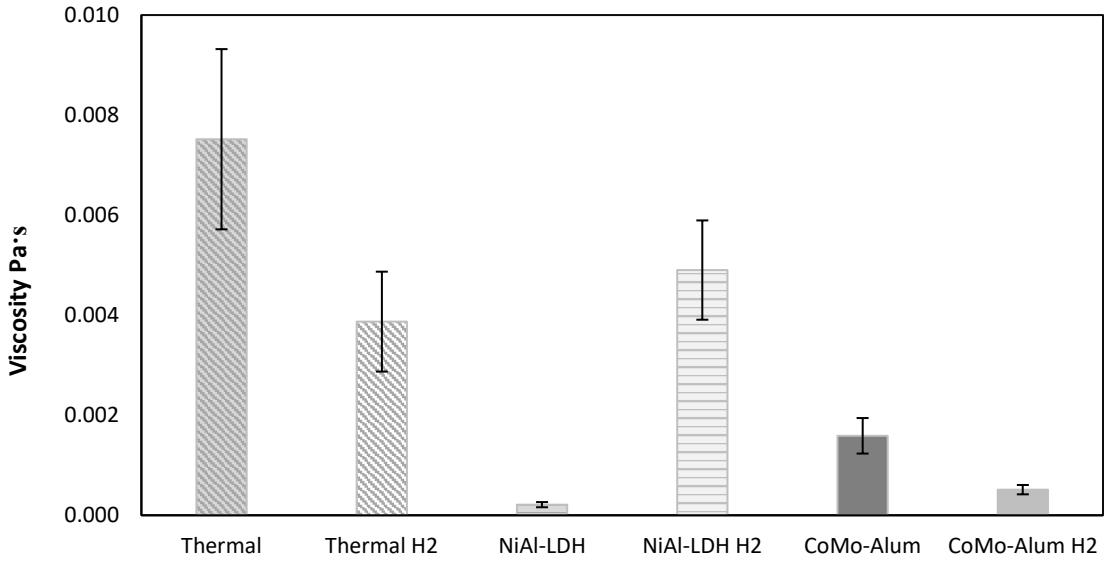

Figure 4.7 Viscosity of the upgraded oil as a function of catalyst type.

It must be noted that the comparatively small standard deviation with respect to Ni-MMO (N_2) corresponds to the fact that the viscosity generated is nearly two orders of magnitude less than the viscosity generated by Thermal (N_2). Taking this into account, the error is consistent with the other conditions.

It is clear that the liquid produced using Ni-MMO reflects chemical structures that allow the liquid to flow more easily. More to the point, the catalyst which produced the lowest yield of asphaltenes was Ni-MMO (N_2), with an average of 5.4%, while CoMo-Alumina (N_2) and thermal (N_2) yield averaged 6.4% and 7%, respectively. In previous research, the role of anionic clays has extended to aromatic removal (8). Consequently, the role of collapsed (delaminated) anionic clays may extend to adsorbents of asphaltenes. It has been demonstrated previously that a significant increase in asphaltene adsorption onto nano-particulated alumina occurs with an increasing NiO loading, suggesting it could be a valuable in-situ upgrading material for asphaltene removal (28). This explanation justifies a possible reaction mechanism for a decrease in viscosity following in-situ delamination of Ni-MMO, which produce several nickel and aluminium oxide phases. The increase in viscosity following the addition of H_2 as the reaction gas falls in-line with the increased asphaltene content of the oil. Under a H_2 environment, the asphaltene content was as follows, 10, 4.4 and 6.7%, for Ni-MMO, CoMo-Al_2O_3 and thermal, respectively. As such, it may be prudent to distinguish between two predominant roles of the Ni-MMO additive under both reaction gases. Firstly, under a N_2 atmosphere, the role of an asphaltene sorbent may be more significant, while under a reducing atmosphere of H_2, the hydrogenation reaction pathway may be more prominent, albeit less significant compared to a typical HDS catalyst. This

latter pathway is thought to cap the asphaltic radicals with activated hydrogen at the relevant metal active sites. This pathway can therefore be recognised as a method to suppress coke formation, which is proven by the corresponding mass balance, at the expense of having higher resistance to flow through pipelines and a higher asphaltene content which is deleterious to pipeline infrastructure.

4.3.2.4 Effect of catalyst on distillate products

Figure 4.8 highlights the relationship between percentage yield and TBP, achieved using an Agilent 8950 GC under a C7-C44 calibration mix and reference gas oil mix. When a heavy oil has been upgraded, either thermally or catalytically, the expectation is that higher boiling point fractions are converted into lower boiling point fractions. Accordingly, an expected shift to the left will be observed on percentage yield vs boiling point graph, thereby demonstrating a higher yield for the lower boiling point components.

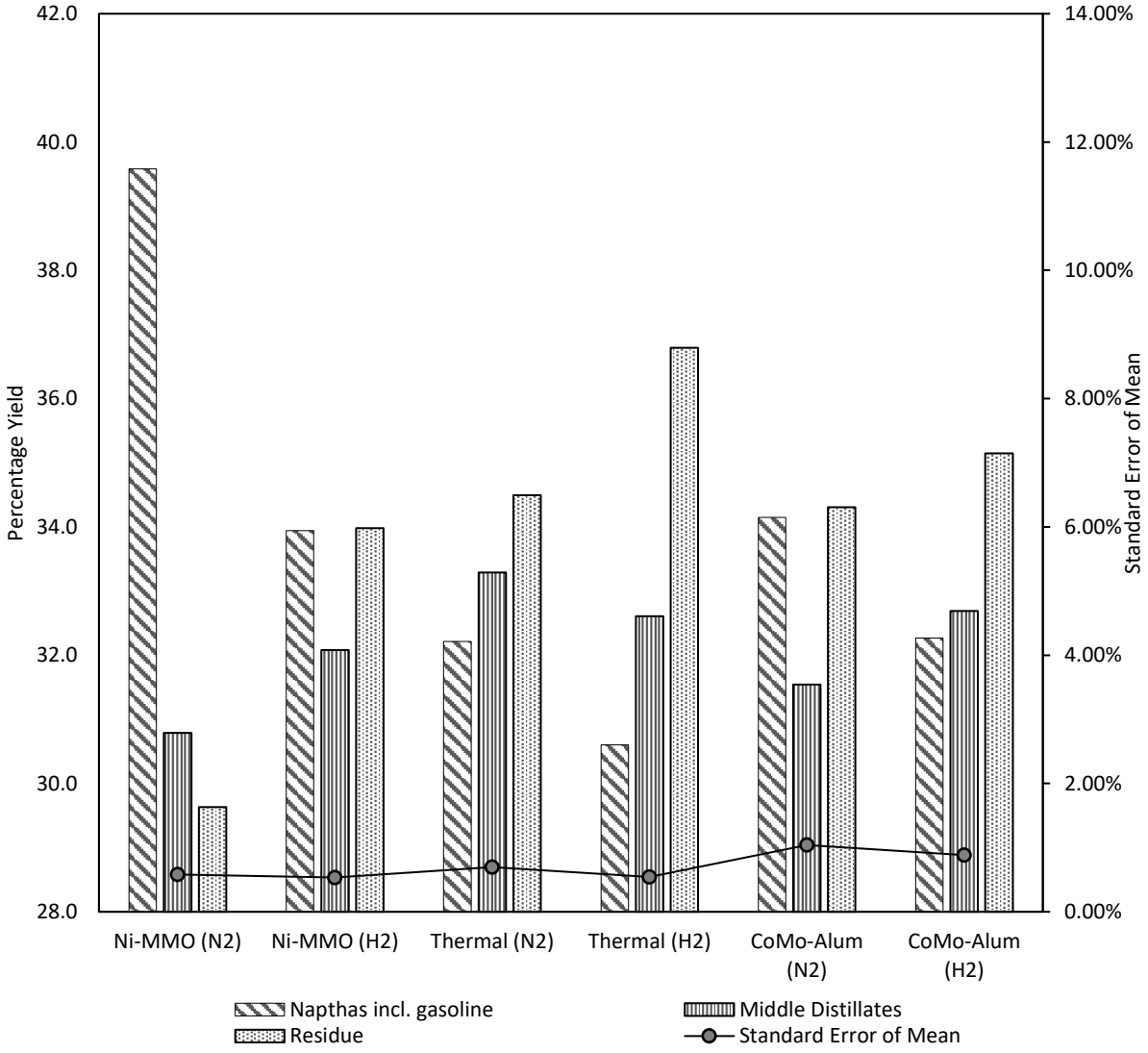

Figure 4.8 Distillate fractions by boiling point of upgraded liquid oil.

Simulated distillation results from Figure 4.8 highlight the following naphtha (gasoline) fraction trend: Ni-MMO (N_2)> CoMo-Al_2O_3 (N_2)> Ni-MMO (H_2)> Thermal (N_2)> CoMo-Al_2O_3 (H_2)> Thermal (H_2). The middle distillate fractions highlight the trend: Thermal (N_2)> CoMo-Al_2O_3 (H_2)> Thermal (H_2)> Ni-MMO (H_2)> CoMo-Al_2O_3 (N_2)> Ni-MMO (N_2). Finally, the residue

trend highlights: Thermal (H_2)> CoMo-Al_2O_3 (H_2)> Thermal (N_2)> CoMo-Al_2O_3 (N_2)> Ni-MMO (H_2)> Ni-MMO (N_2).

If this data is placed into the context of asphaltene content from Ni-MMO-derived liquid phase, what is shown is a clear correlation. With a lower asphaltene content, a higher yield of comparatively lighter molecules is produced. This is justified due to the relatively high boiling point of asphaltene macromolecules and the LDH's role of removing polyaromatics. Consequently, this corroborates the hypothesis that Ni-MMO (N_2) favours an upgrading reaction pathway as a polyaromatic sorbent due to the abundance of NiO sites. When drawing a comparison between Ni-MMO (N_2) and Ni-MMO (H_2), the results support the idea of abundant free radical stabilisation under a H_2 atmosphere. The notable increase in middle distillates by 1.3% and residue by 4.4% under H_2 supports the idea that active hydrogen species have been abstracted by the catalyst, stemming condensation reactions between hydrocarbon radicals, and thereby inhibiting the formation of mesophase and subsequently petroleum coke. Furthermore, with reference to the mass balance results using Ni-MMO, under a H_2 atmosphere, the liquid yield increased from 70.3 to 78.9% that further demonstrates the significance of activated hydrogen abstraction in inhibiting coke formation. It should, however, be noted that the fraction distribution is very similar to the distribution when using CoMo-alumina as the active catalyst. Given that the asphaltene content, however, was significantly higher than both the CoMo-alumina and thermal upgraded oil under the same conditions, it also signifies the importance of the different upgrading mechanism prevalent with the Ni-MMO catalyst compared to thermal upgrading.

When using the CoMo-alumina catalyst, again a similar but less significant correlation highlights an increase of middle distillates, by 1.2%, and heavy residues, by 0.8%, at the expense of light naphtha when using a H_2 reaction gas. Consequently, a similar hypothesis may be applied, indicating that wide-scale free radical termination was achieved under a H_2 atmosphere due to the abundance of active hydrogen species, while cracking was predominant under a N_2 atmosphere owing to the acidic sites present in the alumina support. The latter reaction condition consequently yielded a greater proportion of light naphtha, accompanied by a higher yield of coke, due to over-cracking and limited radical stabilisation (14), which is correctly highlighted in the mass balance.

Under a thermal reaction regime, the higher boiling point products are favoured when using H_2. This a result of activated H_2 acting as stabilising agents following C-C cleavage of the larger hydrocarbon molecules. Under a N_2 atmosphere, the lack of hydrogen accelerates over-cracking reactions leading to a higher proportion of light naphtha and gaseous products, the latter of which is demonstrated by the mass balance.

4.3.3 Effect of catalyst on petroleum coke

The following sections outline characterisation of the solid component using elemental analysis, SEM images and thermal stability of the coke. The properties of coke produced from the upgrading of hydrocarbon liquids are important to study as they can highlight a preferential reaction pathway for particular catalysts and operating conditions. Furthermore, from a refinery perspective there are important economic implications

governed by the coke properties. Various different coke morphologies exist including shot-type, associated shot-type, sponge-type and acicular-type (29,30). Depending on its grade, the coke may have value as fuel-grade i.e. blended with coal for use in power plants and also for use as electrode materials in aluminium manufacture. Additionally, there has been interest in using activated high-sulphur petroleum coke as a natural gas adsorbent to minimise the economic constraints on the transportation of natural gas, accommodated by cost-intensive technologies such as Compressed Natural Gas (CNG) or Liquified Natural Gas (LNG) (31). Secondly, the morphology of the coke produced can also affect the process capacity of a refinery (29). Shot-coke forms spherical-ellipsoidal shaped particles that are easily removed from units such as the delayed Coker drums, which can have a significant benefit on process economics.

4.3.3.1 Elemental Analysis (CHNS)

Elemental analysis of the resulting petroleum coke particles was studied once they were thoroughly washed with toluene solvent and vacuum dried to dissolve and remove all of the liquid hydrocarbon components. Elemental analysis of the solid residue left behind lead to significant insights into the chemical reactions taking place during upgrading.

Table 4.5 Elemental analysis of coke phase, obtained from CHNS combustion tube experiments.

Sample	Carbon (wt%)	Nitrogen (wt%)	Hydrogen (wt%)	Sulphur (wt%)	Hydrogen/carbon ratio
Thermal (N_2)	89.4	1.39	4.89	4.71	0.055
Thermal (H_2)	88.4	1.58	6.63	5.40	0.052
Ni-MMO (N_2)	85.7	1.38	4.54	8.39	0.053
Ni-MMO (H_2)	84.3	1.61	4.46	9.62	0.053
CoMo-A (N_2)	88.1	1.56	4.94	5.43	0.056

A significant trend given in the table above highlights the wt% of sulphur per unit mass of petcoke produced during the upgrading. The wt% of sulphur reduces in the following order Ni-MMO (H_2)> Ni-MMO> CoMo-alumina (H_2)> Thermal (H_2)> Thermal (N_2).

The increased sulphur content in the petcoke substantiates previous proposed mechanism of liquid desulphurisation in the presence of Ni-MMO, drawing parallels with Lakhova et al. (32). Once the removal of anions and interlayer water has been achieved, the LDH is subsequently left with positively-charged metal oxide layer in the form of Ni-MMO. The polyaromaticity of the oil is responsible for high polarity in heavy oils, largely in itself produced by heteroatoms such as sulphur. While Mostafa and Mohamed (8) have previously witnessed a role of CoMo-LDH as an additive to remove sulphur and polyaromaticity in heavy oils, the generation of Ni-MMO may provide this re-uptake of

sulphur-containing polyaromatics. The collapsed clay nuclei may subsequently agglomerate to form Ni-MMO and polyaromatic-containing epicentres that function to activate and remove additional deprotonated thiophenic-type components within the oil, thereby forming large petcoke composites enriched in sulphur species.

The slightly higher percentage of sulphur present in the coke produced during Ni-MMO under a H_2 atmosphere responds to the fact that as a percentage, the amount of coke produced was much lower and therefore the higher molecular weight sulphur becomes a more significant fraction. Given that the petcoke produced from the Ni-MMO (N_2) and (H_2) was 10.4% and 6.4%, of the total reaction products respectively, it can be calculated that the total quantity of sulphur in this coke is 0.87% and 0.62%, respectively when using the wt% data from the elemental analysis. Therefore, it can be deduced that the sulphur-containing components are preferentially removed from the reaction mixture by the Ni-MMO under N_2. While under a H_2 atmosphere, partial reduction of the mixed oxides may partially inhibit this fixing of sulphur species into the petcoke, while promoting the capping of asphaltic radicals. It has been reported that metal oxide catalysts have been used successfully in asphaltene sorption (21). This is in agreement with the reduced quantity of asphaltenes, middle distillates and residue fractions, in addition to the lower viscosity when using Ni-MMO under a N_2.

Looking at the H/C ratio, a slight decrease can be noticed from thermal upgrading to catalytic upgrading when using Ni-MMO (under N_2 atmosphere). This is interesting as it is well known that the coking process contributes to the transfer of hydrogen from the condensing residues and asphaltenes (10). The results therefore indicate that when using

the Ni-MMO there is increased efficiency in the transfer of the hydrogen. This agrees with the presence of Lewis basic O^{2-} active sites on the Ni-MMO. This thereby improves the quality of the oil and corroborates with the viscosity data.

4.3.3.2 Morphology of petroleum coke

Analysing the SEM images of the petcoke, shown in Figure 4.9 (a-d), it is clear that thermal and Ni-MMO-derived coke types comprise these small (semi-)spherical coke particles, indicating the formation of shot-type coke. However, the CoMo-Al_2O_3-derived petcoke demonstrates a large proportion of mm-scale sponge-type properties. A highly fractured morphology with a multiplicity of pores and bubbles can be seen in Figure 4.9 (e-f), lending itself to the sponge-type coke classification.

Shot-type of coke is typically formed in delayed Coker units. In this instance, it is thought to be formed when both existent and cracked light ends volatilise during the upgrading, leaving a suspension of spherical-shaped heavy tar droplets. The highly exothermic reaction of asphaltene polymerisation is thought to contribute the heat required to generate this coke classification, while aided by the turbulent conditions resultant from high fluid velocities under agitation (30). The viscosity of the droplets increases dramatically forming immature coke balls; fail to reintegrate into the bulk liquid phase essentially fixing this macroscopic phase of petcoke. While under thermal upgrading it is expected that shot-type coke is produced, the generation of similar petcoke under Ni-MMO highlights an economic advantage over the coke produced by CoMo-alumina. Furthermore, the mechanism of coke

formation clearly diverges from conventional catalyst, which can be summarised as the fixing of larger polyaromatic compounds out of solution into the Ni-MMO-polyaromatic hybrid epicentres, accommodating an intense pseudo-coking reaction.

The SEM images in Figure 4.9 highlight slight differences in morphological texture between the two shot-type petcokes. Bonding between a proportion of the particles is produced under thermal upgrading. This is suggestive of bonded or matrix-shot according to Siskin et

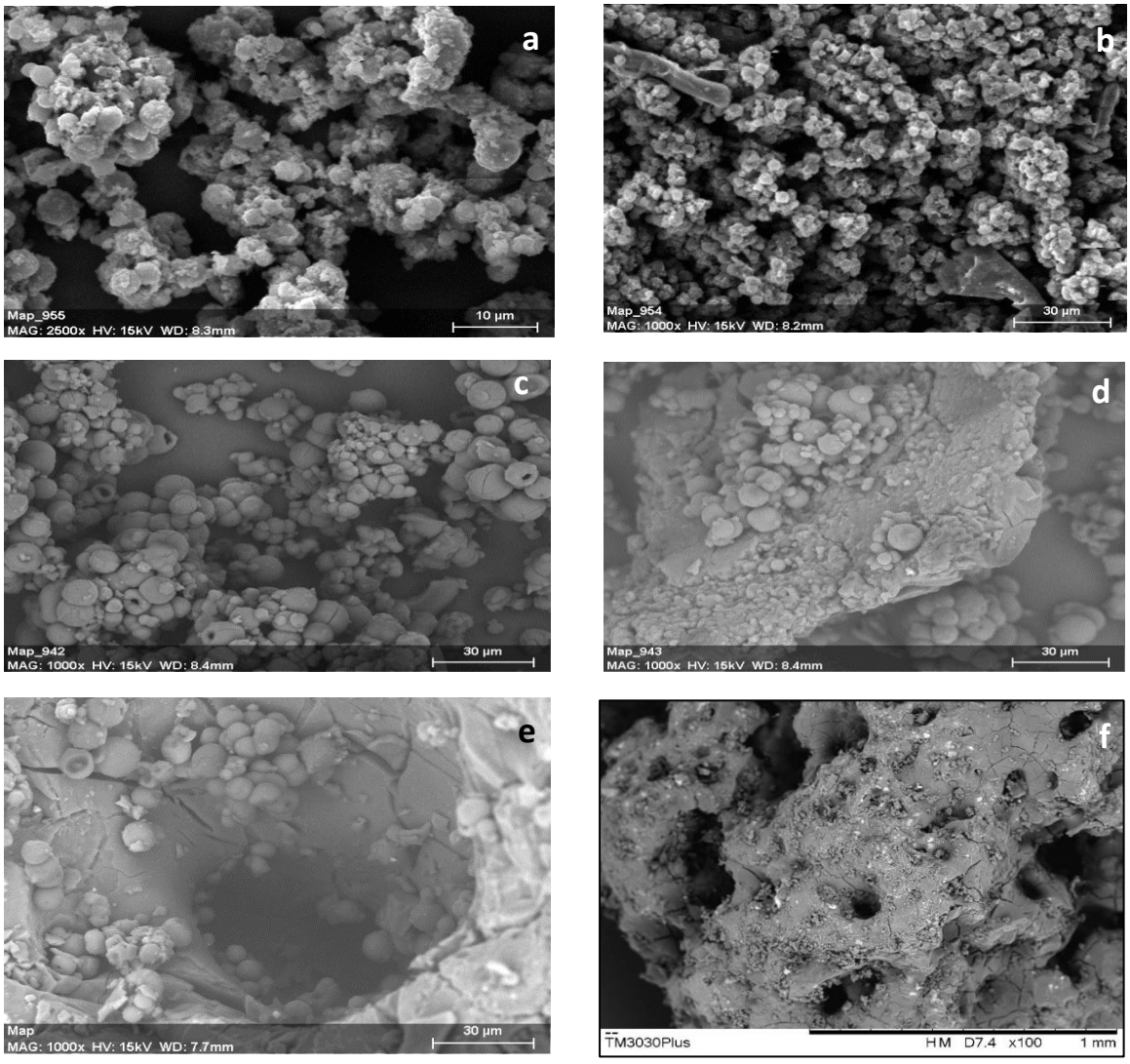

Figure 4.9 SEM of petcokes with respective magnifications (a) NiAl-LDH at x2500 (b) NiAl-LDH at x1000 (c) Thermal at x1000 (d) Thermal at x1000 (e) CoMo-Alumina at x1000 (f) CoMo-Alumina at x100.

al. (29), whereas under Ni-MMO catalyst treatment, the coke appears mainly as agglomerated or clustered coke. An additional difference between Ni-MMO and thermal petcoke presides over the relative morphological smoothness of the particles. Looking at the thermal-derived petcoke images, the particles are highly spherical with relative smooth surfaces, while the particles generated with the Ni-MMO catalyst, although too resemble microspheres, are observed as less rounded with a rougher surface morphology. This is suggestive of the difference in C:H and C:S ratios highlighted in the elemental analysis. Ibrahim (30) reviews the form of carbon comprising the shot-type coke, highlighting its lenticular concentric pattern giving rise to non-linear, rounded microstructures. However, if the sulphur content is particularly high via adsorbed sulphur and related polyaromatic species, this may disrupt the smooth non-linear pattern, thereby generating rough structures forming semi spherical coke particles.

4.3.3.3 TGA of produced petroleum coke

Figure 4.10 demonstrates the relationship between change in mass (%), temperature (˚C) and rate of mass change when the petcoke is exposed to ramping temperature up to 900˚C at a rate of 10˚C/min in the presence of air. What can be observed are clear thermal decomposition curves generating gaseous products. There is an obvious difference between burn off curves relating to the catalyst condition. The difference in burn off curves is suggestive of the structures present within the petcoke samples. When assessing the peaks on the rate of mass loss curves, the peaks for thermal upgrading is much broader, indicating

that certain species prevalent within this petcoke require a higher temperature for oxidation.

A clear observation is the symmetry of the thermal and CoMo-Al_2O_3 burn off curves, while that of the Ni-MMO-derived coke yields an alternative burn off curve profile. The mass loss curve representing this latter catalyst condition peaks sharply at 498℃ before undergoing a

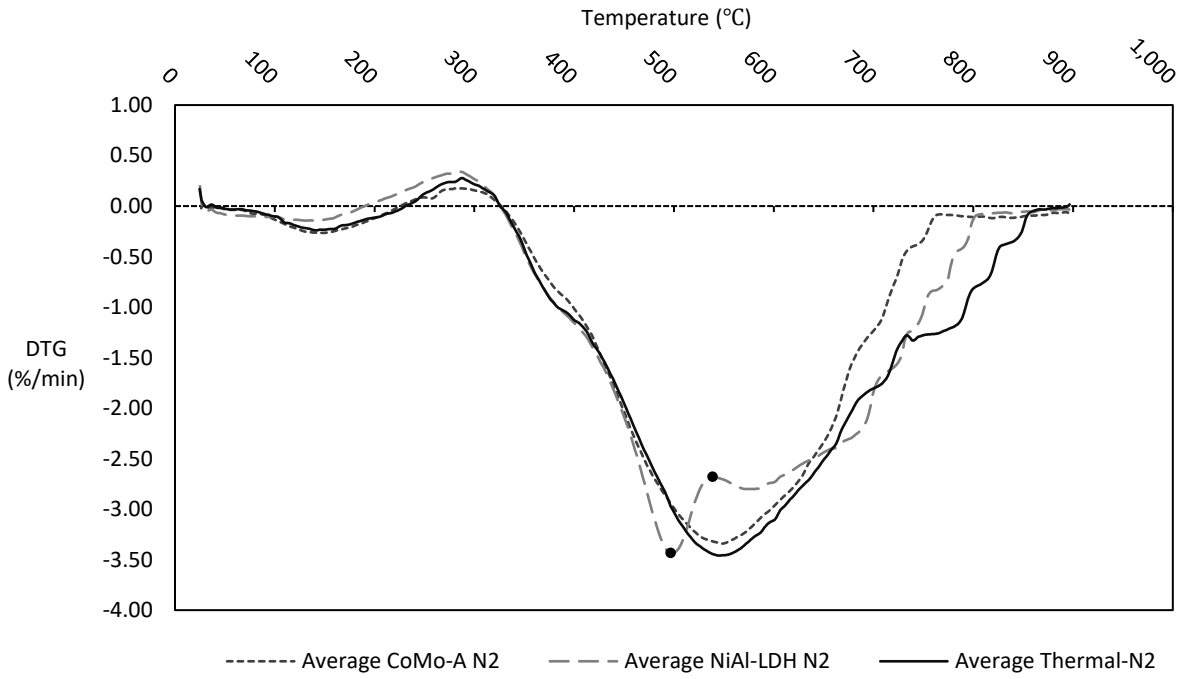

Figure 4.10 Thermo-gravimetric analysis of the produced coke, after residue and asphaltenes have been dissolved out using toluene and subsequent drying under vacuum filtration.

sharp reduction in the rate of mass loss from a peak of -3.44%/min to approximately -2.68%/min. The consistency of the Ni-MMO-derived curve is highlighted by the standard deviations for both the temperatures and rates of mass loss for the distinct peak and subsequent inflection over the three repeats. These points are indicated by the successive black circles in Figure 4.10 with the standard deviations calculated at 8.94℃, 0.21%/min and

6.75℃, 0.2%/min, respectively. Additionally, this mass loss curve is shifted to the right from 638℃, relative to the CoMo-Al_2O_3-derived curve. This relates to the fact that a higher proportion of the petcoke components is present which have a higher oxidation temperature. Organic sulphur in the petcoke can be present in many forms. Thiophenes are typically responsible for a large proportion of the sulphur content and are attached to the aromatic skeleton of the petcoke. Sulphur may also be present as side-chains of polycyclic-aromatics and naphthenic molecules. However, the inorganic sulphur can be present on the coke surface (32). The abundance of sulphur in the Ni-MMO-derived petcoke poses an explanation for the differences in these burn-off profiles. Additionally, the preferential polyaromatic removal pathway of the Ni-MMO is clearly reflected in the curve shift to the right relative to CoMo-Al_2O_3-derived petcoke. This corresponds to an increase in higher oxidation temperature hydrocarbons.

Consequently, the difference in burn off curves highlights the problems associated with subscription to the methodology in which a set temperature range is applied and the mass loss within this range is assumed to be the petcoke. This latter method has been widely used in earlier works and therefore fails to discriminate between the various elemental and structural properties of different petcoke types (4,12,15). Consequently, this technique has limitations which can lead to unnecessary inaccuracies. Therefore, petcoke from each upgrading reaction type should be individually analysed so that accurate inferences may be made about the elemental constituents and structure of the petcoke. Moreover, it has been highlighted previously that the TGA curves of spent hydroprocessing catalyst and asphaltenes extracted using the n-heptane solvent method (ASTM D3279) show oxidation in

the same region which suggests TGA alone cannot be used to differentiate between the two components, asphaltene and coke (34). This re-enforces the need for adequate toluene washing to remove the components that do not represent petcoke.

4.4 Conclusions

The challenges facing the refining of heavier oil feeds has led to the investigation of an alternative, economical catalyst. Catalytic upgrading was carried out in a stirred batch reactor, conditions of which were taken from a previously established optimisation study relating specifically to the THAI-CAPRI method, an in-situ thermal EOR incorporating a pelleted catalyst fixed-bed. A high-surface area Ni-enriched Mixed Metal Oxides (Ni-MMO) catalyst was used as an ultradispersed variation of the fixed-bed production liner, simulating upgrading with a different contacting pattern. The Ni-MMO was compared with a hydroprocessing catalyst, CoMo-Al_2O_3 and thermal upgrading under N_2 and H_2 atmospheres. The results show that the Ni-MMO catalyst condition was the most sensitive to the atmosphere composition. Ni-MMO (N_2) proved to generate the lowest liquid phase viscosity at 0.2 mPa·s coupled with the highest percentage of light naphtha at 39.6%. Subsequent elemental analysis on the Ni-MMO (N_2) and -(H_2) derived petcoke has shown quantities of sulphur of 0.87 wt% and 0.62 wt%, respectively. Ni-MMO (N_2) produced NiO following dehydration and dehydroxylation. This led to the formation of pseudo-petcoke nuclei by providing adsorption sites for sulphur-rich poly-aromatic components, stimulating a significant desulphurisation pathway. This was accompanied by a significant increase in the

gas and coke phases at 10.6 and 18.3%, respectively. Conversely, for Ni-MMO (H_2) the sulphur content of the coke reduced by 29.0% to a total 0.62 wt%. The presence of hydrogen partially reduced the catalyst, stimulating hydrogenation reactions which act to cap radical adducts and prevent the formation of mesophase. This is evidenced by the increase in liquid phase by 12.2% and a reduction of petcoke and gas phases to 6.4 and 13.8%, respectively. It is therefore clear that the introduction of a suitable hydrogen donor during THAI-CAPRI will increase the quantity of liquid phase. Furthermore, the refinery catalyst demonstrated the most significant reduction, by 37.6%, in liquid sulphur phase activity. However, with subsequent manipulation of both the LDH precursor and modification to the resultant Ni-MMO, an increased catalytic upgrading activity of may pave the way for more economical and easily synthesised catalysts in the subsurface and surface refining industry.

4.5 References

[1] BP. BP Energy Outlook 2018 edition. 2018.

[2] Meyer RF, Attanasi ED, Freeman PA. Heavy oil and natural bitumen resources in geological basins of the world. US Geol Surv 2007;Open File-:36. doi:10.1007/BF01944169.

[3] Xia TX, Greaves M. In situ upgrading of Athabasca Tar Sand bitumen using THAI. Chem Eng Res Des 2006;84:856–64. doi:10.1205/cherd.04192.

[4] Al-Marshed A, Hart A, Leeke G, Greaves M, Wood J. Optimization of Heavy Oil

Upgrading Using Dispersed Nanoparticulate Iron Oxide as a Catalyst. Energy and Fuels 2015;29:6306–16. doi:10.1021/acs.energyfuels.5b01451.

[5] (EPA) EPA. Control of Air Pollution From Motor Vehicles: Tier 3 Motor Vehicle Emission and Fuel Standards AGENCY: Environmental Protect 2014;79.

[6] Cavani F, Trifirò F, Vaccari A. Hydrotalcite-type anionic clays: Preparation, properties and applications. Catal Today 1991;11:173–301. doi:10.1016/0920-5861(91)80068-K.

[7] Clause O, Goncalves Coelho M, Gazzano M, Matteuzzi D, Trifirò F, Vaccari A. Synthesis and thermal reactivity of nickel-containing anionic clays. Appl Clay Sci 1993;8:169–86. doi:10.1016/0169-1317(93)90035-Y.

[8] Mostafa MS, Mohamed NH. Towards novel adsorptive nanomaterials: Synthesis of Co2+Mo6+ LDH for sulfur and aromatic removal from crude petrolatum. Egypt J Pet 2016;25:221–7. doi:10.1016/j.ejpe.2015.05.013.

[9] Zhao R, Yin C, Zhao H, Liu C. Synthesis, characterization, and application of hydotalcites in hydrodesulfurization of FCC gasoline. Fuel Process Technol 2003;81:201–9. doi:10.1016/S0378-3820(03)00012-2.

[10] Rana MS, Sámano V, Ancheyta J, Diaz JAI. A review of recent advances on process technologies for upgrading of heavy oils and residua. Fuel 2007;86:1216–31. doi:10.1016/j.fuel.2006.08.004.

[11] Gray MR. Upgrading Oilsands Bitumen and Heavy Oil. The University of Alberta Press; 2015.

[12] Hart A, Greaves M, Wood J. fixed-bed and dispersed catalytic upgrading of heavy crude oil using-CAPRI. Chemical Engineering Journal. 2015;282:213–23. doi: 10.1016/j.cej.2015.01.101

[13] Hart A, Leeke G, Greaves M, Wood J. Down-hole heavy crude oil upgrading by CAPRI: Effect of hydrogen and methane gases upon upgrading and coke formation. Fuel 2014;119:226–35. doi:10.1016/j.fuel.2013.11.048.

[14] Hart A, Omajali JB, Murray AJ, MacAskie LE, Greaves M, Wood J. Comparison of the effects of dispersed noble metal (Pd) biomass supported catalysts with typical hydrogenation (Pd/C, Pd/Al2O3) and hydrotreatment catalysts (CoMo/Al2O3) for in-situ heavy oil upgrading with Toe-to-Heel Air Injection (THAI). Fuel 2016;180:367–76. doi:10.1016/j.fuel.2016.04.064.

[15] Brown AR, Hart A, Coker VS, Lloyd JR, Wood J. Upgrading of heavy oil by dispersed biogenic magnetite catalysts. Fuel 2016;185:442–8. doi:10.1016/j.fuel.2016.08.015.

[16] Bi W, McCaffrey WC, Gray MR. Agglomeration and deposition of coke during cracking of petroleum vacuum residue. Energy and Fuels 2007;21:1205–11. doi:10.1021/ef0602630.

[17] Zarezadeh-Mehrizi M, Afshar Ebrahimi A, Rahimi A. Comparison of γ and δ-Al2O3 supported CoMo catalysts in the hydrodesulphurisation of straight-run gas oil. Sharif University of Technology 2019;26:1555-1565. doi:10.24200/sci.2019.50969.1948

[18] IHS. Light and Heavy Naphtha : International Market Analysis. 2017.

[19] Hunter KC, East ALL. Properties of C - C Bonds in n -Alkanes : Relevance to Cracking Mechanisms. J. Phs. Chem. A 2002:1346–56. doi: 10.1021/jp0129030

[20] Hart A, Lewis C, White T, Greaves M, Wood J. Effect of cyclohexane as hydrogen-donor in ultradispersed catalytic upgrading of heavy oil. Fuel Process Technol 2015;138:724–33. doi:10.1016/j.fuproc.2015.07.016.

[21] Franco C, Patiño E, Benjumea P, Ruiz MA, Cortés FB. Kinetic and thermodynamic equilibrium of asphaltenes sorption onto nanoparticles of nickel oxide supported on nanoparticulated alumina. Fuel 2013;105:408–14. doi:10.1016/j.fuel.2012.06.022.

[22] Hart A, Shah A, Leeke G, Greaves M, Wood J. Optimization of the CAPRI process for heavy oil upgrading: Effect of hydrogen and guard bed. Ind Eng Chem Res 2013;52:15394–406. doi:10.1021/ie400661x.

[23] Javadli R, De Klerk A. Desulfurization of heavy oil-oxidative desulfurization (ODS) as potential upgrading pathway for oil sands derived bitumen. Energy and Fuels 2012;26:594–602. doi:10.1021/ef201448d.

[24] Mckenna AM, Marshall AG, Rodgers RP. Heavy Petroleum Composition. 4. Asphaltene Compositional Space 2013. doi:10.1021/ef301747d.

[25] Hart A. The novel THAI–CAPRI technology and its comparison to other thermal methods for heavy oil recovery and upgrading. J Pet Explor Prod Technol 2014;4:427–37. doi:10.1007/s13202-013-0096-4.

[26] Gateau P, Hénaut I, Barré L, Argillier JF. Heavy Oil Dilution. Oil & Gas Science and

Technology 2004;59:503–9. doi: 10.2516/ogst:2004035

[27] Ilyin S, Arinina M, Polyakova M, Bondarenko G, Konstantinov I, Kulichikhin V, et al. Asphaltenes in heavy crude oil: Designation, precipitation, solutions, and effects on viscosity. J Pet Sci Eng 2016;147:211–7. doi:10.1016/j.petrol.2016.06.020.

[28] Franco CA, Nassar NN, Montoya T, Ruíz MA, Cortés FB. Influence of asphaltene aggregation on the adsorption and catalytic behavior of nanoparticles. Energy and Fuels 2015;29:1610-1621. doi:10.1021/ef502786e.

[29] Siskin M, Kelemen SR, Gorbaty ML, Ferrughelli DT, Brown LD, Eppig CP, et al. Chemical approach to control morphology of coke produced in delayed coking. Energy and Fuels 2006;20:2117–24. doi:10.1021/ef060261f.

[30] Ibrahim HA. Thermal Treatment of Syrian Shot Coke. Recent Advances in Petrochemical Science (RAPSCI). 2017;2:1–5. doi: 10.19080/RAPSCI.2017.02.555588

[31] Zhang H, Chen J, Guo S. Preparation of natural gas adsorbents from high-sulfur petroleum coke. Fuel 2008;87:304–11. doi:10.1016/j.fuel.2007.05.002.

[32] Lakhova A, Petrov S, Ibragimova D, Kayukova G, Safiulina A, Shinkarev A, et al. Aquathermolysis of heavy oil using nano oxides of metals. J Pet Sci Eng 2017;153:385–90. doi:10.1016/j.petrol.2017.02.015.

[33] Birghila S, Carazeanu I. Evaluation of the Physical-Chemical Properties in Petroleum Coke 2013;6:28–31. doi:10.3968/j.aped.1925543820130602.1758.

[34] Barman BN, Skarlos L, Kushner DJ. Simultaneous determination of oil and coke

contents in spent hydroprocessing catalyst by thermogravimetry. Energy and Fuels 1997;11:593–5. doi:10.1021/ef9601632.

Chapter 5

Comparative study on the hydrogenation of naphthalene over both alumina-supported and anionic clay-derived MMO-supported Mo catalysts

5.1 Introduction

Polyaromatic Hydrocarbons (PAH) comprise the organic group containing two or more aromatic rings bonded together. These compounds represent a deleterious fraction in hydrocarbon fuels, leading to an incomplete combustion and consequently soot production, in addition to a reduction of the cetane number in diesel fuels (1). Environmental legislation is turning towards ever more stricter guidelines that include reducing such compounds (2). These compounds are prevalent in lower quality heavy oils. A unique conceptualisation of the In Situ Combustion (ISC) process utilises a horizontal well with catalyst pellets packed in the annular space. This is known as the Toe-to-Heel Air Injection and Catalytic Process In-situ process (THAI-CAPRI) (3), which has the potential to emanate refinery units such as primary and secondary stage hydrotreating reactors given the complex temperature zones up to 450 ℃. This is particularly relevant at lower temperatures observed under the wet-mode ISC conditions in addition to thermal EOR mechanisms such as In Situ Upgrading Technology (ISUT) which generates fields of temperature zones reaching 320 ℃ (4,5). However, identifying a material which could adequately refine or remove PAH compounds at a relatively price competitive margin promotes further investigation into the use of this technology.

While the PAH components in heavy oil typically involve very complex molecules, the use of a model compound such as naphthalene is useful to understand the selectivity and pathways governing polyaromatic group hydrogenation (6). Tetrahydronaphthalene (tetralin), a hydrogenated derivative of naphthalene, has been used previously to represent deleterious aromatics in fuel feeds (7). Hydrogenation of this molecule leads to- the formation of both cis- and trans-decahydronaphthalene (decalin) via the intermediate pathway involving octahydronaphthalene ($\Delta^{1,9}$ – octalin). These two products, however, comprise contrasting reactivities to ring-opening and ring-contraction.

Cis-decalin is far less thermodynamically stable, which results in greater selectivity to ring-opening reactions via selective hydrodecyclisation (8). This conversion process results in the production of alkylated single-ring naphthenes, from multi-ting naphthene precursors such as decalin, generating an improved cetane number (9). Consequently, this justifies the effort to maintain a high cis/trans -decalin ratio. In previous works, the impact of tetralin concentration on the cis/trans ratio was shown to be negligible until most of the tetralin had undergone hydrogenation (10). Upon reaching the high conversion, the cis/trans ratio approached an equilibrium. It was suggested that the competition for catalytic adsorption sites was responsible for inhibiting cis to trans isomerization up until significant tetralin conversion. Wang et al. (11) synthesized a chromium-based Metal Organic Framework (MOF) for use in tetralin hydrogenation reactions spanning 140 to 220 ℃ across a range of 30 to 70 bar H_2. The results indicated that a highly enriched cis/trans ratio was achieved

across all levels of tetralin conversion, due to a greater adsorption facility for tetralin by the highly porous MOF support.

The choice of catalytic material is important as it can significantly affect the adsorption and dissociation energy barriers required for hydrogen activation and subsequent hydrogenation of the target molecule (12). Previous studies have examined the effect of hydrogen activation of individual Pd atom surface sites and the impact of particle size and dispersion on observed chemistry. A study conducted by Yu et al. (13) summarized the beneficial impact of contiguous Pd active sites over a bimetallic catalyst, facilitating a greater dissociative adsorption of hydrogen over a bimetallic catalyst. It was suggested that the contiguous Pd sites could be retained through either heat treatment or depositing a greater coverage of Pd. It has been found that when embedding Pd into Au, monomers are prevalent at lower coverages while an increased coverage generates clusters of Pd which can have an impact on dissociation, spill over and desorption of hydrogen (12).

Most catalytic studies in this area of oil processing focus on second-stage hydrotreating (HDT) and hydrogenation (HYD) reactions using noble metals deposited over protonic supports (14,15). This includes Al_2O_3-supported platinum and palladium catalysts (10). This electron-deficiency, however, can result in over-cracking and an overproduction of coke and catalyst deactivation. This can be mitigated by using more neutral supports such as silica-alumina supported noble metals or non-acidic supports (16–20). Works using supports such as zirconium-doped mesoporous silica have been used in the hydrogenation of tetralin, highlighting very active catalysis at 350 ℃ and 6.0 MPa hydrogen pressure (21). Research has also recently been undertaken to assess the impact of both noble and group VI metals

over basic carriers in both HYD and hydrodesulfurisation (HDS) reactions (8,22–25). It has been shown that a 2 wt.% concentration of alkaline-earth metals dispersed over the conventional acidic support led to greater activity of the platinum during the hydrogenation reaction of naphthalene (8). The works in Escobar et al. (8) added to previous experimental work wherein basic supports were investigated and hypothesized to interact with the metallic Ru nanoparticles, producing dual-site heterolytic hydrogen splitting and surface ionic hydrogenation pathways (24). Bimetallic Pd-Pt catalysts supported by Mg-Al mixed oxide was also synthesized to assess its activity for hydrogenation and hydrogenolysis of high molecular weight compounds as well as its thio-resistance, a necessary property given the presence of S-containing compounds in hydrotreated feeds (26). The results indicated that the catalyst exhibited high activity to decalin production, however, upon decreasing the Pd/Pt ratio the hydrogenation products decreased while the role of Pt-catalyzed hydrogenolysis reactions increased. Furthermore, hydrogenolysis reactions did not contribute to the formation of tar which was in turn attributed to the lack of strong BrØnsted acid sites exhibited by the basic mixed oxide support. Previous works have adopted a pseudo first order kinetic constant regime with respect to naphthalene concentration during the comparison of the catalysts (8,20).

Previous studies (8) have generated encouraging results which have prompted an assessment of whether a novel Mo-doped Ni-enriched Mixed Metal Oxide (Mo-MMO) could provide an economical alternative to naphthalene hydrogenation, a compound used to represent deleterious compounds found in heavier oil reservoirs and thereby directed for refinement in first and second-stage HDT and HDA units. Layered Double Hydroxides (LDH)-

derived mixed metal oxides (MMOs) have been largely studied in the literature in various reactions, owing to their tunability, resulting in variations in electronic configuration, dispersion and surface area and reducibility, which have fundamental impacts on their performance as catalysts (27,28). Furthermore, the synthesis of LDHs remains an inexpensive alternative to typical highly tuned supports, due to the relative ease of coprecipitation and the ability to use a variety of waste streams for metal salt precursors (29,30). The MMOs that are obtained following LDH heat treatment generate a high surface area, homogenous solid solution of oxides which can have shown to be appropriate catalytic supports for HDT reactions (31).

LDH-derived MgAl(O) supports have previously been the subject of a series of successful HYD experiments using the toluene model compound (32). This study uniquely explores the possibility of using Ni-enriched, LDH-derived MMOs as supports doped with Pd and Mo using the incipient wetness impregnation technique.

This study seeks to constrain the reaction rate constant kinetic parameters from batch reactor experiments involving Ni, Mo and Pd-bearing catalysts on naphthalene hydrogenation to tetralin and decalin. A comparison of cis/trans-decalin ratios is made as a function of tetralin conversion during the hydrogenation reaction highlighting the apparent differences between the metal classes and both basic and acidic-enriched support materials introduced into the reaction. This provides insights into how effectively the catalysts can generate the compound, cis-decalin, which is more easily upgraded during further hydrodecyclisation treatment.

5.2 Experimental

5.2.1 Catalyst synthesis

A Ni-enriched LDH was synthesized using the co-precipitation method. Two metal salts $Ni(NO_3)_2{\cdot}6H_2O$ and $Al(NO_3)_3{\cdot}9H_2O$, were added to distilled water in the appropriate molar ratios to reach a 3.3:1 Ni:Al ratio in a 0.3M 200mL. The metal salt solution was sequentially pumped into a second solution containing sodium carbonate adhering to the appropriate ratio $[CO_3^{2-}]/[M^{3+}]$ = 0.5, to commence the in situ formulation of anionic clay. A NaOH solution was used to control the pH to promote LDH precipitation in a pH range of 9 to 10 and a stirring speed was set at 500 rpm. Precipitation occurred over the period of 12 h at 60 ℃ to promote adequate crystallization.

Following this precipitation and crystallization procedure, the resultant LDH was washed with deionized water to remove impurities. The samples were subsequently calcined at 450℃ for 4 h using a heating ramp rate of 10 ℃ min^{-1}. Following this oxidation process, the resultant Ni-MMO was doped with Mo under incipient wetness impregnation in an excess of toluene. A $MoCl_5$ (anhydrous) salt was added in the appropriate ratio to achieve 10 wt% Mo. This method was carried out under constant stirring and a temperature of 60℃ for 12 h. Upon completion of the Mo-impregnation, the resultant Mo-doped MMO was calcined in air at a temperature of 450℃ for 4 h using a ramp rate of 10 ℃ min^{-1}, to remove any remaining impurities. The process was repeated for the generation of a Pd-MMO species using $PdCl_2$ salt.

The Pd/Al_2O_3 catalysts are a pre-formulated series of industry catalysts containing 1 wt%, 2 wt% and 5 wt% Pd, defined in previous studies and characterized in section 5.2.2 (33,34).

5.2.2 Catalyst Characterisation

A Bruker D2 X-ray diffractometer (cobalt source and nickel filter) was used to generate Powder X-ray Diffraction (PXRD) patterns. The method included a scan speed of 30 min with a step size of 0.370 over a 2-theta range 10-100˚ to determine the atomic arrangement of the mineral crystals.

Changes to the catalyst structure as the temperature increased during calcination were analyzed using a NETZSCH TG 209 F1 to obtain a detailed Thermo-Gravimetric Analysis (TGA). The method required 22 mg of catalyst set into a platinum crucible, with a heating rate of 10 K min^{-1} from 25℃ to the maximum temperature of 900℃, under a constant flow set at 10 mL min^{-1} of air.

XRF was conducted on the sample using a S8 TIGER equipped with a high intensity 4 kW Rhodium X-ray tube, two collimators at 0.23° and 0.46° and five analyzer crystals. Confirmation of the elemental constituents following impregnation of the molybdenum species was obtained.

BET analysis was performed using a Micromeritics ASAP2020 at the University of Warwick. To sufficiently evacuate the pores in the catalysts, the degassing procedure involved heating the samples to 350℃ and holding for a duration of 6 hours.

Temperature Programmed Reduction (TPR) and Desorption (TPD), performed by University of Manchester, to evaluate the reduction temperature of the Ni-MMO and number of acid sites present in the catalyst, respectively. The method included loading 20 mg of the catalyst into a quartz U-tube reactor and analyzing the sample using

a Quantachrome ChemBet Pulsar equipped with a Thermal Conductivity Detector (TCD). The temperature ramp programme included room temperature to 900℃ at a rate of 10℃ min^{-1}while simultaneously recording the intensity of H_2 uptake, the source of which was a H_2 5% in Ar gas mix. A NH_3 5% in He gas mix was substituted into the apparatus when carrying out the TPD measurements. In this instance, approximately 40 mg of the catalyst was heated under He to 300 ℃ prior to holding for the duration of 1 h and subsequently cooling to room temperature. The NH_3 5% gas mix was then introduced for 2 h, followed by the replacement of the He gas, and a ramping programme as before from room temperature to 900 ℃ under a 10 ℃ min^{-1} ramp rate.

The distribution of the active metal species in the catalysts was mapped using an Hitachi TM3030 Scanning Electron Microscopy (SEM) and Energy Dispersive X-ray spectrometer (EDS). A carbon disc was used to mount the sample.

5.2.3 Naphthalene hydrogenation

The reaction was conducted in a 100 mL stainless steel Anton Parr batch reactor, conditions of which were chosen to reflect second-stage hydrotreating as use in previous work (8), at a fixed temperature of 250℃, a stirring speed of 1000 rpm, a H_2 atmosphere of 40 bar and catalyst to reactant ratio of 0.12g/0.18g, raising to 0.24g/0.18g with the Ni and Mo catalysts, while the synthesized Mo-MMO catalyst was also used in a single loading 0.12g/0.18g to investigate the cis and trans decalin relationship. The high H_2 pressure can also be equated to subsurface near-wellbore zones, where rapid dehydrogenation could theoretically take place in addition to concentrated hydrogen donor solvent injections. The stirring speed was

selected to eliminate diffusion limitations prevalent in the three-phase heterogeneous reaction and therefore ensure the experiments were under direct kinetic control. During the 20 min heating-up stage, a N_2 atmosphere was added to prevent any reaction prior to the reaction temperature set-point of 250℃. At this temperature a 0.5mL vial was collected and analyzed to confirm the initial concentration of the reactants corresponded with the solution prior to heating. The N_2 was released and H_2 at 40 bar was added to the reaction vessel. This was denoted as the time for reaction commencement. Liquor from the reaction was collected in vials at 20 min intervals for a 2 h period. The progression of the reaction was measured while the rate constants, k_1 and k_2 were derived reaction using a pseudo-first order kinetic model. The pressure was maintained at 40 bar and each vial collected represented a homogenous solution of suspended catalyst, reactant and product compounds at each time point.

All liquid samples were filtered using a micromembrane to remove the catalyst particles, generating a clear liquid. The residual samples were then analyzed using Agilent Technologies 6890N GC with a corresponding 7683 B Series injector. An Agilent 19091J-413 capillary column (nominal length, diameter and film thickness at 30.0m, 320.0 µm and 0.25 µm, respectively) was used accompanied with the following method: equilibration time of 3 min, with a ramp from 80℃ to 135℃ over 9 min and second stage to 300 ℃ over 4 min. The components were separated according to boiling point. The identified reaction products using the GC included first and second stage hydrogenation products, tetralin, cis decalin and trans decalin, respectively. Five-point calibrations were made both isolated in the

solvent and in the presence of the other products/reactants, to ensure no complications were prevalent in the analysis of reactant and product mixtures.

5.3 Results and Discussion

5.3.1 Catalyst characterization

5.3.1.1 TGA

Thermogravimetric analysis of the synthesized nickel-enriched anionic clay highlights the process of MMO formation. The mass loss was measured as a function of time. Figure 4.3 in section 4.3.1.2 highlights two distinctive peaks representing zones of mass loss which can be attributed to the loss of surface and interstitial water, in addition to interstitial decarboxylation and dehydroxylation of the metal hydroxide layers, respectively. This transition is in agreement with the literature (35), subsequently, resulting in a calcination process which produces a nickel-enriched metal oxide layer.

5.3.1.2 XRD

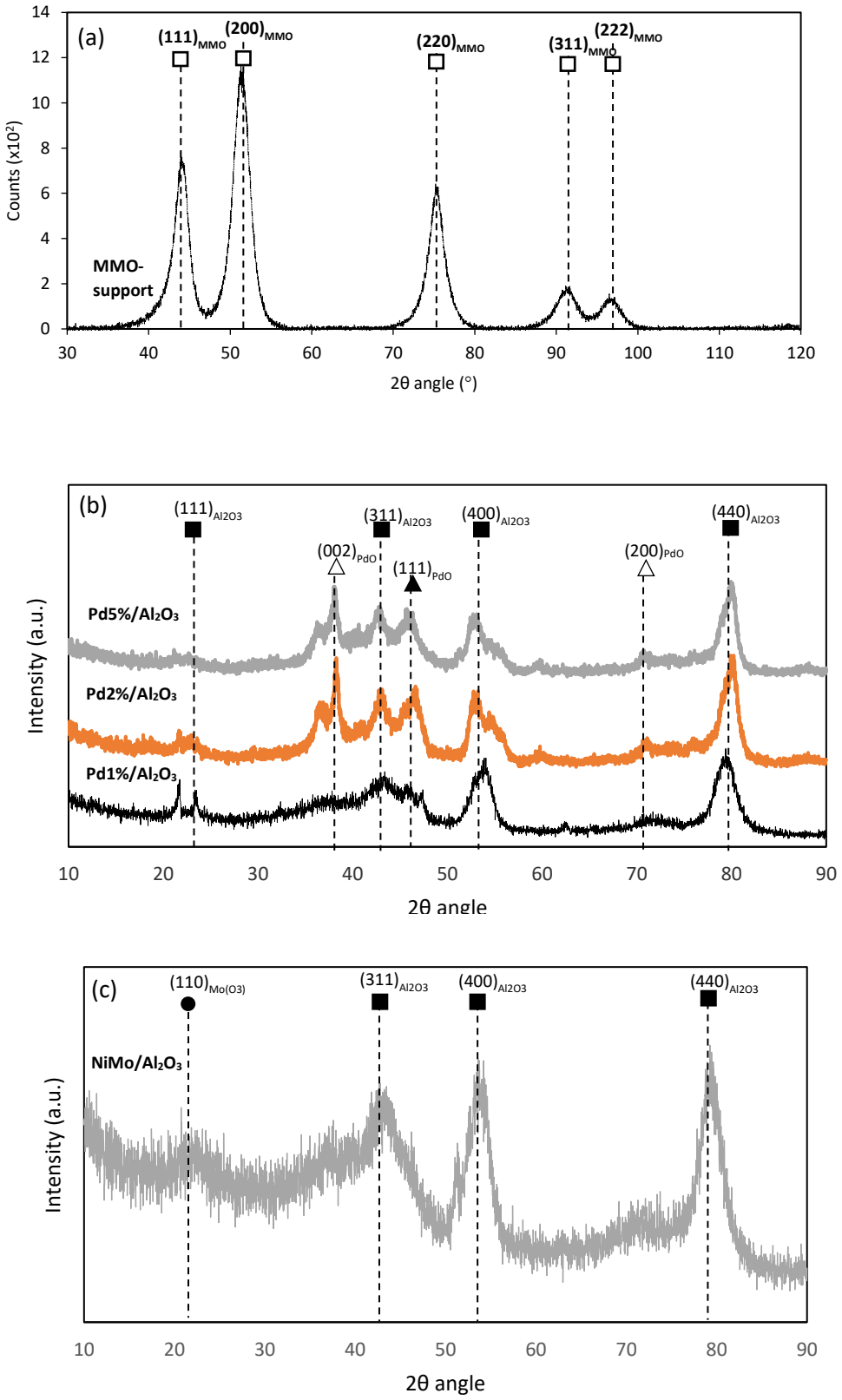

Figure 5.1 PXRD of (a) MMO following calcination at 450 °C, (b) $Pd_{1\%-5\%}$/alumina and (c) NiMo/alumina, the peaks of which are correlated to the 2 theta angles depicted in the figures.

The nickel-enriched anionic clay was subject to a calcination process at 450 °C. This was to ensure the material was completely delaminated forming high surface area polyphasic metal oxide sheets. The XRD pattern in Figure 5.1 (a) highlights the residual components of the material detailing peaks matched to the nickel oxide, Bunsenite mineral as recorded on Powder Diffraction File database, no. 00-047-1049, with corresponding peak indices (111), (200), (220), (311) and (222), from low to high 2θ, respectively. It is assumed that while poor crystallization has led to the absence of aluminium in the XRD profile, both quasi-amorphous spinel type and nickel-doped alumina phases can be found in the MMO.

The reflection peaks relating to the Al_2O_3 and PdO phases, present in all of the alumina-supported Pd catalysts illustrated in Figure 5.1 (b), demonstrate the successive planes of (311), (400) and (440) and, (002) and (200), respectively, reported by JCPDS no. 10-0425.

When analyzing the XRD diffraction pattern for $NiMo/Al_2O_3$, it is evident that the crystallization of the material is poor. However, the Al_2O_3 peaks of (311), (400) and (440) are clear, while the MoO_3 species present can be identified with the (110) peak. The nickel, however, is not observed due to its very small molar loading.

Table 5.1 Calculated molar ratios for the nickel and molybdenum catalysts using XRF analysis.

Element	**Catalyst**	
	Mo-MMO	**$NiMo/Al_2O_3$**
Ni	1.09	0.07
Al	0.36	1.25
Mo	0.09	0.09

The XRF results confirm the presence of a nickel-aluminium mixed oxide in a molar ratio of 3.3:1:0.25 Ni:Al:Mo, with an 8.6 wt% loading of Mo, while the refinery catalyst demonstrates an enrichment of aluminium relating to the acidic alumina support accompanied by surface nickel impregnation on the same order as the molybdenum, demonstrated in Table 5.1.

5.3.1.3 BET

The surface texture measurements of the catalysts are highlighted in Table 5.2. It is clear that the $NiMo/Al_2O_3$ demonstrates the highest surface area, coupled with the greatest pore volume and comparatively large pore size. When drawing comparisons with the LDH-derived catalyst, it is clear that the greater porosity and surface area observed over the $NiMo/Al_2O_3$ catalyst should theoretically provide for a higher activity in terms of upgrading

larger components typically found in heavier oil feeds. When contrasting the Pd-based catalysts, it is evident that while the $Pd_{5\%}/Al_2O_3$ is outperformed on pore volume and surface area, the average pore size is superior. This is a characteristic that will inhibit the coking of pore throats during upgrading of heavier feeds.

Table 5.2 Textural properties of the catalysts used in this study, derived from BET analysis.

	Mo-MMO	**$NiMo/Al_2O_3$**	**$Pd_{1\%}/Al_2O_3$**	**$Pd_{2\%}/Al_2O_3$**	**$Pd_{5\%}/Al_2O_3$**
Pore volume (cc g^{-1})	0.39	0.67	0.48	0.63	0.38
Surface area (m^2 g^{-1})	141.62	220.58	186.88	119.15	110.37
Average pore size (Å)	54.5	60.7	51.3	10.6	69.7

5.3.1.4 TPR and TPD

The peaks of reduction and extent of NH_3 desorption across the temperature range 0-900°C is shown in Figure 5.2 with the total acidity defined in Table 5.3

NH_3 (5%)-TPD was performed to investigate the acidic properties of the catalyst. The peaks can be separated into three predominant groups, representing the strength of the acid site. As temperature increases, the strength of the acid site increases, generating bands of weak,

medium and strong acid sites, the temperature ranges of which follow the approximation 100-200℃, 250-350℃ and 450+℃. The total number of acid sites has been calculated at 0.368 mmol/g for the Ni-MMO support and 2.04 mmol g^{-1} for the molybdenum-doped MMO. The Mo-doped MMO demonstrated a sharper peak with a signal of 89 mV, an order of magnitude higher than the support, at 168℃. This was followed by a smaller secondary peak at 490℃ and ultimately indicates a significant presence of acid sites which are active at lower temperatures following Mo-impregnation.

Comparatively, the $NiMo/Al_2O_3$ catalyst exhibited broader peaks over a greater temperature range indicating the presence of stronger acid sites. The $Pd_{1\%}/Al_2O_3$ material exhibited two smaller peaks at low temperatures, 163 and 273℃, before reaching a more significant and

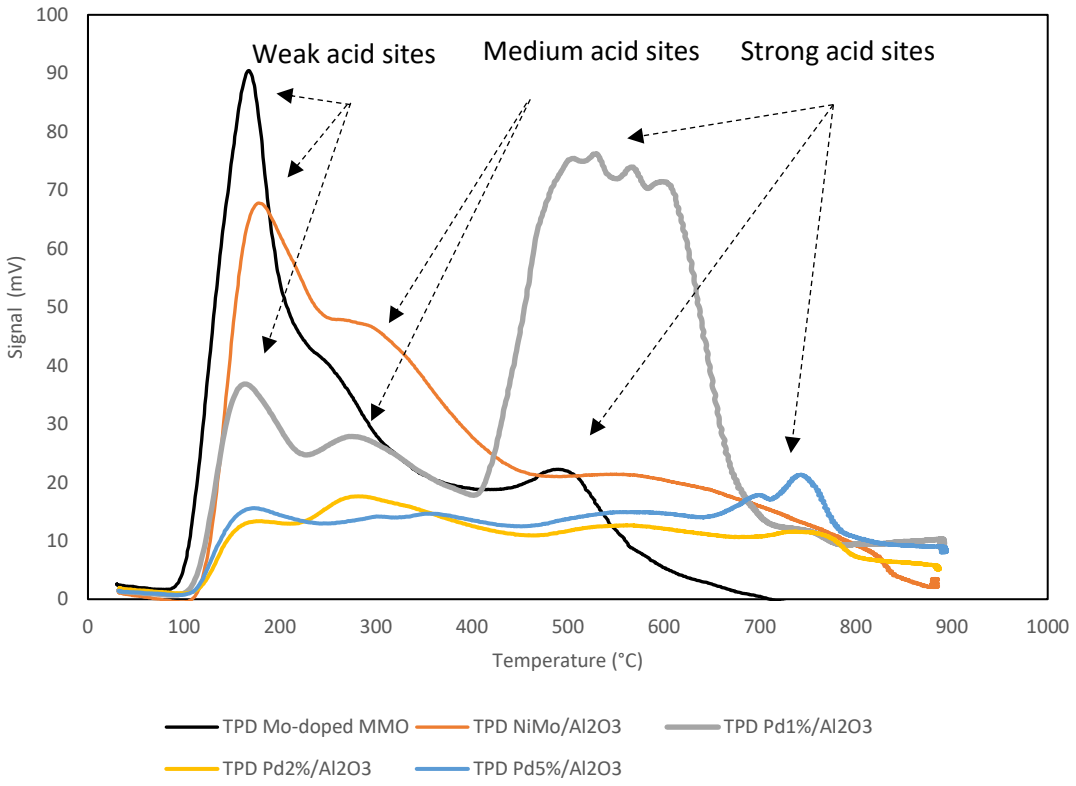

Figure 5.2 TPD profiles for the Mo-doped Ni-MMO species, $NiMo/Al_2O_3$ catalyst and $Pd_{1\%}$ - $Pd_{5\%}/Al_2O_3$.

broader peak between 510 and 610℃, indicating the dominance of stronger Lewis acid sites. The $Pd_{2\%}$ and $Pd_{5\%}/Al_2O_3$ catalysts, exhibited a low intensity broad

peak ranging from 100 to 900℃, while the latter comprised a small peak at 744℃. For comparison, a γ-alumina catalyst bearing molybdenum, promoted by cobalt, exhibits a total acid site count of 1.513 mmol g^{-1} when using NH_3 as the adsorption agent (36).

Table 5.3 Acid site count using TPD NH_3

Catalyst	**Acidity via NH_3 desorption (mmol g^{-1})**
MMO	0.368
Mo-MMO	2.04
$NiMo/Al_2O_3$	2.64
$Pd_{1\%}/Al_2O_3$	2.79
$Pd_{2\%}/Al_2O_3$	0.84
$Pd_{5\%}/Al_2O_3$	1.01

5.3.1.5 TEM & SEM

The images in Figure 5.3 (a-b) highlight the morphological structure of the heat-treated LDH structure. An approximation of the particle size pertains to approximately 200 nm crystallites. The plate-like agglomerates are typical of the rhombohedral crystallites in LDH-

derived materials. The $NiMo/Al_2O_3$ image, Figure 5.3 (c), demonstrated less well-defined tubular morphology, approximating 50nm in length and 5nm in transverse length.

TEM imaging in Figure. 5.3 (d) reveals the Al_2O_3 product in $Pd_{2\%}/Al_2O_3$ consists of disordered stacking nanofibers of length concentrating around 100nm, with a transverse width of less than 10nm. The $Pd_{1\%}/Al_2O_3$ morphology, shown in Figure 5.3 (e), demonstrates very similar attributes, approximating the same dimensions. The $Pd_{5\%}/Al_2O_3$, demonstrates a sphere

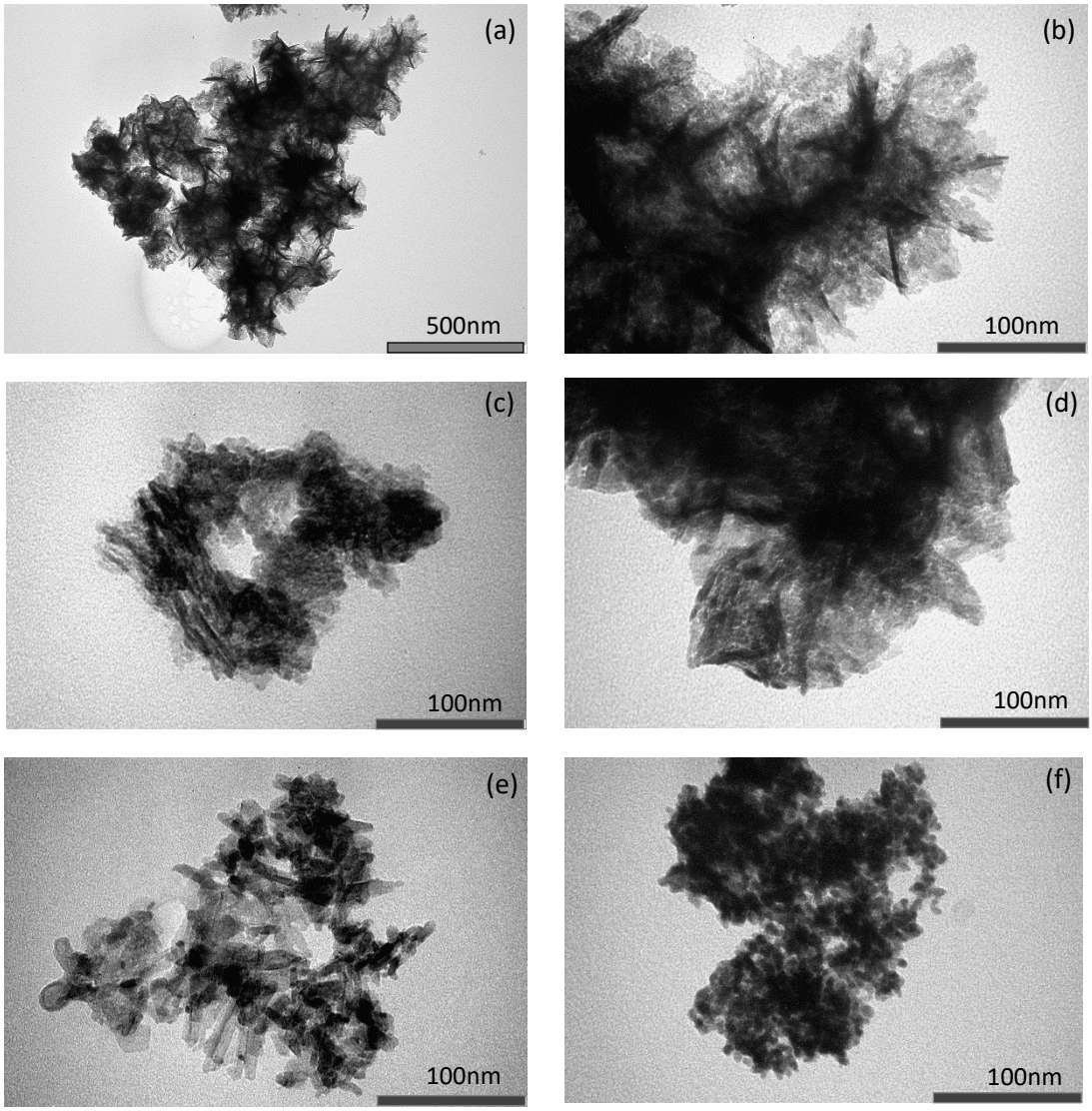

Figure 5.3 TEM imagery to elucidate crystal structure and shape (a) Mo-MMO (b) $NiMo/Al_2O_3$ (c) $Pd_{1\%}/Al_2O_3$ (d) $Pd_{2\%}/Al_2O_3$ and (e) $Pd_{5\%}/Al_2O_3$.

morphology, the diameter of which does not generally exceed 10nm which can be observed in Figure 5.3 (f).

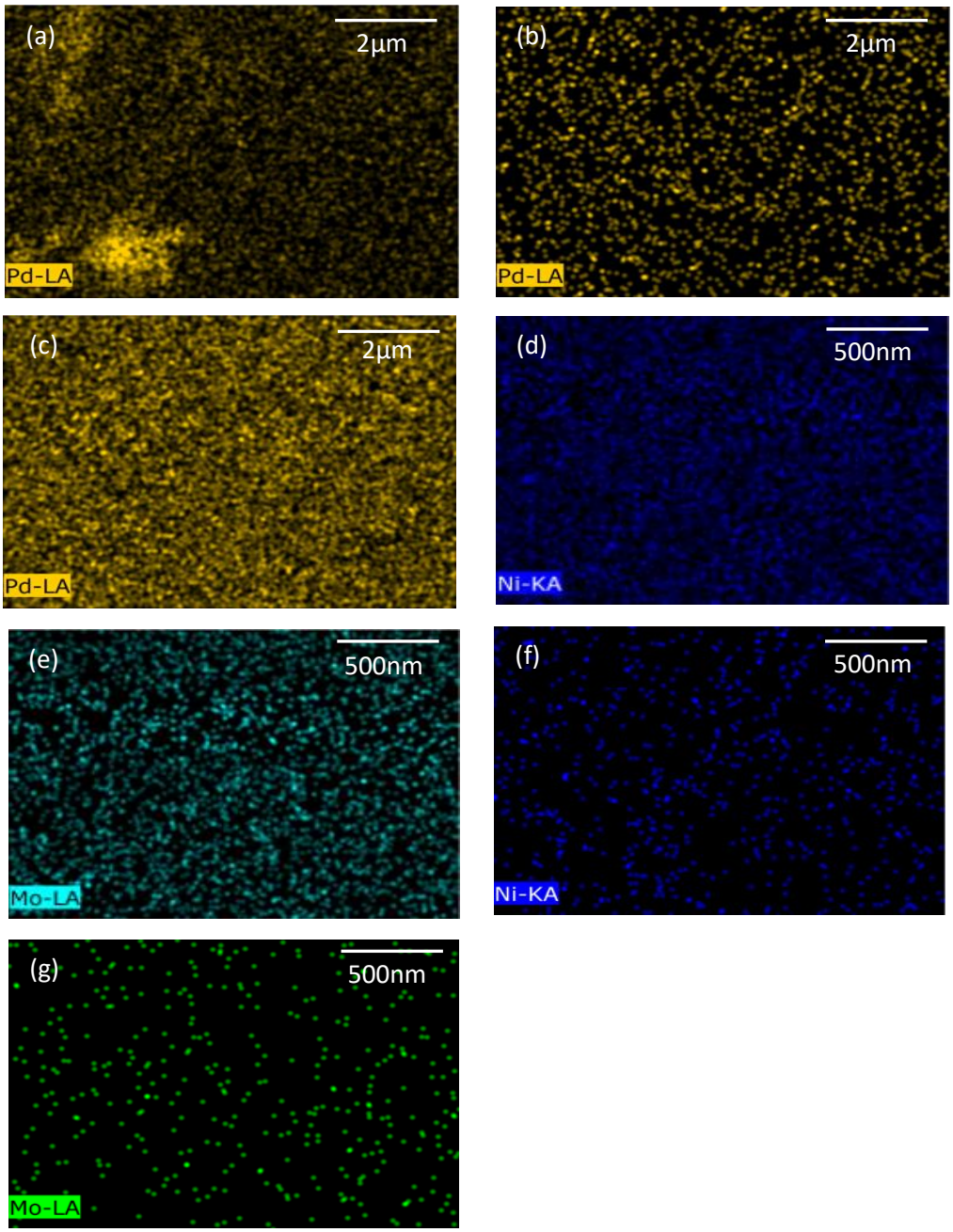

Figure 5.4 EDX analysis on the Pd/Al_2O_3 catalysts highlighting the distribution of Pd over the catalysts as a function of wt.% for (a) $Pd_{1\%}/Al_2O_3$ (b) $Pd_{2\%}/Al_2O_3$ and (c) $Pd_{5\%}/Al_2O_3$, in addition to the distribution of Ni and Mo over Mo-MMO (d&e) and $NiMo/Al_2O_3$ (f&g), respectively.

The EDS analysis of the Pd/Al_2O_3 catalysts clearly indicates the increased concentration of Pd deposited over the Al_2O_3 support as the loading increases. With $Pd_{1\%}/Al_2O_3$ in Figure 5.4 (a), the dispersion is not homogenous, rather areas of highly dispersed and agglomerated Pd exist, which is observed as random bright spots occupying the frame. As the concentration increases to $Pd_{2\%}$, as observed in Figure 5.4 (b), the Pd is more homogenous in its dispersion with higher density Pd epicentres deposited across the support. As the concentration increases to $Pd_{5\%}$ in Figure 5.4 (c), it is clear that again even richer epicentres of Pd exist, surrounded by less dense agglomerations of Pd, while the dispersion is such that only a small fraction of the frame is Pd-deficient. This correlation may be linked to the sequential reduction of surface area exhibited by the catalysts with the trend as follows $Pd_{1\%}>Pd_{2\%}>Pd_{5\%}$, demonstrated in Table 5.2.

The distribution of Ni and Mo over the Mo-MMO and $NiMo/Al_2O_3$ catalyst show that the textural properties of anionic clay-derived MMO and Al_2O_3 supports affect the dispersion of the active species significantly. With the Mo-MMO support, the nickel is embedded as nickel oxides in a solid solution of both nickel and aluminium oxides making up the MMO. This leads to a more homogenous distribution, as highlighted in Figure 5.4 (d). The $NiMo/Al_2O_3$ catalyst is limited by both the concentration of nickel embedded on the support, as the content of nickel in the catalyst is comparatively lower, as well as the nature of its deposition through impregnation, subsequent to the preparation of the alumina support. As a result, Figure 5.4 (f), highlights the heterogenous dispersion with a lower Ni signal.

There is a clear difference in Mo distribution between the catalysts. As shown in Figure 5.4 (e), the distribution of the Mo is more homogenous over the Mo-MMO catalyst, while also

exhibiting a comparatively higher signal. The heat treated anionic-clay-derived MMOs form large high surface area planar oxide layers with a more limited pore network as attested in Table 5.2. Consequently, it is expected that the Mo deposition is concentrated on the surface of the catalyst, while Mo incorporation into an Al_2O_3-supported catalyst, which is characterized by a high pore volume, will generate a greater distribution of internal Mo active centres not observed by the EDS analysis, hence the distribution of isolated Mo centres in Figure 5.5 (g).

5.3.2 Kinetic Study

Naphthalene undergoes partial hydrogenation to tetralin before complete hydrogenation to decalin, according to Scheme 5.1.

Scheme 5.1. Naphthalene hydrogenation reaction pathways.

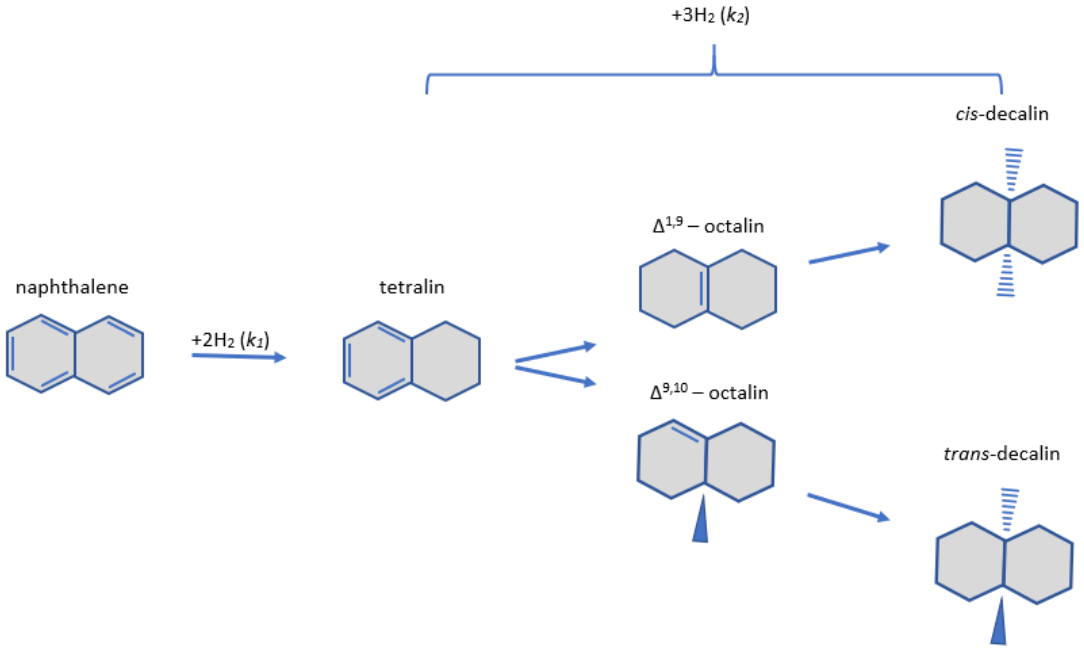

Decalin, however, comprises two particular isomers, cis- and trans-, where cis- is typically favoured for improving the cetane number. The pseudo-first order model, used to derive values for k_1 and k_2, was selected as the enrichment of H_2 comprising the sole component in the reaction gas (H_2 >> Naphthalene) meant that it could be regarded as constant. Similar to previous works (8), the reaction mechanism can then be defined by the following set of equations, the complete derivation of which is included in Appendix A for reference:

$$[N] = [N_0] \times e^{-k_1 t} \quad [5.1]$$

$$[D] = [N_0] \times [1 + (k_1 e^{-k_2 t} - k_2 e^{-k_1 t})/(k_2 - k_1)] \quad [5.2]$$

$$[T] = [N_0] \times [1 + k_1 (e^{-k_1 t} - e^{-k_2 t})/(k_2 - k_1)] \quad [5.3]$$

where N, D and T stand for the naphthalene, decalin and tetralin concentrations, respectively; and N_0 is the naphthalene initial concentration. The reaction rate coefficients k_1 and k_2, shown in Table 5.4, were obtained simultaneously by minimizing the objective function, sum of squares of residuals (SSR), between the experimental and model-calculated naphthalene, tetralin and decalin concentration data points. The solver used was a non-linear Generalized Reduced Gradient (GRG) on Microsoft Excel.

The yields of naphthalene, tetralin and decalin for each catalyst regime are demonstrated in Figure 5.6. The experimental and modelling results are presented graphically in Figure 5.7 while the corresponding parity plots are shown in Figure 5.8.

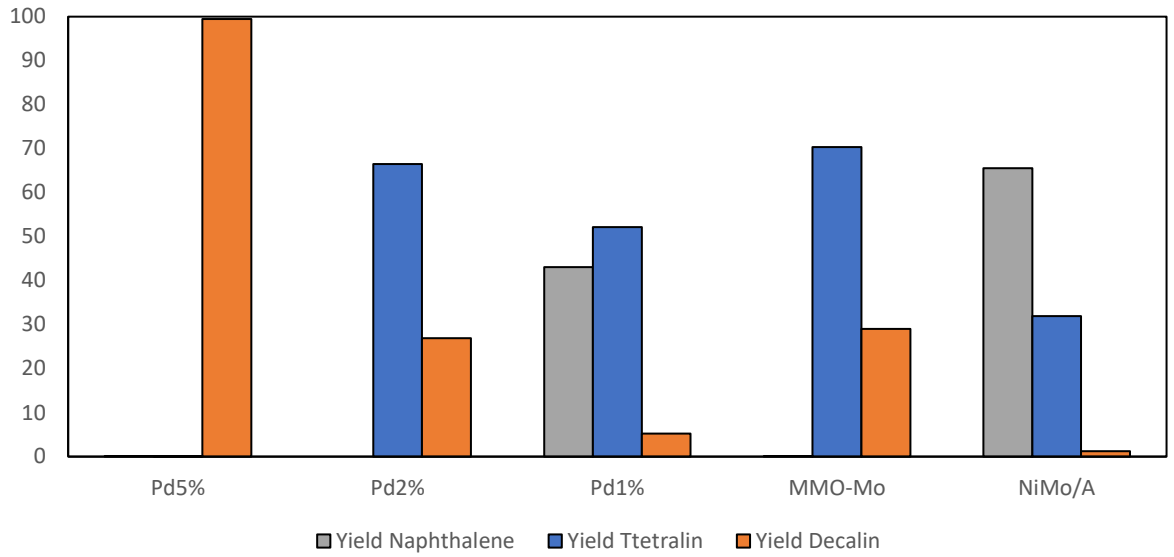

Figure 5.5 Yield of naphthalene, tetralin and decalin (cis & trans) for each catalyst regime.

In terms of the catalytic activity as shown in Figure 5.5, the $Pd_{5\%}/Al_2O_3$ catalyst is significantly more active than any of the other catalysts in the hydrogenation of naphthalene as can be observed by the conversion. $Pd_{5\%}/Al_2O_3$ achieves a yield of 99.5% decalin while as the concentration of the Pd loading decreases over the alumina support, so does the total decalin yield, to 26.9 and 5.3% for $Pd_{2\%}$ and $Pd_{1\%}$, respectively. The yields of decalin for the Ni and Mo-bearing catalysts at 29 and 1.2% for Mo-NiMMO and $NiMo/Al_2O_3$, respectively.

In terms of tetralin formation, the lowest yield follows the following trend: $Pd_{5\%}/Al_2O_3$ < Mo-NiMMO < $Pd_{2\%}/Al_2O_3$ < $Pd_{1\%}/Al_2O_3$ < $NiMo/Al_2O_3$. It is clear that the NiMo/ Al_2O_3 has the worst selectivity for the hydrogenation products after the reaction time. The majority of the product is naphthalene, whereas for all of the other catalytic regimes it is clear that either

hydrogenation products, tetralin or decalin are favoured. The only catalyst with a clear selectivity towards decalin products is the $Pd_{5\%}/ Al_2O_3$.

When modelling according to pseudo-first order kinetics, K_1 and K_2 values were determined as shown in Table 5.4. The model used is presented graphically in Figure 5.6 in relation to the experimental results. The order of k_1 persists as follows: $Pd_{2\%}/Al_2O_3$ > $Pd_{5\%}/Al_2O_3$ > Mo-MMO > $Pd_{1\%}/Al_2O_3$ > $NiMo/Al_2O_3$. The order of k_2 values persists as follows $Pd_{5\%}/Al_2O_3$ > $Pd_{2\%}/Al_2O_3$ > Mo-MMO > $Pd_{1\%}/Al_2O_3$ > $NiMo/Al_2O_3$. As the Pd loading increases it would be expected that k_1 and k_2 values would increase, however, the reduction of k_1 values at a certain maximum contravenes this prediction.

Table 5.4 Calculated reaction rate constants, assuming pseudo-first order kinetics, for naphthalene conversion to tetralin and tetralin conversion to decalin, denoted k_1 and k_2, for each catalyst condition.

Catalyst	**Pseudo-first order kinetic rate constant**	
	k_1 (min^{-1})	k_2 (min^{-1})
$Pd_{5\%}/Al_2O_3$	0.0690	0.2240
$Pd_{2\%}/Al_2O_3$	0.1059	0.0031
$Pd_{1\%}/Al_2O_3$	0.0069	0.0012
$NiMo/Al_2O_3$	0.0036	0.0006
Mo-MMO	0.0353	0.0028

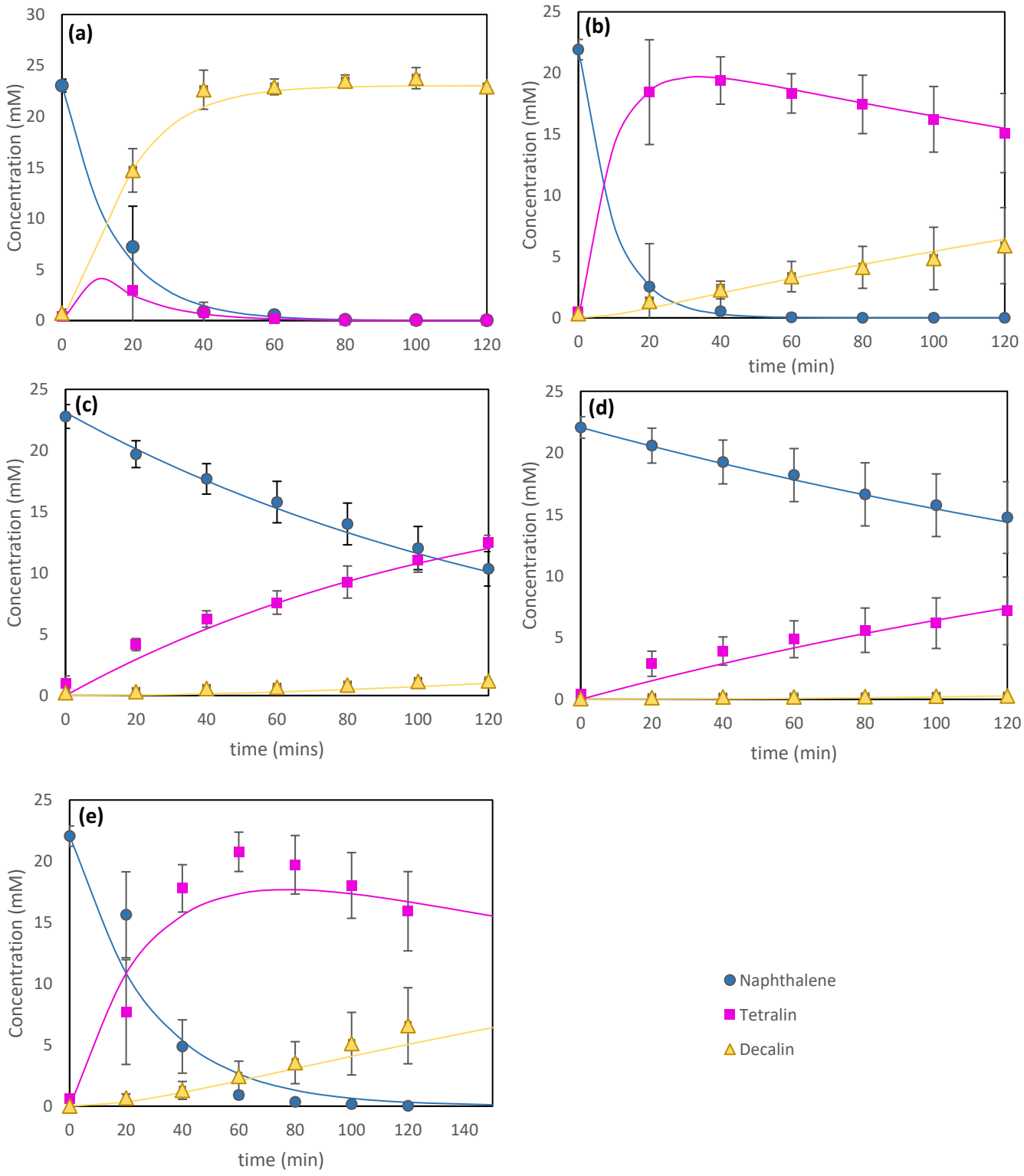

Figure 5.6 Plots of naphthalene, tetralin and decalin concentration against time using the experimentally-derived data and pseudo-first order kinetic model for each catalyst (a) $Pd_{5\%}$/alumina, (b) $Pd_{2\%}$/alumina (c) $Pd_{1\%}$/alumina (d) NiMo/alumina (e) Mo-MMO.

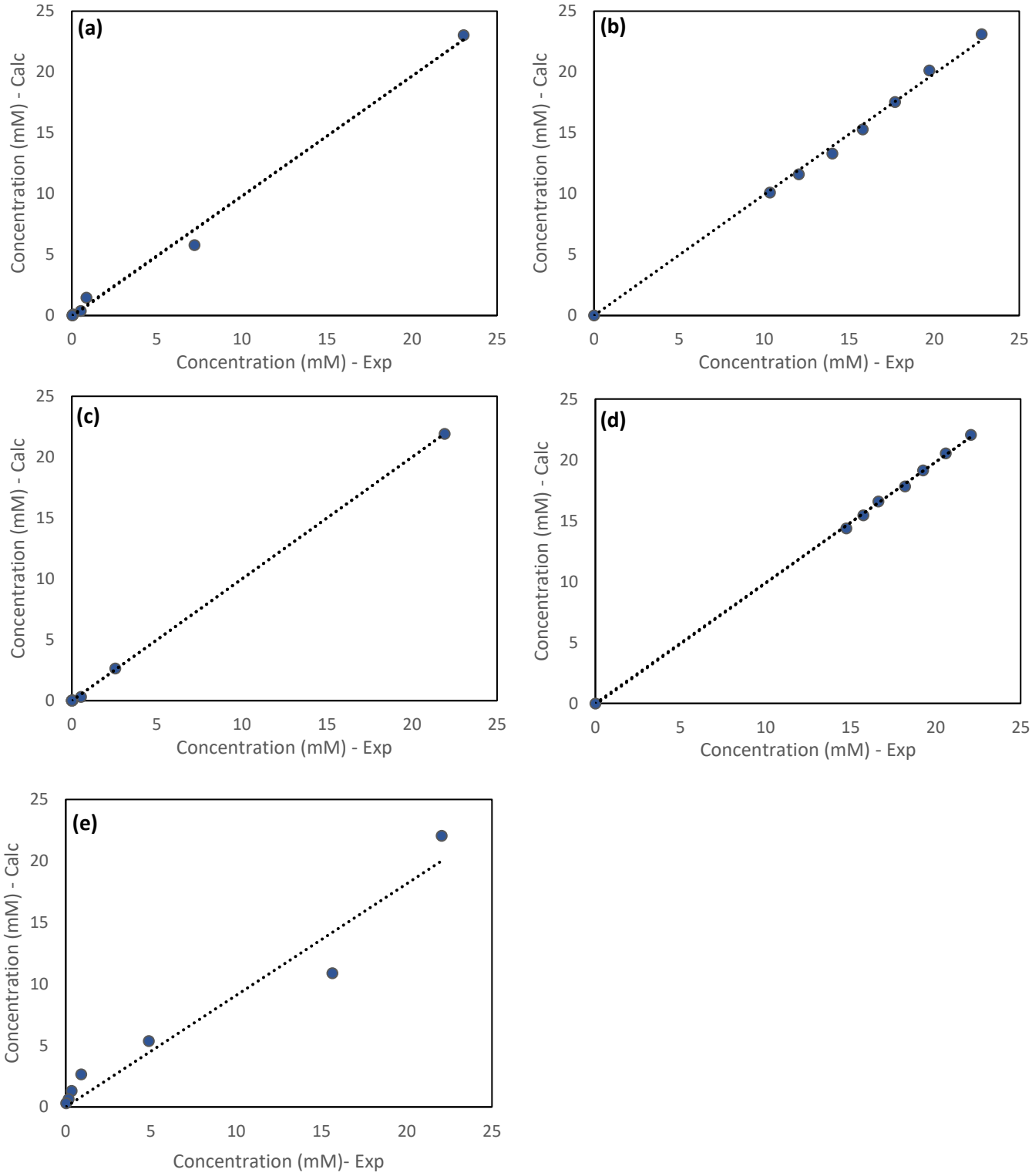

Figure 5.7. Parity plots for naphthalene concentration (a) Pd5%/alumina (b) $Pd_{2\%}$/alumina and (c) $Pd_{1\%}$/alumina (d) NiMo/alumina, and (e) Mo-MMO.

When using the $Pd_{5\%}/Al_2O_3$ coupled with this pseudo-first order reaction model, it becomes clear that the assumption of the second step being the rate determining step ($k_1 >> k_2$) does not hold. This is a detour from almost all conventional assumptions which also makes the simplified form provided in Escobar et al. (8), used for the platinum catalyst, non-applicable in this instance. It is clear that the advancement of catalytic activity provided by the $Pd_{5\%}/Al_2O_3$ is a superior material to be used in the more severe second-stage aromatic hydrogenation reactions. The results demonstrate that adsorption of tetralin is not a limitation with the abundance of palladium species on a $Pd_{5\%}/Al_2O_3$ under the reaction conditions used in this study. This therefore accelerates both cis and trans decalin formation and contradicts conventional k_1 and k_2 relationship assumptions. It is possible that the greater coverage of Pd over alumina which has generated a higher density of Pd clusters on the support, as seen in Figure 5.4 (c) derived from the EDS analysis, is impacting the interactions on the surface of the catalyst. Coupled with the sphere-like morphology exhibited by the $Pd_{5\%}$, demonstrated in Figure 5.3 (f) with a higher average pore size than the other catalysts demonstrated in Table 5.2, this has potentially provided the opportunity for tetralin to migrate to and bond with the active centres more readily. Competing against initial naphthalene molecules, tetralin can take advantage of greater dissociative adsorption for hydrogen activation, and subsequent conversion to decalin, as observed previously in Yu et al. (13). As a result, it is suggested that the tetralin to decalin conversions is not structure-sensitive in the presence of $Pd_{5\%}$ dispersed over Al_2O_3.

While this confirms the advantage of a noble metal-enriched catalytic support in aromatic hydrogenation applications, the high cost and poor sulfur tolerance remains a significant

drawback, particularly when dealing with sulfur-rich feeds typically observed in heavier oils. That said, when using $Pd_{1\%}/Al_2O_3$, the hydrogenation reaction proceeds at a much poorer rate with poor naphthalene conversion to tetralin, in addition to tetralin conversion to cis and trans decalin as shown in Figure 5.6 (c). The k_1 and k_2 values are one and two orders of magnitude lower than k_1 and k_2 for $Pd_{5\%}/Al_2O_3$, respectively.

In conventional catalytic regimes, the naphthalene to tetralin conversion is several orders of magnitude greater than the conversion of tetralin to the decalin isomers (17). It has been suggested previously that when using a $NiMo/Al_2O_3$ catalyst, the strong adsorption of naphthalene on the active centres inhibits tetralin conversion to decalin until the naphthalene has been completely converted (37). The Mo-MMO catalyst broadly concedes to this convention where after 120 min all of the naphthalene has been converted to tetralin whereas the tetralin has been unable to undergo complete conversion to decalin species, as observed in Figure 5.6 (e). However, it is noted that in this study, with the exception of $NiMo/Al_2O_3$ where only an insignificant conversion of tetralin to decalin occurs, tetralin hydrogenation is simultaneously produced before naphthalene hydrogenation is completed. Accordingly, the data highlights k_1 values as an order greater than the k_2 values. As a result, the mechanism suggested by Su et al. (37) can be expanded upon. A distinctive difference in aromaticity prevalent between naphthalene and tetralin compounds results in a clear deviation to the hydrogenation reactivity when using a nickel-based catalyst. Tetralin exhibits a greater Pi-electron density than naphthalene which consequently generates a higher aromatic ring resonance energy. This higher energy inhibits hydrogenation reactivity when using non-noble metal species, leading to a stark difference between k_1 and k_2 values.

Furthermore, the difference in hydrogenation mechanisms of naphthalene and tetralin has been studied previously when in the presence of a Ni/Al_2O_3 catalyst (7). While the weak aromaticity of naphthalene accommodates its conversion to tetralin under Pi/sigma adsorption which demands a single active site, the conversion of tetralin occurs through the Pi-adsorbed species, due its more potent aromaticity. It has previously been found that when using a Ni/Al_2O_3 catalyst, multiple Ni atoms are required to generate a tetralin hydrogenation active site and as a result the tetralin molecule can be considered catalyst structure-sensitive (7). It may therefore be expected that the homogenous spread of Ni and Al in the MMO may promote more hydrogenation of naphthalene on the molybdenum oxide slabs, as compared to the $NiMo/Al_2O_3$ catalyst. A high conversion of naphthalene could then be responsible for the availability of the active sites to accommodate tetralin conversion, whereas in the $NiMo/Al_2O_3$ catalyst, the reduced dispersion due to the far lower concentration of the nickel promotor, as observed in the EDS analysis Figure 5.5 (f), will generate more isolated metallic active sites forming a bottle-neck in the reaction, leading to a reduced tetralin conversion and very limited decalin formation as observed in Figure 5.5, with a total decalin yield of 1.2%. It is evident that the Mo-MMO catalyst is more comparable to the $Pd_{2\%}$/alumina, the latter's reaction progression of which is shown in Figure 5.6 (b), with a final yield of 29.0%. Comparatively, the activity of $NiMo/Al_2O_3$ is more comparable to $Pd_{1\%}/Al_2O_3$, though generates less tetralin and decalin than the $Pd_{1\%}/Al_2O_3$ catalyst.

In a previous study, it was concluded that the addition of a basic site-enriched catalyst support may augment the hydrogenation of naphthalene and tetralin, until a certain basic

site concentration is reached whereupon the benefits are negated (8). It is clear from the activity of tetralin conversion, variation in support materials which leads to variations in the electronic configuration of the catalyst, that a distinct mechanism for the transformation of tetralin into its hydrogenated products is apparent between the catalyst regimes. To highlight these differences in catalytic activity and preferential pathways for tetralin hydrogenation, plots of cis/trans-decalin vs concentration of decalin formed were analyzed.

5.3.3 Cis/trans-decalin ratio

It is observed in Figure 5.9 (a) that when the Mo-MMO catalyst is used with the same catalyst to reactant ratio as the palladium-based catalysts, the cis/trans ratio begins at a comparatively high level compared to the other catalysts shown in both Figures 5.9 (a) and (b), at approximately 1.30. It begins to decline significantly as tetralin conversion to decalin ensues. However, when the basic site-enriched Mo-MMO support catalyst to reactant ratio is doubled to Mo-MMO double loading, for the same concentration of decalin, a greater concentration of trans-decalin is apparent initially with a cis/trans ratio of 0.32, and the trend is reversed leading to a gradual increase to 0.68 as the tetralin is converted. When using the acidic Al_2O_3-supported NiMo catalyst (used with double loading only), as shown in Figure 5.8 (c), the cis/trans ratio begins at 1.49 and gradually decreases with tetralin conversion to decalin, reaching a final ratio of 1.09. This trend is similar to that of the Mo-MMO single loading at the early tetralin conversion stage. When comparing the double loadings of $NiMo/Al_2O_3$ and Mo-MMO catalysts, the disparity between cis/trans ratio is clear. While the reaction has not proceeded to the same extent, it is clear that early

conversion of the double loading Mo-MMO yields an enriched trans-decalin product in direct contradiction to $NiMo/Al_2O_3$. However, as tetralin conversion to decalin increases, so the concentration ratio appears to converge. It has been postulated that the concentration of both the cis and trans isomers is dependent on two factors: (i) Isomerization activity of the catalyst and (ii) decalin-tetralin adsorption competition (10). At low conversion of tetralin, the basic sites on the Mo-MMO catalyst are responsible for promoting isomerization to trans-decalin. There is however a significant reduction in cis- isomerization to trans- decalin as the tetralin concentration decreases, after which the conversion stabilizes resulting in a trans-depleted decalin product with a 0.62 cis/trans ratio. The

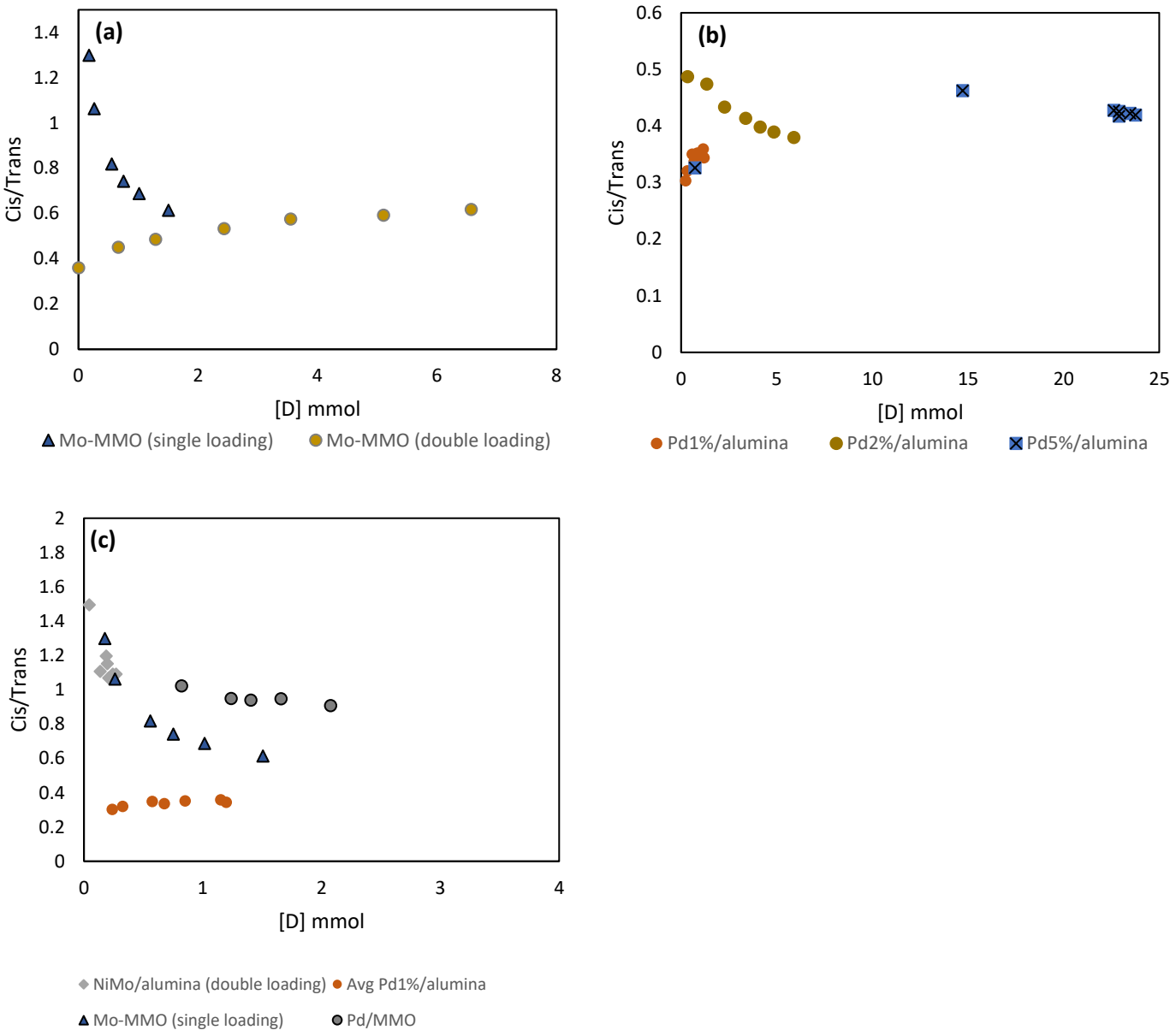

Figure 5.8 Plots of cis/trans ratio against decalin concentration for (a) two separate catalyst loadings of Mo-MMO and (b) including $Pd_{5\%}$/alumina, $Pd_{2\%}$/alumina and $Pd_{1\%}$/alumina and (c) NiMo/alumina, Pd-MMO, Mo-MMO (single loading) and $Pd_{1\%}$/alumina.

observed results agrees with Rautanen et al. (7) wherein long experiments resulting in poor tetralin conversion have resulted in an increase in cis-decalin. This is exemplified with the Mo-MMO single loading and $NiMo/Al_2O_3$, observed in Figure 5.8 (c), wherein as the tetralin

conversion slowly increases, rapid cis to trans isomerization takes place, particularly in the case of NiMo/Al_2O_3.

Furthermore, increases in competition for adsorption sites could greatly reduce the occurrence of the cis-trans isomerization reaction (10,38). This is because although it has been previously reported that the cis to trans isomerization has a higher rate constant than tetralin hydrogenation, the tetralin molecules form a rigid parallel morphology against the surface of the catalyst compared to the hinged cis-decalin molecule (10). This may explain the disparity between the single and double loadings of Mo-MMO, whereupon increasing the availability of adsorption sites, an increase in the cis to trans isomerization activity was observed i.e. the presence of tetralin was unable to block the active sites. This is also supported by the enhanced activity of cis to trans isomerization of Ni compared to Pd (10).

There is a clear difference between nickel and molybdenum-containing catalysts and the palladium bearing catalysts. With the latter, at both high concentration and low concentration on Al_2O_3, with both high and low conversion to decalin, the cis/trans ratio remains in favour of trans-decalin as highlighted in Figure 5.8 (b). The ratios for $Pd_{1\%}$, $Pd_{2\%}$ and $Pd_{5\%}$ end with 0.34, 0.38 and 0.42, respectively. This would suggest that there is a clear tendency to produce the trans-isomer under palladium irrespective of tetralin concentration. This corroborates with previous research which has shown that palladium occupies a higher trans-selectivity than its nickel-containing catalyst counterparts (7,10). The comparative enrichment of trans-decalin, however, has been attributed to a very low intrinsic isomerization activity on the palladium catalyst which essentially stabilizes the produced cis/trans ratio throughout the entire tetralin conversion progression (10).

An underlying mechanism has been suggested by Dokjampa et al. (10), which speculates the cis/trans ratio is reliant on the orientation of the $\Delta^{1,9}$ – octalin intermediate. Hydrogen incorporation into this octalin species is especially fast in the case of nickel catalysts, while the palladium catalyst accommodates a roll over on the surface, culminating in an orientation wherein the H atom in position 10 of the ring is facing away from the surface. This can be inferred considering the conformation of $\Delta^{1,9}$ – octalin on the catalyst surfaces; the syn nature of hydrogen addition requires the addition of H atoms to a double bond from the same side. Moreover, while the $\Delta^{9,10}$ – octalin exclusively produces cis decalin, the greater hydrogenation rate of $\Delta^{1,9}$ – octalin over noble metal catalysts, with the 10 atom facing away from the catalytic surface, greatly reduces isomerization to $\Delta^{9,10}$ – octalin resulting in a greater amount of trans-decalin production (7).

When using nickel and molybdenum catalysts, it is perhaps evidenced that the greater initial concentration of cis relative to trans is indicative of a preferred orientation of the $\Delta^{1,9}$– octalin wherein the hydrogen atom in position 10 faces towards the surface. The addition of hydrogen atoms to positions 1 and 9 occurs on the same side thereby producing cis-decalin (10). This is graphically demonstrated in Figure 5.9 over the Mo-MMO catalyst.

It is clear that at a lower concentration of palladium, which inhibits the progression of the decalin formation, there are distinctive trends in the cis/trans progression.

The $Pd_{1\%}/Al_2O_3$ catalyst demonstrates the lowest intrinsic cis/trans ratio out of all of the catalysts. The trend as tetralin conversion continues highlights a clear increase in the cis/trans ratio from 0.30 to 0.36 and then reduction to 0.34. This modest progression may result from a sudden competition for active sites between tetralin and cis-decalin, favouring tetralin conversion. As further $\Delta^{1,9}$ – octalin is produced from the tetralin, there may be greater inhibition of surface roll over which accommodates a higher concentration of cis-decalin. This is then followed by the sequential appropriation of active sites by the cis-decalin as its concentration continues to increase, thereby resulting in a final decline to 0.34 cis/trans ratio, i.e. favouring cis to trans isomerization.

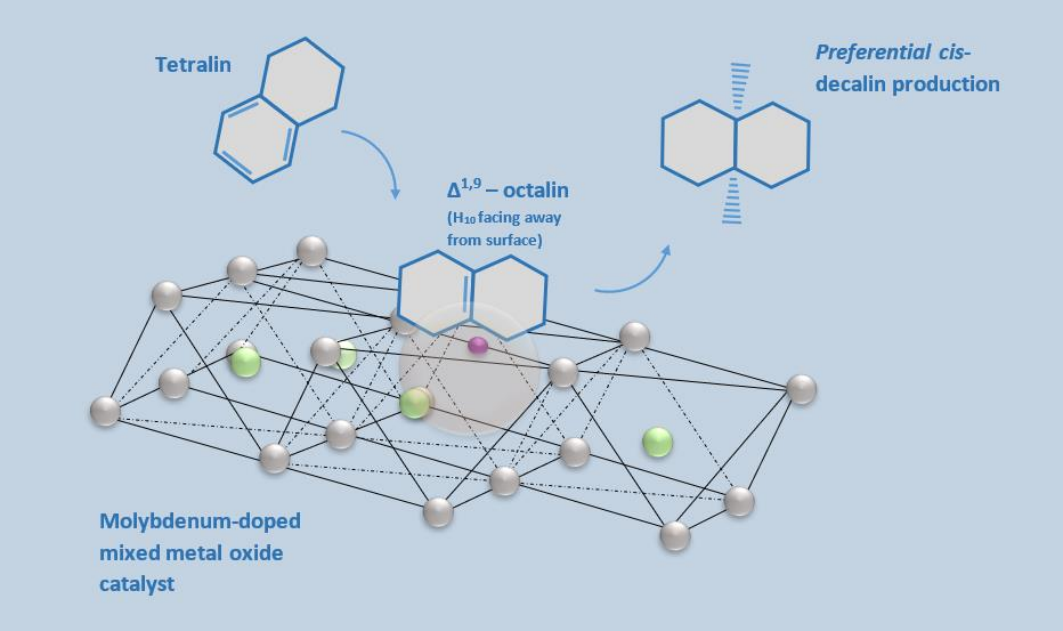

Figure 5.9 Demonstrations of tetralin to cis-decalin conversion through the orientation of intermediate $\Delta^{1,9}$octalin over the Mo-MMO catalyst surface.

The $Pd_{2\%}/Al_2O_3$ catalyst conversely demonstrates a modest decline in cis/trans ratio as the reaction proceeds. This indicates that as the concentration of cis decalin increases, the active sites are appropriated by the cis decalin in spite of the tetralin molecules, resulting in higher cis to trans conversion. Moreover, a great amount of $\Delta^{1,9}$ – octalin rollover on the

surface occurs to extend trans-decalin production. While, the $Pd_{5\%}/Al_2O_3$ catalyst induces a fairly constant cis/trans relationship, it must be stated that the reaction proceeds at a far more significant rate so is not directly comparable. The data obtained from comparable decalin concentrations, i.e. during the early stages of the reaction highlight an initial cis/trans ratio of 0.32 followed by a rise to 0.46 and reduction to 0.42 which is consistent for the subsequent data points. There is a clear agreement with the assumption that initially tetralin occupation of the active sites is favoured over both residual naphthalene and cis-decalin, however as tetralin conversion increases the $\Delta^{1,9}$ – octalin, with the hydrogen in position 10 facing away from the surface, is favoured by the orientation and abundance of the active sites on the catalyst, thereby yielding trans-decalin.

Interestingly, when looking at Figure 5.8 (c) relating to the Pd/MMO, the cis/trans decalin ratio follows a trend similar to that of the Mo-MMO, migrating from 100% cis-decalin down to a cis/trans ratio of 0.91 as the tetralin conversion increases, however with a more severe inhibition of cis-to-trans decalin isomerization reaction compared to the other catalysts. This is in clear contrast to the $Pd_{1\%}/Al_2O_3$, and given the similar low tetralin conversion during the reaction, the contrast is clearly a result of the mixed oxide support and its electronic interaction with the palladium active centres which do not benefit from the presence of enhanced acidity which characterizes alumina supports. Preferential trans-decalin formation has previously been correlated with enhanced acidity on Al_2O_3-supported noble metal catalysts (39). Additionally, the $\Delta^{1,9}$ – octalin intermediate may be prevented from changing its orientation, as a result of rapid hydrogenation which would result in the enrichment of cis-decalin in the product (10). Furthermore, greater naphthalene conversion to tetralin and

then cis-decalin for the same reaction time may also be accounted for by the lack of cis-to-trans isomerization reactions. The significantly greater cis/trans ratio is important in increasing the cetane number of fuels.

5.4 Conclusions

Mixed metal oxide carriers bearing a 3.3:1 Ni:Al ratio were synthesized from anionic clay species. The incipient wetness impregnation method was used to deposit molybdenum onto the surface of the support. The catalytic materials were tested in liquid-phase naphthalene hydrogenation at 250°C and 40 bar H_2. When comparing the Ni and Mo catalysts, the higher the loading of Ni present over the catalyst, the higher the conversion of naphthalene. It is also evident that when contrasting different Pd loadings over alumina, a higher loading of Pd produces a higher yield of decalin with the total yield ranging from 99.5 to 5.9% conversion for $Pd_{5\%}$ and $Pd_{1\%}$, respectively. Reaction rate constants were derived from a pseudo-first order kinetic pathway describing naphthalene to tetralin (k_1) and tetralin to decalin (k_2) hydrogenation. The Mo-MMO catalyst achieved comparable reaction rates to $Pd_{2\%}/Al_2O_3$ at double concentration, exceeding $Pd_{1\%}/Al_2O_3$, and $NiMo/Al_2O_3$. When using $Pd_{5\%}/Al_2O_3$, tetralin hydrogenation was favoured over naphthalene hydrogenation culminating in a k_2 value of 0.224 compared to a k_1 value of 0.069, detouring from the conventional assumption that $k_1 > > k_2$.

Furthermore, when considering the impact of catalyst on the cis/trans ratio against decalin concentration, it is apparent that when using Pd and Mo-MMO, higher rates of cis-decalin production are observed initially, followed by a decline to a lower cis/trans ratio over the

course of the reaction. However, when the MMO-support loading is increased, the relationship becomes inverse wherein the products initially contain a comparatively low cis-decalin concentration, highlighting the increase in cis- to trans- conversion sites. This is followed by an inhibition of cis to trans isomerization and therefore a progressively more cis-decalin enriched product, mirroring that of the $NiMo/Al_2O_3$ catalyst. It is clear that a control over the cis- and trans- decalin products is available when using the novel Mo-MMO catalyst in varied catalyst loading. In comparison, the Pd/alumina catalysts generate a much lower cis/trans ratio irrespective of tetralin concentration and palladium abundance, highlighting palladium's distinct activity for cis- to trans- decalin isomerization. While trans-decalin is thermodynamically more stable, cis-decalin is more active towards ring-opening. This is important as it possess a greater selectivity to indanes and alkyl-cyclohexanes which are favoured products in the HDA process. Consequently, NiMo-bearing catalysts, although offering poorer performance may provide greater advantages in simultaneous HYD and HDA processes. It is also evident that the enriched nickel mixed metal oxide doped with molybdenum offers benefits over the conventional refinery catalyst due to the comparative ease of synthesis of the Layered Double Hydroxide starting material in addition to more economic methods of formulation. Future work should include both the impact of sulfur on the hydrogenation process and catalyst performance, as well as hydrodecyclisation of the cis-decalin product to yield alkyl naphthenes.

5.5 References

1. Taillades-Jacquin M, Jones DJ, Rozière J, Moreno-Tost R, Jiménez-López A, Albertazzi S, et al. Novel mesoporous aluminosilicate supported palladium-rhodium catalysts for

diesel upgrading. II. Catalytic activity and improvement of industrial diesel feedstocks. Appl Catal A Gen. 2008;340(2):257–64.

2. European Environment Agency. Fuel quality in the EU in 2016 [Internet]. Luxembourg; 2016. Available from: https://www.eea.europa.eu/publications/fuel-quality-in-the-eu#tab-news-and-articles

3. Hart A, Leeke G, Greaves M, Wood J. Down-hole heavy crude oil upgrading by CAPRI: Effect of hydrogen and methane gases upon upgrading and coke formation. Fuel [Internet]. 2014;119:226–35. Available from: http://dx.doi.org/10.1016/j.fuel.2013.11.048

4. Bagci SA. Wet Forward Combustion for Heavy Oil Recovery. Energy Sources, Part A Recover Util Environ Eff. 2006;28(3):221–32.

5. Elahi SM, Ahmadi Khoshooei M, Carbognani Ortega L, Scott CE, Chen Z, Pereira-Almao P. Chemical insight into nano-catalytic in-situ upgrading and recovery of heavy oil. Fuel [Internet]. 2020;278(May):118270. Available from: https://doi.org/10.1016/j.fuel.2020.118270

6. Shen Z, He P, Wang A, Harrhy J, Meng S, Peng H, et al. Conversion of naphthalene as model compound of polyaromatics to mono-aromatic hydrocarbons under the mixed hydrogen and methane atmosphere. Fuel [Internet]. 2019;243(November 2018):469–77. Available from: https://doi.org/10.1016/j.fuel.2019.01.148

7. Rautanen PA, Lylykangas MS, Aittamaa JR, Krause AOI. Liquid-phase hydrogenation of naphthalene and tetralin on Ni/Al2O3: Kinetic modeling. Ind Eng Chem Res.

2002;41(24):5966–75.

8. Escobar J, Barrera MC, Santes V, Terrazas JE. Naphthalene hydrogenation over Mg-doped Pt/Al2O3. Catal Today [Internet]. 2017;296(January):197–204. Available from: http://dx.doi.org/10.1016/j.cattod.2017.04.064

9. Rabl S, Haas A, Santi D, Flego C, Ferrari M, Calemma V, et al. Ring opening of cis-decalin on bifunctional Ir/- and Pt/La-X zeolite catalysts. Appl Catal A Gen [Internet]. 2011;400(1–2):131–41. Available from: http://dx.doi.org/10.1016/j.apcata.2011.04.026

10. Dokjampa S, Rirksomboon T, Osuwan S, Jongpatiwut S, Resasco DE. Comparative study of the hydrogenation of tetralin on supported Ni, Pt, and Pd catalysts. Catal Today. 2007;123(1–4):218–23.

11. Wang Q, Hou Y, Zhao H, Li Y, Jia A. Highly Selective Hydrogenation of Tetralin to cis-Decalin Using Ru Catalyst. ChemistrySelect. 2019;4(19):5796–8.

12. Lucci FR, Darby MT, Mattera MFG, Ivimey CJ, Therrien AJ, Michaelides A, et al. Controlling Hydrogen Activation, Spillover, and Desorption with Pd-Au Single-Atom Alloys. J Phys Chem Lett. 2016;7(3):480–5.

13. Yu WY, Mullen GM, Mullins CB. Hydrogen adsorption and absorption with Pd-Au bimetallic surfaces. J Phys Chem C. 2013;117(38):19535–43.

14. Zhang P, Wu T, Hou M, Ma J, Liu H, Jiang T, et al. The hydrogenation of aromatic compounds under mild conditions by using a solid Lewis acid and supported palladium catalyst. ChemCatChem. 2014;6(12):3323–7.

15. Yoshimura Y, Toba M, Matsui T, Harada M, Ichihashi Y, Bando KK, et al. Active phases and sulfur tolerance of bimetallic Pd-Pt catalysts used for hydrotreatment. Appl Catal A Gen. 2007;322(SUPPL.):152–71.

16. Wan G, Aijun D, Zhen Z, Guiyuan J, Dengqian Z, Ruili L, et al. Al2O3-TiO2/Al2O 3-TiO2-SiO2 composite-supported bimetallic Pt-Pd catalysts for the hydrodearomatization and hydrodesulfurization of diesel fuel. Energy and Fuels. 2009;23(1):81–5.

17. Kirumakki SR, Shpeizer BG, Sagar GV, Chary KVR, Clearfield A. Hydrogenation of Naphthalene over NiO/SiO2-Al2O3 catalysts: Structure-activity correlation. J Catal. 2006;242(2):319–31.

18. Venezia AM, La Parola V, Pawelec B, Fierro JLG. Hydrogenation of aromatics over Au-Pd/SiO2-Al2O 3 catalysts; Support acidity effect. Appl Catal A Gen. 2004;264(1):43–51.

19. Navarro RM, Pawelec B, Trejo JM, Mariscal R, Fierro JLG. Hydrogenation of Aromatics on Sulfur-Resistant PtPd Bimetallic Catalysts. 2000;194:184–94.

20. Lu CM, Lin YM, Wang I. Naphthalene hydrogenation over Pt/TiO2 - ZrO2 and the behavior of strong metal - Support interaction (SMSI). Appl Catal A Gen. 2000;198(1–2):223–34.

21. Rodríguez-Castellón E, Díaz L, Braos-García P, Mérida-Robles J, Maireles-Torres P, Jiménez-López A, et al. Nickel-impregnated zirconium-doped mesoporous molecular sieves as catalysts for the hydrogenation and ring-opening of tetralin. Appl Catal A Gen. 2003;240(1–2):83–94.

22. Escobar-Alarcón L, Klimova T, Escobar-Aguilar J, Romero S, Morales-Ramírez C, Solís-Casados DA. Preparation and characterization of Al2O3-MgO catalytic supports modified with lithium. Fuel. 2013;110:278–85.

23. Caloch B, Rana MS, Ancheyta J. Improved hydrogenolysis (C-S, C-M) function with basic supported hydrodesulfurization catalysts. Catal Today. 2004;98(1-2 SPEC. ISS.):91–8.

24. Fang M, Sánchez-delgado RA. Ruthenium nanoparticles supported on magnesium oxide : A versatile and recyclable dual-site catalyst for hydrogenation of mono- and. J Catal [Internet]. 2014;311:357–68. Available from: http://dx.doi.org/10.1016/j.jcat.2013.12.017

25. Chen W, Nie H, Li D, Long X, van Gestel J, Maugé F. Effect of Mg addition on the structure and performance of sulfide Mo/Al2O3 in HDS and HDN reaction. J Catal [Internet]. 2016;344:420–33. Available from: http://dx.doi.org/10.1016/j.jcat.2016.08.025

26. Albertazzi S, Busca G, Finocchio E, Glöckler R, Vaccari A. New Pd/Pt on Mg/Al basic mixed oxides for the hydrogenation and hydrogenolysis of naphthalene. J Catal. 2004;223(2):372–81.

27. Clause O, Goncalves Coelho M, Gazzano M, Matteuzzi D, Trifirò F, Vaccari A. Synthesis and thermal reactivity of nickel-containing anionic clays. Appl Clay Sci. 1993;8(2–3):169–86.

28. Zhao R, Yin C, Zhao H, Liu C. Synthesis, characterization, and application of

hydotalcites in hydrodesulfurization of FCC gasoline. Fuel Process Technol. 2003;81(3):201–9.

29. Kaur G, Couperthwaite SJ, Millar GJ. Acid Mine Drainage Treatment Using Bayer Precipitates Obtained from Seawater Neutralization of Bayer Liquor. Glob Challenges. 2018;2(12):1800061.

30. Douglas GB. Contaminant removal from acidic mine pit water via in situ hydrotalcite formation. Appl Geochemistry [Internet]. 2014;51:15–22. Available from: http://dx.doi.org/10.1016/j.apgeochem.2014.09.005

31. Álvarez R, Tóffolo A, Pérez V, Linares CF. Synthesis and characterization of CoMo/Zn-Al mixed oxide catalysts for hydrodesulphuration of thiophene. Catal Letters. 2010;137(3–4):150–5.

32. Zhang Y, Cheng H, Lu X, Ding W, Zhou G. Influence of rare earth promoters on the performance of Ni/Mg(Al)O catalysts for hydrogenation and steam reforming of toluene. Rare Met. 2009;28(6):582–9.

33. Bennett JA, Creamer NJ, Deplanche K, Macaskie LE, Shannon IJ, Wood J. Palladium supported on bacterial biomass as a novel heterogeneous catalyst: A comparison of Pd/Al2O3 and bio-Pd in the hydrogenation of 2-pentyne. Chem Eng Sci [Internet]. 2010;65(1):282–90. Available from: http://dx.doi.org/10.1016/j.ces.2009.06.069

34. Hart A, Omajali JB, Murray AJ, MacAskie LE, Greaves M, Wood J. Comparison of the effects of dispersed noble metal (Pd) biomass supported catalysts with typical hydrogenation (Pd/C, Pd/Al2O3) and hydrotreatment catalysts (CoMo/Al2O3) for in-

situ heavy oil upgrading with Toe-to-Heel Air Injection (THAI). Fuel [Internet]. 2016;180:367–76. Available from: http://dx.doi.org/10.1016/j.fuel.2016.04.064

35. Cavani F, Trifirò F, Vaccari A. Hydrotalcite-type anionic clays: Preparation, properties and applications. Catal Today. 1991;11(2):173–301.

36. Zarezadeh-Mehrizi M, Ebrahimi AA, Rahimi A. Comparison of γ and δ-Al2O3 supported CoMo catalysts in the hydrodesulfurization of straight-run gas oil. Sci Iran. 2019;26(3 D):1555–65.

37. Su X, An P, Gao J, Wang R, Zhang Y, Li X, et al. Selective catalytic hydrogenation of naphthalene to tetralin over a Ni-Mo/Al2O3 catalyst. Chinese J Chem Eng. 2020;28(10):2566–76.

38. Jongpatiwut S, Li Z, Resasco DE, Alvarez WE, Sughrue EL, Dodwell GW. Competitive hydrogenation of poly-aromatic hydrocarbons on sulfur-resistant bimetallic Pt-Pd catalysts. 2004;262:241–53.

39. Popescu (Stanica) AI, Bombos M, Popovici RD, Bombos D, Bolocan I. Hydrogenation of Naphtalene on Pt-Pd Catalyst. Rev Chim. 2017;68(2):210–4.

Chapter 6

A conceptual approach to offshore wet-combustion for co-production of catalytically upgraded oil and hydrogen gas in the North Sea

6.1 Introduction

The aim of this section of the study is to understand both the oil and H_2 potential of developing an offshore heavy oil field using wet-mode *in situ* combustion to generate heat in the reservoir. The work focuses on a 500ft x 500 ft well pattern comprising a vertical injector and horizontal producer, modelled using the Marx and Langenheim steam heating model (1), in addition to a number of extensively used oil burning correlations used in the Nelson & McNeil ISC planning methodology (2). The combustion characteristics of the oil were determined in order that the thermal energy expelled from the reaction could be used as a basis for the heat injection approximation, the latter of which is crucial in estimating the production potential of *in situ* steam generation. The stream of gases produced from previous field pilots has highlighted a rich stream of hydrogen gas, with field data highlighting in excess of 20 mol.%, which can be used in both hydrogenation reactions within the reservoir, as well as a source of "transparent" hydrogen production (3,4). The contribution of in situ dehydrogenation to the hydrogen potential of a reservoir has been considered in this study. Experimental work on tetralin dehydrogenation has been included to highlight optimised temperatures for generating hydrogen in the presence of clay

minerals, analogous to those which may be located in reservoir mineral complexes. A comparison to thermal dehydrogenation and a Pd-based catalytic liner, the latter of which experimented with a specific temperature window, have been used as a comparison to demonstrate whether dehydrogenation reactions, in the presence of reservoir minerals, should be considered seriously.

While not exclusive to any particular types of fields, this TEOR technique has been the source of interest in developing less mobile, poorer quality heavy oils which suffer from poor production levels (2,5,6). Furthermore, partially water-flooded and low value heavy oil fields could also represent increasingly attractive targets for In-Situ DeHydrogenation (ISDH) as well as in-situ Water Gas Shift (WGS) projects. An abundance of low value heavy oil fields and fields situated within mature basins makes this latter technology an attractive option.

In a financial and environmental climate, wherein, higher quality transport fuels are required, this TEOR may provide a solution to bridge the gap between the reality that low sulphur, lighter oil supplies are needed and the manifestation of an industry becoming increasingly dependent on clean fuels, such as hydrogen (7).

6.1.1 Wet-mode combustion

The majority of heat generated in dry combustion is predominantly stored in the burned rock fabric and therefore cannot be used for oil displacement. In the wet-mode process, illustrated in Figure 6.1, the steam and water banks ahead of the combustion front increase in size thereby mobilising more of the oil, while also conditioning the reservoir volume

ahead of the combustion front and limiting the extent of gas override. The ratio of injected water to air will determine the type of water combustion which can be split into three further categories of incomplete wet combustion, normal wet combustion and super wet combustion (2).

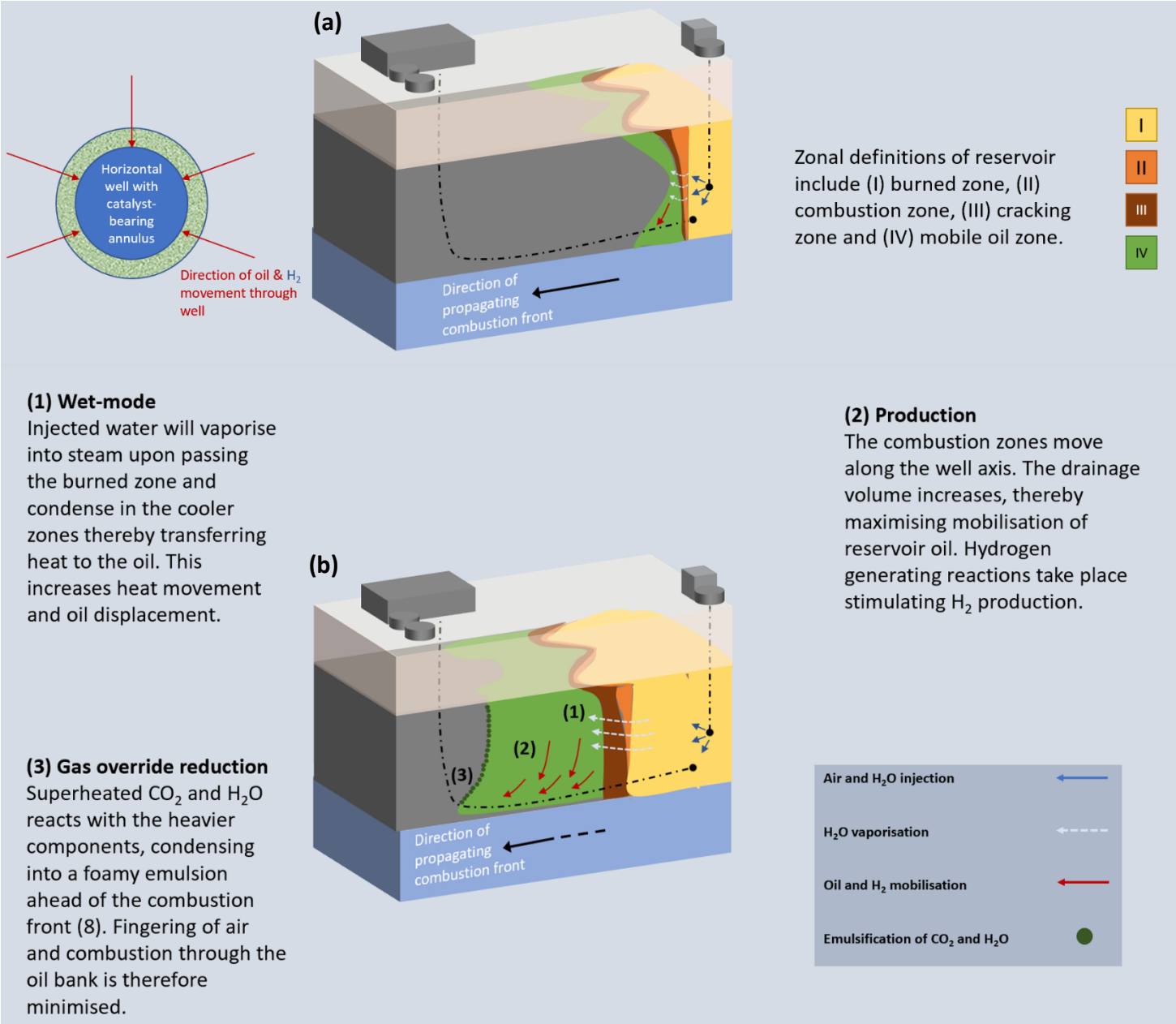

Figure 6.1 (a) Schematic of THAI with corresponding zones as shown in Figure 2.5 **(b)** Schematic of THAI at time *n*, illustrating the lateral movement of the thermal zones along the axis of the production well, while demonstrating the processes involved in and benefits of wet-mode combustion.

6.1.2 Hydrogen Generation

A number of reactions can take place within the different zones under in-situ combustion, both hydrogen generating and hydrogen consuming. It is therefore difficult to predict hydrogen production when any hydrogen produced can be consumed in reactions which take place in the different zones. A great number of these reactions can occur, linked with the different thermal zones of the THAI process. The main contributions to hydrogen generation during in-situ combustion (3), together with the equations, can be found in Table 6.1. It is clear that gas mass transport velocity is crucial in efficiently removing the hydrogen gas from any hydrogen consuming reaction zones to maximise hydrogen recovery (8).

Table 6.1 An estimation of the location of various reactions, predominant in both hydrogen generation and hydrogen generation.

Reaction		**Estimated Zone**
$C + H_2O \rightarrow CO + H_2$	Coke gasification	Zone (I)
$C + 1/2O_2 \rightarrow CO$	Coke oxidation	Zone (II)
$C + 2H_2 \rightleftharpoons CH_4$	Methanation	Zone (I-II)
$CO + H_2O \rightleftharpoons CO_2 + H_2$	WGS	Zone (II – IV)
$CH_4 + H_2O \rightleftharpoons CO_2 + 3H_2$	Steam reforming	Zone (II -IV)

It has been proven at Wolf Lake, when water is co-injected with air under combustion, a fraction of the produced gas can consistently contain 10-20% H_2 (3,4). Under dry

combustion, in the same field, this reduced to 0% which highlights the necessity of a co-injection mechanism comprising air and steam – though this field development specific, as such, dry combustion projects may still produce H_2 to lesser extent.

More recent laboratory data have shown that the hydrogen generation is optimised within the temperature range of 320 and 380°C. If thermal cracking and low temperature oxidation persist, this temperature range can be sustained. The implications of this suggest that a lower proportion of oxygen should be included within the injection fluid to minimise heat generation. Consequently, less oxygen is available to react with hydrogen gas, and more carbon will be available to react with steam and therefore promote hydrogen formation through the gasification, WGS and steam reforming reactions (9).

6.1.3 North Sea

While the North Sea Basin is considered mature, the Central North Sea may offer motivation for TEOR and/or ISDH development. Firstly, the North Sea has been producing oil since the 1970s. Consequently, there is a wealth of valuable data derived from exploratory wells, production wells and seismic acquisitions over the last 50 years. The geology of the North Sea is well studied and resources are readily available. In addition, high resolution 4D seismic studies have been employed to visualise flow patterns over time which can help to remove uncertainty in predicting fluid migration (10). Perhaps more importantly, there is a vast quantity of heavy oil reservoirs, containing up to 10 billion STB, of which only a small

fraction are currently being developed (11). Notable examples of mature heavy oil fields include but are not limited to the Bentley, Mariner and Alba fields. Additionally, the heavy oil reservoirs present favourable properties with high porosity and permeability in addition to being vast in size. Consequently, the development of TEOR techniques in such reservoirs could accommodate significant increases in productivity and offer a chance to increase the quality of the oil before reaching the surface. Furthermore, the problems associated with high integrity overburden are not problematic in the North Sea as reservoir depth is significantly greater than the 150-200m minimum stipulation, which is used in the event of poor confinement, while remaining relatively shallow in offshore terms (12). Moreover, the infrastructure that exists across many of the North Sea fields offers the potential to retrofit existing facilities rather than re-design and install completely new structures. The use of existing water-flood infrastructure for HPAI had a positive impact on economics for both the Coral Creek and Ekofisk field studies (13,14).

The wide-scale use of water injectors is also relevant because the use of water as a pressure maintenance method works under the principle of 'bottoms-up' oil displacement. While this is highly effective as an EOR, large swathes of oil-saturated rock are left in what is known as attic oil deposits, especially when dealing with thick reservoirs >20ft (13). As a result, this segregation allows the air injection process to mobilise the residual saturations of oil, which have been left uncontacted by the water-flooded reservoir.

6.1.3.1 The Ekofisk and Maureen fields

The Ekofisk field, a fractured carbonate reservoir with an estimated 6.4 billion bbl STOOIP, in the Norwegian sector of the North Sea has been the subject of high pressure air injection consideration (14). The design of the processing facilities and required investment was a substantial consideration. An air injection platform, fully equipped with high capacity compressors, as well as a gas process processing platform, containing gas sweetening, nitrogen reinjection and recompression packages, in addition to existing well upgrading were all requirements for the project (14). Simulations indicated that as air enters the matrix porosity, lighter oil fractions are stripped out by diffusion and gravity to drainage into the fracture, leaving the heavier ends to be oxidised. It was also indicated that a stable combustion front could form with a low risk of oxygen breakthrough. A major drawback, however, was the fact that the simulations suggested that the majority of the reservoir volume would be excluded from the oxidation zone and therefore the contribution of oxidation to recovery was minimal in this instance. To apply full field-scale air injection, it was deemed necessary to recomplete 30 production and 30 injection wells and install an air injection platform with gas handling facilities. The evaluation finalised a capital expenditure estimate of 2.7 billion USD which is a considerable investment. However, the project was deemed unviable given an additional oil recovery estimate of 5% and the combination of capital and operating expenditure, taking into account project uncertainties (14). It was decided that further work to delineate the uncertainties was not necessary as technologies such as continued water injection were more competitive.

Fraim et al. (15) conducted a preliminary accelerating rate calorimeter and combustion tube experimentation on a North Sea prospect, the Maureen field. Waterflood oil recovery achieved up to 53% of the OOIP, however a residual oil saturation in the reservoir at 0.23 estimated a further 175 $x10^6$ bbl remaining. The air injection process was subsequently modelled in the mode of a miscible gas (hot carbon dioxide/steam flood) EOR using the history matched waterflood model. The model comprised a 3D, 3-phase black oil simulator using six discrete geological layers. This study was particularly positive yielding results which suggested an incremental oil recovery up to 26.3 MM STB or 6.6% OOIP, up to 4 API point increase in oil quality at a maximum cost of $1.5 US/bbl (15).

6.2 Methods

6.2.1 Reservoir Selection Criteria

The Selection of appropriate reservoirs is key to implementing a successful combustion project. Within guidelines previously stipulated, geological characterisation is crucial. Combustion is suitable for reservoirs exhibiting good sand continuity and lateral extent, while situated in traps with a high overburden integrity (2). Economically-successful projects have been conducted in depths varying from 300 to nearly 12,500ft (2). Ideally a trade-off is needed to ensure sufficient air injection pressure can be introduced and retained by competent overburden while also preventing an excessive cost of air injection related to higher depth prospects. While 50ft has been mentioned as an upper thickness limit, one

reason for this is due to its ability to auto-ignite. However, with the adequate inclusion of bottom-hole ignition system management, this problem can be overcome. Table 6.2 details reservoir characteristics which have been suggested as ideal candidates for ISC.

Reservoir heterogeneities can severely inhibit a combustion flood, e.g. excessively fractured systems or high permeability thief zones, unique reservoir management systems can be installed to accommodate variations in reservoir architecture. Moreover, when faced with natural channel or induced channel structures, a pressure-up blowdown combustion process was developed for the Wolf Lake project. Production wells are restricted at the time of heat breakthrough to the producer. Once the channel system is sufficiently pressurised, the injection process is paused and the production wells are opened without restriction. The channels become saturated with oil, hosting the combustion. Once the reservoir is blown-down sufficiently, the entire process is repeated (4).

Using the criteria provided in Table 6.2, reservoirs in the North Sea were identified as potential offshore targets for the ISC process.

Table 6.2 Reservoir characteristics with corresponding limits deemed appropriate for *in situ* combustion recovery.

Parameters	**Sarathi (1999)** (2)	**Turta (2013)** (12)
Oil viscosity (cp)	<5,000	60 -10,000
Oil API Gravity	10-40	-
Oil Composition	Low asphaltenes, <50 ppm heavy metals	-
Reservoir Depth (ft)	300 – 12,500	
Reservoir Thickness (ft)	5 – 50 (up to 150 have been economically successful)	>9
Reservoir Permeability (mD)	Not critical	>100
Reservoir Porosity	>0.18	>0.18
Oil Saturation	>0.09	>0.07
Reservoir Mineralogy	Low in pyrite, calcite and siderite (coke promoters)	-
Fracture Networks	Undesireable	No

6.2.2 Analytical Model

A step-by-step procedure for implementation of this technique can be based on Nelson and McNeil's method comprehensively explained by Sarathi (2) analytical design procedure, based on a modification to the steady state radial flow equation. This yields a reasonable plan based on preliminary combustion tube data and a wealth of real-world data taken from both real-time data and post-mortems of successful and failed projects. As this procedure does not discriminate between shallow and deep prospects and the data it is based on spans shallow reservoirs to those >10,000ft in depth, there is no reason that it cannot be adapted for offshore production. As a result, rather than technical constraints providing the barrier to trialling this EOR offshore, it will predominantly revolve around economic constraints and company policy.

In the absence of combustion tube experimentation, regression correlations have been used to determine the fuel deposition and air requirement parameters based on work in Chu (2). With these parameters, the Nelson and McNeil (2) analytical method can be employed to realise important parameters including injection well bottom-hole pressure and oil recovery, which can be used to aid in the engineering of an ISC project. While the method is based upon a number of assumptions, it has been produced and validated by a wealth of field experience which enable the engineer to derive reasonable results. Furthermore, a number of averages have been taken to demonstrate reservoir properties, The 5-spot well pattern used in the Nelson and McNeil method has been converted into a horizontal production well pattern. An understanding of the current horizontal well regime in the Alba field has been

used in the model to derive an alternative route to production using horizontal wells in a configuration similar to the THAI process. This horizontal well configuration serves to increase contact between producer and combustion front, reducing gas override and incorporating a short-displacement mechanism. A dual-vertical injection and single horizontal production pattern in staggered line drive has been selected as the desired configuration, suggested as a suitable well pattern by Xia et al. (16).

The method however, does not consider the non-linear growth of the heated zone ahead of the combustion front. This must be considered as this significant heat transfer throughout the reservoir will have the effect of mobilising additional oil-derived from the comparatively larger steam and condensation zones ahead of the combustion front, when comparing to dry combustion. This would therefore yield higher production rates at any given time, particularly where horizontal producers are present. Furthermore, this also has the effect of reducing the total volume of oil used for a fuel source. Consequently, this study has uniquely applied the Marx and Langenheim heating model, as shown in Ahmed and Meehan (1), which can approximate the areal extent of the heated steam zone as a function of time from which an estimate of additional oil mobilisation can be calculated given the extent of steam zone growth, as would be present in wet combustion. It is assumed that the steamed zone will mobilise the oil at an efficiency level pre-determined, at a calculated oil displacement flow rate. The residual saturation of oil will be cracked, vaporised and mobilised by the mobile combustion front upon contact.

A sensitivity analysis has been employed based on a variety of saturation levels to discriminate between the difference in oil saturations which reflect attic oil and waterflooded packages within a mature, previously-developed, reservoir. Furthermore, the combustion front velocity has also been considered in the sensitivity analysis to understand its effect on the total time required for pattern area depletion.

No indication of chemical upgrading has been incorporated into the model and as such the monetary value associated with these chemical reactions has not been determined, rather it is acknowledged that it will have a positive effect on the quality of oil and therefore the project economics.

6.2.2.1 Model Assumptions

The equations detailed in this section are supplemented with the following nomenclature.

Nomenclature

As(t)	extent of "steamed area" as a function of time
Erfc	complementary error function
t_D	dimensionless time
λ_R	thermal conductivity of cap and base rock, BTU/hour-ft-°F
q_{od}	displaced oil rate, bbl/day
P_{iw}	bottom hole pressure of injection well, psia
P_w	bottom hole pressure of production well, psia
i_a	maximum air rate, SCF/day
t_1	time to reach maximum air rate, day
S_{oi}	initial oil saturation
S_{or}	residual oil saturation
S_w	water saturation
ρ_o	oil density, lb/ft^3
ρ_w	water density, lb/ft^3
ρr	rock density, lb/ft^3
C_o	specific heat of oil, BTU/lb-°F
C_w	specific heat of water, BTU/lb- °F
C_r	specific heat of rock, BTU/lb-°F
μ	viscosity, cP
h	pattern thickness, ft
d	pattern depth, ft
L	pattern length, ft
a	distance between wells, ft
r_w	radius of production well, ft
K	permeability, mD
K_a	permeability with respect to air, mD
M	volumetric heat capacity of reservoir, BTU/ft^3-°F
M	fuel deposit, lb/ft^3
H_0	heat injection rate, BTU/hour, adapted for ISC process - BTU/lb coke based on 80% fuel to steam efficiency; 11,500 – 14,000
Φ	porosity
ΔT	change in temperature, °F
T_f	Formation temperature, °F

The thermal conductivity of the reservoir in question was estimated using the Tikhomirov relationship (1) demonstrated by Equation [6.1].

$$\textbf{[6.1]}\ \lambda_R = \frac{6.36(e\text{^}(0.6\ \rho_r + 0.6\ S_w))}{(0.556\ T_f + 255.3)^{0.55}}$$

This is a function of the dry rock density (ρ_r), water saturation fraction (S_w) and the formation temperature (T_f).

A prediction of fuel deposition was derived using a correlations derived by Chu (2), demonstrated in Equation [6.2].

$$\textbf{[6.2]}\ M = -0.12 + (0.00262*h) + (0.000114*K) + (2.23*\ S_{oi}) + (0.000242*((h*K)/\ \mu)) - (0.000189*d) - (0.000652*\ \mu)$$

This regression correlation is used as a preliminary approximation for fuel deposition as a function of reservoir thickness, permeability of the formation, oil saturation fraction, viscosity at reservoir temperature and formation depth.

The heat injection rate was estimated using the BTU hr^{-1} liberated from the *in situ* coke lay-down and combustion, demosntrated in Equation [6.3].

$$\textbf{[6.3]}\ H_0 = [(BTU\ lb^{-1})\ *coke\ lb\ *\ M*h*(burn\ rate)*L]$$

This is a function of the predicted coke formation (coke lb) and BTU lb^{-1}, burn rate of the process (ft day^{-1}), pattern length (L) and pattern thickness (h).

An estimate of the steam zone growth as a function of time is quantified using Equation [6.4], taken from the Marx & Langenheim steam heating model (1).

$$\textbf{[6.4]}\ A_s(t) = \left[\frac{(H_0*M*h*D)}{(4*43560*(\lambda_R)^2*\Delta T}\right] * (G*t_D)$$

The production derived from combustion component is assumed linear over time as the production well is horizontal and therefore a short-displacement mechanism ensues with a constant velocity (5,16). To account for the convergence of the combustion front into the "steamed" zone, the heat loss function has been utilised to generate production data relating to the particular area at time, using Equations [6.5-6.6].

$$\textbf{[6.5]}\ G*t_D = e^{tD}erfc(\sqrt{t_D}) + 2\sqrt{[(t_D/n)-1]}$$

$$\textbf{[6.6]}\ t_D = [(4*(\lambda_R)^2)/(M^2*h^2*D)]$$

The volumetric heat capacity of the formation (*M*) is given by Equation [6.7],

$$\textbf{[6.7]}\ M = \Phi(S_{oi}\rho_{oi}C_{oi} + S_w\rho_wC_w) + (1 - \Phi)\,\rho_rC_r$$

dependent on the density at reservoir temperature (T_f), specific heat and saturation fraction of the oil and water phases (C_o, C_w, S_o, S_w, respectively) in addition to specific heat of the formation (C_f), density of the formation at reservoir temperature (ρr) and the formation porosity (Φ).

The steam-related production data is derived using Equation [6.8],

$$\textbf{[6.8]}\ q_{od} = 4.275*[(H_0*\Phi*(S_{oi}-S_{or}))/(M*\Delta T)]*(\ e^{tD}erfc(\sqrt{t_D}))$$

This is calculated as a function of the volumetric heat capacity of the formation (*M)*, saturation difference between initial oil and residual oil (S_{oi}-S_{or}), porosity (Φ) and the complementary error function ($e^{t_D}erfc(\sqrt{t_D})$) to account for heat loss .

Several assumptions in the Nelson & McNeil model (2) were used to predict the mobilisation and production of oil from the combustion front affected rock volume. The required injection pressure (P_{iw}) is derived from a modified version of the steady state radial diffusivity equation as shown in Equation [9], values of which are demonstrated in Appendix C. The areal sweep efficiency of the burned region in the combustion zone is based on a dimensionless flow term set at 52.5%. The volumetric sweep efficiency (V_e) of the burned region in the combustion zone is set at 100%, 75% and 50% for direct comparison. The unburned region constitutes volume of oil-bearing rock post-steam and post-combustion, as a function of the volumetric efficiency. Theoretically, the only oil left behind is that missed by the combustion front which has been suggested to retain a figure near zero in the literature (2,17).

The fuel deposit of the reservoir pattern in question was used to calculate the equivalent heat injection rate, BTU as a function of time as shown in Equation [6.6], required to calculate steam growth.

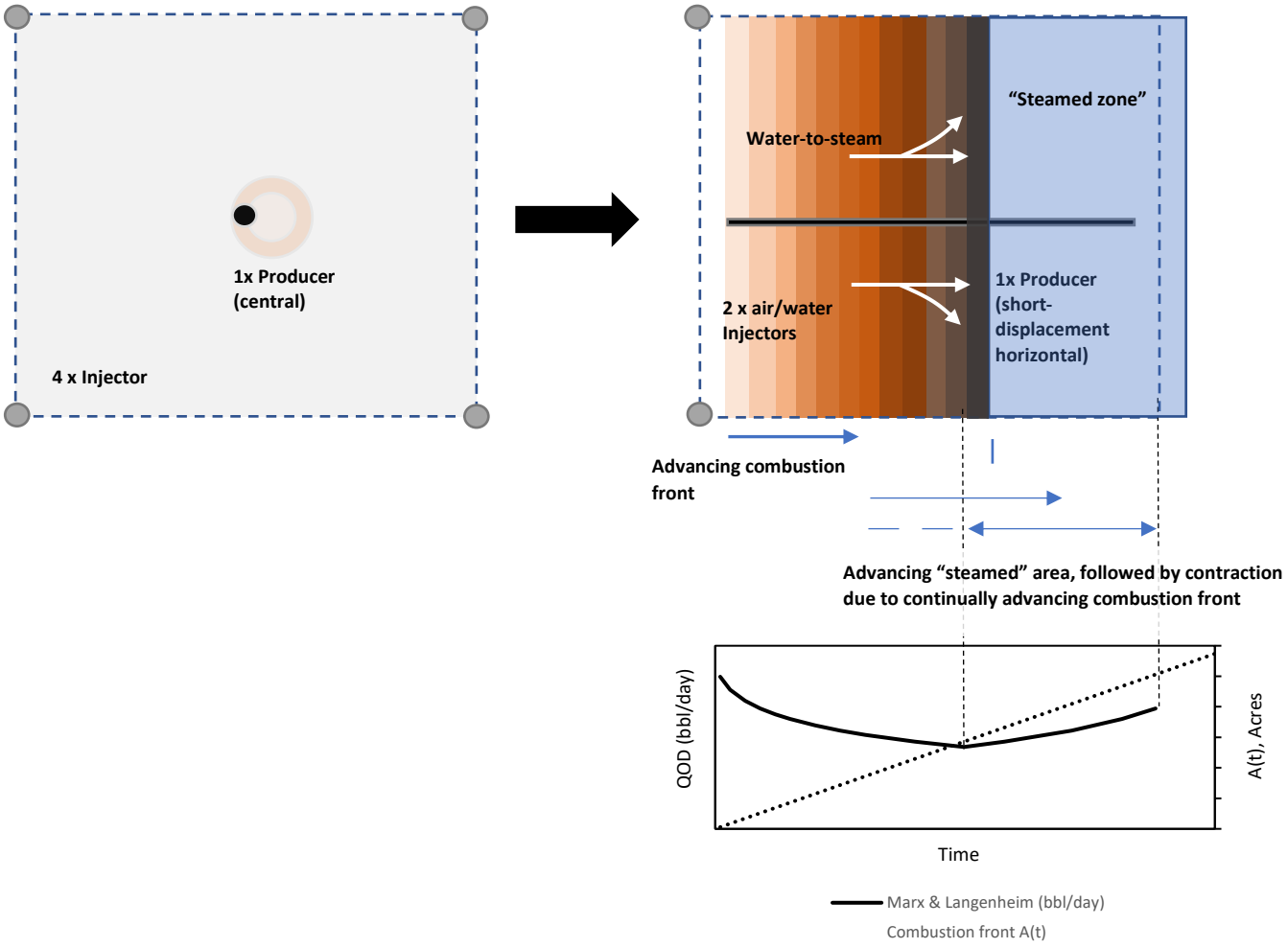

Figure 6.2 Areal schematic of the THAI well design as a conversion from a conventional 5-spot well pattern, highlighting dimensions used in the analytical model.

6.2.3 Estimating Amount of Hydrogen

It is useful to look at hydrogen as a fuel substitute in terms of barrels of oil equivalent (boe) as a clearer comparison can be made. This is a unit of energy based upon the amount of

BTUs available in one barrel of oil or 158.9 litres. Given both the predicted number of barrels liberated from the pattern, in addition to the bbl/boe ratio derived from typical dehydrogenation reactions, a tentative figure can be produced to estimate boe H_2 which could be generated in-situ. A comparison has been made to previous literature data, which itself is based on thermal cracking and LTO, which estimates hydrogen production from in-situ combustion of bitumen (8), highlighting the potential to augment production systems thereby favouring H_2 production.

To contrast the theoretical calculations, simulated dehydrogenation of a heavy oil was conducted in a 100 mL stainless steel Anton Parr batch reactor using tetralin as the partially-hydrogenated starting material. In order to integrate the experimental data into the production model, the oil in the model was considered to comprise tetralin i.e. a single component. The conditions were assessed to understand the effect of temperature and pressure on the reaction using a set range governed by both previous works and the ranges estimated within in situ thermal recovery processes. The stirring speed was set at 1000 rpm, a N_2 atmosphere of 40 bar and a catalyst to reactant ratio in the ranges typically used in second-stage hydrotreating reactions, the conditions of which reflect similar values to those used in the reverse dehydrogenation reactions (8). The catalysts used in this study consist of a LDH-derived NiAl(O) and $Pd_{1\%}$/alumina which have been fully characterized earlier in the study. During the 20 min heating-up stage, a low pressure N_2 atmosphere was added to inhibit any reaction prior to the reaction temperature set-point. At this temperature a 0.5mL vial was collected and analysed to confirm the initial concentration of the reactants corresponded

with the solution prior to heating. The gas in the reactor was drawn down before N_2 at 40 bar was added to the reaction vessel. This represents the pressures normally encountered in the reservoir under thermal EOR. This was also critically denoted as the time for reaction commencement. Liquor from the reaction was collected in vials at 20 min intervals for 2 h to measure the progression of the reaction.

All liquid samples were analysed using Agilent Technologies 6890N GC with a corresponding 7683 B Series injector. An Agilent 19091J-413 capillary column (nominal length, diameter and film thickness at 30.0m, 320.0 μm and 0.25 μm, respectively) was used accompanied with the following method: equilibration time of 3 min, with a ramp from 80℃ to 135℃ over a 9 min period and second stage to 300 ℃ over a 4 min period. The components were separated according to boiling point. The identified reaction components included tetralin and naphthalene. Five-point calibrations were made both isolated in the solvent and in the presence of the other products/reactants, to ensure no complications were prevalent in the analysis of reactant and product mixtures.

6.3 Results

6.3.1 Offshore Candidates

While the criterions detailed in Table 6.2 are useful as a starting point, it should be noted success in ISC has been found in varying rock types with varying lithologies. The general guidelines therefore reflect technology at the time of submission while the economic climate will undoubtedly have a significant impact on the viability of such a process. Each

reservoir should be analysed individually and both geological and engineering judgements, based on a combination of field and combustion tube data, need to be made before any pilot study is committed.

The heavy oil reservoirs of the North Sea are located in the Central North Sea area. Within this region there are relatively shallow post-rift Lower Cretaceous or Paleogene reservoir sandstones which reduce the susceptibility to regional rift-induced fracturing. Some of these examples include the Captain and Alba fields. Table 6.3 highlights the properties of these reservoirs and potential suitability to ISC. The calculated thermal properties have been added to Table 6.3[1-2].

Table 6.3 Reservoir characteristics of heavy oil fields situated in the North Sea which may prove adequate ISC and ISDH targets.

Parameters	**Alba field** (10)	**Captain field** (18)
Oil viscosity (cp)	9-6	150-47
Oil API Gravity	19 (S.G. 0.94)	19-21
Oil Composition	-	
Reservoir Depth (ft)	6465 (OWC)	2700
Reservoir Thickness (ft)	*350-400 net to gross (NTG) (Intra-reservoir shales between 20-50ft)	<300

Reservoir Permeability (mD)	2000 – 3000	7000
Reservoir Porosity	0.35	0.28-0.34
Oil Saturation	0.9-0.93 at field sanction	0.84
Reservoir Mineralogy	Clean sands, slightly micaceous with a low detrital clay content	Fine to medium sandstones with very little silt or claystone
Fracture Networks	Limited	Minor diagenetic alteration
Top Seal	Shale	Sola Shale and Chalk Group
[1]Volumetric capacity of reservoir rock (BTU/ft^3-°F)	34.52 (S_o 0.8) 39.90 (S_o 0.6) 45.27 (S_o 0.4)	-
[2]Thermal conductivity of base and cap rock (BTU/hour-ft-°F)	0.975 – 1.044	-

Table 6.3 ***(cont.)***. Reservoir characteristics of heavy oil fields situated in the North Sea which may prove adequate ISC and ISDH targets.

6.3.1.1 Alba reservoir characterisation

The Alba reservoir has been described as a simple binary system of 'clean' unconsolidated sands inter-bedded with thick impermeable shale units. It is an elongate channel-fill structure comprising turbiditic sediment, located in the Central North Sea block, 16/26 approximating 225km NE of Aberdeen (19). It is approximately 9km in length and 1 to 1.5km

in width, dipping gently to the SE. With a STOIIP of approximately 1000 x10^6 bbl, as of 2012 390 x10^6 bbl of oil had been recovered. Coupled with a predicted recovery factor of 0.55, this means that a considerable proportion of oil will be left behind following abandonment. This carefully demonstrates the limit of current technologies which are employed to enhance total oil recovery. However, given in-depth feasibility studies the possibility of integrating high pressure air injection into mature fields both onshore and offshore can seek to demonstrate the capabilities of existing technologies in yielding more efficient production profiles and therefore maximising asset value. Facilities on the field include an ANP platform containing 31 slots (25 platform producers with 6 injector wells), with an additional 12 slot AXS subsea manifold containing 10 producers and 2 injectors with production in excess of 25,000 bopd gross (19).

The Alba field has been subject to a 4D seismic survey (1991, 1998, 2002 & 2008) over the course of the field's production life. This has helped to delineate reservoir saturation, existence of faults including those of which pertain to baffles, in addition to conduits to flow, all with a relative high accuracy. Moreover, the interpretation of the field's geology has evolved over time. It has been suggested that the Upper Jurassic Harlev Formation (East Greenland) demonstrates an accurate analogue to Alba and that a thinning edge model is more accurately applied to the geological regime. As a result, field edge targets have been observed, using the more accurate model and knowledge from reservoir flow pattern, and well-paths determined to uncover un-swept reservoir packages (19,20).

While the Alba reservoir sequences are very thick, the presence of thick interbedded shales may be used to the advantage of the ISC process and a pilot. The thickness of a reservoir is an important factor for auto-ignition but also gas override which will be more significant in thicker reservoirs such as Alba. However, there are a number of field observations which may mitigate this problem rendering it only a superficial setback. Firstly, the presence of thick inter-bedded shales will essentially compartmentalise the reservoir into smaller more convenient sub-units. These serve to isolate certain un-swept edge targets in the reservoir which could be ideal for ISC pilot tests both 'dry' and 'wet'. The shale units can serve as effective vertical baffles by isolating the air injection i.e. preventing gas override thereby producing a more stable combustion front which can sweep through a particular sub-unit more efficiently. Additionally, shale units can be used as an anchoring point to ensure lateral sweep. Reservoirs that have been previously developed with thermal recovery techniques such as the Lower Grand Rapids Formation at Wolf Lake, have also been compartmentalised by thin but effective shale barriers (4). Finally, the presence of horizontal producers as demonstrated in the THAI ISC augmentation can further reduce the risk of gas override. In this instance, the horizontal wells should be completed in parallel with the shale units along Alba's channel transect to maximise recovery.

In the case of both the Alba and Captain fields, the reservoirs have been completed previously using technologically-advanced horizontal producer wells and consequently may be suitable for recompletion. Additionally, the historical use of horizontal wells in itself is an important factor as it diminishes the technical difficulties found in implementing complex

well systems in a reservoir for the first time, while also being able to take advantage of the necessary infrastructure.

For the purposes of preliminary assessment, the Alba field has been selected as the subject for an offshore ISC pilot, making up a 5.73 acre well pattern, which is similar to previously modelled reservoir well patterns (14). Within this pattern area, the following initial saturations (S_0) have been used 0.8, 0.6 and 0.4 which equates to an OIP of 620,000, 470,000 and 310,000 bbls, respectively.

6.3.2 Model Hybridisation

l

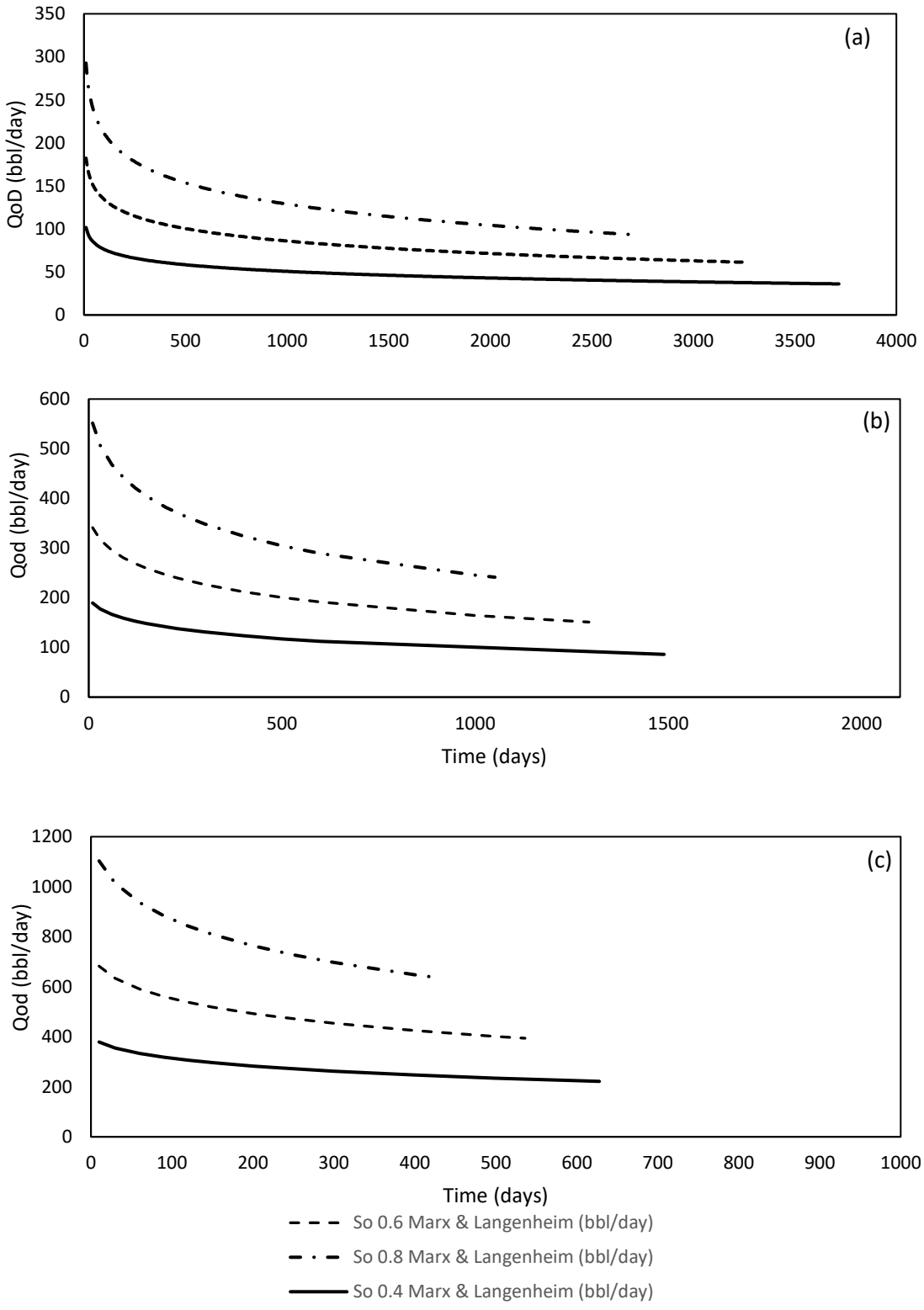

Figure 6.3 Graphical illustration of time taken to complete steam flood and consequent drawdown of flow rate as dictated by enlargement of steam area and the corresponding heat loss function across saturations for burn rates (a) 0.25 ft/day, (b) 0.5 ft/day & (c) 1 ft/day.

saturation decreases, the length of time to produce the total bbls liberated for the set steam efficiency rating increases for each burn rate. The theoretical number of days taken to complete steam flooding for a a given burn rate is demonstrated in Figure 6.3 (a,b,c). For a burn rate of 0.5 ft/day, increasing across saturations S_o 0.8, 0.6 and 0.4, the total time taken reaches 1051 to 1294 to 1489 days, respectively. This correlation is apparent due to the fact that a lower oil saturation equates to a lower amount of heat available which therefore inhibits the growth of the steam zone considerably. Furthermore, while the general trend is similar for each burn rate, as the burn rate decreases, the time taken for each saturation disproportionately increases. This highlights the direct impact of less heat (BTU)/unit time generated from the reduced combustion zone movement on which the steam model is dependent.

In reality, the combustion front migration at rates of 1.0, 0.5 and 0.25 ft/day have reached total pattern length after 500, 1000 and 2000 days, respectively. Consequently, the time taken to complete the steam flood, as predicted by the initial steam model component and equating to the total bbls produced given the steam efficiency rating (55%), becomes unobtainable if the EOR technique incorporates a moving combustion front. This problem in the dual-mode combustion front and steam model can be mitigated, however. As the production profile for the steam flood ensues, it is clear that at a point wherein the total area 'steamed' is at its maximum, the heat loss error function can no longer continue to effect a greater proportion of in situ heat loss. An increase in the heat loss is directly responsible for a reduction in the production rate. This continued reduction in production

rate lends itself to the hugely extended period of time, as predicted by the initial steam model, for the steamed zone to reach maximum pattern area.

The 'steamed' area however is subsequently reduced in size, after a certain "pivot point", by the addition of a mobile combustion front in the process. Using the same heat loss function,

this time correlated with the distance from the pivot point rather than the accumulated

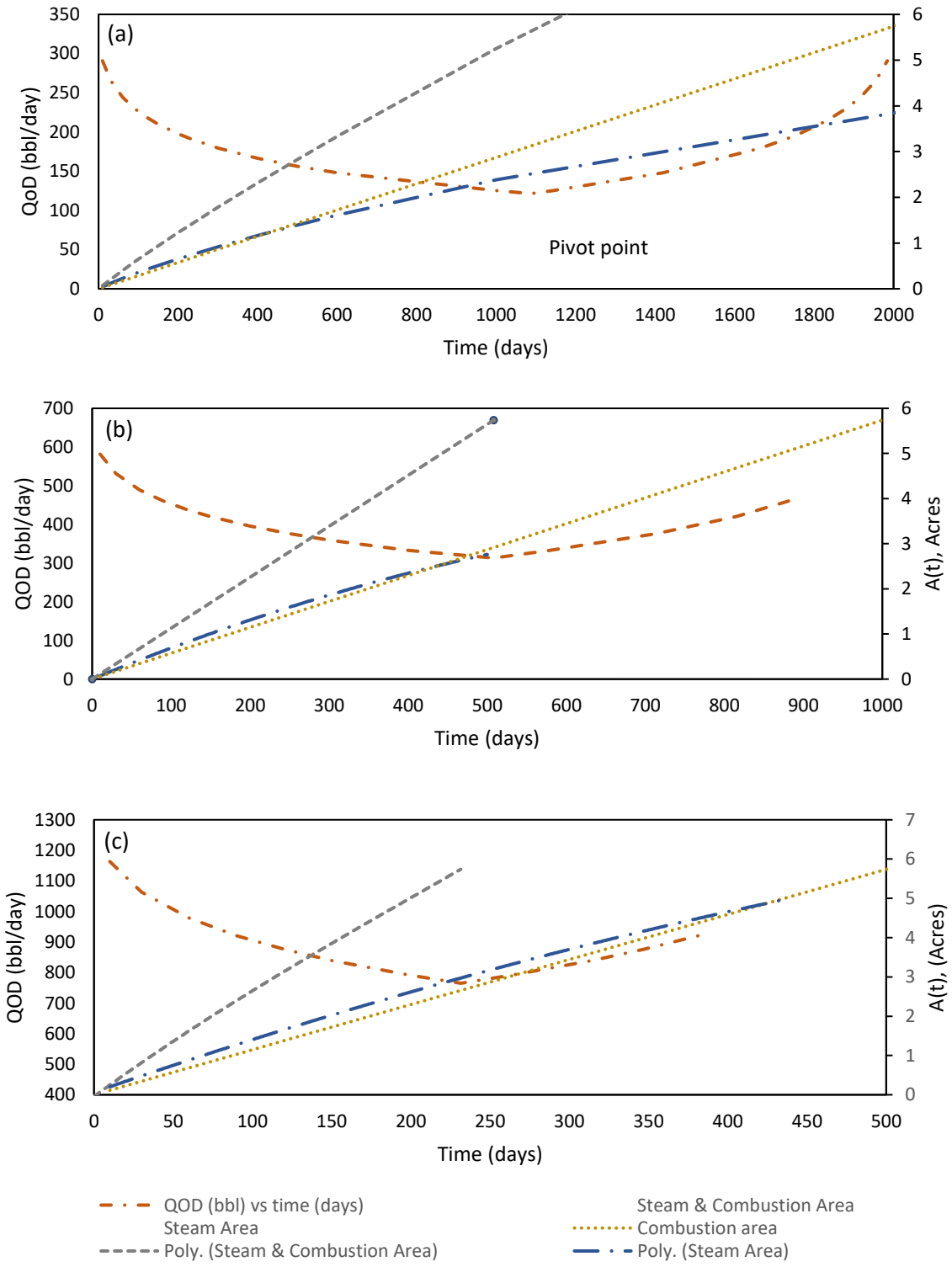

Figure 6.4 Graphical illustration of the growth and subsequent encroachment of the "steamed" zone with time, highlighting the combined areal extent of the steam and combustion (including coked) zones as well as individual progression of the two zones for (a) 0.25 ft/day, (b) 0.5 ft/day and (c) 1 ft/day burn rates, set at 50% volumetric efficiency of the combustion front and total S_o at 0.8.

time, the production ate of the pattern area can be predicted to increase. This increase in production is defined by the reverse of the GtD function and is demonstrated in Figure 6.4 (a,b,c) where QoD (bbl/day) begins to increase at a point defined by the steam reaching its maximum extent in the pattern area. The production for this specific period is calculated from the difference between the estimated total swept for the given steam efficiency and the cumulative production to the point at which the combined steamed and coked region reaches the total pattern area, the "pivot point". For each burn rate at each S_o 0.8, 0.6 and 0.4, the total pattern area, i.e. where the total 'steamed' area is at its maximum, is demonstrated in Table 6.4.

Table 6.4 Time taken to complete areal extent of pattern area with both combustion and steam across different burn rates at different oil saturations.

Burn rate (ft/day)	**S_o 0.8**	**S_o 0.6**	**S_o 0.4**
1.0	237	291	340
0.5	508	613	706
0.25	1105	1304	1474

As the burn rate increases, a disproportionate reduction in the time taken to "steam" the entire pattern area is apparent. With a higher burn rate comes a greater amount of energy which can be carried forward using the water. Consequently, for the same pattern area more steam is available to cover an area at any point in time and therefore the time taken to 'steam' the pattern area is reduced.

This point in time for the model to reach the total pattern area, the pivot point, correlates to the time at which production will be least, i.e. heat loss is highest and therefore dictates a point at which the economics of a project become less favourable according to the Marx & Langenheim model. As a result, it will remain a crucial factor in the planning of a pattern area.

The total time taken for steam-model derived recovery is dictated by this same trend i.e. with a higher burn rate being disproportionately favoured. This is apparent as the model assumption, to incorporate the encroachment of the combustion front into the "steamed" area, has led to the reliance of the predicted production on the now reducing error function, following the "steamed" pattern area pivot, which was used to reverse the time-based uncertainty in terms of the heat generation and loss.

This reconfiguration of the steam model, in the presence of a combustion front, is not without justification as similar trends can be observed in experimental simulations of wet-combustion. The combustion cell experimental run 985 in Xia et al. (16) highlights a significant production increase as the combustion front continued along its axis of movement in the combustion chamber and, in essence progressively compressing the steam zone. Furthermore, Bagci, and Bagci and Kok (21,22) demonstrates subsequent rises in production rate under BKWC1, 2 & 4 wet combustion experiments as the combustion front moves into the latter stages of production. Additionally, under the hybrid of air and steam injection simulations performed by Yang et al. (17), a significant increase in production occurred prior to pattern completion. A comparison made to the simulation of steam EOR

production highlights this effect exhibited, however less pronounced owing to the lack of a continually driving combustion front.

This alteration of the predicted production curve can help to alleviate the problems encountered when incorporating a mobile combustion front, moving over a linear trajectory and encroaching into the consequently depleting steam zone, in combination with the Marx & Langenheim steam model.

The remaining oil remaining is thought to be either consumed in the coking process or produced as upgraded oil. This model has used a set of qualifying areal and invasion efficiencies to estimate a volumetric efficiency for the combustion component. Percentages of 50, 75 and 100 were chosen to demonstrate the effects separating poor and ideal air injection compatibility for the chosen reservoir. That said, it has been widely recorded that a combination of in-situ steam generation and combustion can yield high recovery factors, nearing 90% in some instances (16,17,21).

Descriptions of this component of the process have defined the “bulldozer” effect as acting to either sweep up or burn the residual oil saturation to near zero, culminating in recovery factors up to 90% (17). As a result, this justifies the use of relatively high volumetric sweep efficiency ratings used in the analysis.

Table 6.5 Summary of (a) total recovery factors and (b) contribution by the combustion model, across saturations and combustion volumetric sweep efficiency ratings, at a fixed steam efficiency of 55%.

(a)

$V_{E\ (combustion)}$	**Total Recovery Factor (0.5ft/D)**		
	S_o 0.8 (mmbbl)	**S_o 0.6 (mmbbl)**	**S_o 0.4 (mmbbl)**
100	81.06% (0.51)	77.49% (0.36)	67.14% (0.21)
75	74.43% (0.46)	72.02% (0.34)	63.99% (0.20)
50	68.26% (0.42)	65.94% (0.31)	64.24% (0.19)

(b)

$V_{E\ (combustion)}$	**S_o 0.8** (bopd)	**S_o 0.6** (bopd)	**S_o 0.4** (bopd)
100	32.72% (165)	28.24%(103)	18.77% (39)
75	26.72% (124)	22.78% (76)	14.77% (29)
50	20.10% (83)	15.66% (51)	11.03% (20)

The total recovery factors and contributions of combustion to recovery are demonstrated in Table 6.5. As saturation decreases so does the recovery factor for each burn rate. The highest recovery rate reaches in excess of 81% while the lowest rate reaches only 62%. In reality, the burning characteristics of the oil will have a significant impact on the total recovery. This is in part due to the fact that this will dictate what percentage of the oil will produce coke. The higher the coke formation, the less oil that can be produced. However, if

a greater fuel to steam efficiency is favoured, the excess coke formation may promote greater steam penetration and drainage. In this instance, sacrificing combustion-derived recovery will enhance steam-based recovery further ahead of the combustion front. This in turn can favour the reliance of production on the steam model and promote reactions such as WGS and steam reforming.

What's more, coke formation is predicted from a non-linear function, based on numerous field trials. At lower saturations a higher proportion of the residual oil is transformed into coke, which is required to maintain the combustion front. While resulting in a decreased production of oil, however, this results in a relatively higher amount of BTU/bbl residual oil produced and may serve to provide a more impactful platform upon which to upgrade the oil and produce a higher proportion of hydrogen from the combustion front.

It is clear that the higher the burn rate and S_o, the more favourable the economics from the perspective of time to completion as it yields higher production rates. In terms of ultimate recovery of steam-derived production, this is expected the same as the additional BTU available will aid in the time-dependent expansion of the steam flood and assuming the same flood efficiency, will produce the same amount of initial oil-in-place, just at a different rate. For each saturation, the same proportion of oil production is predicted, given the steam efficiency invasion of 55%.

That said, while the production generated from each mechanism as a proportion of the total favours the steam model, it is the combustion component which remains responsible for the

high temperatures demonstrated in the reservoir, due to the coke production and therefore energy generation. This is in turn important for a number of reasons including;

(i) The oil produced from the residual saturation, following steam flooding, will be upgraded to a greater extent

(ii) More coke will be produced which equates to a greater opportunity for in-situ coke gasification – translating as an ultimately richer source of hydrogen gas

(iii) More dehydrogenation, WGS & steam-metal reactions may occur in the presence of natural catalysts in the reservoir to promote hydrogen production

Additionally, without the combustion front, the steam model production rate would be significantly depressed by the time taken to “steam” the reservoir while the “bulldozer effect” accompanying the combustion front would not be available to seal-off and drain the reservoir nor provide an acceleration to steam growth and recovery during the encroachment period.

Consequently, this prevents the need to make a direct comparison in terms of production for each component – steam and combustion-derived production. In the absence of a combustion front, steam generation would be required at surface using an external energy source. Furthermore, vacuum insulated tubulars would be required to significantly minimise high heat loss along the injection well from platform to sea floor and then to formation (23).

6.3.3 Hydrogen generation

6.3.3.1 Theoretical dehydrogenation

It is important to acknowledge the difficulty in predicting hydrogen gas generation from an in-situ thermal process, which itself remains difficult to model. The abundance of reactions that are plausible remain extensive. Furthermore, it must be stated that potential hydrogen generation reactions will be at least partially inhibited by potential consumption reactions. However, that said, some cases of in-situ combustion have resulted in excess of 0.20 mol.% H_2 in the produced gas (8). In the event that suitable catalytic liners can be installed within the production wells, this may be increased significantly with the promotion of dehydrogenation reactions through use of in-situ mineral structures and/or active deployment of catalysts in the reservoir.

Table 6.6 Summary of example dehydrogenation reactions and hydrogen production from linear to polycyclic hydrocarbons.

Reaction	**Density (kg/m^3)**	**M_w of Feed (g/mol)**	**Feed : hydrogen (molar ratio)**	**bbls feed / boe hydrogen**
$C_nH_{2n+2} \rightleftharpoons C_nH_{2n} + H_2$	730	142.29	1:1	28.8
$C_{10}H_{12} \rightleftharpoons C_{10}H_8 + 2H_2$	970	132.2	1:2	10.1
$C_{10}H_{18} \rightleftharpoons C_{10}H_8 + 5H_2$	896	138.25	1:5	4.6
$C_{14}H_{24} \rightleftharpoons C_{14}H_{10} + 7H_2$	914	192.3404	1:7	4.5

A heavy paraffin such as n-decane represents an example of a compound in a light crude oil. 1 mole of n-decane dehydrogenation will produce 1 mole of decene and 1 mol of hydrogen gas. There are 51.72 lb mol for every 1 boe H_2. Therefore 51.72 lb mol of n-decane will need to undergo dehydrogenation. This equates to 7,359lbs or 28.8 bbls. However, if tetralin is substituted in for n-decane, an example of a component in heavy crude oil, the volume in bbls required to generate 1 boe hydrogen becomes 10.1 bbls. If decalin is substituted, this figure becomes 4.6 bbls, representing a medium crude oil.

With increased condensation of the poly aromatic hydrocarbons, e.g. perhydroanthracene, while a lower lb mol of feed is required to generate the same lb mol of hydrogen, the increase in molecular weight offsets the higher hydrogen storage capacity. As a result, 4.5 bbls perhydroanthracene needs to be dehydrogenated to generate 1 boe hydrogen which is not a significant improvement on the dehydrogenation potential of a component such as decalin. Again, perhydroanthracene is a component which can be used to represent compounds found in heavy oils. In any case, it is still indicated that heavier oils containing a higher abundance of poly aromatic hydrocarbons generate a higher efficiency of conversion to dehydrogenate than their lighter paraffin-enriched counterparts.

The model compounds have been selected to represent the various groups of oil, as characterised in terms by density. However, in reality pseudo-compositional models would be used to predict hydrogen generation as opposed to predictions based on ideal reactions of model compounds, but the trend is clear that a higher abundance of cycloIalkanes is preferred for hydrogen storage, while increasing the level of condensation of the rings to polycyclic structures has little advantage over cyclic structures with less condensation.

This estimation procedure demonstrates the increased amount of hydrogen which may be generated from the oil before it is produced at surface, in addition to hydrogen gas which can be produced due to the gasification of oil during the in-situ combustion process and other in situ reactions as stipulated previously in Table 6.1.

6.3.3.2 Experimental Dehydrogenation

Cycloalkanes have been investigated for use as dehydrogenation agents to yield hydrogen, however there are clear limitations to this reaction scheme. A sufficiently high temperature is required to remove the hydrogen from the cycloalkanes. Additionally, in the presence of a catalyst, the resulting aromatic products compete with the catalyst active sites which can inhibit the efficiency of further cycloalkane dehydrogenation. Tetralin contains an aromatic ring within its structure which can therefore help to alleviate this concern to a degree. The results obtained through thermal and catalytic dehydrogenation of tetralin are presented in Figure 6.5.

It is clear that dehydrogenation in the absence of a catalyst is not insignificant, while in previous works this has been ignored (24). The clear trend in this study highlights that with increasing temperature from 200 up to 300 ℃, there is an increasing yield of tetralin dehydrogenation to naphthalene after 120 minutes of reaction time. However, above this temperature tetralin dehydrogenation begins to decrease. This limitation is likely due to competing hydrogenation and/or ring opening reactions which seek to convert naphthalene back to tetralin or naphthalene ring opening, respectively, due to the sufficiently high temperature required for this process. The greatest yield of conversion for thermal dehydrogenation is 35% at 275 ℃. In terms of hydrogen production, this equates to 0.7 moles of hydrogen production from the conversion of 1 mol of tetralin.

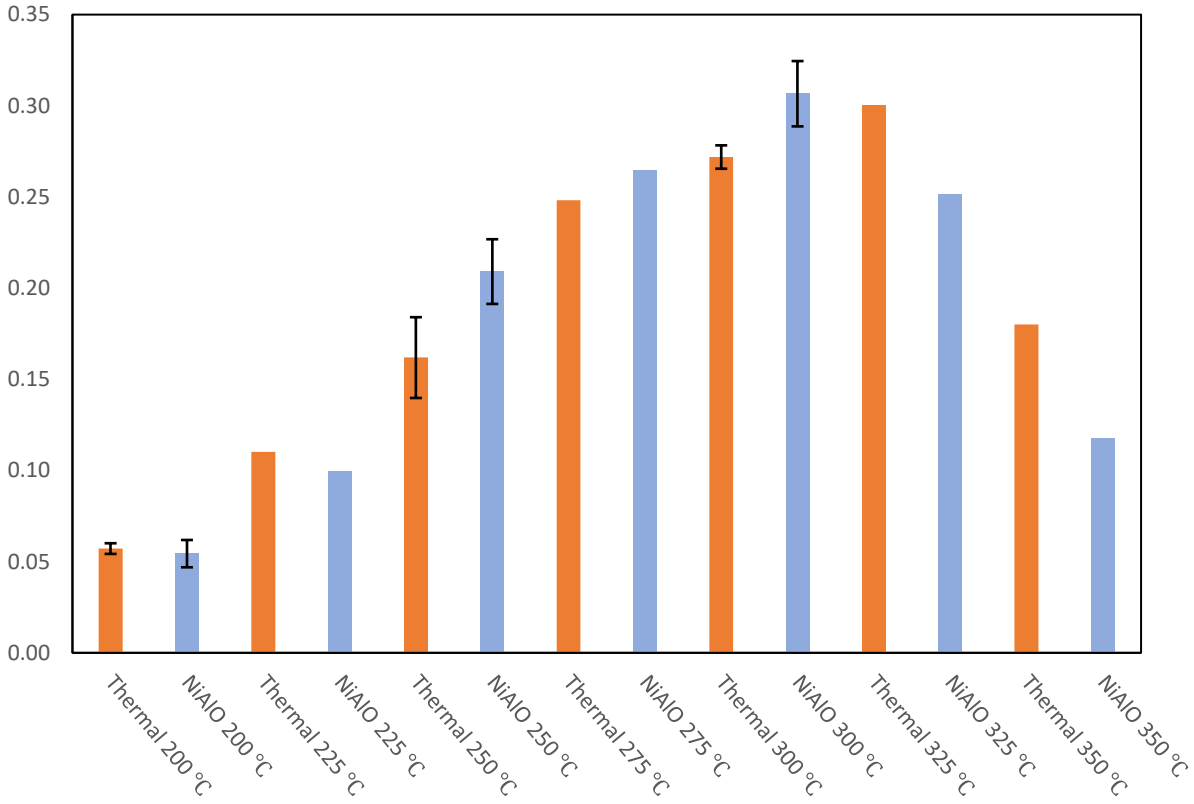

Figure 6.5 Graph to demonstrate percentage conversion of tetralin to naphthalene across the temperature range 150 to 350℃, for both non-catalytic and catalytic conditions.

When the NiAl(O) catalytic material is added to the reaction scheme, interestingly the production of naphthalene is more prominent compared to thermal between 225 and 300℃. The results indicate that above this temperature there is consistently less tetralin conversion compared to thermal dehydrogenation, across a temperature range of 325 to 350℃. Above 300℃, the disadvantage of the NiAlO material to carry out dehydrogenation is suggested to be a result of competing naphthalene hydrogenation reactions. It is clear that for the catalytic material above this temperature, this trend continues significantly

culminating in a relatively poor 12% conversion to naphthalene at 350℃, compared to the thermal regime at 18%. Though the trend can be seen with the thermal regime, the conversion to naphthalene is not inhibited until a temperature of 350℃ is reached.

It was observed that, during the temperature regimes from 325 to 350℃, when using the NiAlO material, the dihydronaphthalene intermediate compound is present in the produced liquid in small quantities. This therefore indicates that the catalytic mechanism changes during this higher temperature regime. Typically, the intermediate structure will be fixed to the active sites, before completing the conversion to the end product of naphthalene. In the instance of elevated temperature, a residual amount of intermediate has been released prematurely. It is suggested that one factor could involve the dual competition of naphthalene and the intermediate with the active site, serving to prevent the completion of dehydrogenation by promoting naphthalene adsorption. This could potentially lead to hydrogenation of naphthalene through the hydrogen transfer mechanism and could explain the relative drop in naphthalene production during this upper temperature range.

Furthermore, when comparing the tetralin percentage change to the naphthalene percentage change, it becomes apparent that there is disparity between the two data sets.

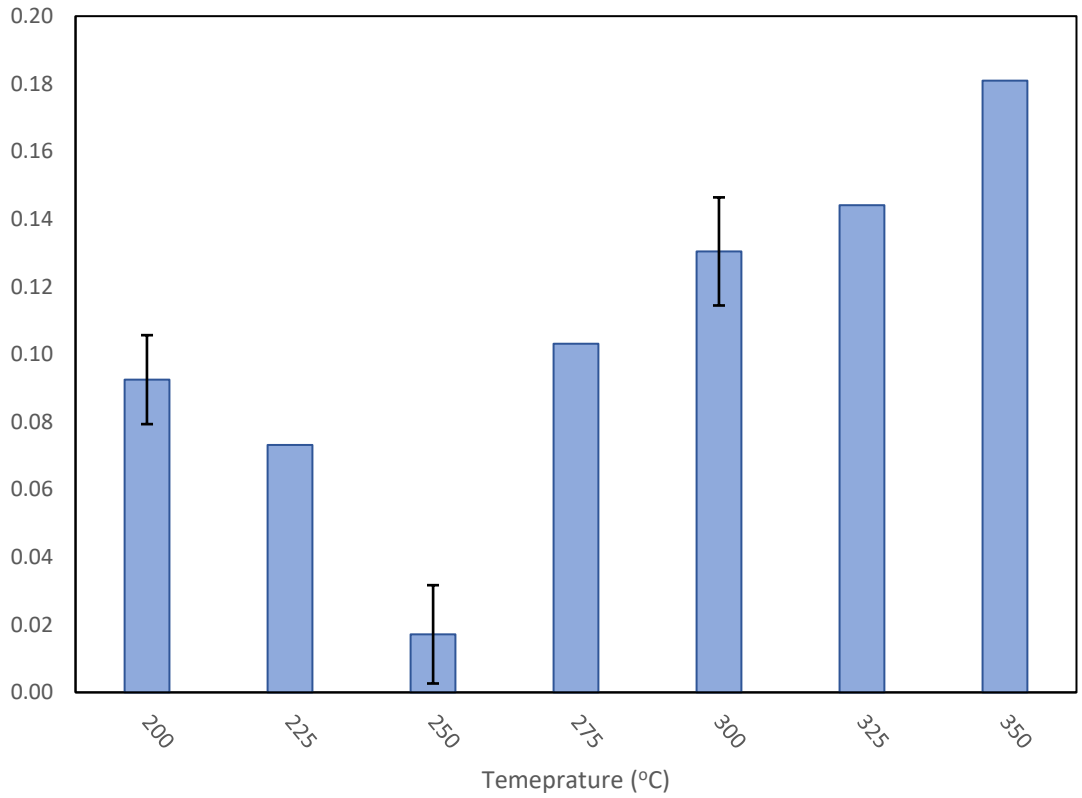

Figure 6.6 Graph to demonstrate disparity between moles of tetralin converted and moles of naphthalene produced.

When considering the NiAlO material, this disparity demonstrated in Figure 6.6, which demonstrates conversion vs temperature (℃), is more prominent at the extreme ends of the temperature range, continually rising from 250℃ through to the highest temperature at 350℃. It is suggested that this is as a result of both the occupation of the active sites by tetralin and naphthalene, particularly at low temperatures where adsorption is facilitated by the high surface mixed oxides which are not sufficiently activated to promote catalysis. This explains the comparatively lower yield of naphthalene compared to thermal at 200-225℃

shown in Figure 6.5. As the temperature increases, however, it is plausible that competing ring-opening reactions involving hydrogenolysis and cracking can explain the deficit. These side-reactions have previously been reported in the dehydrogenation of cyclic hydrocarbons in the presence of base metals such as Ni under high loadings (25). It has been reported that adsorption of hydrogen over cation-oxide sites can be described as heterolytic, facilitating the production of intermediate metal hydride species (26). This process is favoured by the basic properties of oxide species. Production of hydrogen gas is subsequently accommodated by proton abstraction. However, Ni is limited by its high hydrogenolysis reaction rates which can in turn inhibit hydrogen production, particularly at increased temperatures (27). Consequently, it is important to note that uptake of tetralin is not directly correlated to production of naphthalene, and by extension hydrogen generation.

It has previously been hypothesised that aromatic compounds are intercalated into the anionic clay complex due to the vacant interstitial layer, following decarboxylation and dehydration (28). Interestingly, at these lower temperatures, it is plausible that the metal active sites on the catalyst act to inhibit tetralin conversion through the adsorption of naphthalene into the sheet structure. Naphthalene consisting of two aromatic rings is susceptible to intercalation as has been indicated in a previous study which looked at the possibility of poly aromatic hydrocarbons intercalation into the collapsed LDH-derived metal oxide sheet (28). However, while the unavailability of sufficient active hydrogen species prevents significant hydrogenation of naphthalene to tetralin, the reaction progression of tetralin dehydrogenation remains inhibited due to competition for available active sites.

That said, between the range of 250 and 300 ℃ it is clear that tetralin conversion is inhibited only to a lesser extent. This is underpinned by the fact that the NiAlO material consistently outperforms thermal dehydrogenation within this temperature range.

If the experimental results are contrasted against the theoretical hydrogen generation capacity of the model compound in question, it can be demonstrated that the quantity of oil required to generate hydrogen gas is considerably larger than the calculations suggest under the reaction conditions tested. This is demonstrated in Table 6.7 when compared to tetralin conversion potential in Table 6.6. However, it must be noted that this reaction scheme was carried out during a time frame of hours. This however, could be greatly increased with the advent of greater thermal conductivity through the oil reservoir e.g. with heat transfer accommodated by steam injection prior to the ignition cycle. This could in turn expose the oil to the high in situ temperatures for a greater length of time. While the model compound is useful to characterise typically heavier feeds, a greater hydrogen capacity exists for higher molecular weight components which make up a large contribution of the residuum fraction. Additionally, the complex condensation reactions between coke precursor radicals may present another attractive mode for hydrogen generation in the formation of coke which is spatially located ahead of the combustion front.

In a recent study, it was estimated that a bitumen oil field may produce 1250 Sm^3 for each ton of bitumen produced (with a density of 1000 kg/m^3) (8). This equates to bitumen bbl:H_2 boe ratio of 3.3. This is significantly lower than the ratios demonstrated in this study, with the lowest oil:H2 boe ratio reaching 15 equating to a substantial decrease in potential

hydrogen production. That said, this study only considers tetralin dehydrogenation while ignoring the remaining hydrogen generating reactions such as water gas shift, coke gasification, aquathermolysis, and the pyrolysis of different molecular weight species which have a greater capacity for hydrogen generation.Additiounally, the inclusion of experimental data in this study aimed to understand non-ideal conditions which would be rpesent during the in situ thermal process, thereby presenting a more realistic approach to pyrolysis of the model compound used.

Table 6.7 Summary of experimental dehydrogenation reactions under the thermal and catalytic regimes, indicating bbls of oil produced/ boe H_2.

Reaction	**Temperature**	**Catalytic regime**	**bbls feed / boe hydrogen**
$C_{10}H_{12} \rightleftharpoons C_{10}H_8 + 2H_2$	200	Thermal	177
		NiAlO	186
	225	Thermal	92
		NiAlO	101
	250	Thermal	62
		NiAlO	48
		$Pd_{1\%}$/alumina	15
	275	Thermal	41

Table 6.7 *continuation*. Summary of experimental dehydrogenation reactions under the thermal and catalytic regimes, indicating bbls of oil produced/ boe H_2.

		NiAlO	38
	300	Thermal	37
		NiAlO	33
	325	Thermal	34
		NiAlO	40
	350	Thermal	56
		NiAlO	86

During an in-situ thermal EOR, it is important to note that temperature variations are widespread, hence the need to divide the reservoir into thermal zones. During low temperature thermal EOR, it is suggested that dehydrogenation reactions may be favoured if low temperatures can be maintained. However, the mineral content will have an impact on the dehydrogenation reactions. In the presence of clay minerals, which can make up a significant portion of the bulk volume of the reservoir, these reactions may be enhanced at higher temperatures that can be found within either wet-mode in situ combustion or IUT. This is evidenced from the ability of the NiAlO material, a synthetic clay, to outperform thermal dehydrogenation at a temperature range between 250 and 300°C. With this mind, it is clear that the mineralogical properties of a typical oil reservoir may inhibit the generation of hydrogen if the temperature regime is not satisfactorily high at this pressure. Additionally, the organo-metallic structures prevalent within oil will contribute to the coking

of the reservoir. This in turn may provide sufficient metal deposition over the surface of the reservoir minerals which may present enhanced dehydrogenation potential in the reservoir.

What's more, certain mineral groups will undergo transformation which can also serve to promote hydrogen generation. Olivine, a well-known iron and magnesium silicate mineral group can undergo serpentinization between a temperature range of 150 and 350℃. This process uses water to hydrate olivine, generating hydrogen gas as a by-product. Such reservoirs containing olivine include ultra-mafic petroleum reservoirs and therefore may prove to be interesting prospects for in-situ dehydrogenation reactions.

In the region adjacent to the well, the pressure is lowest. As a result, this may be advantageous to help promote dehydrogenation reactions. Consequently, the integration of a catalytic production liner may optimise this process so as to enhance the conversion of cycloalkanes to aromatics and

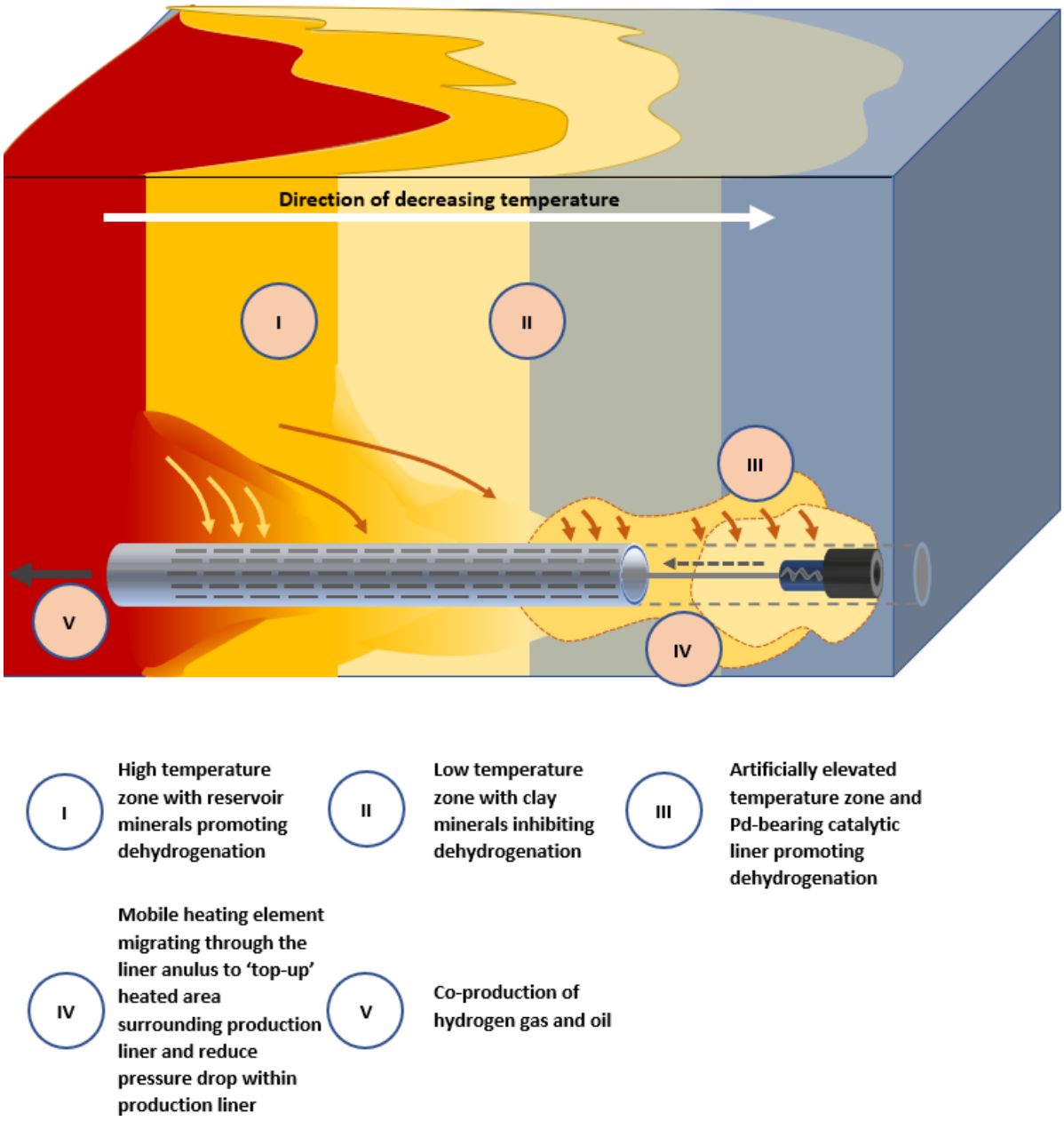

Figure 6.7 Graphical representation of an optimised production liner, featuring both a catalytic liner and localised down-hole heating element, the latter of which can be tuned to a specific temperature range.

hydrogen. This configuration is demonstrated in Figure 6.7 highlighting the temperature regime and reaction pathways within the context of a potential ISDH technique.

Palladium supported by alumina accelerates tetralin dehydrogenation considerably. While the expense of this catalyst can make such a process prohibitive, the palladium-based materials may be incorporated economically through specially-functionalised liners in the production well. Figure 6.8 demonstrates the significant impact of a palladium-based alumina catalyst in tetralin dehydrogenation at a temperature of 250 ℃. While it is clear thermal dehydrogenation marginally surpasses NiAlO at 22 compared to 19% conversion, the $Pd_{1\%}$/alumina catalyst reaches a conversion of 68%. Palladium, like other noble metals, has a tendency to activate C-H bonds, which makes it a superior catalyst for dehydrogenation (25). Moreoever, in the case of palladium a significant population of hydrogen resulting from the dehydrogenation reactions can form in the palladium crystal subsurface, leading to the production of bulk Pd hydride intermediates (29). At a critical point the small interstices in the Pd lattice expands thereby allowing higher density hydrogen clusters. A draw-back, however, concerns the high rate of poisoning in the presence of deleterious components such as sulphur, those of which are typically found in heavy oil reservoirs. This therefore makes Ni-bearing catalysts, with their high sulphur tolerance, more attractive. This promotes the development of multi-stage catalysis in the

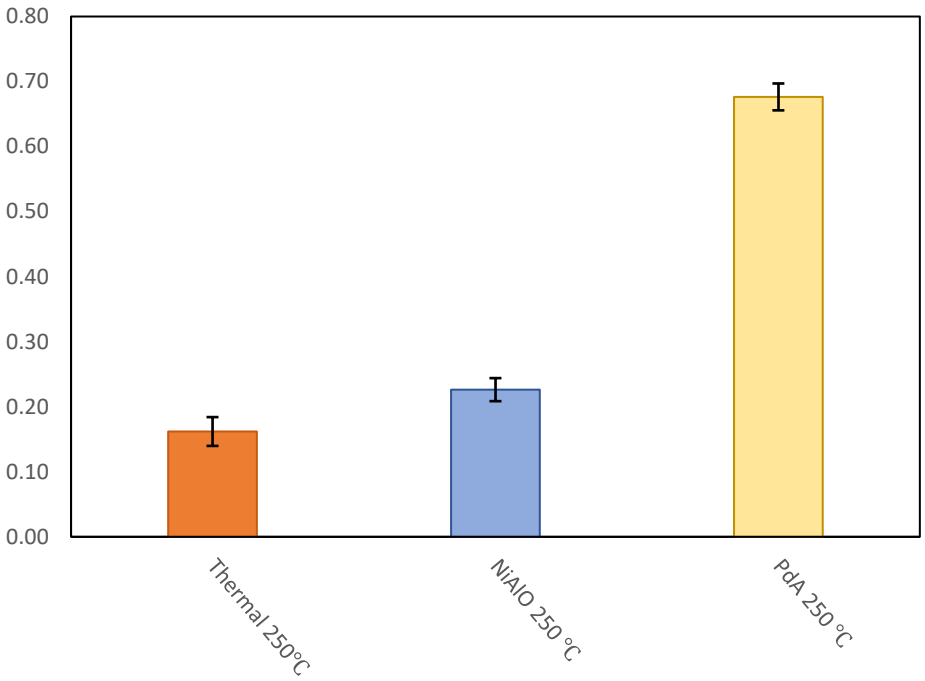

Figure 6.8 Graph to compare the percentage conversion of tetralin to naphthalene across the catalytic regimes at 250℃ and 40 bar pressure.

reservoir, whether orchestrated using in situ minerals or injected adsorptive/catalytic barriers ahead of the catalytic liner.

It should also be noted that under typical oil mixtures, side reactions will occur leading to carbonaceous deposits and subsequent catalyst deactivation. This ultimately can lead to a reduction in the purity of the produced hydrogen via the release of light paraffin gases such as methane and ethane.

A sustained combustion front of oil however, should in theory help activate rock materials such that dehydrogenation reactions become more widespread.

In terms of the actual potential boe H_2 production per day, Table 6.8, demonstrates the actual yield, governed by the dehydrogenation of the model compound used in this study. The quantities provided suggest the range of production of hydrogen across the three burn rates, highlighting the lowest amount produced by the lower burn rate and the maximum amount produced governed by the highest burn rate. It is clear that the flow rates must be carefully considered to justify the economics of the project. Furthermore, when producing H_2 gas, it is important to account for the upgrade of facilities required to carry out sufficient air separation, especially when dealing with the complex stream of gases produced during combustion projects.

It is evident that the range of co-produced H_2 varies significantly, from approximately 1 boe H_2 to 78 boe H_2. It is desirable to increase the burn rate so that the yield of not only H2, but also oil increases appropriately. While this may be achieved through increased air rates, the economic consideration must include the cost of air compression as well as the availability of the capability of the injection well to supply the high air rate. It has been highlighted that many field trials adopt a 0.5 ft/day burn rate which therefore makes this latter range more appropriate to consider in this study (2). In practice, a modified version of the steady-state radial flow equation can be used to estimate injection pressure. To put this into context, however, this represents one well pairing out of numerous well pads which would be required to develop the field economically. What's more, incorporation of hydrogen generating reactions other than single component dehydrogenation will undoubtedly increase the H_2 potential of the single horizontal production well pattern.

It is clear from the retail pump price for hydrogen, according to the statistics for stations in California, $14.99 to 18.71/kg was the range of prices in Q3 2019 (30). This equates to approximately $709 to 885/boe H_2. This feedstock is far more financially significant when drawing comparisons with the average price of an oil barrel, particularly that of heavier feeds. As a result, preference to hydrogen generation should be considered seriously in the economic review of TEOR in heavy oil fields and potentially as stand-alone reasons to develop these unconventional fields (31).

Table 6.8 Summary of daily boe H_2 production from the lowest to highest prediction across the burn rate range, for each temperature and catalyst regime used in the experimental work.

Temperature (°C)	**Catalyst regime**	**H_2 yield (boe H_2 /day)**					
		0.25 ft/day (S_{oi}0.8)		**0.5 ft/day (S_{oi}0.8)**		**1.0 ft/day (S_{oi}0.8)**	
		Low	**High**	**Low**	**High**	**Low**	**High**
200	Thermal	1	2	2	3	4	7
	NiAlO	1	2	2	3	4	6
225	Thermal	1	3	3	6	8	13

	NiAlO	1	3	3	6	8	12
250	Thermal	2	5	5	9	12	19
	NiAlO	3	6	7	12	16	24
	$Pd_{1\%}$/alumna	8	19	21	39	51	78
275	Thermal	3	7	8	14	19	28
	NiAlO	3	8	8	15	20	31
300	Thermal	3	8	8	16	21	31
	NiAlO	4	9	9	18	23	35
325	Thermal	4	9	9	17	23	34
	NiAlO	3	7	8	15	19	29
350	Thermal	2	5	6	10	14	21
	NiAlO	1	3	4	7	9	14

Table 6.8 (cont.). Summary of daily boe H_2 production from the lowest to highest prediction across the burn rate range, for each temperature and catalyst regime used in the experimental work.

6.4 Conclusions

A theoretical approach to offshore wet-combustion with the intention to produce hydrogen gas has been considered as a method to alleviate the currently diminishing reliance on oil, and complement the motivation to redevelop existing oil fields in mature basins. Offshore heavy oil fields can be vast and while the idea of a thermal combustion approach to offshore

oil fields is in its infancy, it may provide a useful alternative for mature basins while experimenting with hydrogen production for use as greener fuel alternatives. A reservoir in a specific basin was selected based on its properties and level of existing infrastructure, to demonstrate its application to in situ thermal EOR. The model in this paper augments the Marx and Langenheim steam model, with the aid of principles used in the Newton & McNeil combustion model concept, to generate production curves from a mature heavy oil field in the North Sea. The heat loss function has been used in both steam zone growth and steam zone encroachment to theoretically provide a more accurate prediction for production since the presence of a mobile combustion front acts to suppress steam growth in a given pattern. The time taken to reach the pivot between growth and encroachment is disproportionately favoured towards higher burn rates and with high saturation (S_0 =0.8) zones, it takes 232, 498 and 1088 days for burn rates of 1.0, 0.5 and 0.25 ft/day, respectively. Residual oil left in the reservoir following the steam flood is assumed to be swept by the combustion front with recovery factors determined in excess of 80%, limited by coke formation. The recovery potential decreases with decreasing saturation in addition to the fact that a higher proportion of the oil is converted to coke at lower saturation levels. The model predicts a steam-derived production decline as the “steamed” area increases due to the increase in heat loss. This is then followed by an increase in production owing to the encroachment of the combustion front into this area.

As the burn rate of the combustion front increases from 0.25 to 1.0 ft/day, the time for total steam-derived recovery decreases disproportionately. It has been shown that for a S_0 0.8

and 1.0 ft/day burn rate steam-derived production ranges from approximately 1100 bopd to 500 bopd over a 237 day period, before increasing to 900 bopd during the combustion zone encroachment period for an additional 150 day period, at which point steam-derived recovery ceases and the remainder of the 'steamed' zone is drained under the thermal 'bulldozer' effect of the combustion front.

An analysis of model dehydrogenation reactions in addition to previously reported hydrogen gas production per unit of bitumen have provided for a tentative examination of the hydrogen potential in the reservoir. It is shown that polycyclic hydrocarbons, those of which characterise heavier feeds, have a greater hydrogen capacity and therefore provide a richer hydrogen source. When drawing comparisons with previously reported bbl oil:boe H_2 ratios from the in-situ gasification of bitumen, the experimental data has highlighted that the dehydrogenation of a model compound, tetralin, is less appreciable in practice over the reaction parameters used in this study. That said, the use of injected water to produce steam may condition the reservoir to sufficient temperature which can accommodate hydrogen generation reactions. This therefore may improve the yield via a time extension of the reaction period. Furthermore, additional experimental work to include additional hydrogen generation reactions will be useful in highlighting a more realistic yield of hydrogen. Competing reactions may occupy the thermal zones which will have an impact on the catalytic performance of in situ reservoir minerals and/or down-hole injected catalytic species. The adsorption capacity of in situ minerals such as clays may inhibit such dehydrogenation reactions. However, the minerals may also serve to provide natural

catalytic supports which can become activated at the high temperatures experienced during the in situ combustion process. These minerals may also act as sites on which catalytically relevant metals may be deposited, derived from the oil in the reservoir. This therefore highlights need to accurately assess the mineralogical properties of a given reservoir to help in the prediction of upgrading potential, be it in terms of heavy oil upgrading or hydrogen generation. An appropriately designed in-situ dehydrogenation and hydrogen capture system may capitalise on the sustained high temperatures generated within the combustion zones to promote desired reactions.

The highest yield of hydrogen was achieved when using a Pd-alumina catalyst. The potential for boe H_2 increased significantly, predicting 78 boe H_2/day under a 1.0 ft/day burn rate through a reservoir with saturation of S_{oi} 0.8. This material represents an analogue to potential catalytic materials installed within the production liner. When using a nickel-enriched MMO, dehydrogenation reactions were more significant over thermal dehydrogenation over a temperature range of 250 to 300 ℃, reaching a maximum of 35 boe H_2 at 300 ℃.

6.5 References

1. Ahmed T, Meehan DN. Introduction to Enhanced Oil Recovery. In: Advanced Reservoir Management and Engineering. 2011. p. 541–85.

2. Sarathi SP. In-Situ Combustion Handbook - Principles and Practices. Natl Pet Technol Off US Dep Energy. 1999;

3. Hajdo, E. L.; Hallam, J. R.; Vorndran LDL. Hydrogen Generation During In-Situ-Combustion. In: SPE California Regional Meeting. Society of Petroleum Engineers; 1985.

4. Hallam, J. R.; Hajdo, E. L.; Donnelly KJTR of B at WL. Thermal Recovery of Bitumen at Wolf Lake. SPE Reserv Eng. 1989;4.

5. Xia TX, Greaves M. In situ upgrading of Athabasca Tar Sand bitumen using THAI. Chem Eng Res Des. 2006;84(9 A):856–64.

6. Hart A. The novel THAI–CAPRI technology and its comparison to other thermal methods for heavy oil recovery and upgrading. J Pet Explor Prod Technol. 2014;4(4):427–37.

7. U.S. Energy Information. Annual Energy Outlook 2020. 2020;

8. Kapadia PR, Kallos MS, Gates ID. Potential for hydrogen generation from in situ combustion of Athabasca bitumen. Fuel [Internet]. 2011;90(6):2254–65. Available from: http://dx.doi.org/10.1016/j.fuel.2011.02.038

9. Kapadia PR, Wang J (Jacky), Kallos MS, Gates ID. Practical process design for in situ gasification of bitumen. Appl Energy [Internet]. 2013;107:281–96. Available from: http://dx.doi.org/10.1016/j.apenergy.2013.02.035

10. Moore I. Alba Field - How seismic technologies have influenced reservoir characterization and field development. Geol Soc Spec Publ. 2015;403(1):355–79.

11. Jayasekera AJ, Goodyear SG. The development of heavy oil fields in the U.K. Continental Shelf: Past, Present and Future. SPE West Reg Meet Proc. 1999;1999-May.

12. Turta A. In Situ Combustion. In: Enhanced Oil Recovery Field Case Studies. 2013.

13. Glandt, A. C.; Pieterson, R.; Dombrowski, A.; Balzarini AM. Coral Creek Field Study: A Comprehensive Assessment of the Potential of High-Pressure Air Injection in a Mature Waterflood Project. In: SPE Mid-Continent Symposium. 1999.

14. Stokka, S.; Oesthus, A.; Frangeul J. Evaluation of Air Injection as an IOR Method for the Giant Ekofisk Chalk Field. SPE Int Improv Oil Recover Conf Asia Pacific, Proc. 2005;

15. Fraim, L. M.; Moffitt, D. P.; Yannimaras VD. Laboratory Testing and Simulation Results for High Pressure Air Injection in a Waterflooded North Sea Oil Reservoir. Spe Annu Tech Conf Exhib San Antonio. 1997;5-8 Octobe.

16. Xia TX, Greaves M, Turta AT, Ayasse C. THAI - A “short-distance displacement” in Situ combustion process for the recovery and upgrading of heavy oil. Chem Eng Res Des. 2003;81(3):295–304.

17. Yang, M.; Harding, G. T.; Chen, Z.; Yu, K.; Liu, H.; Yang, B.; He R. Numerical Modelling of Hybrid Steam and In-Situ Combustion Performance for Oil Sands. In: SPE Reservior Simulation Conference. 2017.

18. Pinnock SJ, Clithero ARJ, Rose PT. The Captain Field , Block 13 / 22a , UK North Sea. 2003;431–41.

19. Hampson JM, Walden SF, Bell C. Maximizing production and reserves from offshore heavy oil fields using seismic and drilling technology: Alba and Captain Fields, UKNS. Pet Geol Conf Proc. 2010;7(0):337–47.

20. Surlyk, F.; Noe-Nygaard N. A Giant Sand Injection Complex: The Upper Jurassic Hareelv Formation of East Greenland. Geol Croat. 2010;56(1).

21. Bagci SA. Wet Forward Combustion for Heavy Oil Recovery. Energy Sources, Part A Recover Util Environ Eff. 2006;28(3):221–32.

22. Bagci S, Kok MV. In-situ combustion laboratory studies of Turkish heavy oil reservoirs. Fuel Process Technol. 2001;74(2):65–79.

23. Offshore. FLOW ASSURANCE Vacuum-insulated tubing helps solve deepwater production problems [Internet]. 2001. Available from: https://www.offshore-mag.com/home/article/16758982/flow-assurance-vacuuminsulated-tubing-helps-solve-deepwater-production-problems

24. Hart A, Adam M, Rigby S. Hydrogenation and Dehydrogenation of Tetralin and Naphthalene to Explore Heavy Oil Upgrading Using NiMo / Al 2 O 3 and CoMo / Al 2 O 3 Catalysts Heated with Steel Balls via Induction. 2020;(May).

25. Gianotti E, Taillades-Jacquin M, Rozière J, Jones DJ. High-Purity Hydrogen Generation via Dehydrogenation of Organic Carriers: A Review on the Catalytic Process. ACS

Catal. 2018;8(5):4660–80.

26. Busca G. Catalysts for Hydrogenations, Dehydrogenations and Metathesis. In: Heterogeneous Catalytic Materials. 2014. p. 345–74.

27. Zaikina OO, Yakovlev VA. High-Loaded Nickel Based Sol–Gel Catalysts for Methylcyclohexane Dehydrogenation. 2020;12–5.

28. Claydon R, Wood J. A Mechanistic Study of Layered-Double Hydroxide (LDH)-Derived Nickel-Enriched Mixed Oxide (Ni-MMO) in Ultradispersed Catalytic Pyrolysis of Heavy Oil and Related Petroleum Coke Formation. Energy and Fuels. 2019;

29. Busca G. Metal Catalysts for Hydrogenations and Dehydrogenations. 2014.

30. Newsom G, Hochschild D, Mcallister JA, Ph D, Monahan P, Barker K. Joint Agency Staff Report on Assembly Bill 8 : 2019 Annual Assessment of Time and Cost Needed to Attain 100 Hydrogen Refueling Stations in California California Energy Commission Project Manager. 2019;(December).

31. Mayyas A, Mann M. Manufacturing competitiveness analysis for hydrogen refueling stations. Int J Hydrogen Energy [Internet]. 2019;44(18):9121–42. Available from: https://doi.org/10.1016/j.ijhydene.2019.02.135

Chapter 7

Conclusions and Recommendations

7.1 Conclusions

The global energy market is currently in a transitional period. The desire for clean energy is steering energy markets away from fossil fuels. However, it is clear that the pace of transition is currently not significant enough to alleviate the increasing demand of energy. This is particularly pertinent given the current geopolitical theatres which are driving less economically independent countries to industrialisation and further integration with the global powers.

Heavy oil and bitumen represent a fraction of fossil fuel which is found in abundance in countries such as Canada, Venezuela and Russia, among others. This energy source, however, comprises undesirable characteristics which typically draws exploration and development focus towards lighter, more easily refined, oil types. This trend has, however, propelled institutions towards research which seeks to upgrade this heavy oil type so that the characteristics are more suitable for use as both fuels and feedstocks for the petrochemical industry, thus making the abundant reserves more attractive. Moreover, research has focused increasingly at the process of pre-refinement which has been conceptualised into a subsurface process, essentially sequestering the deleterious products within the reservoir architecture while producing the less refractory components at surface.

In a market which is constantly driven by innovation to unlock oil resources in ever more challenging environments, including ‘ultra-deep’ offshore prospects or smaller and more

complex reservoir targets, the known reserves of bitumen and heavy oil which exist at comparatively shallow depths may provide a more economical alternative.

In addition, the use of heavy oil has recently been suggested as a source of 'transparent' hydrogen. The high density of hydrogen locked in petroleum coupled with the relatively mild conditions required to extract hydrogen from oil, makes an in-situ thermal EOR process an attractive option in coproducing oil and hydrogen gas, or even purely hydrogen. This is particularly important when considering the huge capital expenditure required to decommission mature fields, even when in many cases a large portion of the oil saturation remains in the reservoir. An abundance of partially-depleted oil reservoirs are transferred to decommissioning programmes. However, the existing infrastructure including platforms and high density well pads could provide an ideal stage to launch end-of-life in-situ burning. This could not only equate to huge reserves of hydrogen gas production to fulfil an increasing demand of this fuel type, but also challenge convention by transitioning late-stage reservoirs towards more carbon-aware projects.

The aims of this study were divided into three parts.

Firstly, heavy oil samples were upgraded in the presence of tailor-made LDH species which could provide analogues to in-situ reservoir minerals. The upgrading goals focused on a reduction of viscosity, asphaltene and heteroatom content, so that a light-naphtha and distillate-enriched oil could be produced. The motivation also included the analysis of residual coke to help demonstrate specific upgrading pathways as well as to understand how coking may affect an in situ thermal EOR. To carry out this work an autoclave batch

reactor was used with parameters based upon earlier work in heavy oil upgrading optimisation.

Secondly, a kinetic study was used to further demonstrate the effectiveness of the synthesised LDH as supports to active upgrading metals such as Mo and Pd typically used in hydrogenation programmes. The study focused on understanding the different catalytic mechanism for upgrading, through the assessment of the hydrogenation products of naphthalene and the variation of ratios of these products. The reactions proceeded in a low temperature high pressure batch reactor under carefully controlled conditions which could represent a number of the lower temperature thermal zones associated with the ISC process.

Thirdly, a broad assessment of a thermal EOR in a mature North Sea reservoir has been carried out. This study focused on modelling heat derived from the associated coke produced in the thermal EOR process, as an energy resource to produce steam in-situ. A Marx and Langenheim steam heating model was adopted to simulate the progression of the steam front through the reservoir and associated production of oil. The amount of oil produced was used in conjunction with experimental work which focused on dehydrogenation of aromatic compounds to provide an estimate of potential hydrogen production.

7.1.1 Ni-MMO as heavy oil upgrading materials

Heavy oil contains a significantly lower H:C ratio and higher quantity of organic heteroatoms and organo-metallic complexes than conventional light oil. Consequently, novel catalytic materials are needed to aid in heavy oil upgrading to remove the deleterious components and support the higher demand for low sulphur and higher value fuels.

Heavy oil upgrading was studied using an inexpensive nickel-aluminium Layered Double Hydroxide (LDH)-derived Ni-enriched Mixed Metal Oxide (Ni-MMO) dispersed catalyst in a Baskerville autoclave. The conditions were set at 425℃, initial pressure of 20 bar, 0.02 Catalyst-To-Oil (CTO) ratio and a residence time of 30 minutes to mimic previously optimised conditions for in-situ upgrading processes.

The extent of the upgrading following catalytic pyrolysis was evaluated in terms of a solid, liquid and gaseous phase mass balance, liquid viscosity reduction, desulphurisation, and True Boiling Point (TBP) distribution.

A typical in-situ activated CoMo-Al_2O_3 commercial hydroprocessing catalyst was used as a reference. It was found that the produced oil from dispersed ultrafine Ni-MMO exhibited superior light oil characteristics.

The viscosity decreased from 811 mPa·s to 0.2 mPa·s while the light naphtha fraction increased from 12.6% of the feed to 39.6%, with respect to the feed. Though CoMo-Al_2O_3 offered the greatest desulphurisation of the oil, the Ni-MMO offered comparable sulphur reductions in both gas environments. The greatest reduction in liquid sulphur content for Ni-MMO occurred under a N_2 gas environment reaching 31.6%, in comparison to CoMo-Al_2O_3

reaching 37.6% under a H_2 gas environment, while thermal up[grading reached a 26.5% reduction under a N_2 gas environment.

Using a thorough suite of analytical techniques on the petroleum coke product, including Thermo-Gravimetric Analysis (TGA) and Scanning Electron Microscopy (SEM), a mechanism has been hypothesised for the upgrading by dispersed Ni-MMO under both N_2 and H_2 atmospheres:

Under a N_2 atmosphere, the Ni-MMO, generated by the in-situ thermal decomposition of the LDH, demonstrate a preferential asphaltene and poly-aromatic adsorption mechanism, generating a poly-aromatic mixed oxide-coke precursor and asphaltene-depleted oil.

While using Ni-enriched mixed oxides under a reducing H_2 atmosphere, hydrogenation reactions become more significant, while asphaltene molecules remain in high abundance within the produced oil. The TGA curves evidence a distinction in the chemical structure of the produced petroleum coke. A distinctive peak at approximately 500℃ appears consistent with elemental analysis highlighting a large and marginal increase in sulphur and nitrogen-bearing components, respectively, present in the solid product in comparison to the other catalytic regimes.

In terms of correlating the data to the in situ thermal EOR process, it is clear that the different catalytic regimes have wider implications. Though it is useful to assess potential catalytic materials in relation to thermal upgrading, the nature of the mineralogical properties of each reservoir, though significant variations of which exist from reservoir to reservoir, it is clear that a purely thermal upgrading mechanism will not be prevalent.

Many reservoirs comprise significant amounts of clay and sandstone. It is clear from this study, that Ni-MMO, an analogue for clay, will steer the reactions in a certain direction. The higher amount of coke produced from the Ni-MMO setting, in particular, may have some significant implications.

Firstly, a relatively higher quantity of coke could provide more energy to sustain a steam-generating zone during wet-mode combustion. Secondly, coke laid-down ahead of the combustion front may also serve as an effective CO_2 trap so as to partition unwanted gases from the resultant gas mix, naturally enriching the desired gaseous products. Thirdly, the ability to sequester poly aromatic hydrocarbons offers a useful tool to both generate a lighter fraction-enriched product while also preventing deleterious deposition in the production lines which act to inhibit flow.

It is also necessary to note that while there will be a partial availability of hydrogen, unless a hydrogen donor is introduced at scale, it is likely that the reaction routes that follow will more closely resemble the data derived from that of an inert atmosphere.

Under such an environment, it is clear that the Ni-MMO produces an oil with more favourable properties including the lowest amount of sulphur, the highest relative amount of light naphtha, and the lowest viscosity. Moreover, the reaction gases evolved are found to be the greatest under this catalytic regime, at 18.3 wt.%. Ordinarily this is not useful as oil is the preferred production fluid, however the reaction gases have an integral contribution to the hydrogen generating reaction schemes. As such, in the context of coproducing hydrogen gas as well as higher quality oil, this could potentially provide a platform from which such reaction schemes are artificially promoted in the reservoir.

7.1.2 Mo-MMO as heavy oil upgrading materials using model compound analogue

Naphthalene was used as a model compound to provide a representation of a typically heavier weight feed which makes up a large constituent of heavier oils. The use of a model compound aimed at highlighting a detailed mechanism while also more closely constraining the differences between catalytic regimes used in hydrogenation.

Mo was deposited over the Ni-MMO, with the intention of generating a clay-like material more capable of carrying out hydrogenation reactions. It also represents a material that can be easily synthesised and may potentially be constructed in-situ given the availability of catalytically active metals in the native oil.

The reaction progress and resultant hydrogenation products were contrasted against a series of Pd-doped and NiMo-doped Al_2O_3 catalysts, typical of industry varieties used in second stage hydrotreating units.

The results showed clearly that hydrogenation activity improved considerably with the increased weighting of Pd over the Al_2O_3 support. The trend was elaborated upon when considering the catalyst architecture. High density Pd clusters were reasoned for the significant advances in magnitude of hydrogenation. When drawing comparisons with the Mo-MMO and NiMo-Al_2O_3 catalysts, it was clear that the abundance of Ni in the solid solution of the MMO support, played a pivotal role in improving hydrogenation activity. The Mo-MMO support generated comparable hydrogenation product yields to $Pd_{2\%}/Al_2O_3$ while the NiMo-Al_2O_3 industrial catalyst, bearing only a small amount of Ni generated the least hydrogenation efficiency with a yield more comparable to $Pd_{1\%}/Al_2O_3$. Reaction rate constants were determined through the use of a pseudo-first order rate model which did

not assume first stage hydrogenation to tetralin was much faster than second stage hydrogenation to decalin, the rate constants of which were denoted k_1 and k_2, respectively. That said, with the exception of $Pd_{1\%}/Al_2O_3$, all of the remaining catalyst species exercised $k_1 > > k_2$.

When analysing the cis/trans yield, it was clear that Pd-bearing catalyst species favour a lower cis/trans ratio. Conversely the Ni and Mo-bearing catalysts favoured a greater cis/trans ratio. The dependence of the cis/trans ratio was hypothesised as a result of the orientation of the $\Delta^{1,9}$ – octalin intermediates, which in turn is related to the electronic properties of the catalyst. This dictates whether sufficient time is allowed for the rollover on the catalyst surface. The significance of this resides with the intended product distribution. Cis decalin is desirable if further ring-opening products, such as indanes and alkyl-cyclohexanes, are warranted, those of which can be more desirable end-components for fuels.

7.1.3 The North Sea as a frontier for in situ heavy oil dehydrogenation

Based on the requirement to explore the considerations needed to transfer lab-simulated the in situ combustion/dehydrogenation process to a field pilot scale, a hypothetical scenario was conceptualised to highlight the initiation of in situ combustion in a partially-depleted North Sea reservoir. The simulated model included a Marx and Langenheim steam heating component, using the production of in situ coke as a fuel source to vaporise injection water. An attempt to incorporate the concept of a linear-moving combustion front in the reservoir was used to demonstrate its impact on the steam front and corresponding

production figures. Estimates of hydrogen gas evolution were provided to highlight the advantages of stimulating an ISC project to coproduce hydrogen and upgraded oil. The estimates were based on laboratory experiments using tetralin as the model compound to undergo dehydrogenation to naphthalene, yielding hydrogen gas as a by-product.

A determination of the production figures from an attic oil accumulation with a saturation of oil at 0.8 was made. The range of burn rates used demonstrated the following approximate range of production figures: 300 to 120, 600 to 300 and 1100 to 500 bopd for 0.25, 0.5 and 1.0 ft/day, respectively. However, the encroachment of the combustion front on the steamed area demonstrated a subsequent rise to 290, 360 and 900 bopd, respectively, before the total volume of the reservoir package has been drained. This subsequent rise occurred due to the encroachment of the combustion zone into the steamed zone at 1104, 508 and 237 days after ignition for combustion zone migration rates of 0.25, 0.5 and 1.0 ft/day, respectively.

The model was tested over different saturation levels, 0.4, 0.6 and 0.8. It was found that the recovery factor decreases with decreasing saturation in addition to the fact that a higher proportion of the oil is converted to coke at lower saturation levels.

Polycyclic hydrocarbons prove to be a rich source of hydrogen in comparison to their lighter counterparts. This makes heavy oil fields more attractive as potential hydrogen sources. The experiments focused on using a Ni-MMO material drawing comparisons to thermal dehydrogenation

Previously reported figures of bbl oil boe H_2 production were used as a base for comparison to the experimental data in this study. While using a single model compound, tetralin, is less

representative of the varied reactions which can take place during the ISC process, it was interesting to look at how the temperature range affected the dehydrogenation potential.

A Ni-MMO catalyst was used as an analogue for in situ clay-type minerals. The results were contrasted against thermal dehydrogenation reactions and a Pd/Al_2O_3 catalyst was used as a base case for a temperature zone of 250℃. The potential for boe H_2 increased significantly when using the Pd/Al_2O_3 catalyst, highlighting a range of 51 to 78 boe H_2/day under a 1.0 ft/day burn rate through a reservoir with saturation of S_o at 0.8. This catalyst represents an analogue which could be emplaced within a bespoke in situ catalytic liner to augment the degree of dehydrogenation. Under a reaction regime with Ni-MMO a higher degree of dehydrogenation occurred over a temperature range of 250 to 300℃, when comparing to thermal dehydrogenation, reaching a maximum of 35 boe H_2/day at 300℃. Thermal dehydrogenation reached a peak of 31 boe H_2/day at 325℃. This may indicate the advantages of in situ mineral types throughout the reservoir when exposed to milder temperature thermal zones. This is particularly relevant to the 'steamed' zones ahead of the combustion front.

7.2 Recommendations

With the global energy market seeking to transition heavily to more renewable sources, it is prudent to understand how the oil industry can also transition into a greener industry. It is clear that hydrocarbons will continue to play an important role in future energy supply. However, it will be key to determine the energy and carbon cost on a reservoir-by-reservoir case so that the industry can focus on oil reserves which require less energy intensive

schemes used in the discovery, development and extraction of the oil. It will therefore be necessary to draw up energy cost comparisons between marginal light oil reservoirs vs large heavy oil reservoirs.

Catalyst development remains crucial in both surface and subsurface oil refining. Cheaper alternatives to conventional commercial varieties will persistently encourage research. Adsorbents which can be tailored for the removal of polycyclic components and heteroatom-enriched oil components are required to efficiently develop 'sour' oil reservoirs. Consequently, further work to constrain the mechanism of how high surface area MMOs can be used to uptake such components is advisable. Specifically, looking at how the exchanged cation type can affect the nano-architecture of MMO will help to determine an optimum species for heavy oil filtering and upgrading. In situ formulation of catalytic materials will provide a more economical alternative to the packing of expensive catalytic materials into the producer well. Consequently, in situ catalyst synthesis development is an important research pathway to explore. Given that anionic clays can be synthesised from multiple sources, it may be useful to formulate a strategy which can help transpose the synthesis into the reservoir using injectant salt solutions as well as in situ minerals.

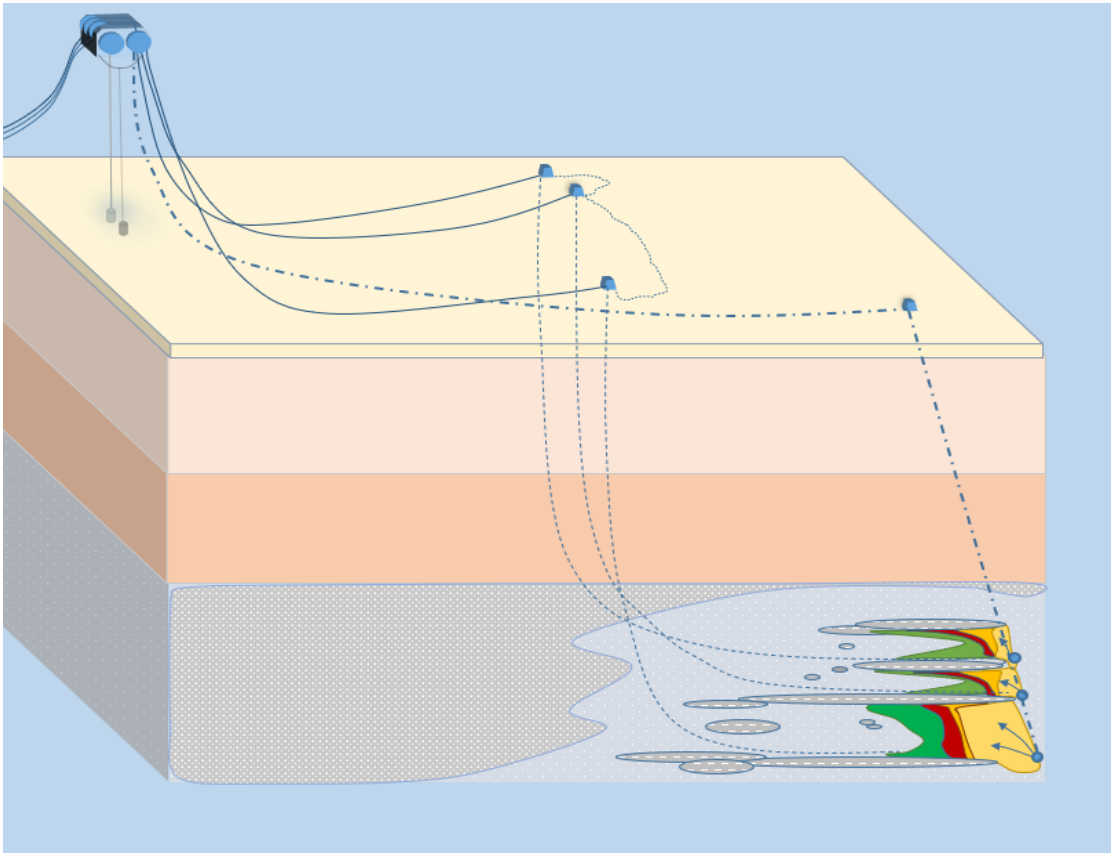

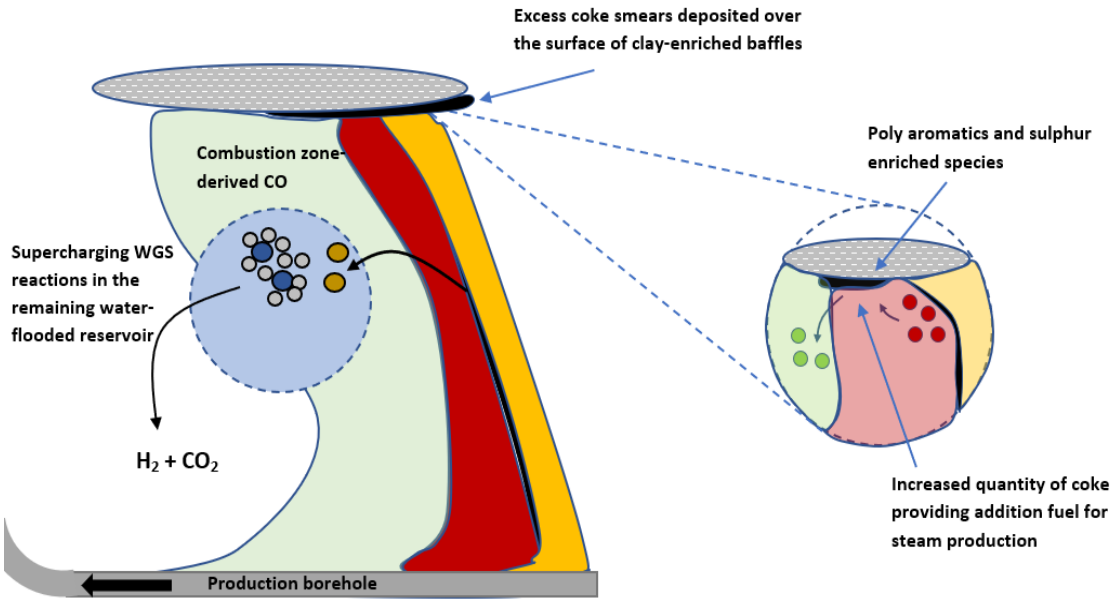

Figure 7.1 A multi pad offshore ISC concept using in situ residual oil as fuel source for WGS reactions.

It is evident that partially-flooded reservoirs may hold a key in heavy oil field development

for hydrogen production. It will therefore be necessary to understand how the WGS reaction can be optimised in situ. The key components of this reaction focus on the availability of steam and carbon monoxide, both of which can be produced in excess when carrying out in situ combustion within a heavily water-flooded field. Understanding how the mineral content within a reservoir can withdraw carbon dioxide from the reservoir gases may demonstrate a potential pathway to supercharging the hydrogen generating capacity of the ISC process via WGS. Furthermore, for a development programme wholly focused on producing H_2 gas, it will be imperative to understand what clay-based reservoir minerals can aid in the transfer of the majority of the in situ residual oil into petroleum coke so that it the oil can be used solely as a fuel source to aid in the WGS reaction.

Optimising the heat availability will improve the feasibility of a project. The design of a localised heating element which can be emplaced along the producer well could play a critical role in controlling specific reaction pathways which can constrain desirable products for the project. Furthermore, this can provide a platform to carry out hydrogen generating reactions closer to the horizontal producer well, therefore, minimising the issues surrounding the impact of gas mass transport velocity on the extrication of hydrogen from the combustion zone.

Finally, a comprehensive economic analysis for offshore platform conversion and well repurposing will be necessary to assess the economic feasibility for the transition from oil production to in situ H_2 generation and production. It will be useful to understand the constraints apparent for offshore development on a region-by-region scale.

Appendix A

Derivation of pseudo first order model

[A.1] $dN/dt = -k_1N$

[A.2] $dT/dt = k_1N – k_2T$

[A.3] $dD/dt = -k_2T$

Initial conditions:

$t = 0$

$N = N0$

$T = 0$

$D=0$

$dN/N = -k_1\,dt$

[A.4] $\int dN/N = -k_1 \int dt$

[A.5] $\ln N = -k_1t + c_1$

From the initial conditions:

$\ln N_0 = -k_1(0)$

[A.6] $c_1 = \ln N_0$

Substitute **[A.6]** into **[A.5]**:

$\ln N = -k_1t + \ln N_0$

$\ln N – \ln N_0 = -k_1t$

$\ln(N/N_0) = e^{-k1t}$

[A.7] $N= N_0e^{-k1t}$

Substitute **[A.7]** into **[A.2]**:

$dT/dt = k_1N_0e^{-k1t} – k_2T$

[A.8] $dT/dt + k_2T = k_1N_0e^{-k1t}$

Solve **[A.8]** using the Integration factor metrhod:

$dx/dt + p(t)x = Q(t)$

$p(t) = k_2$

Integration factor:

$e^{\int Pdt} = e^{\int k2dt} = e^{k2\int dt} = e^{k2t}$

Multiply **[A.8]** by the integration factor:

$e^{k2t}\,(dT/dt + k_2T) = e^{k2t}k_1N_0e^{-k1t}$

[A.9] $e^{k2t}\,(dT/dt) + e^{k2t}(k_2T) = k_1N_0e^{-k1t}e^{k2t}$

If $e^{k2t}T$

$d/dt\,(e^{k2t}T) = e^{k2t}dT/dt + Te^{k2t}k_2$

[A.9] can be re-written as:

$d/dt\,(e^{k2t}T) = k_1N_0e^{-k1t}e^{k2t}$

$d/dt\,(e^{k2t}T) = k_1N_0e^{k2t-k1t}$

[A.10] $d/dt\,(e^{k2t}T) = k_1N_0e^{(k2-k1)t}$

Equation **[A.10]** solved by separating variables:

$\int d(e^{k2t}T) = \int k_1N_0e^{(k2-k1)t}\,dt$

[A.11] $e^{k2t}T = k_1N_0 \int e^{(k2-k1)t}\,dt$

$e^{(k2-k1)t}\,dt$, can be solved by:

$u = (k_2-k_1)t$

$du/dt = (k_2-k_1)$

$du = (k_2-k_1) \quad \rightarrow \quad dt = du/(k_2 - k_1)$

$\int e^{(k2-k1)t}\,dt = \int (e^u\,du)/(k_2-k_1) = 1/(k_2-k_1) \int e^u\,du$

$= 1/(k_2 - k_1)\,e^u = 1/(k_2 - k_1)\,e^{(k2-k1)t}$

[A.11] can be written as:

[A.12] $e^{k2t}T = k_1N_0/(k_2-k_1)\,e^{(k2-k1)t} + c_2$

Dividing **[A.12]** by the integration factor (e^{k2t})

$T = k_1N_0/(k_2-k_1)(e^{(k2-k1)t}/e^{k2t}) + c_2/e^{k2t}$

$T = k_1N_0/(k_2-k_1)e^{(k2-k1)t-k2t} + c_2/e^{k2t}$

$T = k_1N_0/(k_2-k_1)e^{k2t-k1t-k2t} + c_2/e^{k2t}$

[A.13] $T = k_1N_0/(k_2-k_1)e^{-k1t} + c_2/e^{k2t}$

Using the integration factor:

$$0 = k_1N_0/(k_2-k_1)e^{-k1(0)} + c2/e^{k2(0)}$$

$$0 = k_1N_0/(k_2-k_1)+c_2$$

[A.14] $c_2 = -k_1N_0/(k_2-k_1)$

Substitute **[A.14]** into **[A.13]**:

$$T = k_1N_0/(k_2-k_1)e^{-k1t} – k_1N_0/((k_2-k_1)e^{k2t})$$

[A.15] $T = k_1N_0/(k_2-k_1)(e^{-k1t} – e^{-k2t})$

Since $D = N_0 – N – T$

Then:

$$D = N_0 – N_0e^{-k1t} – k_1N_0/(k_2-k_1)(e^{-k1t} – e^{-k2t})$$

$$D = N_0 [1 – e^{-k1t} – k_1/(k_2-k_1) (e^{-k1t} – e^{-k2t})]$$

$$D = N_0 [1 – e^{-k1t} – (k_1e^{-k1t} – k_1e^{-k2t})/(k_2-k_1)]$$

$$D = N_0 [1-e^{-k1t} + (k_1e^{-k2t} – k_1e^{-k1t})/(k_2-k_1)]$$

$$D = N_0 [1 – (k_2-k_1)(e^{-k1t})/(k_2-k_1) + (k_1e^{-k2t} – k_1e^{-k1t})/(k_2-k_1)]$$

$$D = N_0 [1 + (-k_2e^{-k1t} + k_1e^{-k1t} + k_1e^{-k2t} – k_1e^{-k1t})/(k_2-k_1)]$$

[A.16] $D = N_0 [1 + (k_1e^{-k2t} – k_2e^{-k1t})(k_2-k_1)]$